THE ROLE OF GREMLIN1 IN BREAST CANCER DISEASE PROGRESSION:

RELEVANT MOLECULAR AND CELLULAR MECHANISMS

By

Catherine Zabkiewicz

Cardiff China Medical Research Collaborative

School of Medicine, Cardiff University

2021

Thesis submitted to Cardiff University for the degree of Doctor of Philosophy

Acknowledgements

I would like to thank my supervisor Miss Rachel Hargest and Dr Lin Ye for their continued essential guidance and support throughout the process of this research and thesis submission. Professor Wen G. Jiang has provided the opportunity for me to undertake this work within his laboratory at the Cardiff China Medical Research Collaborative, a truly international and welcoming environment, which has allowed my interest in cancer cell biology and my network of fellow scientists and medics to flourish.

This research work was supported with the award of a prestigious Royal College of Surgeons Research Fellowship, generously sponsored by the Freemasons United Grand Lodge of England. This fellowship significantly benefits the integration of laboratory science with the clinical frontline and was instrumental in enabling certain aspects of the research work.

I would also like to thank the many supportive staff within the laboratory – Mrs Fiona Ruge, Dr Andrew Sanders, Dr Jane Lane, and Dr Tracey Martin, who truly made me feel part of the team. Thanks must also go to Dr Stephen Paisey for his work with my *in vivo* model in the PETIC unit, and to Dr Joanna Zabkiewicz for providing both sisterly and scientific advice.

Lastly, but most certainly not least this would not have been achievable without the support and endless patience of my better half David, and my children, Reuben, and Lily.

Summary

Bone Morphogenetic Proteins (BMPs) are members of the Transforming Growth Factor Beta (TGFβ) family, that were discovered for their role in bone development, but have since been found to regulate cellular differentiation and tissue homeostasis. The cellular effect of BMPs is highly regulated, involving secreted antagonist proteins that directly bind BMPs, dampening BMP signalling. BMPs and their antagonists are of interest for their role in tumourigenesis and metastasis in cancer. Due to their significance in bone homeostasis, they are of particular interest in breast cancer, which commonly metastasises to bone. Despite progress in treatment and outcomes, those with metastatic breast cancer have poor survival. A better understanding of breast cancer biology, and development of prognostic markers and therapeutic targets is required for improved patient outcomes.

The Gremlin1 ligands BMP-2, -4 and -7, have been implicated in breast cancer disease progression, but little is known regarding the role of Gremlin1 itself.

This work determined that Gremlin1 expression in breast cancer is upregulated, but that its impact is dependent on the subtype and receptor profile of the breast cancer. There is a strong correlation between Gremlin1 and the Human Epidermal Growth Factor Receptor 2 (HER2), wherein upregulated Gremlin1 is a negative prognostic marker. Upregulation of Gremlin1 in HER2+ breast cancer cells increased proliferation, migration, and markers of epithelial to mesenchymal transition (EMT). *In vivo* Gremlin1 promoted HER2+ tumour growth and metastasis (particularly to bone). Inhibition of HER2 kinase activity abrogated the effect of Gremlin1 overexpression *in vitro*, suggesting a reciprocal relationship between Gremlin1 and HER2. Gremlin1 was also found to increase activity in AKT signalling and upregulates expression of PI3KCA, both important HER2 signalling pathway components. This highlights Gremlin1 as of relevance to HER2+ breast cancers, with a potential role in disease progression and response to HER2 blockade treatments.

Contents

List of figures

List of Tables

Publications and presentations

- **Zabkiewicz, C.,** Resaul, J., Hargest, R., Jiang, W. G., & Ye, L. (2017). 'Bone morphogenetic proteins, breast cancer, and bone metastases: striking the right balance'. *Endocrine-Related Cancer*, *24(10), R349–R366. PMID:28733469*

- Owen S., **Zabkiewicz C**., Ye L., Sanders A.J., Gong C., Jiang W.G. (2017) 'Key Factors in Breast Cancer Dissemination and Establishment at the Bone: Past, Present and Future Perspectives'. *Adv Exp Med Biol. 1026,197-216. PMID:29282685*

Abstracts:

- **Zabkiewicz, C.,** Ye, L., Hargest, R. (2021)'Gremlin promotes tumourigenesis and metastasis in HER2+ breast cancer' (Abstract) *British Journal of Surgery*, *Volume 108, Issue Supplement_1*

- **Zabkiewicz, C.,** Ye, L., Hargest, R. (2020)' A putative role for bone morphogenetic protein antagonist Gremlin1 in HER2 positive breast cancers' *(Abstract)UK Interdisciplinary Breast Cancer Symposium 2020. Breast Cancer Res Treat 180, 527–596 (2020).*

- **Zabkiewicz, C**., Ye, L., Hargest, R. (2019)' A putative role for bone morphogenetic protein antagonist Gremlin1 in HER2 positive breast cancers' (*Abstract)BJS 106(S3)6-27*

- **Zabkiewicz, C.,** Ye, L., Hargest, R., Jiang, W.G(2017) 'Gremlin 1 expression correlates with prognostic features and survival in breast carcinoma' ***(****Abstract)European Journal of Cancer*, Vol. 72, S17–S18

Presentations:

- ' Gremlin -1 promotes tumourigenesis and metastasis in HER2+ Breast Cancer' **ABS prize presentation session winner.** *SARS conference Dublin/Virtual Oct 2020(Oral)*

- ' A putative role for bone morphogenetic protein antagonist Gremlin1 in HER2 positive breast cancers' ***Basic science poster prize finalist.****UK Interdisciplinary Breast Cancer Symposium, Birmingham Jan 2020 (Poster)*

- 'A putative role for Bone Morphogenetic Protein Antagonist Gremlin in HER2 positive Breast Cancers' *SARS, London Jan 2019(Oral)*

- 'A putative role for Bone Morphogenetic Protein Antagonist Gremlin in HER2 positive Breast Cancers' *TSS, Cardiff Sep 2018* ***Trainee prize presentation winner*** *(Oral)*

- 'A Gremlin in the works' ***MIA Science Prize Winner*** *Royal Society of Medicine Surgical section conference, Cardiff Sep 2017 (Oral)*

Abbreviations

AKT Protein Kinase B

APS Ammonium Persulfate

BAMBI BMP And Activin Membrane Bound Inhibitor

BCC Basal Cell Carcinoma

BCS Breast Conserving Surgery

BME Bone Matrix Extract

BMP Bone Morphogenetic Protein

BRCA Breast Cancer gene

BRG Bone Related Gene

BSA Bovine Serum Albumin

BSP Bone Sialoprotein

BSS Balanced Salt Solution

CAF Cancer Associated Fibroblast

CHD1 Cadherin 1

CRC Colorectal Cancer

CRISPR Clustered Regularly Interspaced Short Palindromic Repeats

CS Cowden Syndrome

CTGF Connective Tissue Growth Factor

DAB 3, 3'-diaminobenzidine

DAN Differential screening selected gene Aberrative in Neuroblastoma

DCIS Ductal Carcinoma in Situ

DEPC Diethyl pyrocarbonate

DiI 1,1′-dioctadecyl-3,3,3′,3′-tetramethylindocarbocyanine perchlorate

Dlx5 Distal-less homeobox 5

DMEM Dulbecco's Modified Eagle Medium

DMFS Disease and Metastasis Free Survival

DMH1 Dorsomorphin

DMSO Dimethyl Sulfoxide

DNA Deoxyribonucleic Acid

EDTA Ethylene Diaminetetraacetic Acid

EGFR Epidermal Growth Factor Receptor

ELISA Enzyme Linked Immunosorbent Assay

EMT Epithelial to Mesenchymal Transition

ERα Oestrogen Receptor

ERE Oestrogen Response Element

ERK extracellular signal-regulated kinase

FAK Focal Adhesion Kinase

FCS Foetal Calf Serum

FDG Fluorodeoxyglucose

FGF Fibroblast Growth Factor

FOXA1 Forkhead Box A1

GAPDH Glyceraldehyde-3-Phosphate Dehydrogenase

GATA3 GATA binding protein 3

GC Gastric Cancer

GEO Gene Expression Omnibus

GFP Green Florescent Protein

GSK3β Glycogen Synthase Kinase 3

GTPase Guanosine Triphosphate enzyme

HER2 Human Epidermal Growth Factor Receptor 2

hFob Human Foetal Osteoblast

HGF Hepatocyte Growth Factor

HRP Horse Radish Peroxidase

HRT Hormone Replacement Therapy

HTA Human Tissue Act

HUVEC Human Umbilical Vein Endothelial Cell

ID1 Inhibitor of Differentiation protein 1

IDC Invasive Ductal Carcinoma

IHC Immunohistochemistry

IGF Insulin like Growth Factor

JNK c-Jun N-terminal Kinases

MAPK Mitogen Activated Protein Kinase

M-CSF Macrophage colony stimulating factor

MFP Mammary Fat Pad

MMP Matrix Metalloprotease

MRI Magnetic Resonance Imaging

MSC Mesenchymal Stem Cell

mTOR Mechanism Target Of Rapamycin

MTT 3-(4,5-dimethylthiazol-2-yl)-2,5-diphenyltetrazolium bromide

NFκB Nuclear Factor Kappa B

NPI Nottingham Prognostic Index

OPG Osteoprotegerin

OPN Osteopontin

OS Overall Survival

OSCC Oesophageal Squamous Cell Carcinoma

OSX Osterix

PALB Partner and Localizer of BRCA

PBS Phosphate Buffered Saline

PCR Polymerase Chain Reaction

PDGF Platelet Derived Growth Factor

PDPL Podoplanin

PEI Polyethylenemine

PET Positron Emission Tomography

PI3K Phosphoinositide 3-Kinase

P/KC Protein Kinase C

PR Progesterone Receptor

PRDC Protein Related to DAN and Cerberus (Gremlin 2)

PTEN Phosphatase and Tensin homolog

PTH Parathyroid Hormone

PVDF Polyvinylidene Difluoride

RANKL Receptor Activator for NF-κB Ligand

RAS Rat Sarcoma Virus gene

RFS Relapse Free Survival

Rh Recombinant

Rho RAS Homologue

RNA Ribonucleic Acid

RPMI Roswell Park Memorial Institute

Runx2 Runt related transcription factor 2

SDS Sodium Dodecyl Sulfate

SEM Standard Error of the Mean

SHH Sonic Hedgehog

SLNB Sentinel Lymph Node Biopsy

SMAD Homologue of mothers against decapentaplegic and SMA

SOC Super Optimal broth with Catabolite repression medium

STK11 Serine/Threonine Kinase 11

TCGA The Cancer Genome Atlas

TEMED Tetramethylethylenediamine

TBE Tris Boric Acid EDTA

TBS Tris Buffered Saline

TGFβ Transforming Growth Factor Beta

TMA Tissue Microarray

TMB 3,3′,5,5′-Tetramethylbenzidine

TNBC Triple Negative Breast Cancer

TNFα Tumour Necrosis Factor Alpha

USAG Uterine Sensitisation Associated Gene

VEGF Vascular Endothelial Growth Factor

VEGFR2 Vascular Endothelial Growth Factor Receptor 2

WBRT Whole Breast Radiotherapy

WHO World Health Organisation

Wnt Wingless/Integrated

1 Introduction

1.1 Breast cancer epidemiology

Breast cancer is currently the most common cancer in the UK, accounting for almost a sixth (15%) of all cancer cases and 54,700 cases in women in 2017(CRUK 2021) (Figure 1.1). Worldwide, there were 2.26 million breast cancer diagnoses in 2020, as the most common cancer site, followed by lung cancers with 2.21 million cases (Bray et al. 2018; Ferlay et al. 2019; Huang et al. 2021).

Figure 1-1 The 20 most common cancers in the UK, 2017(Graph Credit with open access permission, Cancer Research UK)

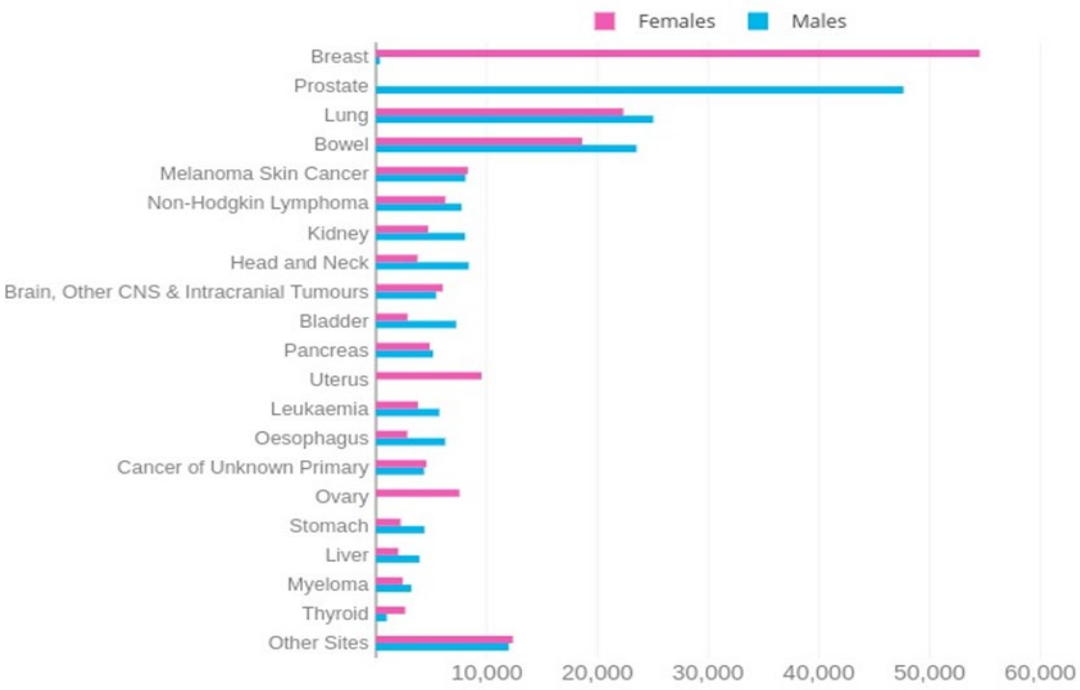

Less than 1% of breast cancer diagnoses are in men, and these account for less than 0.1% of cancer deaths, thus, male breast cancer is considered rare, with little published data (Ferzoco and Ruddy 2016; CRUK2021). For this reason, further reference to breast cancer in this work can be assumed to regard female breast cancer only. There is wide geographical variation in incidence of breast cancer, with predominance in the western world, and lowest incidence in south central Asia, middle, and eastern Africa (Figure 1.2) (Bray et al. 2018).

Figure 1-2 GLOBOCAN worldwide breast cancer incidence and mortality per 100,000 women, 2018

Adapted from Bray et al, (with open access permission)(Bray et al. 2018)

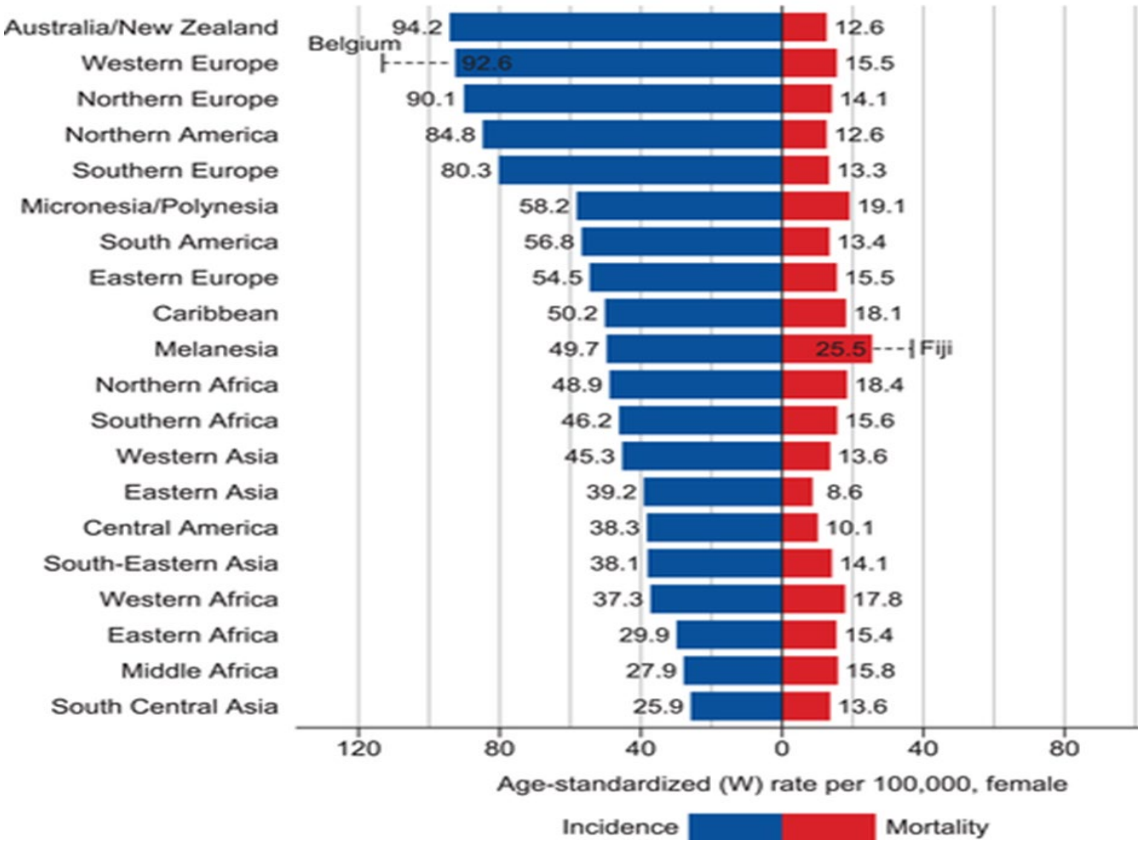

The major driver for this geographical variation in incidence is thought to be related to non-hereditary elements and risk factors, as low risk populations migrating to high-risk areas attain higher incidence levels in subsequent generations and vice versa as acculturation occurs (Ziegler et al. 1993; Ziadeh et al. 2017).

In nearly all regions of the world, breast cancer incidence has been steadily rising since records were initiated in the 20th century, making breast cancer an ongoing vital area of cancer research (Figure 1.3 A). In the UK, incidence has risen steadily and continues to do so (Figure 1.3 B), currently 1 in 7 women in the UK will be diagnosed with breast cancer during their lifetime (Smittenaar et al. 2016). Thus, breast cancer is a significant ongoing concern for the UK health service, and the public.

Figure 1-3 Breast cancer incidence trends over time

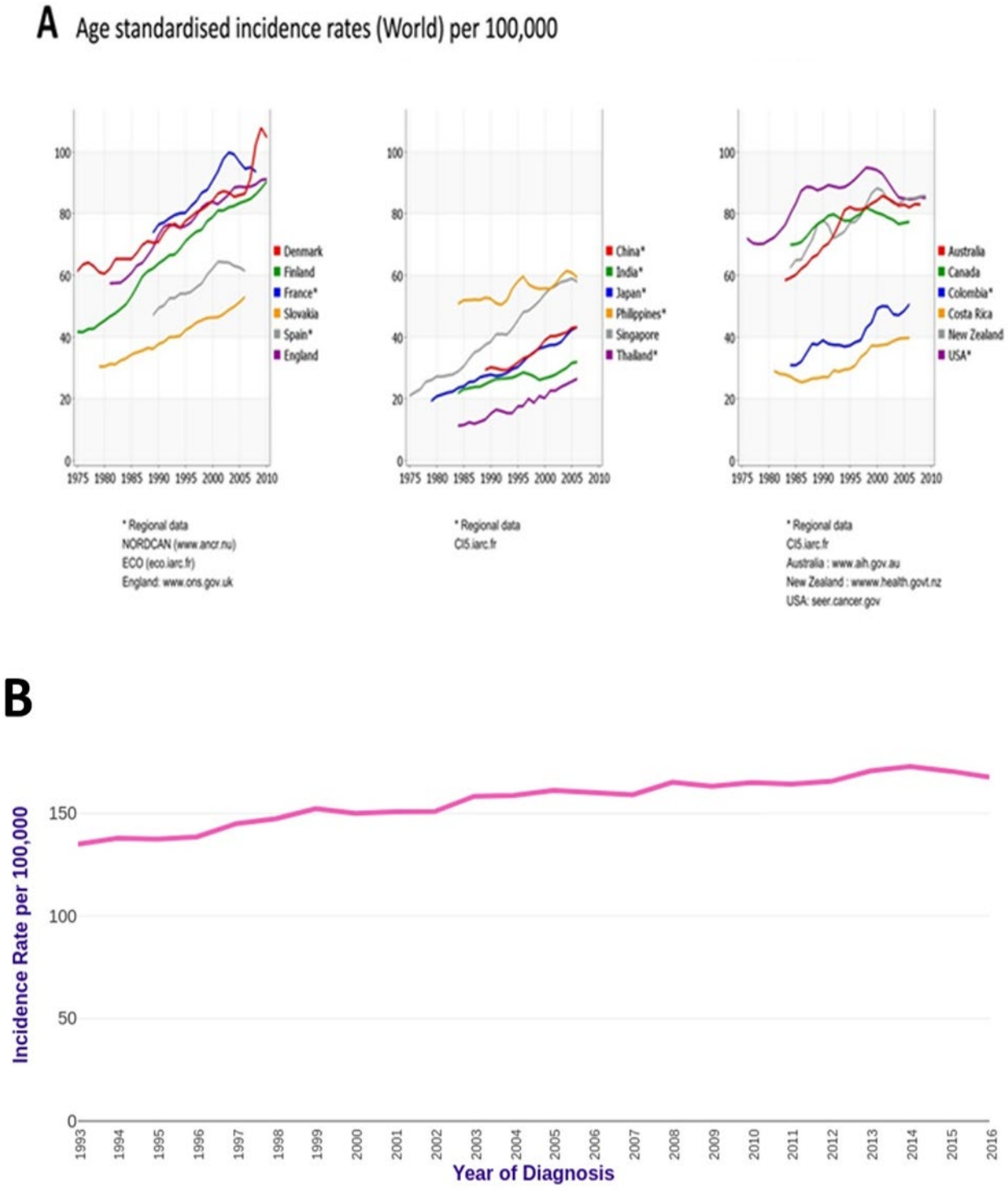

A) Age standardised breast cancer incidence per 100,000 women over time in different regions and countries of the world. Adapted with open access permission from International Agency for Research on Cancer factsheet 15 (Cancer 2012)

B) Age standardised breast cancer incidence per 100,000 women in the UK from 1993 to 2016. Graph Credit with open access permission, Cancer Research UK 2021

1.2 Breast cancer risk factors

1.2.1 Age

Increasing age is the most significant risk for breast cancer, with a median age at diagnosis of 61 years. However, the rate of increase does slow and flatten after the menopause (Rojas and Stuckey 2016).

1.2.2 Reproductive and biological factors

Risk of breast cancer is related to exposure to endogenous hormones produced by the ovaries (oestrogen and progesterone). Those with early menarche or late menopause also have 2-3-fold increased relative risk and those who undergo bilateral oophorectomy before age 35 reduce their risk of breast cancer to 40% of those who have natural menopause. Use of exogenous oestrogens, such as oral contraceptive and hormone replacement therapy (HRT), for extended periods of time, also increase their breast cancer risk by a small margin compared to those who do not. HRT gives the effect of delaying menopause, and increases breast density, making it more difficult to detect cancers on screening mammograms. However, despite an increased risk, HRT does not increase breast cancer mortality, and cancers in the context of HRT tend to be less advanced (McPherson, Steel et al. 2000).

Since pregnancy and breastfeeding reduce the lifetime number of natural menstrual cycles, nulliparous women have increased risk compared to those with children (with increasing number of live births associated with decreased breast cancer risk), and women who have their first child after age 30 have twice the risk of breast cancer compared to those who have their first child before age 20. In addition, pregnancy and breast feeding directly affect the development and differentiation of breast cells, which may impact the likelihood of cancerous changes (McPherson et al. 2000; Rojas and Stuckey 2016).

1.2.3 Genetic and Inherited factors

Somatic mutations account for most breast cancer cases, as only 5-10% are inherited. Those with bilateral breast cancers, combination of breast and other epithelial cancers or early onset breast cancers, are more likely to be carrying a genetic mutation that predisposes to breast cancer. Risk of breast cancer increases dependent on family history. For example, risk increases if one or more

first degree relatives develops it under the age of 50, with higher risk the younger the relative is at diagnosis (McPherson et al. 2000). Genetic risk is also higher in those with immediate family members that have had triple negative, bilateral or male breast cancer. African American women diagnosed with breast cancer under the age of 35 are also more likely to have a breast cancer genetic mutation.

In 60 - 90% of hereditary breast cancer cases it is due to mutation in BRCA1 and BRCA2 (BReast CAncer genes), inherited in an autosomal dominant manner. These genes are both involved in DNA repair responses and cell cycle mechanisms (Peshkin et al. 2010; Lee et al. 2020). Patients with BRCA1 mutations have a 65% risk of developing breast cancer by age 70, and those with BRCA2 have a 45% risk. BRCA1 mutations are correlated with more aggressive breast cancers, of higher grade and with lower expression of hormone receptors (Peshkin et al. 2010; Lee et al. 2020). In addition to an increased risk of breast cancers, BRCA variants also have increased risk of melanoma, ovarian, endometrial, pancreatic, colorectal, and prostate cancers (McPherson et al. 2000; Peshkin et al. 2002; Lee et al. 2020).

Other high risk gene mutations for breast cancer include TP53, which is a tumour suppressor gene for a transcription factor that regulates cell cycle, is antiproliferative and mutated frequently in many types of cancers. Mutation in TP53 is found in 30% of all breast cancers, however the clinical relevance of somatic TP53 mutations is not always clear. High rates of somatic TP53 mutation are found in triple negative tumours and BRCA1/2 germline mutation carriers. In Li Fraumeni syndrome (LFS) a germline TP53 mutation leads to increased risk of a wide spectrum of cancers, however, for women with LFS, breast cancer is the most common, with a 49% risk of developing it by age 60 (Masciari et al. 2012).

PTEN (Phosphatase and Tensin homolog) is another tumour suppressor gene that is regularly found to be mutated in breast cancers and regulates cell signalling pathways that control cellular proliferation and cell cycle progression. PTEN also promotes apoptosis. Cowden’s Syndrome(CS) is an autosomal dominant inherited condition with germline mutation in PTEN, characterised by developing breast, endometrial and thyroid malignancies, along with benign hamartomas (Kimura et al. 2017). Lifetime breast cancer risk in CS is 25-50%, with an average age of diagnosis between 38 and 50 years old (Pilarski 2009).

PALB2 germline mutations resulting in loss of function disrupt the localisation of BRCA2 in the nucleus and its function in DNA damage repair. It has therefore recently been found that the risk of breast cancer in those with germline PALB2 mutation is equivalent to that of BRCA2 mutation, with a mean cumulative risk of 35% by age 70, and an odds ratio of 3.94 compared to those without PALB2 mutation (Rahman et al. 2007; Evans and Longo 2014).

STK11 slows cellular division and promotes apoptosis. Inherited mutations in this gene lead to Peutz-Jeghers syndrome, whereby benign hamartomatous polyps develop in the gastrointestinal tract. It also increases the risk of developing several cancers including colonic, pancreatic and testicular/ovarian as well as a lifetime risk of breast cancer of 24-54% (Rousset-Jablonski and Gompel 2017).

CHD1(E-Cadherin) belongs to a family of proteins that are vital for cell-cell adhesion and transmission of signalling for control of cellular differentiation. It can also prevent uncontrolled cellular proliferation and motility. Mutation of CDH1 leads to a 39% lifetime risk of mainly lobular breast cancers and also a 56-70% lifetime risk of gastric cancer (hereditary diffuse gastric cancer) (Rousset-Jablonski and Gompel 2017).

1.2.4 Lifestyle and co-morbidity factors

Obesity is an increasing health issue in the developed world, resulting in an altered physiology and hormonal environment that can lead to several diseases and increased risk of several cancers (Jiralerspong and Goodwin 2016; Rojas and Stuckey 2016).

Gain of weight, during middle adulthood, is associated with a near two-fold increased risk of breast cancer in post-menopausal women, in particular those cancers that express oestrogen receptors. Conversely, obesity in pre-menopausal women decreases the overall relative risk of breast cancer (for African and white pre-menopausal women), but increases the odds ratio of breast cancers lacking hormone receptors (‘triple negative’ breast cancer/TNBC) (Jiralerspong and Goodwin 2016; Soguel et al. 2017)

Obesity has also been found to be an independent risk factor for worse survival from breast cancer, with a linear relationship between breast cancer specific mortality and increasing BMI (body mass index). Breast cancer cells express

insulin receptors, with insulin circulating at higher concentrations in obesity, resulting in binding of insulin to receptors on breast cancer cells and activation of PI3K (Phosphoinositide 3-Kinase)/AKT and MAPK (Mitogen Activated Protein Kinase) signalling pathways that promote proliferation. Women with Type 2 diabetes have been found at meta-analysis to have a 20 % increased risk of breast cancer (Liao et al. 2011; Goodwin and Stambolic 2015; Rojas and Stuckey 2016). Given the above findings, it is perhaps no surprise that regular physical activity reduces breast cancer risk (Jiralerspong and Goodwin 2016; Rojas and Stuckey 2016).

Alcohol intake has consistently been correlated with risk of developing breast cancer, with a pooled analysis adjusted for other risk factors demonstrating that each additional 10g of alcohol per day equates to an estimated 7% increased breast cancer risk (Hamajima et al. 2002). This association is controversial, as other studies have shown that the risk is not seen in cohorts of alcoholics, with one study showing a reduced risk of breast cancer in those consuming 10-12g of wine per day compared to non-drinkers (Rojas and Stuckey 2016).

Finally, smoking is historically not thought to influence breast cancer. However, a recent study associated smoking with breast cancer incidence, particularly an increase in those breast cancers expressing hormone receptors (Goldvaser et al. 2017). A large cohort study from the UK examined 102,927 women, and found a hazard ratio of 1.24 for breast cancer in smokers compared to never smoked, with particularly strong association if smoking commenced in adolescence or peri-menarche (Jones et al. 2017).

1.2.5 Factors intrinsic to the breast

Breast epithelium and stroma, from within which breast cancer arises, appears radiopaque on mammograms, with mammographic breast density (the proportion of dense breast tissue within the total breast area) associated with an increased risk of breast cancer (odds ratio 4.7). Breast density reduces with increasing age, BMI, parity, and breast feeding. It is also influenced by HRT use, which implies density is a product of endogenous and exogenous hormonal influence (Barrett-Lee et al. 2009; Rojas and Stuckey 2016).

Mammographically dense tissue makes it more difficult to detect breast cancers, and those that originate in mammographically dense tissue are more commonly associated with higher pathological grade, lymphovascular invasion and advanced stage when compared to tumours in radiolucent breast tissue (Rojas and Stuckey 2016).

Women with previous diagnosis of atypical epithelial hyperplasia of the breast, have a four to five fold increased risk of developing breast cancer than those with no history of benign breast proliferative changes (McPherson et al. 2000). Other proliferative lesions without atypia, such as adenosis and radial scars, have a relative risk of breast cancer of 1.88. For those with proliferative benign lesions and a family history of breast cancer, there is a 2.5-fold increased breast cancer risk compared to those without family history(Dyrstad et al. 2015; Rojas and Stuckey 2016). Non-proliferative lesions, such as cysts and fibroadenomas, in one meta-analysis conferred a relative risk of breast cancer of 1.55 (95 % CI 1.26–1.90) and 1.41(95 % CI 1.11–1.80) respectively, compared to standard population risk (Dyrstad et al. 2015; Rojas and Stuckey 2016), however, other studies have found no significant increased risk of breast cancer in those with non-proliferative benign breast disease(classed in this study as fibrocystic tissue, cysts and fibroadenomas, without features of ductal hyperplasia, sclerosing adenosis or papilloma) compared to standard population, unless in the presence of a strong family history of breast cancer(Hartmann et al. 2005). Using the same cohort as Hartmann et al, a more recent study demonstrated a greater incidence of breast cancer compared to standard population incidence in benign breast disease overall (BBD, i.e. non-proliferative disease, proliferative disease without atypia and atypical ductal hyperplasia), with a standardised incidence ratio (SIR) of 1.50 (95% CI 1.39– 1.62).Those whose BBD was a simple fibroadenoma had a similar SIR of 1.49 (95% CI 1.26– 1.74), but those with complex fibroadenoma(defined as containing cyst diameter 3 mm or larger, sclerosing adenosis, epithelial calcifications or papillary apocrine metaplasia) had a SIR of 2.27 (95% CI 1.63–3.10) .It was felt this increased risk in complex fibroadenoma was more attributable to the associated proliferative changes, rather than the fibroadenoma itself(Nassar et al. 2015).In addition, these results may be biased by the fact they are based on only surgically excised lesions, which will have a different breast cancer risk profile to fibroadenomas that are not excised .A retrospective longitudinal study suggested that the SIR of breast cancer in those with clinically

and radiologically diagnosed fibroadenoma is 0.97 (95% CI = 0.7-1.4) compared to a SIR of 2.0 (95% CI 1.4-2.7) for biopsied or excised fibroadenoma(Ciatto et al. 1997).

Any prior radiation exposure to the chest wall/breast region, or during childhood/puberty when the breast is rapidly developing, will lead to an increased risk of breast cancer later in life. Teenage girls exposed to radiation during the second world war had a doubling of breast cancer risk, and those receiving chest radiation at a young age for Hodgkin's lymphoma had a cumulative risk of breast cancer of 29% by age 55 (McPherson et al. 2000; Rojas and Stuckey 2016).

1.3 Breast cancer mortality and survival

Despite attracting the largest share of research funding for several years (Kamath et al. 2019), and significant reductions in mortality (Figure 1.4A), breast cancer is still the leading cause of cancer death in women worldwide, accounting for 15% of all female cancer deaths (Bray et al. 2018) (Figure 1.4 B). There is geographical variation in mortality (Figure 1.2). Trends of decreasing mortality are seen in more economically advanced western countries with the highest incidences (Figure 1.4A). For England, those in the most economically deprived areas experience a 6% higher mortality from breast cancer compared to those in the least deprived areas(UK 2014). These geographical differences worldwide will be influenced by variations in accuracy and recording of data, as well as the healthcare provisions with differing available resources in detecting and treating breast cancer, heightened awareness or less stigma amongst populations in which it is a more common disease, presentation at different stages of disease, and biological differences in the subtypes of breast cancers common amongst different populations.

Figure 1-4 Worldwide mortality burden of Breast Cancer

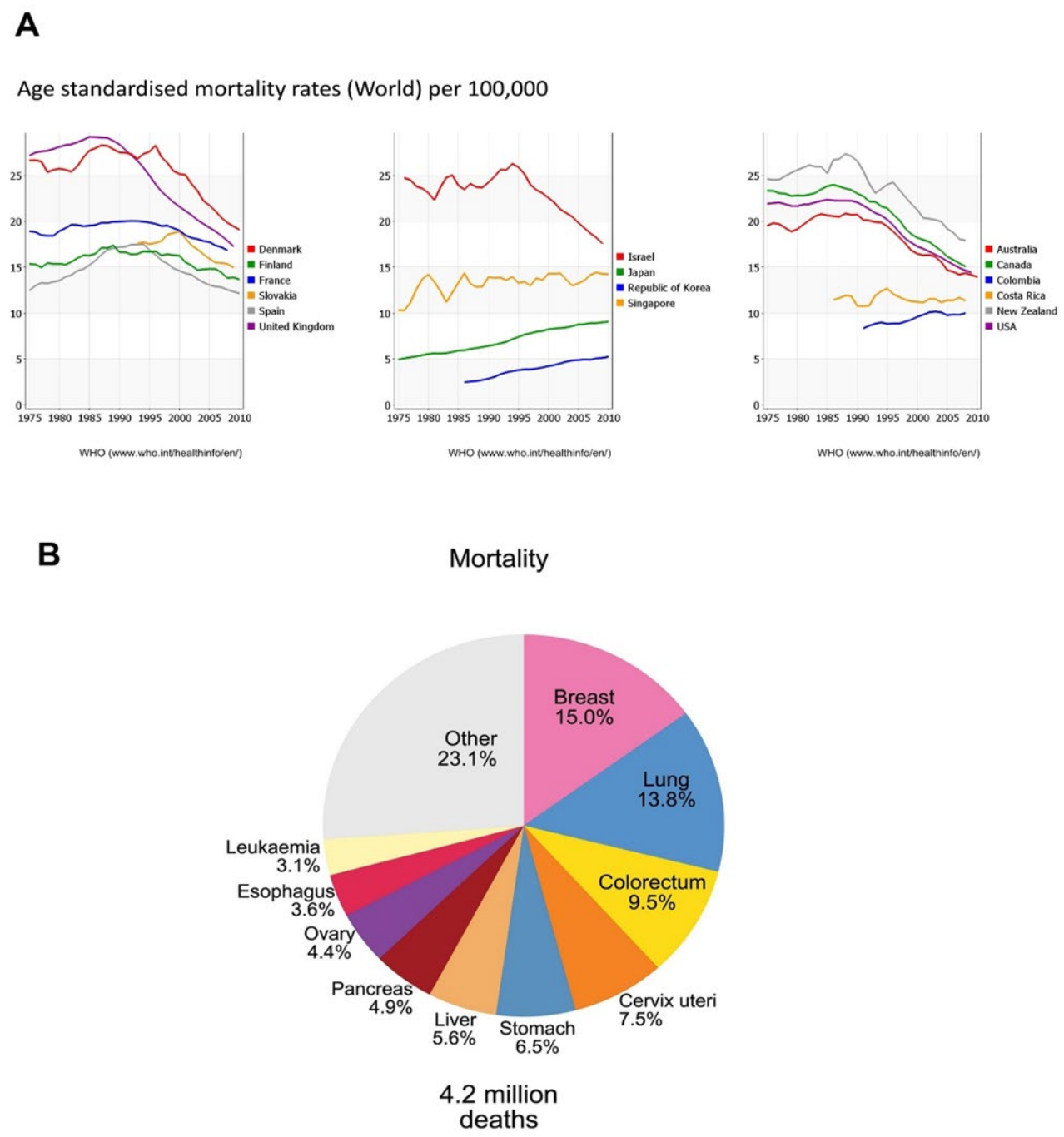

A) Age standardised mortality rates per 100,000 population over time. Adapted with open access permission from International Agency for Research on Cancer factsheet 15 (Cancer 2012)

B) Percentage of 4.2 million cancer deaths in women worldwide in 2018 by cancer type. Adapted from Bray et al with open access permission (Bray et al. 2018)

Although the incidence of breast cancer has increased in England and Wales, the 10-year net survival in breast cancer of all stages at diagnosis has improved from

40% in the 1970s to 78% in 2010-11(Figure 1.5). This could be attributed to multiple factors, including population behaviours, screening and improvements in diagnostic methods, such as breast magnetic resonance imaging (MRI) and digital mammography(Saadatmand et al. 2015). Changes in surgical management such as the more selective sentinel lymph node biopsy (SLNB) of the axillary nodes rather than the traditional full lymph node dissection, resulted in more accurate pathological scrutiny and stage migration than previously, with the potential benefit of adjuvant treatments that would not otherwise have been offered(Vanderveen et al. 2006; Meiers et al. 2013). Alterations in use and precision of radiotherapy and improved targeting of hormone blockade treatments and chemotherapies, with evolution of our understanding of breast cancer biology have also led to improved outcomes (Saadatmand et al. 2015).

Figure 1-5 Age standardised 10-year net survival in women (age 15-99), England and Wales, 1971-2011. Graph Credit with open access permission from Cancer Research UK 2021.

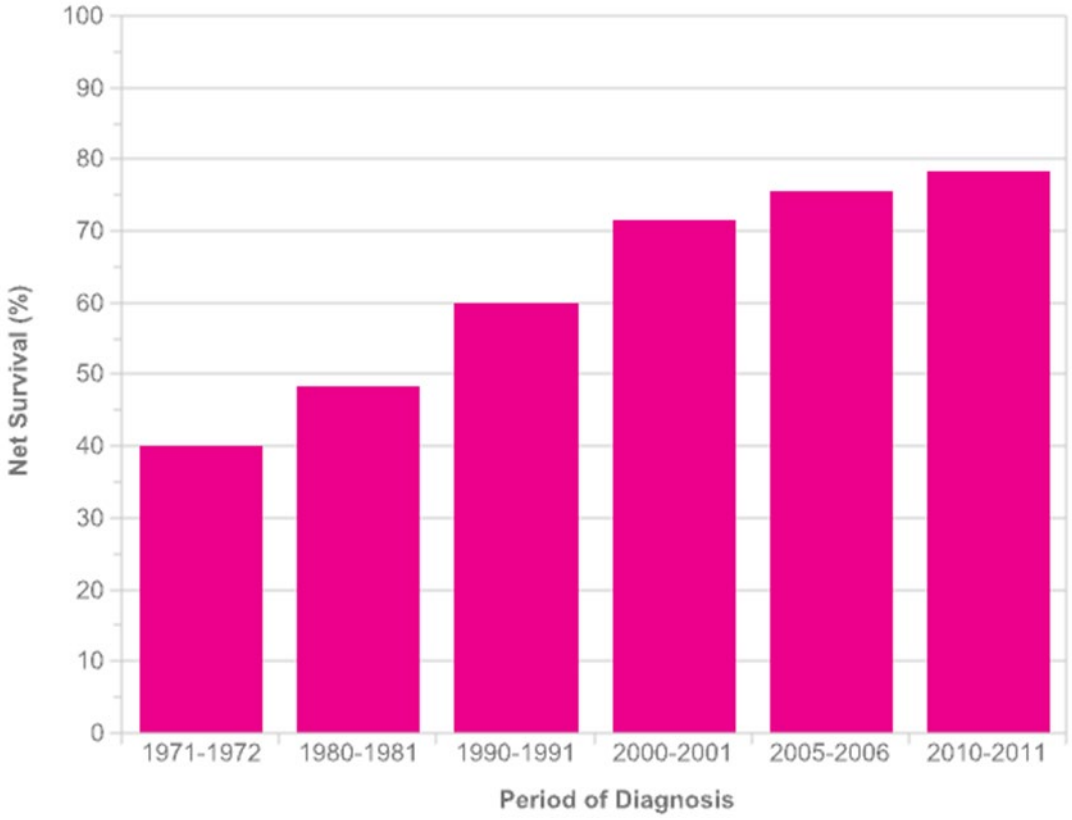

This survival data does not reflect the vast difference in survival between those diagnosed at an early stage and those who already have *de novo* metastatic disease at diagnosis (Table 1.1). In England and Wales, those with advanced stage 4 disease and distant metastases at diagnosis have a significantly lower 5-year survival of 26.2% even compared to stage 3, which is advanced loco-regional disease, with a 5-year survival of 72%. This highlights that although *de novo* stage

4 disease is a relatively small proportion of all breast cancer cases, the majority of whom are early stage with good survival, metastatic breast cancer is an area where improvements in biological understanding and treatment should be made.

Table 1-1 Breast Cancer 5-year net survival by stage in England and Wales 2013-2018.

Stage	Number of Cases	Net Survival (%)	Lower Confidence Interval (%)	Upper Confidence Interval (%)
1	83,026	97.9	97.3	98.5
2	79,397	89.6	89	90.2
3	18,369	72	70.5	73.5
4	10,294	26.2	24.8	27.7
Unstageable	422	-	-	-
Unknown stage	18,830	69.1	68	70.3

(Credit to Cancer Research UK, data from Office for National Statistics. Open access permission. Unstageable/unknown are those without complete staging data)

1.4 Breast cancer pathology

Cancer occurs when cells within the body become abnormal and develop mechanisms that allow the cells to evade the normal checks and balances of cellular homeostasis, such as self-sufficient growth and metabolism, resistance to growth inhibition, evasion of cell death programmes and immune response controls plus limitless replication. Underlying these traits will be genetic and epigenetic changes that aid in driving the process (Hanahan and Weinberg 2000,2011). In addition, cancer is an evolutionary process, whereby those abnormal cells that acquire advantageous properties can also be influenced by the selection pressures of the environment within which they sit (tumour microenvironment or TME) (Fouad and Aanei 2017). The cells that consequently

form a clinically detectable tumour will thus have undergone clonal selection and expansion because of these varying selection pressures, ultimately giving rise to both intratumour heterogeneity (diversity within the tumour) and intertumoural heterogeneity (diversity between individual tumours). This is a core principle particularly for breast cancers, where complexity and heterogeneity must be 'unpicked' to determine treatment strategy, thus, there are different ways in which breast cancers are classified and treated.

1.4.1 Histopathological classification

The World Health Organisation (WHO) has defined different breast tumours (Lokuhetty et al. 2019) (Table 1.2) based on their histopathological appearance and cytology, but also with regard to the tumour's localisation, clinical features, molecular features, aetiology and pathogenesis.

Breast tumours are divided into epithelial tumours of the breast, tumours of the nipple, and mesenchymal tumours of the breast (Table 1.2). Epithelial tumours are the most common, and within the category are a variety of sub classifications. The most common breast tumour overall is invasive ductal carcinoma of 'no special type' (NST). These comprise 80% of all breast tumours and thus further discussion of invasive breast cancer will refer to invasive ductal carcinoma NST unless otherwise specified.

Breast tumours are also histopathologically graded using the Nottingham system, which provides a reflection of how 'abnormal' the breast cells appear based on tubule formation, mitoses (dividing cells) and nuclear pleomorphism (Rakha et al. 2010; Nicolini et al. 2018). Each of these factors is assessed by a pathologist and scored, and a grade given based on the total. Grade 1 tumours are most like normal breast cells and Grade 3 the least normal. The tumour grade can be utilised, along with tumour size and number of lymph nodes involved, in the Nottingham Prognostic Index score, which stratifies patients in terms of predicted survival (Sejben et al. 2020).

Table 1-2 WHO Classification of Breast Cancers

EPITHELIAL TUMOURS	EPITHELIAL TUMOURS	MESENCHYMAL TUMOURS
Precursors:	**Rare or Salivary gland type:**	**Vascular:**
Usual ductal hyperplasia	Acinic cell carcinoma	Haemangioma
Columnar cell lesions	Adenoid cystic carcinoma	Angiomatosis
Atypical ductal hyperplasia	Secretory carcinoma	Post radiation angiosarcoma
Adenosis and benign sclerosing lesions:	Mucoepidermoid carcinoma	Primary angiosarcoma
Sclerosing adenosis	Polymorphous adenocarcinoma	**Fibroblastic and myofibroblastic:**
Apocrine adenosis	Tall cell with reversed polarity	Inflammatory fibroblastic
Microglandular adenosis	**Neuroendocrine**	Myofibrosarcoma
Radial scar		Fibrosarcoma
Adenomas:	**TUMOURS OF NIPPLE**	Leiomyosarcoma
Tubular	Syringomatous	Rhabdosarcoma
lactating	Nipple adenoma	(Phyllodes)
Ductal	Paget disease of breast	(Fibroadenoma)
Epithelial-Myoepithelial:		
Pleomorphic adenoma		
Adenomyoepithlioma(benign/malignant)		
Papillary:		
Intraductal Papilloma		
Papillary DCIS		
Encapsulated/solid/invasive papillary carcinoma.		
Non-Invasive Lobular Neoplasia:		
Atypical lobular hyperplasia		
Lobular carcinoma in situ		
Ductal carcinoma in situ (DCIS)		
Invasive breast carcinoma:		
No special type		
Microinvasive		
Invasive lobular		
Tubular		
Cribriform		
Mucinous		
Mucinous cystadenocarcinoma		
Invasive micropapillary		
Carcinoma with apocrine differentiation		
Metaplastic		

1.4.2 Biological markers

In addition to histopathological grading, invasive breast carcinomas are also classified by immunohistochemistry (IHC), expression of clinical biomarkers which include oestrogen receptors (ER), progesterone receptors (PR) and the human epidermal growth factor receptor 2(HER2). This histopathological classification determines treatments offered, and thus forms part of standard pathology reporting of invasive breast cancers in the UK (NICE 2018), Europe, and the USA (Harris et al. 2016; Cardoso et al. 2019).

Historically, it has been noted for many decades that breast cancer growth can be stimulated by oestrogen, and thus, breast cancers with ER may benefit from treatments that block oestrogen (Williams and Lin 2013; Duffy et al. 2017). ERα is upregulated or overexpressed in 70% of invasive breast cancers (Carroll 2016; Siersbæk et al. 2018). Its main function in normal breast cell biology is genomic and transcriptional regulation in response to oestrogen exposure, for example, it has a DNA binding region and can directly interact with oestrogen response elements (EREs) that regulate target gene expression. This is thought to also require co-ordination of several additional co-factor proteins such as FOXA1 and GATA3 (Carroll 2016). ERα can indirectly affect gene expression via interactions with transcription factors and co-regulators of transcription. In breast cancer these functions become dysregulated, and oestrogen binding of the ERα results in aberrant and uncontrolled gene transcription and cell division (Carroll 2016). In addition to these core functions within the nucleus, ERα has also been shown to interact with cell membrane receptors and intra cellular cytoplasmic downstream signalling pathways. For example, epidermal growth factor(EGF) can phosphorylate ERα via mitogen activated protein kinase (MAPK), inducing activation of ERα independent of oestrogen stimulation (Siersbæk et al. 2018). ER and PR expression are assessed using IHC and reported using a standardised score (such as the Allred score, which combines percentage nuclear stain with intensity of stain) (NICE 2018).

PR expression is utilised in breast cancer traditionally as a marker of ER activity, as PR is a target gene regulated by ER, and is thus often expressed in ER+ breast cancers (Siersbæk et al. 2018). Historically, it was thought that those ER+ breast cancers demonstrating a loss of PR expression, reflected a functionally disrupted ER response and therefore may not benefit from oestrogen targeted therapies as much as those patients who were highly ER and PR positive. Although studies

have shown that ER+/PR- cancers do have a worse prognosis, the PR status has no bearing on recurrence after tamoxifen treatment, and ER-/PR+ cancers, although rare, do not have a statistically significant response to tamoxifen treatment (NICE 2011; Hefti et al. 2013).

Despite its historically uncertain and passive role, PR status is assessed and reported for all breast cancer patients. PR expression has also been gaining interest once more, as it has been determined that an active PR can sequester ER away from the ERE sites that result in tumour proliferation. Thus, active PR could inhibit the ER effects (Carroll et al. 2017; Siersbæk et al. 2018). This is currently the subject of the phase II PIONEER trial (A Pre-operative Window Study of Letrozole Plus PR Agonist (Megestrol Acetate) Versus Letrozole Alone in Post-menopausal Patients With ER-positive Breast Cancer) (Baird 2017), examining the use of a PR agonist in post-menopausal, ER positive breast cancer patients in the window between diagnosis and surgery and comparing the changes in tumour proliferation markers between initial tumour biopsy, and tumour specimen at operation after treatment, compared with control.

The HER2 status of breast cancer was recognised as important in the 1980s, as amplification of the HER2 gene was found to associate with more aggressive disease, high recurrence, and poor patient outcomes. HER2 is a transmembrane receptor, that is present in an active conformation, and although it has no confirmed identifiable ligand, will dimerise with other EGF receptors in order to affect cellular functions such as proliferation and cell cycle (Mitri et al. 2012). Around 20% of breast cancers demonstrate HER2 amplification and these patients will benefit from treatment targeting HER2, such as Trastuzumab and Pertuzumab (NICE 2011; Mitri et al. 2012). HER2 amplification is given an IHC score of 0 to 3+, with a positive 3+ result when more than 10% of cells demonstrate compete cell membrane staining (again, a combination of proportion of cells expressing the protein, and the intensity). An IHC result of 2+ is ambiguous and results in further tests to define HER2 status, using fluorescent in situ hybridisation (FISH) to look at HER2 gene copy number (Cardoso et al. 2019). An IHC result of 0/1+ is deemed negative for HER2 amplification.

Finally, those patients who do not have any of these clinical biomarkers present are deemed ‘Triple Negative’ breast cancers (TNBC) and will not significantly benefit from the treatments targeting these biomarkers. However, these patients may be suitable for other chemotherapeutic options. Classifying and selecting

patients for adjuvant therapeutics is becoming increasingly complex as breast cancer research has evolved, with multiple subtypes of breast cancer identified based on molecular profiling and gene expression panels, to determine which patients will benefit from which treatments.

1.4.3 Molecular classification

Many patients experience relapse or progression of disease, even after treatment selected by the above biological markers, reflecting our lack of full understanding of breast cancer biology and the heterogeneity therein. The biological markers are a simplistic stratification tool, and with development of high throughput gene expression molecular profiling of breast cancers, several subtypes have been identified (Eroles et al. 2012; Yersal and Barutca 2014) (Summarised inTable1.3) that share some crossover with the biological markers.

Table 1-3 Most common Breast Cancer molecular subtypes

Molecular subtype	Features
Luminal A 50-60% of tumours	ER/PR strongly +, HER2 -, Low Ki-67 Best Prognosis, hormone targeted therapy
Luminal B 10-20% of tumours	ER /PR + moderate, HER2+ or -, Ki-67 High Prognosis worse than Luminal A, hormone therapy +/- HER2 therapy
HER2 enriched 15-20% of tumours	ER/PR-, HER2+ Aggressive. Respond to HER2 targeted therapy +/- Chemotherapy.
Basal Like/Triple Negative 10-20% of tumours	ER/PR-, HER2- EGFR+, CK5/6+, p53 mutation Aggressive. Associated with BRCA1 gene mutation. Chemotherapy treated.

These intrinsic molecular subtypes were first published in 2000 by Perou et al (Perou et al. 2000), where gene expression profiling was used to classify 65 breast cancer samples from 42 patients, using cDNA microarrays encompassing around 8,000 genes. They initially identified four groups (Luminal like, Basal like, HER2+ and Normal like) and suggested that these tumours were biologically distinct and may need treating as such.

The Normal like group is rare and poorly characterised. There are features of adipose gene expression, but they do not demonstrate any markers that fit into the other subtypes and are often grouped with samples of normal breast tissue. Researchers have since postulated the Normal like group is a technical artifact in samples of normal breast tissue and not clinically relevant, thus this group is not often included as a true molecular subtype (Prat and Perou 2011; Eroles et al. 2012).

Since the seminal work by Perou et al, the Luminal group has been further divided into Luminal A and B. Luminal A breast cancer is the most common subtype and expresses ER and PR highly, as well as genes activated by ER signalling. These cancer cells share gene expression similarity with luminal cells lining the mammary ducts. Luminal A breast cancers have low proliferation markers such as Ki-67 (Table 1.3). The GATA3 gene is highly expressed in Luminal A and encodes for a transcription factor known to be important in differentiation and homeostasis of luminal epithelial breast cells, and the functioning of oestrogen and androgen signalling. Luminal A breast cancers have the best prognosis of all the subtypes, with lower relapse rates and longer survival times. This subtype has a propensity to metastasise to bone rather than other organ sites (Sørlie et al. 2001; Bastien et al. 2012; Eroles et al. 2012).

The less common Luminal B breast cancers are similar in some features to Luminal A, such as expression of ER, and bone as a common metastatic site, but there the similarity ends. Luminal B are more aggressive, with high markers of proliferation including Ki-67, with some expressing HER2 and EGFR. Luminal B have a much worse prognosis than Luminal A, even when treated with ER blockade, with higher recurrence in other organs such as the liver and lower survival rates. These tumours respond better to chemotherapy, but not as well as in other subtypes such as HER2 enriched and basal tumours (Sørlie et al. 2001; Sotiriou et al. 2003; Eroles et al. 2012). This results in difficulties successfully treating this subtype.

HER2 enriched subtype demonstrates high expression of the HER2 gene and proliferation genes, with low ER/PR expression. A large proportion also have p53 mutations. Seventy percent of tumours defined as HER2 enriched subtype on microarray will have corresponding protein overexpression on IHC, but not all, which demonstrates the incongruity between the molecular gene level and the protein level, and how clinical biological markers may not be directly comparable to the molecular intrinsic subtype (Sotiriou et al. 2003; Bastien et al. 2012; Eroles et al. 2012; Cheang et al. 2015). Historically, HER2 enriched subtype had a poor prognosis but, with the use of HER2 blockade treatments such as Trastuzumab and Pertuzumab, and given the higher chemosensitivity of this subtype, survival has much improved.

The basal subtype of breast cancer is highly invasive with poor survival, given the propensity towards metastasis in visceral organs such as liver, lung, and brain. The gene expression profile has similarities to the myoepithelial, or basal cells of the breast, highly expressing cytokeratin CK5/6, EGFR, and p53 mutations. Tumours with germline mutation in the BRCA1 gene are basal like (Bertucci et al. 2012; Alluri and Newman 2014). Basal tumours clinically present with large, high grade locally advanced disease in younger age groups, with a predominance in patients of African heritage. They do not express the clinical biological markers (ER/PR/HER2), and thus the terms “basal -like” and “triple negative” are often used interchangeably. However, not all clinically triple negative breast cancers will have a basal phenotype (Eroles et al. 2012; Alluri and Newman 2014).

The identification of molecular subtypes of breast cancer paved the way towards expansion of personalised medicine, as the subtypes demonstrate significant difference in incidence, survival, and response to treatments (Carey et al. 2006; Cheang et al. 2009; Hugh et al. 2009; O'Brien et al. 2010; Liu et al. 2016). UK guidance does not require reporting of intrinsic subtype for treatment or prognostic decisions, whereas European guidelines recommend tumours are grouped into intrinsic subtypes for treatment decisions using IHC and histology as surrogate for gene expression. They also suggest Ki-67 index maybe additionally useful, although this is not mandated.

However, multigene DNA or RNA profile assays are now available for use in clinical circumstances, for identifying recurrence risks and those who may benefit most from certain treatments. In the UK, Endopredict, Oncotype DX Breast Recurrence Score or Prosigna are recommended to guide adjuvant chemotherapy

options for patients with ER +/ HER2 – early breast cancer, where there is no spread to local lymph nodes or beyond. The patient must be assessed as having intermediate risk of recurrence using validated tools such as Nottingham Prognostic Index(Todd et al. 1987), or the online PREDICT tool(Wishart et al. 2010), as it is these ‘borderline’ cases in which the extra information provided by a gene assay may aid in decision making (Table 1.4).

Table 1-4 Prognostic tools approved for use in the UK

Prognostic Tool	Reference source	Method
PREDICT	https://breast.predict.nhs.uk/	Uses clinicopathological parameters from 5,000 previous breast cancer patients linked to outcome to estimate average survival and average benefit from different treatments. Validated on 23,000 patients.
Nottingham Prognostic Index (NPI)	(Todd et al. 1987)	(0.2 x size in cm) +Node status +Grade = NPI N1 = 0 nodes+, N2 = 1-3 nodes+, N3 = >3 nodes+ Grade 1 = 1, Grade 2 = 2, Grade 3 = 3 5-year survival and prognosis are given correlated to Index score.
Endopredict® (Second generation assay)	https://myriad.com/	Formalin fixed samples in paraffin, RNA extracted and real time reverse transcription polymerase chain reaction (RT-PCR) for panel of 8 genes (AZGP1, BIRC5, DHCR7, IL6ST, MGP, RBBP8, STC2, UBE2C), 3 normalisation genes (CALM2, OAZ1, RPL37A) and 1 control gene (HBB). Molecular score combined with tumour size and node status to give % risk of 10-year distant recurrence and estimated benefit of chemotherapy at 10 years.
Oncotype DX® (First generation assay)	https://www.oncotypeiq.com/	Formalin fixed surgical samples in paraffin, RNA extracted and RT-PCR for panel of 16 genes (Ki-67, STK15, Survivin, CyclinB1, MYBL2, Stromelysin3, Cathepsin L2, GRB7, HER2, ER, PR, Bcl2, SCUBE2, GSTM1, BAG1, CD68) and 5 reference genes (Beta-Actin, GAPDH, RPLPO, GUS, TFRC). Result gives recurrence score, risk of distant recurrence over 10 years and average chemotherapy benefit
Prosigna® (Second generation assay)	https://www.nanostring.com/ (Wallden et al. 2015)	Formalin fixed surgical samples in paraffin, RNA extracted and analysis of 50 genes (PAM50), for intrinsic subtyping. Nanostring platform uses fluorescent labelling of mRNA transcripts of interest rather than RT-PCR. 50 genes of interest, and 8 reference genes, plus positive and negative controls. Recurrence score is given by gene expression panel subtype, tumour size, node status and proliferation score (derived from 18 of the panel genes). Gives probability of distant recurrence over 10 years.

1.4.4 Diagnosis staging and treatment

In the UK, patients will present with breast cancer via a symptomatic or screening pathway. All patients will be ‘triple assessed’ with a physical examination by a clinician, radiologic assessment of breast and axilla (most commonly using mammograms and focused ultrasound (USS), with breast MRI in selected patients) and pathological biopsy (NICE 2018). Using this assessment, the cancer can be staged provisionally before treatment based on clinical and radiographic assessment, and/or formally after surgery with pathological assessment, using the American Joint Committee on Cancer (AJCC) anatomical TNM system, whereby T relates to tumour size, N is involvement of locoregional lymph nodes and M the status of any metastasis to other organs (Table 1.5). In the most recent edition of this staging tool, a prognostic stage can also be given, which incorporates tumour grade, biomarkers, and multigene panel results with the anatomical stage (Koh and Kim 2019; Magnoni et al. 2019).

For early breast cancer, with no evidence of spread to locoregional lymph nodes, patients are offered surgery to the breast and SLNB to stage the axilla (NICE 2018). Surgical options for the breast include breast conserving surgery (BCS) with post-operative radiotherapy, or mastectomy. Either approach can incorporate reconstructive oncoplastic techniques (NICE 2018; Cardoso et al. 2019). SLNB is used to stage the axillary nodes, where pre-operative axillary USS+/- biopsy has not detected axillary disease. If one or more nodes has macrometastases, the patient can be offered further surgery to remove the remaining lymph nodes or axillary radiotherapy, or if undergoing post-operative whole breast radiotherapy (WBRT), with only 1 or 2 involved sentinel nodes, they can choose to forego further axillary treatment(NICE 2018; Cardoso et al. 2019). Other adjuvant treatment after breast surgery includes assessment of biological markers and use of appropriately targeted agents.ER+ disease is treated with oestrogen blockade, HER2+ disease with Trastuzumab (Herceptin). Post-menopausal women with node positive disease are offered bisphosphonates. Those assessed as higher risk for disease recurrence are also offered adjuvant chemotherapy with a taxane and anthracycline regime. Chemotherapy can be used pre-operatively to downstage larger tumours to achieve BCS. Neoadjuvant Trastuzumab and Pertuzumab can also be added to chemotherapy for HER2+ disease that has high recurrence risk (NICE 2018).

Adjuvant and neoadjuvant treatments have significant side effects and toxicity, and although tools such as PREDICT have started to quantify the relative benefits of breast cancer treatments to help stratify patients to certain regimes, there is still further work to be done to predict those who will respond or relapse, and who will suffer the most severe side effects.

Table 1-5 American Joint Committee on Cancer 8th Edition TNM Breast Cancer Staging*

	TUMOUR		NODES		METASTASIS
TX	Cannot be assessed	Nx	Cannot be assessed	Mx	Not assessed
T0	No evidence of tumour	N0	No nodal metastases	M0	No clinical or radiographic evidence of metastasis
Tis	carcinoma *in situ or* Paget's disease of the nipple	N0(i+)	Malignant cell cluster <0.2mm	M0(i+)	Molecular or microscopic detection - Circulating tumour cells
T1	≤ 20 mm	N0(mol+)	No cells but +RT-PCR	M1	Distant metastases in organs or non-regional nodes
T1mi	≤ 1 mm	N1mi	Micrometastasis 0.2-2mm		
T1a	> 1 mm but ≤ 5 mm	N1a	Metastases 1-3 nodes		
T1b	> 5 mm but ≤ 10 mm	N1b	Metastases in ipsilateral internal mammary sentinel node		
T1c	> 10 mm but ≤ 20 mm	N1c	N1a and N1b		
T2	> 20 mm but ≤ 50 mm	N2	Metastases in 4-9 nodes		
T3	> 50 mm	N2a	4-9 axillary nodes (at least one deposit >2mm)		
T4	any size- invasion of local structures	N2b	Metastases in clinically detected internal mammary nodes, with pathologically negative axillary nodes		
T4a	Extension to chest wall beyond pectoralis	N3	Metastases in 10+ nodes		
T4b	Skin involvement	N3a	Metastases in 10 + axillary nodes or infraclavicular nodes		
T4c	Both T4a and T4b	N3b	N1a or N2a with N2b OR N2a with N1b		
T4d	Inflammatory carcinoma	N3c	Metastasis in ipsilateral supraclavicular nodes		

**Categories can be prefixed with 'c' for clinical or radiological assessment, 'p' for pathological assessment and 'y' if the patient has had neoadjuvant treatment. For T stage, if tumour is multifocal, the largest tumour size denotes the T stage with the prefix m for multifocal.*

1.4.5 Breast cancer metastasis

As described, the treatment and prognosis for breast cancer patients alters significantly once the primary tumour has metastasised Estimates suggest 20-30% of those diagnosed with early breast cancer will go on to develop metastases (Wang et al. 2019), which results in significant morbidity and mortality. Patients do not die due to their primary tumour, but as a result of metastatic disease. The process of cancer metastasis has therefore been the subject of significant research efforts examining the metastatic 'cascade' – those stepwise changes that are still not fully understood, in which cells of the primary tumour escape their boundaries and migrate via the lymphatics or bloodstream to other organs, establishing new colonies or secondaries.

One of the initial changes in cancer cells that results in progression to metastasis is the epithelial to mesenchymal transition (EMT), whereby tumour cells become more migratory and invasive. Changes occur in the polarity of the cancer cells and their adherence properties. Epithelial cancer cells usually interact with each other and support cell functions via adhesion molecules such as E- Cadherin, tight junctions, adherent junctions, desmosomes, and gap junctions. When EMT occurs, the cancer cells can be independent of these adhesional interactions and become motile, allowing the cancer cells to migrate and invade(Mittal 2018; Ribatti et al. 2020).

The microenvironment around the tumour cells is also important in promoting EMT. Cells surrounding the cancer includes stromal cells, fibroblasts, and immune response cells. These microenvironment cells produce cytokines such as Transforming Growth Factor Beta (TGFβ), Tumour Necrosis Factor Alpha (TNFα) and growth factors such as Vascular Endothelial Growth Factor (VEGF), Epidermal Growth Factor (EGF) and Fibroblast Growth Factor (FGF)(Mittal 2018; Ribatti et al. 2020).

These cytokines promote upregulation of transcription factors within the cancer cells that control genes vital for EMT. These important transcription factors that increase during EMT include zinc finger transcription factors SNAI1 (Snail) and SNAI2 (Slug), helix loop helix factors (Twist1 and 2) and Zinc finger E-box Binding homeobox proteins ZEB1 and ZEB2(Mittal 2018; Ribatti et al. 2020).

Genetic changes that occur in EMT as a result of these transcription factors include the down regulation of E- Cadherin, resulting in increased motility of the

cancer cells, and upregulation of mesenchymal phenotype genes such as N-Cadherin, Fibronectin, Vimentin, and secreted matrix metalloproteases (MMPs) which favours invasiveness and the ability of the cancer cells to escape their primary tumour environment. After intravasation into lymphatics and blood vessels, tumour cells then circulate and extravasate at distant organ ‘targets (Mittal 2018; Cominetti et al. 2019; Ribatti et al. 2020).

The ‘seed and soil’ hypothesis was first postulated in the 1880s, whereby the tumour cells or ‘seed’ have certain characteristics that mean they will only grow in certain ‘soil’ or target organ environments (Langley and Fidler 2011). Breast cancer does show a preferential metastatic pattern with the main metastatic sites being bone, lung, liver, and brain. In a recent database review of patients with metastatic breast cancer, 40% had bone metastasis only, 11% lung only, 7% liver and 1.5% brain, with 33% displaying metastases to multiple sites (Wang et al. 2019). There is also an association of metastatic patterns with pathological subtypes based on receptor expression. For example, from a large database of 243,896 patients with metastatic breast cancer, Wu et al found that bone metastases were the most common for all subtypes, and very common in ER+/HER2- and ER+/HER2+ subtypes. HER2+ tumours had a higher propensity to brain and liver metastases compared to other subtypes, whilst TNBC tended towards lung metastases (Wu et al. 2017).

Bone metastasis significantly reduce patient’s quality of life due to symptoms of bone pain, hypercalcaemia, pathological fracture, neurological sequalae of spinal metastasis, and they have been shown to decrease patient survival(Zhang et al. 2018). Bone Morphogenetic Proteins (BMPs), as the name suggests, have been known for their role in bone turnover and homeostasis, and indeed, are used clinically in orthopaedic applications to enhance bone fusion and healing. More recently interest has grown in relation to their role in malignancy, in particular bone metastasis.

1.5 Bone morphogenetic proteins

Bone Morphogenetic Proteins were first discovered in the 1960s by Dr Marshall Urist, who found a secreted protein dimer that induced osteogenesis in a rat model (Urist and Strates 1971). This was classed as a member of the TGF-β super family, and since then a total of 15 mammalian BMPs have been identified, which regulate a wide variety of processes beyond bone, including cellular differentiation and stem cell regulation, proliferation, apoptosis and motility, particularly in embryonic development and tissue homeostasis (Nohe et al. 2004; Ye et al. 2009; Davis et al. 2016). Naturally, because of these vital homeostatic roles, dysregulated BMP signalling has been implicated in several cancers, including breast cancer, but often with contradictory results dependant on the BMP and tumour type involved (Alarmo and Kallioniemi 2010; Chi et al. 2019).

1.5.1 BMP signalling, crosstalk, and regulation

When a BMPs binds to BMP receptors, this induces intracellular signalling through two different pathways, canonical BMP signalling and non-canonical BMP signalling, dependent on how the BMP interacts with the receptors.

If the BMP binds to Type I and Type II BMP receptors that are already formed into a complex together, this induces canonical signalling, whereby the receptor complex recruits and phosphorylates Smad proteins (homologues of the Drosophila protein, mothers against decapentaplegic (Mad) and the Caenorhabditis elegans protein Sma). Smads 1,5 and 8, once phosphorylated are activated to translocate to the nucleus, along with Smad-4, which assists the translocation into the nucleus, and this Smad complex then acts as a transcription factor, regulating BMP responsive genes in association with transcriptional co-activators or co-repressors (Figure 1.7)(Bragdon et al. 2011; Brazil et al. 2015). Target genes include the inhibitors of differentiation/DNA-binding proteins (IDs), which regulate cell cycle and cellular differentiation. ID1 has been implicated in invasiveness, EMT and metastasis in breast cancer (Zhao et al. 2020). In non-canonical BMP signalling, the BMP ligand binds a Type I BMP receptor which then recruits the Type II receptor into the complex instead, triggering a Smad-independent pathway, which involves various branches of the mitogen-activated protein kinase (MAPK) pathways: RAS(Rat sarcoma virus guanosine triphosphate enzyme), ERK (Extracellular signal regulated kinase),

PI3K/AKT(phosphatidylinositol 3-kinase and Protein kinase B), P/KC (Protein Kinase C)and Rho-GTPase(Ras homologous guanosine triphosphate enzyme) depending on which BMP ligand and receptors are recruited. MAPK signalling controls cellular growth and apoptosis and has long been implicated in breast cancer progression and resistance to chemotherapy(Haagenson and Wu 2010; Khojasteh Poor et al. 2021).

Figure 1-6 BMP signalling pathways and regulation

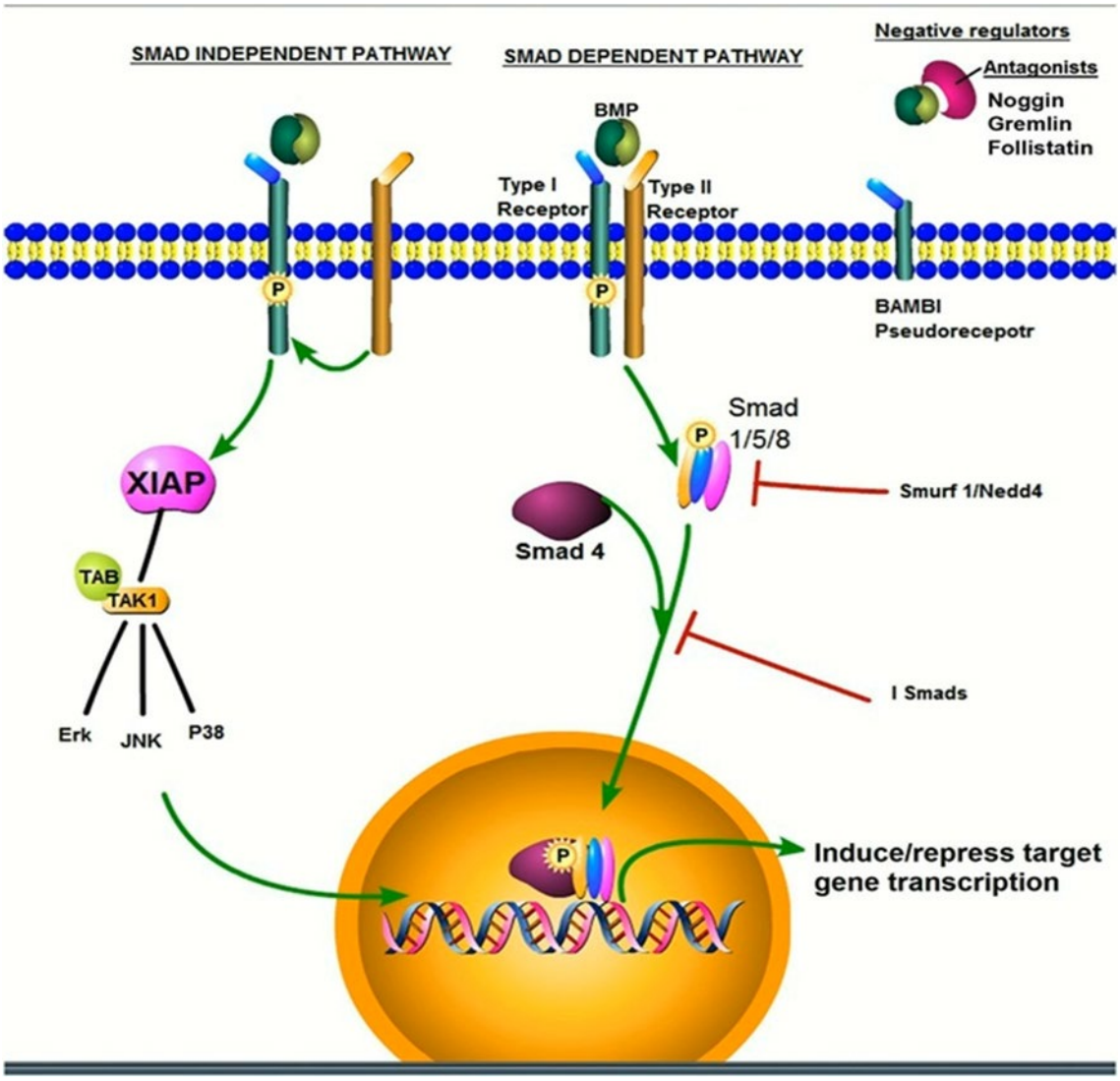

When a BMP ligand binds to a preformed complex of type I and II tyrosine kinase receptors an intracellular signalling cascade is initiated, with phosphorylation of Smad1/5/8 which, with the co factor Smad 4 translocates to the nucleus and interacts with transcription factors to alter target gene expression. This can be negatively regulated intracellularly by Smad specific E3 ubiquitin protein ligase 1(Smurf1), Neuronal precursor cell-expressed developmentally downregulated 4(Nedd4, another E3 ubiquitin ligase), and inhibitory Smads (I Smads – Smad 6 and 7). Other negative regulators include the pseudoreceptor BAMBI and secreted antagonists, which bind BMP ligands and prevent interaction with BMP receptors. When a BMP ligand binds a type I receptor initially and then recruits other receptors into the complex, this results in activation of MAPK(ERK, JNK,P38) pathways via linking proteins such as XIAP(X linked Inhibitor of Apoptosis Protein), TAK1(TGFβ activated kinase 1) and TAB (TAK1 Binding Protein).Image adapted from Zabkiewicz et al, open access permission (Zabkiewicz et al. 2017).

Elements of the canonical and non-canonical BMP pathways are also able to interact with other intracellular signalling pathways, with evidence of signalling crosstalk with other members of the TGF-β super family, such as Transforming Growth Factor β(TGFβ), Epidermal Growth Factor(EGF), hepatocyte growth factor (HGF) and Wnt(Wingless/Integrated) signalling (Schwalbe et al. 2003; Ye et al. 2007; Ye et al. 2008; Guo and Wang 2009; Augeri et al. 2016).

For example, MAPKs induced by other cell signalling pathways, can phosphorylate Smad1/5/8, inhibiting translocation to the nucleus, and can also induce Smad ubiquitination regulatory factor 1 (Smurf1), which is a ligase of Smad 1/5/8, leading to Smad 1/5/8 degradation, with resulting suppression of BMP target genes (Sapkota et al. 2007; Guo and Wang 2009).

As well as MAPKs downregulating canonical BMP signalling, EGF/MAPK signalling have been shown to upregulate BMP gene expression (Clement et al. 1999), and EGF treatment of breast cancer cells *in vitro* upregulates BMP-4 signalling via the Smad pathway (Laulan and St-Pierre 2015).

There is also a reciprocal influence of BMP signalling on MAPK pathways, for example, BMP-2 treatment of mesangial renal cells negatively regulates EGF-induced MAPK activity and gene transcription (Ghosh Choudhury et al. 1999),and BMP-2 induced upregulation of p21 prevents EGF- induced proliferation of MDA-MB-231 breast cancer cells(Ghosh-Choudhury et al. 2000b).

Proliferation and metastasis of SK-BR-3 breast cancer cells is inhibited by BMP-9 decreasing HER2(Human Epidermal Growth Factor Receptor 2) expression and inactivating ERK1/2 and PI3K/AKT signalling pathways (Ren et al. 2014a). In addition, knockdown, or suppression of BMP-6 in the breast cancer cell line MCF-7 induces activation of the ERK pathway and increased proliferation (Lian et al. 2013).

Importantly in breast cancer, there is evidence that crosstalk occurs between BMP signalling and the clinical biomarkers, in particular ER. Oestrogen regulates expression of BMP receptors, which are found more highly expressed in poor prognosis ER positive carcinomas, and ER can also affect the function of BMPs by directly interacting with Smad1 and 5, inhibiting their phosphorylation (Yamamoto et al. 2002; Helms et al. 2005).

Canonical BMP-2 signalling can inhibit oestradiol induced proliferation of ER+ breast cancer cell lines, whilst BMP-6 and -7 have been found to inhibit oestradiol induced p38 MAPK activity (Ghosh-Choudhury et al. 2000a; Takahashi et al. 2008). In breast tumour tissues and cell lines, BMP-6 and -7 expression correlates with the expression of ER (Schwalbe et al. 2003; Ong et al. 2004; Zhang et al. 2005; Alarmo et al. 2006).

In ER+ breast cancer cell lines the BMP-6 promoter region has oestrogen response elements whereby oestrogen activates BMP-6 expression (Zhang et al. 2005). In contrast to several studies demonstrating BMP and ER signalling interactions, evidence for BMP cross talk with HER2 signalling specifically is very limited and is an underexplored area.

Other mechanisms of inhibition and control of BMP signalling (Figure 1.7) are important for both normal tissue development and in cancer pathogenesis. BAMBI (BMP and activin membrane bound inhibitor) is a pseudoreceptor related to type I receptors, which limits BMP function. It is present in breast cancer cell lines and expression has been noted as upregulated in cancers, but as it also abrogates TGF-β signalling, the pro-oncogenic effect may not be specific to BMPs (Wang and Cui 2015; Pawlak and Blobe 2021).

Further control of BMP signalling is via Inhibitory Smads (I-Smads) such as Smad 6 and 7, which are induced by canonical BMP signalling and prevent complex formation between Smad1/5/8 and Smad-4, thus acting as a negative feedback loop on BMP signalling (Figure 1.7) (Miyazono et al. 2010; Bragdon et al. 2011).

Finally, an emerging area of interest in breast cancer pathology is BMP antagonists. In normal cellular function, secreted antagonists block the binding of BMPs to their receptors by directly binding to the BMP ligands (Figure 1.7). There are 11 currently known antagonists, which bind to different BMP ligands, and whilst some may share limited structural similarities, have large diversity(Todd et al. 2020). These antagonists are often BMP transcription target genes, forming an important regulatory feedback loop for normal tissue development (Alarmo and Kallioniemi 2010; Walsh et al. 2010). There have been studies describing a role for BMP antagonists in many different cancers, including colonic, lung, ovarian, brain, liver, kidney, and breast(Walsh et al. 2010; Todd et al. 2020). Gremlin1, a BMP antagonist and the subject of this thesis, has been well characterised in several cancers(Walsh et al. 2010; Todd et al. 2020), and thus is an emerging topic of

interest in breast cancer, which will be described further in following sections (Section 1.6).

1.5.2 BMPs and the bone environment

As essential bone development and homeostasis regulators, BMPs have been of great interest in bone metastases. In normal bone physiology and turnover(Figure 1.7), BMP signalling controls differentiation of mesenchymal stem cells (MSCs) into osteoblast progenitors in conjunction with other cell signalling pathways such as TGF-β, IGF(Insulin like Growth Factor), PTH(Parathyroid Hormone)and Wnt(Wingless/Integrated)(Rahman et al. 2015; Sanchez-Duffhues et al. 2015).The effect of BMPs on MSCs is to upregulate expression of important osteoblast differentiation genes such as runt related transcription factor 2(Runx2), distal-less homeobox5(Dlx5) and Osterix (Osx), that differentiate MSCs into osteoblast progenitor cells. Osteoblast progenitors, driven by Runx2, Dlx5 and Osx. then enter a proliferative phase with maturation into osteoblasts(Capulli et al. 2014; Sanchez-Duffhues et al. 2015).

Mature osteoblasts build bone by secreting type 1 collagen, proteoglycans, osteocalcin, osteonectin and osteopontin to form a non-mineralised bone matrix called osteoid. Osteoid eventually becomes mineralised as tricalcium phosphate crystals form, which is further hydroxylated to hydroxyapatite forming mineralised bone(Capulli et al. 2014; Al-Bari and Al Mamun 2020). Osteoblasts that are encased in mineralised bone matrix can then further differentiate to become osteocytes. Osteocytes sit within the bone matrix; their branched cellular processes extend throughout the bone inside a network of interconnecting canaliculi and orchestrate bone remodelling responses of osteoblasts and osteoclasts to mechanical and biological stimuli(Capulli et al. 2014; Al-Bari and Al Mamun 2020).

Bone remodelling requires resorption of old mineralised bone by osteoclasts. Osteoclasts have a different lineage to osteoblasts and are derived from haemopoietic stem cells Osteocytes and osteoblasts produce two main cytokines, macrophage colony stimulating factor(M-CSF) and Receptor Activator of NF-κB ligand(RANKL)which promote osteoclast differentiation(Huntley et al. 2019). The final stage of osteoclast differentiation is fusing of several osteoclast precursors into a giant multinucleated cell, and activation of this multinucleate cell into a mature bone resorbing osteoclast. RANKL is a vital driver throughout this process, whilst another molecule Osteoprotegerin (OPG), secreted by osteoblasts, acts as a decoy receptor for RANKL, inhibiting osteoclastogenesis and controlling bone resorption(Huntley et al. 2019; Al-Bari and Al Mamun 2020).

Osteoclast maturation and function can be indirectly influenced by BMPs, with certain BMPs shown to enhance osteoclast differentiation by upregulating RANKL and downregulating OPG expression in osteoblasts(Sanchez-Duffhues et al. 2015; Huntley et al. 2019). Evidence for direct effects of BMPs on osteoclast function is still at an early stage, but there are studies demonstrating osteoclasts express BMPs, and that BMP-2 can directly enhance osteoclast survival and proliferation(Huntley et al. 2019; Lademann et al. 2020)

Osteoclasts secrete proteases and acids to dissolve mineralised bone, which results in release of growth factors embedded in the bone, including TGFβ, IGF, platelet derived growth factor (PDGF) and BMPs. This acts in normal homeostasis to activate and recruit osteoblasts to the resorption area, with resulting new bone formation(Huntley et al. 2019; Lademann et al. 2020)(Figure 1.7).

Figure 1-7 Bone Homeostasis

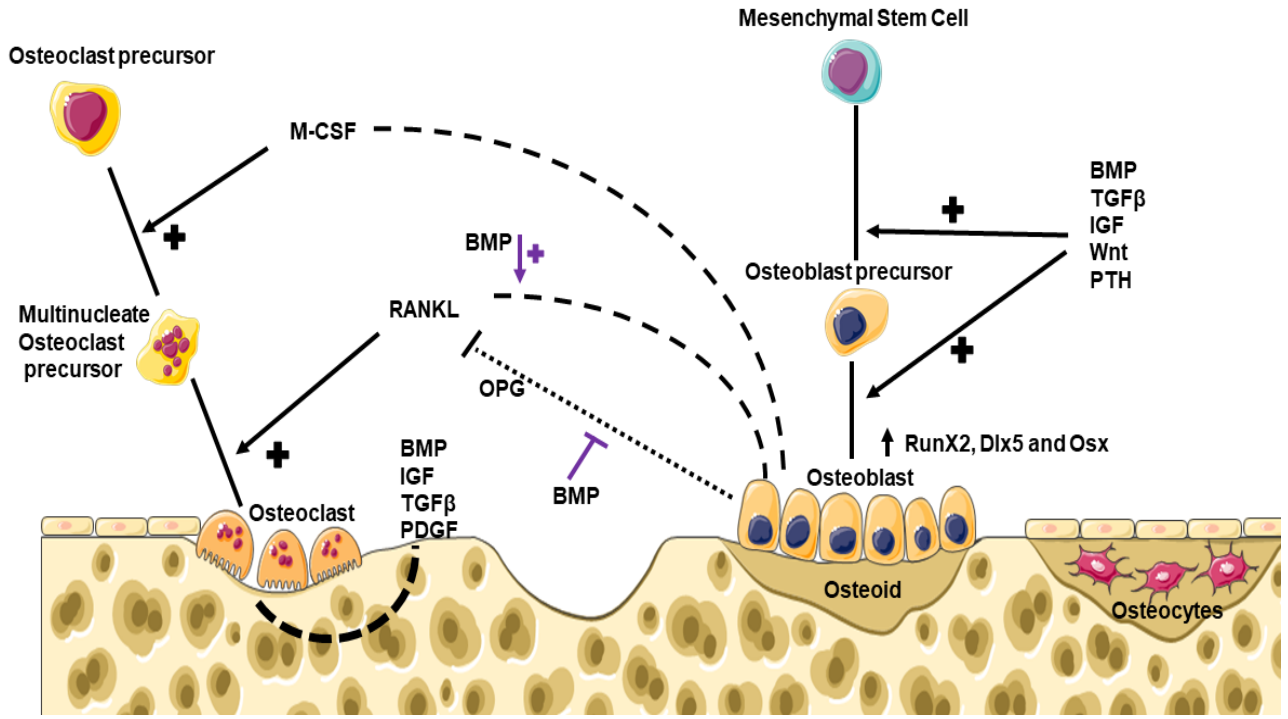

Bone homeostasis requires balance between bone resorbing osteoclasts and new bone formation by osteoblasts. Osteoclasts absorb bone in response to stimuli (e.g., low calcium, low bone loading, hormones, and cytokines), releasing growth factors and molecules such as transforming growth factor-β (TGFβ), insulin-like growth factor (IGF), platelet-derived growth factors (PDGFs) and bone morphogenetic proteins (BMPs). Osteoblast differentiation from mesenchymal stem cells is promoted by BMP, TGFβ, IGF, Parathyroid hormone (PTH) and Wnt (Wingless/Integrated). Osteoblasts lay new bone but to ensure controlled homeostasis, osteoblasts, and osteocytes release RANKL (Receptor activator of nuclear factor kappa-B ligand) and M-CSF (Macrophage colony stimulating factor) which promote osteoclast formation and function. Osteoblasts also secrete Osteoprotegerin (OPG), which is a decoy receptor for RANKL. Secreted BMPs cause osteoblasts to increase RANKL expression and decrease OPG (Purple lines/arrow), indirectly promoting osteoclast function, and therefore has a role in both bone formation and resorption.

Given such a role for BMPs in bone homeostasis, it is logical to consider the role of BMPs in bone metastasis, the leading site of metastasis in breast cancer. Bone metastasis result in either excessive bone formation(osteoblastic) or resorption (osteolytic), or a mixture of these processes. The majority of breast cancer metastasis are purely osteolytic(Li et al. 2014). This is thought to occur due to breast cancer metastatic cells within the bone microenvironment upregulating the secretion of RANKL from osteoblasts, and down regulating OPG, shifting the bone homeostasis towards stimulation of osteoclasts which then resorb bone. The resorption of bone further releases TGFβ, IGF, PDGF (Platelet Derived Growth Factor) and BMPs, which supports the survival of the cancer cells within the metastatic niche(Suvannasankha and Chirgwin 2014; Yardley 2016).

Many studies have demonstrated a pro bone metastatic role for BMP signalling. Breast cancer cells can acquire an osteoblast-like phenotype, by ectopically expressing bone matrix proteins such as bone sialoprotein (BSP), osteopontin (OPN), osteoprotegerin (OPG) and osteoblast-specific cadherins (Ibrahim et al. 2000; Kapoor et al. 2008). Tan and co-workers (Tan et al. 2016) showed that breast cancer cells with induced EMT exhibited an elevated level of these bone-related genes (BRGs) on exposure to BMP-2, and Scimeca et al (Scimeca et al. 2018) identified breast osteoblast like cells with significantly higher expression of BMP-2 and -4, in primary tumours of patients with known bone metastases, which was also found in samples of the bone metastases themselves. They postulate that BMP signalling induces EMT and osteoblast like breast cancer cells, which then predicts the organotropism of metastasis to bone.

Transcriptional pathways induced by BMPs are found to be active in bone metastatic lesions from breast primary tumours *in vivo* (Katsuno et al. 2008) and BMP-7 overexpression is seen in primary tumours associated with bone metastases (Alarmo et al. 2008).In murine 4T1E/M3 mammary cells, which are highly metastatic to bone, expression of BMP-7, BMP Receptors and the BMP signalling pathway is upregulated (Sakai et al. 2012).Knockdown of BMP receptor 1a in breast cancer cells, inhibiting BMP signalling, reduced bone metastatic lesions *in vivo*, thought to be mediated *in vitro* by suppression of production of RANKL by the cancer cells, which is important for osteoclastogenesis (Liu et al. 2018). Conversely, in one study, BMP-9 suppresses the growth of tumour cells in bone through a process that involves downregulation of Connective Tissue Growth

Factor (CTGF), a secreted protein involved in bone homeostasis and associated with promoting bone metastases (Ren et al. 2014b).

Therapeutic strategies to target BMP signalling in bone metastasis are of great potential, as currently, treatment of bone metastasis is palliative and the only treatments for preventing skeletal related events (such as pathological fracture or spinal cord compression) focus on inhibiting osteoclast function. Bisphosphonates are used to increase bone density and reduce fracture risk, as they are selectively taken up by osteoclasts, inactivating the osteoclasts and reducing bone resorption, which helps to reduce the impact of symptoms and bone related events in metastatic breast cancer(Shao and Varamini 2022). Bisphosphonates are utilised in advanced bone metastatic breast cancer, but are also now recommended for post-menopausal women with early breast cancer, as evidence has shown a very small reduction in bone metastasis and breast cancer mortality(absolute risk reduction of 2.2% and 3.3% respectively)(NICE 2017,2018).

Denosumab is a monoclonal antibody against RANKL, reducing osteoclast differentiation. It is recommended (and thought to be more effective than bisphosphonates) for reducing skeletal related events in bone metastatic breast cancer but has not been shown to delay or prevent bone metastasis in early-stage breast cancer(NICE 2018; Coleman et al. 2020).

Antagonism or inhibition of BMP signalling is under explored in this setting however, and thus far of the endogenous BMP antagonists, only Noggin has been seen to be expressed at low levels in osteolytic breast cancer cell lines(Schwaninger et al. 2007). At high expression levels, Noggin has been seen to inhibit the growth, migration, and invasion of breast cancer cell lines, but conversely promoted bone metastasis in a mouse model *in vivo* (Ye et al. 2009; Guo et al. 2012; Tarragona et al. 2012). There is a small molecule inhibitor of the BMP type I receptor, named LDN-193189, which has been shown to prevent prostate tumour growth and osteoblastic bone lesions in a mouse model(Lee et al. 2011). However, in a breast cancer mouse model, treatment with LDN-193189 increased osteolytic bone metastasis(Vollaire et al. 2019).Although well tolerated in mice, thus far, this small molecule BMP inhibitor has not passed toxicology studies for use in humans, but others BMP inhibitors are in development that may well prove useful in the future application of BMP antagonism to breast cancer metastasis(Sanchez-Duffhues et al. 2020).

1.6 BMP antagonist Gremlin1

The BMP antagonist Gremlin1 is becoming well characterised as having a role in several specific pathological conditions, particularly in fibrotic and inflammatory conditions (Figure1.8) where Gremlin1 expression is increased in conjunction with raised TGFβ (Transforming Growth Factor β), a multipotent growth factor that is well known for its role in promoting fibrosis, inflammation and epithelial to mesenchymal transition (EMT)(Dituri et al. 2019; Chung et al. 2021). There is large interplay between BMPs and TGFβ, with BMP signalling inhibiting TGFβ. In fibrosis and inflammation, TGFβ signalling increases Gremlin1 expression, thereby indirectly and reciprocally decreasing BMP activity, which then further allows TGFβ to escape the inhibition of BMP signalling and tip the balance towards highly active TGFβ induced inflammation and fibrosis (Figure 1.8)(Dituri et al. 2019).

Figure 1-8 Main function of Gremlin1 in development and pathogenesis

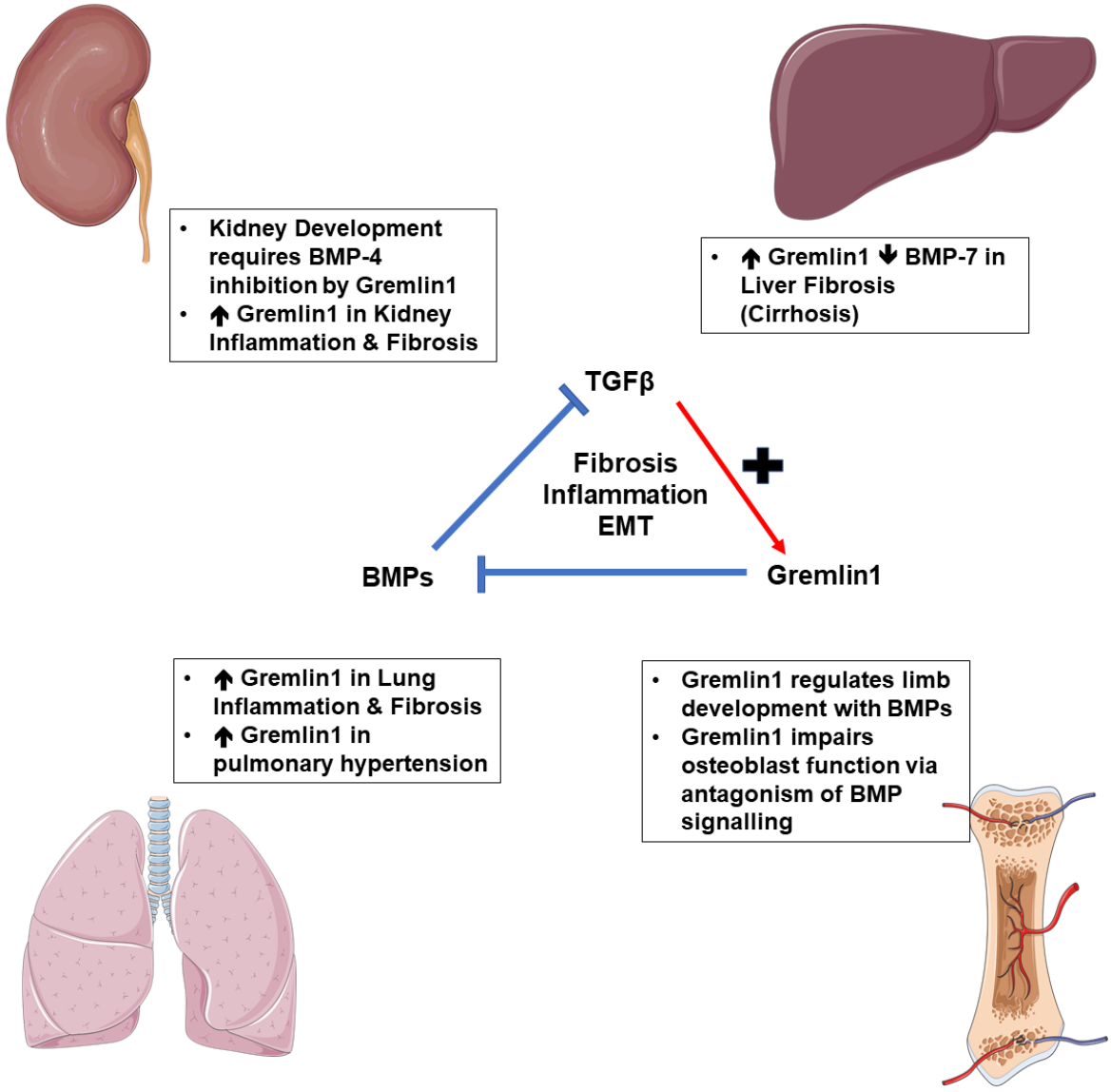

Gremlin1 is important in the development of the limbs and the kidney, whereby in normal circumstances Gremlin1 controls the level of BMP signalling that is regulating developmental processes. For example Mice with GREM1 gene knockout have decreased leg development and kidney abnormalities(Canalis et al. 2012). Most interesting however is the extensive studies that have shown Gremlin1 is prominent in promoting inflammation and fibrosis in the lungs(Costello et al. 2010), kidney(Mezzano et al. 2018) and liver(Yang et al. 2012).Gremlin1 is thought to be a target gene of TGFβ signalling, being upregulated by TGFβ, and in turn, inhibiting or suppressing BMP signalling. This reduction in BMP signalling then further releases inhibition of TGFβ, the increase in which promotes local inflammatory responses via effects on immune cells and release of proinflammatory cytokines, increases fibrosis, and results in cellular changes and transformation of epithelial cells into mor motile, fibroblast type cells(or mesenchymal type cells)otherwise known as epithelial to mesenchymal transition(EMT)(Dituri et al. 2019).

The cellular processes seen in fibrosis and inflammation are also often found in the development and progression of malignancy(Chung et al. 2021). BMPs and their antagonists have been explored in the context of many different cancers, with distinct and sometimes opposing roles depending on which BMP ligand, antagonist, or cancer setting is being studied(Alarmo and Kallioniemi 2010; Walsh et al. 2010; Brazil et al. 2015; Todd et al. 2020).

There has been increasing interest in the role of BMP antagonist Gremlin1 in malignancy, with dysregulated GREM1 seen in colon, gastric, lung, skin, pancreatic and breast cancers(Todd et al. 2020)(See Table 1.6). As described in more detail below, there are changes seen in GREM1 at a genetic level, that may predispose to cancers forming, and then further interplay between TGFβ and Gremlin1 in the cancer associated supporting stromal cells that then promote the step wise progression of cancer cell EMT, invasion, migration and finally metastasis (Figure 1.9). As one of the most well characterised BMP antagonists, Gremlin1 is of great interest in the setting of malignancy, as both a potential risk factor and prognostic marker, and potential therapeutic target(Todd et al. 2020). Indeed, a phase I/II clinical trial of an Anti-Gremlin1 antibody(UCB6114) for the treatment of solid cancers was announced in 2020, but has not yet completed recruitment(Sarker et al. 2022).

Figure 1-9 Gremlin1 and its role in Cancer

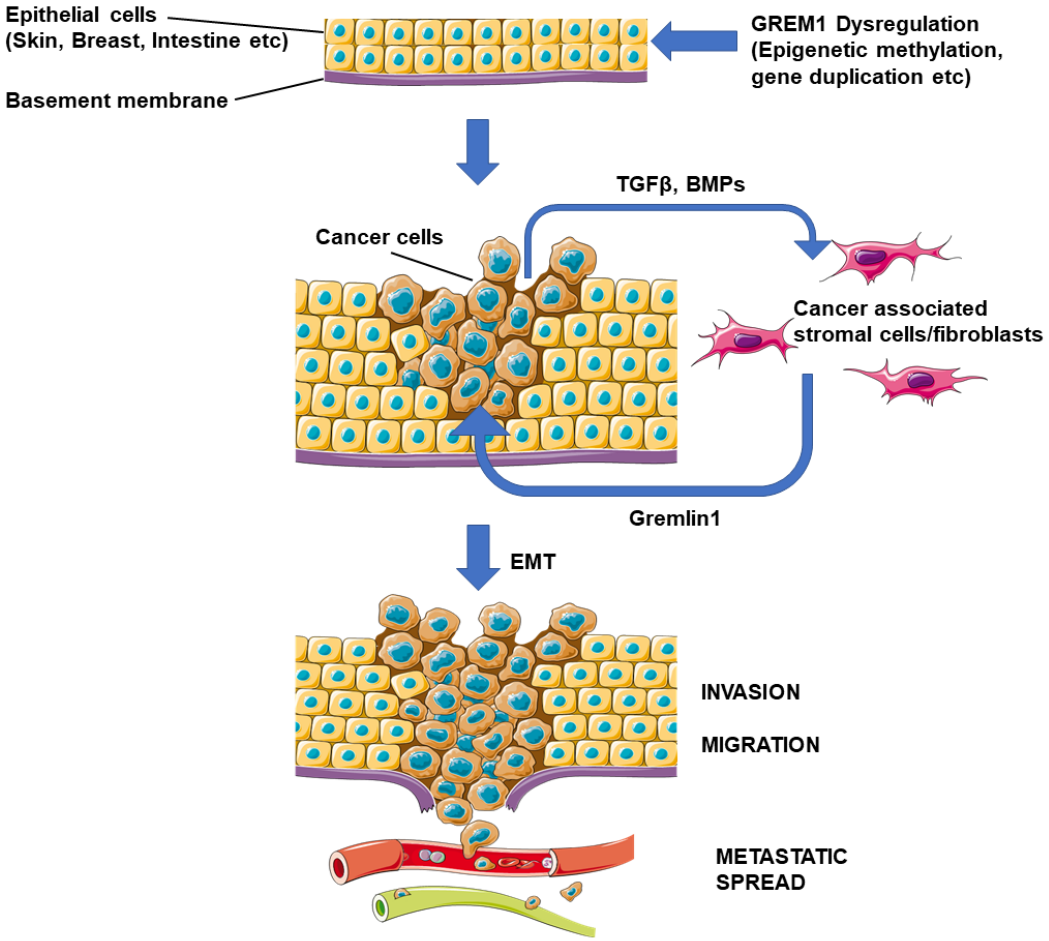

In epithelial cells of organs, GREM1 expression may become dysregulated. For example a GREM1 gene duplication in the epithelial cells of the colon have been shown to be the cause of increased GREM1 expression, and a resultant polyposis syndrome that leads to colorectal cancers(Jaeger et al. 2012).In breast cancers, epigenetic changes such as hypermethylation of the GREM1 gene is found(Li et al. 2015). Once GREM1 expression is dysregulated and cancer cells develop, the interaction with surrounding stromal cells in the tumour microenvironment such as cancer associated fibroblasts and mesenchymal stem cells, promotes the survival and growth of the cancer cells(Karagiannis et al. 2015; Jang et al. 2017). High GREM1 expression has been seen in these stromal cells in several different cancers(Hong et al. 2018; Ren et al. 2019), thought to be induced by cytokines such as Transforming Growth Factor β(TGFβ) and Bone Morphogenetic Proteins (BMPs) from the cancer cells. Gremlin1 then supports the survival of the cancer cells, promoting epithelial to mesenchymal transition(EMT)(Hong et al. 2018; Liu et al. 2019; Ren et al. 2019; Sun et al. 2020), whereby the cancer cells become more invasive and migratory, allowing them to escape the confines of the basement membrane and invade into the lymphatics and blood vessels, a key step in metastatic spread.

1.6.1 Structure

The GREM1 gene is located on Chromosome 15(15q13.3) and encodes a 184 amino acid peptide which is secreted into the extracellular space and can also be cell associated (Church et al. 2015). Originally identified in rat fibroblasts and termed Down regulated by Mos (Drm), it was found to be similar in structure to the tumour suppressor gene DAN (differential screening-selected gene aberrative in neuroblastoma) due to its cysteine knot. Drm in rat fibroblasts was secreted into media, but also seen as cell associated, present on the external surface of cells, as well as in the endoplasmic reticulum and Golgi apparatus. The Xenopus and human homologs later identified, were termed Gremlin1(Topol et al. 2000). Gremlin1 structure is thought to contain an N terminus signalling sequence, a glycosylation site, several phosphorylation sites, and a nuclear localisation signal sequence (Topol et al. 2000; Wordinger et al. 2008). There are two known splice variants-the full protein at 184 a.a (21kDa,28kDa when glycosylated), and one of 143 a.a (16kDa) and a possible third non-functional 42a.a (4.3kDa) protein (Wordinger et al. 2008).

The cysteine knot domain, a cysteine rich region at the C terminus, is common to this group of BMP antagonists, which, although they do not share particularly high sequence identity, share similarity in certain structural characteristics. The variation in number of residues between the bonding cysteines at the C terminus allows further division of BMP antagonists into subgroups, of which, Gremlin1 belongs to the CAN (Cerberus and DAN) subfamily of BMP antagonists(Walsh et al. 2010; Kisonaite et al. 2016).

1.6.2 Functional effect

Kisonaite et al (Kisonaite et al. 2016) have determined the crystal structure of Gremlin1 (Figure 1.10), noting that in solution Gremlin1 forms dimers, and can form oligomers with BMP-2, sequestering it into larger complexes.

Figure 1-10 Structure of Protomer Human Gremlin1

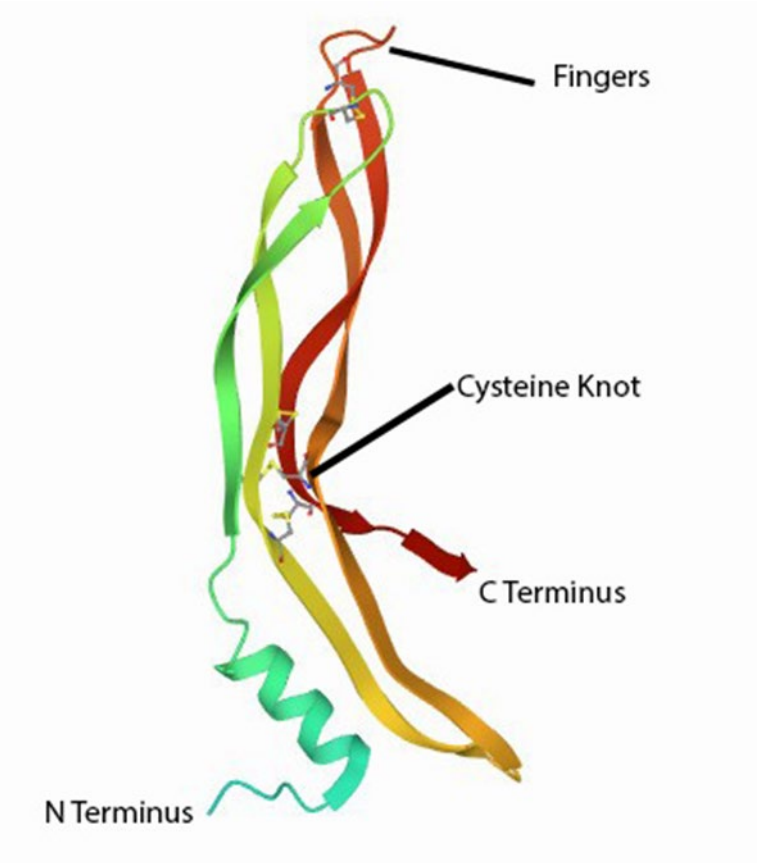

Gremlin 1 typically exists as a non-covalently linked homodimer. Seen here is the protomer, consisting of anti-parallel β strands with a cysteine knot of 6 cysteine residues at the core. The 'fingers' are linked by a disulfide bond. At the N terminus is an α helix thought to assist in dimer stabilisation(Kisonaite et al. 2016). Image adapted from public access protein data bank

They also studied the interaction between Gremlin1 and BMP-2 receptor site mutants. Although mutations in the BMP-2 receptor binding sites reduced binding affinity between Gremlin1 and BMP-2, it did not stop Gremlin1 binding to BMP-2, raising the possibility that Gremlin1 does not only antagonise BMP activity by blocking receptor binding sites. Removing the Gremlin1 N terminus also did not affect Gremlin1's interaction with BMP-2 but did reduce its biological activity in cellular assays compared to full length Gremlin1. It is suggested that this indicates the Gremlin1 N terminus may exert effects outside of those on BMP signalling.

Alborzinia et al fluorescently labelled BMP-2 to examine how BMP-2 is regulated by various antagonists including Gremlin1. They found Gremlin1 increases BMP-2

endocytosis and cellular uptake in HeLa cells, the rate of which is dependent on Gremlin1 concentrations (Alborzinia et al. 2013). As well as BMP-2, Gremlin1 is thought to antagonise BMPs -4 and -7.

Church et al found that Gremlin1 has the strongest affinity for BMP-2, followed by BMP-4 and the weakest affinity with BMP-7 in human renal cells (HK-2). This is consistent with the findings of Kim et al., who found, using an enzyme immunoassay, that Gremlin1 interacts with BMP-2 and -4, but not BMP-7 in A549 lung cancer cells (Kim et al. 2012). Church et al treated renal cells with Gremlin1, followed by treatment with BMP-2 or -4 and examined Smad1/5/8 phosphorylation, and compared this to BMP signalling activity when Gremlin1 was added after BMP treatment rather than before. They conclude that Gremlin1 exerts its antagonism whilst in solution with BMP ligands, rather than when in membrane bound form (Church et al. 2015). However, Gremlin1 can also specifically bind to BMP-4 precursor protein inside cells, which prevents the production and secretion of mature BMP-4 protein and thus down-regulates BMP-4 ligand signalling(Sun et al. 2006).

There is some evidence that Gremlin1 can interact with heparan sulfate. Heparan sulfates are complex carbohydrate chains found in all animal tissues, both bound to cell surface membranes and in the extracellular matrix, that can interact and influence the function of cytokines, growth factors and cell receptors(Li and Kusche-Gullberg 2016). Alborzinia et al found that BMP antagonists such as Gremlin1 and Noggin can increase the endocytic uptake of BMP-2 in a dose concentration dependant manner and may include cooperative binding whereby Gremlin1 interacts with potential coreceptors such as heparan sulfate. Inactivation of heparan sulfates with heparinase III reduced BMP-2 endocytosis in the presence of Noggin, although this was not examined specifically with Gremlin1 (Alborzinia et al. 2013). This interaction of Gremlin1 with heparan sulfate is interesting, as it may mean Gremlin1 can have effects outside of BMP signalling, with other receptors.

More recently Mitola et al reported that *in vitro* Gremlin1 binds to the Vascular Endothelial Growth Factor Receptor 2 (VEGFR2) in a BMP independent function. This receptor and its ligands, vascular endothelial growth factors (VEGF), are important in the formation of new blood vessels(neoangiogenesis). Mitola et al found Gremlin1, via binding with VEGFR2 in vascular endothelial cells, induced neoangiogenesis in chick embryos *in vivo* (Mitola et al. 2010). Chiodelli et al found

that heparan sulfate proteoglycans on vascular endothelial cells, and in extracellular matrix, can bind Gremlin1 and help mediate its engagement and autophosphorylation of the VEGFR2 (Chiodelli et al. 2011). Interestingly, Grillo et al also show that mutated Gremlin1(Gremlin ^{C141A}) which forms monomers as opposed to dimeric form, can bind to VEGFR2, but does not result in receptor dimerisation or internalisation, and resulted in reduced phosphorylated VEGFR2 and reduced sprouting angiogenesis in vascular endothelial cells compared to wild type Gremlin1 dimers (Grillo et al. 2016).

Within these studies it was also seen that Gremlin1 was able to directly bind to the surface of the vascular endothelial cells, via heparan sulfate proteoglycans, and induced angiogenesis in a BMP independent manner, causing phosphorylation of FAK and ERK1/2 (Stabile, Mitola et al. 2007). Interestingly, Grillo et al (Grillo et al. 2016) produced a Gremlin1 monomer, mutated to prevent homodimerization, and this retained BMP antagonist activity, but engaged with VEGFR2 in a non-productive manner, acting as an antagonist instead, suggesting that Gremlin1 needs to be in dimer form to promote neoangiogenesis via VEGFR2.

In contrast, a different research group (Dutton et al. 2019) treated endothelial cells with VEGF(Vascular Endothelial Growth Factor) and /or recombinant Gremlin1, and could not confirm that Gremlin1 induced VEGFR2 phosphorylation or interfered with VEGF induced VEGFR2 signalling. Although contradictory, these studies nevertheless highlight the interesting potential role of Gremlin1 in angiogenesis, an important step in the metastatic cascade, and the fact that Gremlin1 has functions independent of BMP antagonism. Indeed, Kim et al found Gremlin1 can bind to cancer cells independent of VEGFR2, and independent of BMPs, and postulate there may be different motifs in Gremlin1 that have separate functions, which echoes Kisonaite et al's work on Gremlin1 structure, and the importance of the N terminus as having function outside of BMP binding(Kim et al. 2012; Kisonaite et al. 2016).

Functions and cellular effects of Gremlin 1 are summarised in Figure 1.10.

Figure 1-11 Cellular Effects of Gremlin1

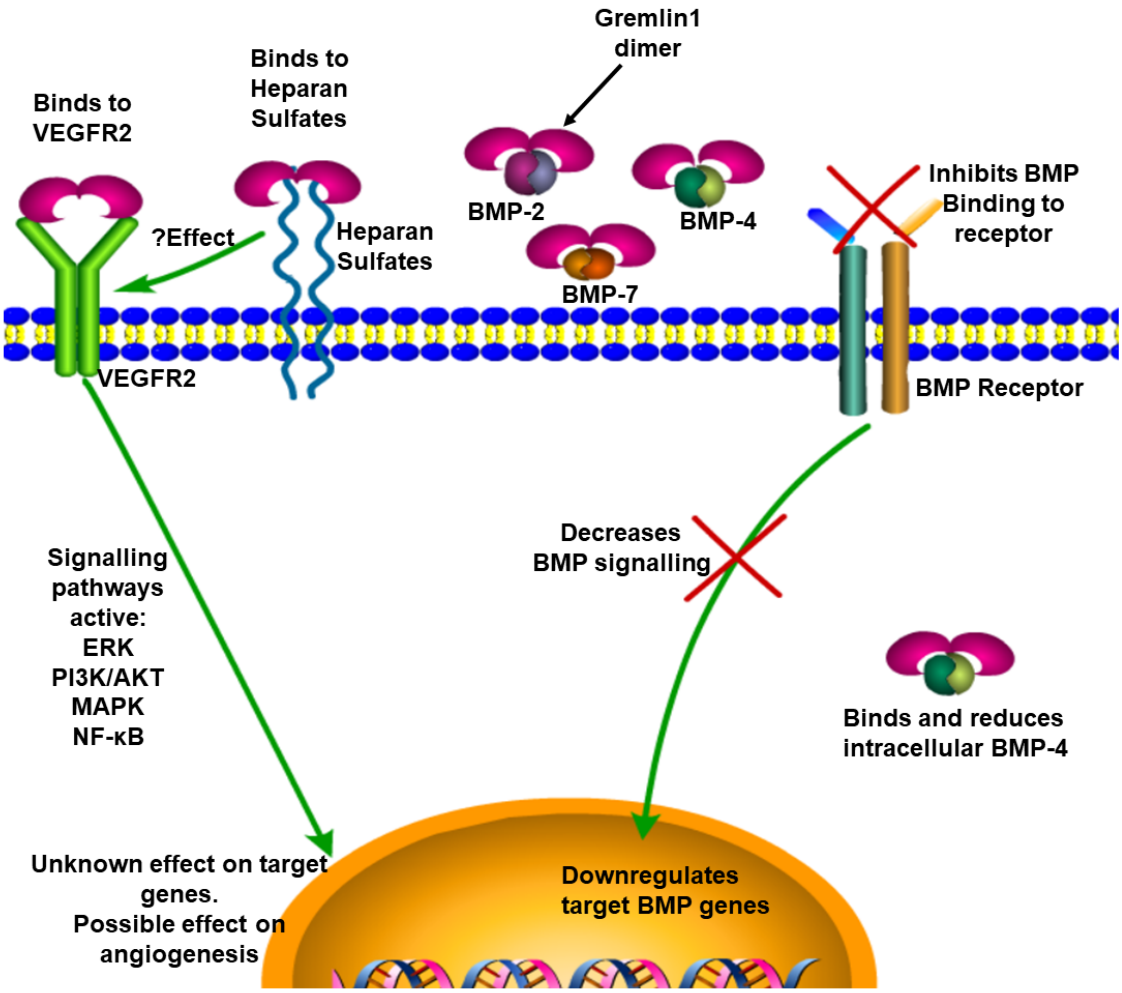

As a secreted antagonist of BMPs-2, -4 and -7, Gremlin1 dimers in the extracellular space bind to these BMPs and prevent their interaction with BMP receptors at the cell membrane, resulting in decreased BMP signalling and down regulation of BMP target genes.Gremlin1 has to be in solution with the BMPs to have its inhibitory effect, rather than Gremlin1 being bound to the cell membrane(Church et al. 2015). Gremlin1 does not seem to antagonise BMPs by directly blocking their BMP receptor binding site, and the mechanism by which it inhibits BMP interaction with its receptor is unknown(Kisonaite et al. 2016). Gremlin1 binds to BMP-2 and -4 with more affinity than BMP-7(Church et al. 2015) and as well as inhibiting BMPs in the extracellular space, Gremlin1 can also bind and inhibit BMP-4s actions intracellularly too(Sun et al. 2006).

In addition to, and independent of BMP antagonism, Gremlin1 has been shown to bind to heparan sulfates, complex carbohydrates that help facilitate the action of cytokines, growth factors and cell membrane receptors. Several studies suggest that Gremlin1 dimers can directly interact with the vascular endothelial growth factor receptor 2(VEGFR2),which may be further facilitated by heparan sulfates, activating signalling pathways in vascular endothelial cells and promoting new blood vessel formation (neoangiogenesis)(Mitola et al. 2010; Chiodelli et al. 2011; Grillo et al. 2016).

1.7 The role of Gremlin1 in development and pathogenesis

1.7.1 Bone

As BMPs regulate bone development and homeostasis, it is logical to postulate that BMP antagonists such as Gremlin1 may also have a role in limb and bone development or pathogenesis. Gremlin1, BMPs, SHH (Sonic Hedgehog) and FGF (Fibroblast Growth Factor) 4 and 8 all tightly regulate limb patterning, as has been demonstrated in chick and mouse embryos (Khokha et al. 2003; Verheyden and Sun 2008). Grem1 null mice, in those that survive, demonstrate abnormal limb development compared to control mice, being reduced in femoral length. These mice also demonstrate an osteopenia, although this is transient, and subsequent post-natal bone formation and mineralisation reverses the osteopenia (Canalis et al. 2012). Indeed, conditional GREM1 inactivation in matured osteoblasts results in increased bone volume (Gazzerro et al. 2007). It is thought these effects occur through the antagonism of BMPs by Gremlin1, as in bone marrow stromal cells Gremlin1 reduced BMP/Smad signalling and impaired osteoblast numbers and function (Gazzerro et al. 2005). The role of Gremlin1 in bone metastasis has yet to be explored.

1.7.2 Kidney

Gremlin1 null transgenic mice display abnormalities in nephric development (Michos et al. 2004; Canalis et al. 2012). As kidneys develop, Gremlin1 and BMP-4 interact within the metanephric mesenchyme to control ureteric bud formation, and renal epithelial branching. It is the antagonism of BMP signalling that enables this process, as when Gremlin1 is deleted, leaving BMP-4 unopposed, renal agenesis occurs, which can be rescued by deletion of one BMP-4 allele. The implication being that it is the decrease in BMP-4, facilitated by Gremlin1, that is required for kidney development (Michos et al. 2007). GREM1 mRNA levels are seen to be increased in several nephropathies, in particular, injury to renal tubular epithelial cells found in diabetic nephropathy, acute kidney injury, glomerulonephritis and chronic allograft nephropathy (Walsh et al. 2008; Rodrigues-Diez et al. 2012; Droguett et al. 2014; Lavoz et al. 2018; Mezzano et al. 2018; Droguett et al. 2019). When GREM1 was targeted for knockdown in murine renal tubular epithelial cells, there was reduced fibrotic response and less renal damage histologically in response to a folic acid induced renal injury (Church et al.

2017). Conversely, an overexpression of GREM1 in tubular renal epithelial cells increased murine susceptibility to renal damage compared to control (Droguett et al. 2014). TGFβ is heavily involved in driving the cellular processes underpinning nephropathy, with Walsh et al reporting that TGFβ induced increased Gremlin1 in human kidney epithelial cells, as well as increased Gremlin1 expression at mRNA and protein levels in diabetic nephropathy patient renal biopsies, compared to healthy control tissue (Walsh et al. 2008). In high glucose induced renal damage in a mouse model, Gremlin1 protein expression increased, particularly in the renal glomeruli, interstitium and tubules. This expression was attenuated by application of GREM1 SiRNA to the mice, which also improved the mouse creatinine levels and extent of proteinuria (Zhang et al. 2010). Further to this, Lavoz et al injected recombinant murine Gremlin 1 into mouse kidneys *in vivo* and demonstrated, compared to control, that VEGFR2 and NF-κB pathways were activated, with concomitant increase in infiltrating inflammatory cells and renal expression of pro inflammatory chemokines. This effect was abrogated by treatment with a VEGFR2 specific kinase inhibitor(Lavoz et al. 2015).

1.7.3 Lung

As in kidney fibrosis, the balance of TGFβ and BMP signalling has been implicated in pulmonary fibrosis, inflammation and hypertension (Costello et al. 2010). It appears that attenuation of BMP signalling and the concomitant increase in TGFβ, is the driver for these processes. GREM1 is upregulated in idiopathic pulmonary fibrosis in humans, and in a murine model of pulmonary fibrosis (Myllärniemi et al. 2008; Murphy et al. 2016). At the genetic level, Heron et al examined patients with sarcoidosis and those that were homozygous for a particular GREM1 allele with a specific single nucleotide polymorphism, had greater disposition to pulmonary fibrosis (Heron, van Moorsel et al. 2011).

In a study of pulmonary fibrosis, an adenovirus encoding GREM1, or empty control was administered to the respiratory tract of rats. The overexpression of GREM1 caused transient reduction in Smad1/5/8 phosphorylation, alveolar epithelial injury, lung fibrosis and accumulation of myofibroblasts (Farkas et al. 2011). TGF-β induced epithelial to mesenchymal transition (EMT) in lung epithelial cells, contributed to fibrosis and was associated with an increase in GREM1 mRNA

expression. Overexpression of GREM1 in lung epithelial cells enhanced TGF-β induced EMT (Koli et al. 2006).

Graham et al postulate that TGFβ signalling decreases expression of miR-27b, with concomitant increase in Gremlin1 expression in pulmonary cells. miR-27b was found to directly bind to GREM1 3'UTR reducing and regulating GREM1 mRNA levels. This suggests TGFβ regulates Gremlin1 via miR-27b. Inhibiting miR-27b ,or adding recombinant Gremlin1 to pulmonary cells, enhanced the expression of genes known to promote fibrosis (Graham et al. 2014).

Upregulated Gremlin1 has been seen in the lungs of patients with pulmonary hypertension and selectively within murine lung under hypoxic conditions (Costello et al. 2008; Cahill et al. 2012). It is also elevated in the peripheral circulation of pulmonary hypertension patients and correlated with patient functional status and survival (Wellbrock et al. 2015). In a mouse model of chronic hypoxia and pulmonary arterial hypertension, GREM1 mRNA was upregulated in lung and right ventricular tissue compared to normoxic control, while an anti-Gremlin1 antibody reduced pulmonary vascular remodelling and right ventricular hypertrophy compared to control (Ciuclan et al. 2013).

1.7.4 Liver

In a mouse model of hepatic fibrosis, administration of BMP-7 improved liver function and suppressed expression of TGF-β1, interestingly, expression of Gremlin1 was increased (Yang et al. 2012). A further study in rats, of induced hepatic fibrosis, showed elevated TGF-β1 and Gremlin1 expression and lowered BMP-7 expression in fibrotic livers compared to control (Zhao et al. 2014). Increased Gremlin1 expression has also been seen in fully transdifferentiated hepatic stellate cells (myofibroblasts) (Boers et al. 2006). Although the mechanism for Gremlin1 involvement is yet to be elucidated, whether because of TGFβ signalling in fibrosis, or as a negative feedback loop from BMP-7 signalling, it has been proposed as a potential biomarker for hepatic fibrosis.

mRNA expression of Gremlin1 and BMP-7 was examined in 35 cases each of chronic hepatitis, cirrhosis (the end stage of hepatic fibrosis) and hepatocellular carcinoma (HCC). Gremlin1 was seen at higher levels in cirrhosis and HCC compared to hepatitis. Gremlin1 expression was positively correlated with BMP-7

expression in the cirrhosis group, further supporting the interplay of Gremlin1 and BMP-7 in fibrotic processes (Guimei et al. 2012).

1.8 The role of Gremlin1 in cancer

The initiation and progression of cancer is intrinsically linked to the microenvironment with which the cancer cells interact, this includes stromal cells such as fibroblasts, immune cells, vasculature, and extracellular matrix components such as collagens (Chandler et al. 2019).

With the evidence that Gremlin1 may promote pro-fibrotic environments, including TGF-β signalling, elements of vascular remodelling and interact in angiogenesis, via influences on VEGF and FGF signalling, it is no surprise that there are an increasing number of studies examining the role of Gremlin1 in cancers.

In an early study of Gremlin1/Drm in tumourigenesis, overexpression of Drm in Daoy and Saos-2 cells inhibited tumourigenesis, reduced phosphorylated p42/44 MAPK and increased protein levels of $p21^{Cip1}$, which arrested cell cycle and suppressed cellular transformation (Chen et al. 2002). Namkoong et al published the mRNA expression levels of GREM-1 and Gremlin1 protein levels, in a variety of human normal and cancer tissues. They found the Gremlin1 homolog PIG-2 expressed in human muscle, colon, and small intestine. In cell lines it was strongly expressed in the lung cancer cells A549, and highly expressed in lung cancers compared to normal lung tissue. It was also upregulated in ovarian, kidney and breast cancers in comparison to normal tissues (Namkoong et al. 2006). Further to this, others have further examined Gremlin1 effects in human cancers.

When lung cancer cells A549 are treated with recombinant Gremlin1, cell morphology becomes fibroblast like and E-Cadherin expression decreases. When A549 cells overexpress GREM1, cells become more migratory and proliferative *in vitro* compared to control. These effects were abrogated when cells were treated with Gremlin1 neutralising antibody. GREM1 overexpressing A549 cells also grew to larger volumes in an *in vivo* xenograft mouse model (Kim et al. 2012). Gremlin1 was also seen to be more highly expressed in terms of both mRNA and protein, in non-small cell lung cancer tissues compared to normal lung tissue samples and was more highly expressed in a gefitinib resistant lung cancer cell line compared to control. Subsequent GREM1 silencing with siRNA resulted in an increased gefitinib induced apoptosis (Yin et al. 2016). Gremlin1 was highly expressed in 8

malignant mesothelioma samples, compared to paired normal pleural tissue, and in 4 of 6 malignant mesothelioma cell lines. When Gremlin1 was knocked down in those highly expressing cell lines (H290 and H2450) proliferation was significantly reduced (Wang et al. 2012). In another study using 3D culture, low GREM1 expressing mesothelioma cells did not show as much proliferation, branching, and invasion, as high GREM1 expressing cells. GREM1 silencing in these highly expressing, invasive cells abrogated the invasiveness and branching, and reduced expression markers of EMT such as SNAI2 (Slug) (Yin et al. 2017).

Honma et al studied Gremlin1 using IHC in 159 gastric cancers (GC). This study showed that 63% of tumours were negative for Gremlin1 staining, and these cases had more advanced pathological features and a poorer survival rate, suggesting in gastric cancers, that Gremlin1 may be a positive prognostic marker (Honma et al. 2018). This is supported by a publication in the same year by Yamasaki et al who examined 232 gastric cancer tumours and found around 50% were Gremlin1 negative and, those that were, had poor pathological features and significantly worse survival than the Gremlin1 positive tumour patients. Unlike the study by Honma, multivariate analysis in this cohort did not identify Gremlin as an independent prognostic marker (Yamasaki et al. 2018). In addition, a recent study by Sun et al (Sun et al. 2020), with a much larger patient cohort, suggested that GREM1 is upregulated in GC, and *in vitro* GREM1 overexpression in GC cell lines resulted in increased proliferation, migration, and expression of EMT related genes.

In human oesophageal squamous cell carcinomas (OSCCs), as studied by Hong et al, GREM1 overexpression was seen. When GREM1 was silenced in mesenchymal stromal cells (MSCs), oesophageal carcinoma cell lines displayed less proliferation and invasion. This suggests BMP signalling mediated by surrounding stromal cells is tumour suppressive in OSCCs and Gremlin1 is tumour promoting(Hong et al. 2018) .

In basal cell carcinomas (BCCs,) Kim et al found GREM1 expression mainly in activated cancer associated myofibroblasts at the tumoral-stromal interface, suggesting that GREM1 expression can be a marker for activated myofibroblasts in the cancer stroma or in scar tissue (Kim et al. 2017). This is supported by an earlier work from Sneddon et al, who found Gremlin1 highly expressed in the stroma of human BCC, and the application of Gremlin1 to cultured BCC cells *in vitro* promoted their proliferation (Sneddon et al. 2006). In contrast, in the *in vitro*

microenvironment for SK-MEL-28 melanoma cells, Gremlin1 secreted by embryonic stem cells inhibited SK-MEL-28 proliferation. On Gremlin1 knockdown in the microenvironment, the melanoma cells increased proliferation and anchorage independent growth (Kim et al. 2011).

In colorectal cancer (CRC), expression of Gremlin1 has been associated with cancer associated fibroblasts at tumour invasion fronts, promoting EMT within colorectal cancer cells (Karagiannis et al. 2015). Higher Gremlin1 expression has been shown to differentiate colorectal carcinoma from adenoma (Galamb et al. 2008) and, indeed, in corroboration with higher levels of BMP antagonists, other studies have shown that although BMP signalling is active in colonic adenoma, it becomes suppressed in colorectal carcinoma, as Gremlin1 levels rise (Kodach et al. 2008a; Kodach et al. 2008b; Karagiannis et al. 2015; Karagiannis et al. 2016). When GREM1 is silenced in colorectal cancer cells, cellular proliferation, migration and EMT is reduced (Liu et al. 2019). Patients with hereditary mixed polyposis syndrome have been found to have a duplication upstream of the GREM1 locus, associated with increased Gremlin1 expression particularly within the colonic epithelial cells, whereas in those without this polyposis syndrome, Gremlin1 is predominantly found in subepithelial myofibroblasts (Jaeger et al. 2012). The increased colonic epithelial Gremlin1 expression has been found, in a mouse model, to disrupt normal gradients of morphogens such as BMPs, and results in certain cells re-acquiring ’stem’ like traits as a precursor to intestinal neoplasia (Davis et al. 2015). In contrast to the above conclusions that Gremlin1 promotes colorectal carcinogenesis, Pelli et al (Pelli et al. 2016) examined 148 CRCs and found high GREM1 expression associated with better clinicopathological features and improved survival outcomes. While Jang et al found high stromal GREM1 expression correlated with low lymphovascular invasion and better clinical outcomes (Jang et al. 2017).

Converse to most findings, Gremlin1 expression in pancreatic neuroendocrine tumours was associated with favourable features, such as high micro vessel density, well differentiated tumours and improved progression free survival, compared to those tumours with low Gremlin1 staining (Chen et al. 2013). The association of Gremlin1 expression with tumour microvasculature and angiogenesis was also examined in a study of pituitary adenomas, whereby Gremlin1 was seen to co-localise with tumour vasculature and expression was strongly correlated with increased micro vessel density (Koketsu et al. 2015).

1.8.1 Gremlin1 in breast cancer

With regards to Gremlin1 in breast cancer, up until very recently, there had been no published literature and the role of Gremlin1 in breast cancer was relatively unexplored. Li et al performed sequencing analysis of 48 genes in 180 breast cancer patients compared to paired normal tissues. It was determined that GREM1 was hypermethylated in breast cancers, as one of 13 hypermethylated genes proposed for candidate biomarkers in predicting breast cancer (Li et al. 2015). In the final months of this doctoral work, there were two published studies regarding Gremlin1 in breast cancer. Firstly, Ren et al (Ren et al. 2019) determined that GREM1 was highly expressed in breast cancer stroma, and that this correlated with poor prognosis. They also found that when conditioned media was collected from breast cancer cells, GREM1 mRNA expression was increased in cancer associated fibroblasts (CAFs), and treatment of CAFs with TGFβ-3 promoted GREM1 mRNA expression. The GREM1 expression inducing effect of the conditioned medium was abrogated by the addition of a TGFβ-neutralising antibody. GREM1 knockdown in CAFs decreased expression of TGFβ signalling components and the ability of CAFs to remodel collagen. This interestingly fits with some of the above studies, regarding the interaction of Gremlin1 and TGFβ in fibrosis.

In the same study, administration of recombinant Gremlin1, or GREM1 overexpression in immortalised MCF10A breast cancer cells, resulted in higher 'stemness' markers such as CD44. In GREM1 overexpressing MDA MB 231 cells, markers of EMT increased at the mRNA level. These cells were then injected into embryonic zebrafish and demonstrated increased extravasation (as a reflection of invasive capacity), compared to non-GREM1 overexpressing control cells. In 3D co-culture, CAFs cultured with MCF-7 or MDA MB 231 cells increased invasiveness, but this invasion was reduced when co-cultured with GREM1 knockdown CAFs or *in vivo* when injected into embryonic zebrafish.

Publishing around the same time, Neckmann et al (Neckmann et al. 2019) (who share one author with Ren et al) developed a murine model, whereby the metastatic 66c14 murine cell line, and non-metastatic 67NR murine cell line were compared in terms of secretome, both *in vitro* and when grown as tumours, in BALB/c nude mice. They found GREM1 mRNA more highly expressed in 66c14 cells and higher Gremlin1 protein in 66c14 on Western blot, as well as higher secretion of Gremlin1 by these cells compared to 67NR. GREM1 was upregulated

in 66c14 cells on RNA-seq, as were other extra cellular and intracellular BMP antagonists. Interestingly stem cell marker CD44 was low in 66c14 cells compared to 67NR, the opposite to what might be expected in a more metastatic line with more BMP antagonism. Other pathways active in stem cell maintenance were, however, upregulated in 66c14 cells. In identifying a possible link between more metastatic breast cancer and high Gremlin1, the authors generated GREM1 depleted 66c14 cells. These cells displayed no difference in growth or colony formation *in vitro* and could not form tumours in immunocompetent mice. With immunocompromised mice, the GREM1 depleted cells formed smaller primary tumours and did not metastasise to the lungs compared to control 66c14 cells. The GREM1 depleted cells also were unable to penetrate a monolayer of vascular endothelial cells as an *in vitro* marker of extravasation, and an initial metastatic step, although statistical significance figures were not given, and the effect was slight.

These initial works suggest that Gremlin1 may be a promoter of breast cancer, either directly via epigenetic changes such as hypermethylation of GREM1, or indirectly via a role in the tumour microenvironment and promotion of EMT.

Table 1-6 Summary of Gremlin1 effects in Development and Disease

Tissue	Gremlin 1 effect on development/pathology	Mediating pathways	Reference
Bone	GREM1 required for normal limb development. Impairs mature osteoblast function	Embryological FGF and BMP	(Gazzerro et al. 2007; Verheyden and Sun 2008)
Kidney	Required for ureteric bud and epithelial branching	Gremlin1 antagonism of BMP-4	(Michos et al. 2007)
	Increased GREM1 in nephropathy. Gremlin 1 induces renal damage and inflammation	TGFβ induced GREM1 increase. VEGFR2 and NF – KB mediated inflammation	(Walsh et al. 2008; Lavoz et al. 2015)
Lung	GREM1 increased in pulmonary fibrosis and pulmonary hypertension	Gremlin1 attenuates BMP signalling, allowing increased TGFβ mediated EMT/fibrosis	(Koli et al. 2006; Costello et al. 2010; Farkas et al. 2011)
	Elevated GREM1 in Lung cancer tissue and cell lines. Confers Gefitinib resistance in vitro	Unknown ? EGFR	(Yin et al. 2016)
Liver	Elevated GREM1 in fibrosis, cirrhosis, and HCC	Increased TGFβ and reduced BMP signalling	(Guimei et al. 2012; Yang et al. 2012; Zhao et al. 2014)
Stomach	Gastric cancer associated with high GREM1 expression	Unknown	(Sun et al. 2020)
Colon	Hereditary Polyposis with GREM1 duplication GREM1 high expression in CRC cells promotes EMT in vitro.	Postulated BMP antagonism and disruption of normal morphogen gradients	(Kodach et al. 2008a; Jaeger et al. 2012; Davis et al. 2015; Karagiannis et al. 2016)
Pancreas	Neuroendocrine tumours with high Gremlin 1 = better clinical outcomes	Unknown but postulated Gremlin 1 alters micro vessel density	(Chen et al. 2013)
Breast	GREM1 hypermethylated in breast cancer High GREM1 in metastatic murine model	Unknown	(Li et al. 2015; Neckmann et al. 2019)
Microenvironment stromal cells	GREM1 in cancer stroma increased oesophageal cancer proliferation. High GREM1 in stroma of Basal Cell carcinoma, High GREM1 in stem cells inhibits melanoma. High GREM1 in colonic stroma = better clinical outcome in CRC High GREM1 in cancer associated fibroblasts at invasion front in CRC. High GREM1 in breast cancer stroma correlates with poor prognosis	Unknown Suggestion TGFβ from breast cancer cells promotes GREM1 in CAFs.	(Kim et al. 2011; Karagiannis et al. 2015; Jang et al. 2017; Kim et al. 2017; Hong et al. 2018; Ren et al. 2019)

1.9 Overview and Conclusion

Outcomes for early-stage breast cancer have improved vastly over the last four decades. Methods of prognostication and treatment have evolved through the genomic era, with a recognition that breast cancer is an umbrella term for a heterogeneous collection of breast malignancies that have differing molecular profiles, displaying phenotypes that respond differently to treatment. This has driven huge developments in 'personalised' medicine, and improvements in survival, but the disparity in morbidity and mortality for those with, or at risk of developing metastatic disease remains significant.

Given the propensity of breast cancer to metastasise to bone, and their significant role in both bone homeostasis and cancers, the role of BMPs in breast cancer has become an increasingly studied area. The interaction of BMP signalling with vital clinical biomarkers, such as the oestrogen receptor signalling pathway, has further highlighted the potential for BMPs in this field, and in more recent years efforts have been made to develop therapeutics targeting elements of the BMP pathways, and in particular, antagonism of BMP actions. As an example, Dalantercept is a ligand trap protein, targeting BMP receptors and preventing their interaction with BMP-9 and -10 which results in inhibition of BMP regulated angiogenesis. Although Phase II Clinical trials for renal cell carcinoma did not show any improvement in survival, further trials in other cancers and with other BMP receptor inhibiting agents are awaited (Sanchez-Duffhues et al. 2020). BMP antagonism and its role in breast cancer progression and metastasis, particularly to bone, is poorly understood but is evidently an area of both research and therapeutic interest.

Gremlin1 is a BMP antagonist that has roles in fibrosis, inflammation, angiogenesis, and malignancy, as well as bone development. It is therefore the most prominent BMP antagonist with potential to further understand and target progression and metastasis of breast cancer. Gremlin1 is known to interact with other receptors and pathways independent of BMP signalling, such as Vascular Endothelial Growth Factor Receptor 2, and this has additional implications for what its role may be within the different subtypes of breast cancers, defined and treated by their clinical biomarkers and receptors. Whilst initial studies have suggested Gremlin1 promotes breast cancer, this will further explore the role of BMP antagonist Gremlin1 with specific focus on HER2+ breast cancer progression and metastasis, which has yet to be examined.

1.10 Thesis Hypothesis and Aims

Given the influence of BMP signalling in breast cancer progression and metastasis, particularly in the bone environment as outlined in this chapter, and the interaction of BMP signalling with other signalling pathways pertinent to subtypes of breast cancers such as ER and EGFR, we hypothesise that the BMP antagonist Gremlin1 is also able to affect breast cancer progression and metastasis and may influence cellular functions differently depending on breast cancer subtype, particularly in HER2+ breast cancers.

The aims are as follows:

- To examine comparative expression of GREM1/Gremlin1 in breast cancer and normal breast tissues in a patient cohort utilising qPCR and immunohistochemistry, and collating publicly available expression data, with comparison of expression with clinical pathological information.
- To determine an overview GREM1 expression in breast cancer cell lines and then manipulate GREM1 in these cell lines, to examine *in vitro* effects on cellular functions such as proliferation, migration, and invasion in different representative breast cancer subtypes.
- To further analyse the relationship between Gremlin1 and the different molecular subtypes of breast cancer using a tissue microarray, with subsequent focus on Gremlin 1 in HER2 positive breast cancers. In addition, utilising GREM1 overexpression in HER2+ breast cancer cells to examine effects on cellular functions and markers of EMT.
- To examine potential mechanisms of the relationship between HER2 and Gremlin1 in breast cancer cells, utilising HER2 specific small molecule inhibitors and HER2 knockdown, to examine the effect on Gremlin 1 expression. Recombinant Gremlin 1 treatment of HER2+ cells will also allow examination of the effect on HER2 and intracellular signalling cascades.
- The effect of GREM1 overexpression in HER2+ cancer cells on metastases of breast cancer will be examined *in vitro,* with models of the bone environment, *in vivo* utilising a mouse model of both primary tumour growth within the murine mammary fat pad and of metastases via an intracardiac injection model.

2 General Methods and Materials

2.1 General Materials and Solutions

2.1.1 Materials and Solutions for Cell Culture

0.05M Ethylene Diaminetetraacetic Acid (EDTA) trypsin

A stock solution of 10x trypsin-EDTA solution was purchased from Sigma-Aldrich, Inc. (Dorset, UK) and was diluted to a working concentration of 1x with sterile water. This solution was aliquoted into 25ml universal containers and stored at -20°C until required.

Antibiotics

An antibiotic solution for use in cell culture was prepared by dissolving 3.3g penicillin, 5g streptomycin and 12.5mg Amphotericin B in dimethyl sulfoxide (DMSO) in 500ml Balanced Salt Solution (BSS). The solution was filtered prior to use and stored at -20°C. One 5ml aliquot of antibiotics was added to each 500ml media bottle required prior to use.

Foetal Calf Serum (FCS)

FCS was purchased from Sigma-Aldrich, Inc. (Dorset, UK) and aliquoted into 25ml aliquots in universal containers and stored at -20°C until required. Two 25ml aliquots of FCS were added to each 500ml media bottle required, giving a final volume of 10% FCS for standard cell culture. FCS from the same batch was used throughout all experimental work.

Phosphate Buffered Saline (PBS)

A stock solution of 10x phosphate buffered saline (P5943) was purchased from Sigma-Aldrich, Inc. (Dorset, UK), autoclaved and diluted in sterile water to a concentration of 1x PBS. This was aliquoted into 25ml sterile universal containers and stored at room temperature until required.

2.1.2 Primers

Primers were designed in Primer BLAST (National Centre for Biotechnology Information, Bethesda, USA) and synthesised by Sigma (Sigma-Aldrich, Inc., Dorset, UK). All primers used have been previously tested within the laboratory for efficacy. Primer sequences are outlined in Table 2.1.

Table 2-1 Table of Primers (Z-Sequence in bold)

Primer target	Application	Primer	Sequence 5' – 3'
GREM1	PCR/qPCR	Forward (SGF1)	TGCTGGAGTCCAGCCAAGA
GREM1	PCR/qPCR	Reverse (SGR1)	GCACCAGTCTCGCTTCAGGTA
BMP-2	PCR/qPCR	Forward (SGF1)	TGTATCGCAGGCACTCAGGTCA
BMP-2	PCR/qPCR	Reverse (SGR1)	CCACTCGTTTCTGGTAGTTCTTC
BMP-4	PCR/qPCR	Forward (SGF1)	CTGGTCTTGAGTATCCTGAGCG
BMP-4	PCR/qPCR	Reverse (SGR1)	TCACCTCGTTCTCAGGGATGCT
BMP-7	PCR/qPCR	Forward (SGF1)	GAGTGTGCCTTCCCTCTGAACT
BMP-7	PCR/qPCR	Reverse (SGR1)	AGGACGGAGATGGCATTGAGCT
HER2	PCR/qPCR	Forward (SGF1)	GGGAAGAATGGGGTCGTCAAA
HER2	PCR/qPCR	Reverse (SGR1)	CTCCTCCCTGGGGTGTCAAGT
GAPDH	PCR/qPCR	Forward (SGF1)	TGCACCACCAACTGCTTAGC
GAPDH	PCR/qPCR	Reverse (SGR1)	GGCATGGACTGTGGTCATGAG
GREM1	qPCR	Forward (F1)	CTGCTGAAGGGAAAAAGAA
GREM1	qPCR	Reverse (zR1)	**ACTGAACCTGACCGTACA**CGACTGAGTCTGCTCTGAGT
ID1	qPCR	Forward (F1)	TCAACGGCGAGATCAG
ID1	qPCR	Reverse (zR1)	**ACTGAACCTGACCGTACA**GATCGTCCGCAGGAA
Vimentin	qPCR	Forward (F1)	ACTGAACCTGACCGTACACA
Vimentin	qPCR	Reverse (zR1)	**ACTGAACCTGACCGTACA**CATCTTCGTGGAGTTTCTTCA
Snail (Snai1)	qPCR	Forward (F1)	CAGAAAGTTTTCCACCAAAG
Snail (Snai1)	qPCR	Reverse (zR1)	**ACTGAACCTGACCGTACA**AAATGTGAGCAATTCTGCTT
Slug (Snai2)	qPCR	Forward (F1)	ATTCTCAACCCCATCT
Slug (Snai2)	qPCR	Reverse (zR1)	**ACTGAACCTGACCGTACA**TTCTCCACTTGATTTC CATT
E- Cadherin (CDH1)	qPCR	Forward (F8)	CAGAAAGTTTTCCACCAAAG
E- Cadherin (CDH1)	qPCR	Reverse (zR8)	**ACTGAACCTGACCGTACA**AAATGTGAGCAATTCTGCTT
P27	qPCR	Forward (F2)	GGAATAAGGAAGCGACCTG
P27	qPCR	Reverse	**ACTGAACCTGACCGTACA**CACCGTCTGAAACATTTTCTTC

		(zR2)	
P21	qPCR	Forward (F1)	GCGATGGAACTTCGACTTTG
P21	qPCR	Reverse (zR1)	**ACTGAACCTGACCGTACA**GGGCTTCCTCTTGGAGAAGAT
Cyclin D1	qPCR	Forward (F1)	CGGTGTCCTACTTCAAATGT
Cyclin D1	qPCR	Reverse (zR1)	**ACTGAACCTGACCGTACA**AAGCGGTCCAGGTAGTTC
PI3KCA	qPCR	Forward (F10)	TGCTAAAGAGGAACACTGTC
PI3KCA	qPCR	Reverse (zR10)	**ACTGAACCTGACCGTACA**GGTACTGGCCAAAGATTCAA
PDPL	qPCR	Forward (F8)	GAATCATCGTTGTGGTTATG
PDPL	qPCR	Reverse	**ACTGAACCTGACCGTACA**CTTTCATTTGCCTATCACAT
GAPDH	qPCR	Forward (F1)	AAGGTCATCCATGACAACTT
GAPDH	qPCR	Reverse (zR1)	**ACTGAACCTGACCGTACA**GCCATCCACAGTCTTCTG

2.1.3 Antibodies

Antibodies utilised are listed below in Table 2.2

Table 2-2 Antibodies

Antibody	Host species	Molecular weight	Resolving Gel %	Standard concentration used	Manufacturer
β Actin	Goat	42kDa	8	1:500	Santa Cruz (Sc 1615)
Gremlin1	Mouse	18-25kDa	15	1:500	Santa Cruz (C7 sc 515877)
ID1	Mouse	45-50kDa	8	1:250	Santa Cruz (Sc 101068)
Snail (Snai1)	Goat	25-30kDa	15	1:250	Santa Cruz (sc10432)
Slug (Snai2)	Rabbit	30kDa	15	1:250	Santa Cruz (Sc 15391)
Vimentin	Mouse	54-57kDa	8	1:250	Santa Cruz (Sc 6002)
E- Cadherin (CDH1)	Mouse	80-120kDa mature	8	1:250	R&D (BTA 1)
HER2(Neu)	Mouse	69kDa	8	1:250	Santa Cruz (Sc 3B5)
pSmad 1/5/8	Goat	50-60kDa	8	1:200	Santa Cruz (Sc 12353)
pAKT	Rabbit	57kDa	8	1:200	Santa Cruz (Sc 33437)
pERK	Mouse	44kDa	8	1:200	Santa Cruz (Sc 7383)
Anti-Mouse IgG	Rabbit	N/A	N/A	1:1000	Sigma Aldrich (A 9044)
Anti-Rabbit IgG	Mouse	N/A	N/A	1:1000	Sigma Aldrich (A 3687)
Anti-Goat IgG	Rabbit	N/A	N/A	1:1000	Sigma Aldrich (A 5420)

2.1.4 Specialised Reagents

Additional special reagents utilised in select experiments are listed in Table 2.3

Table 2-3 Specialised Reagents

Reagent	Description/Mechanism of action	Concentration	Manufacturer
CP724714	A potent small molecule inhibitor highly selective only for HER2 with IC50 of 10nM	Used at 40nM	(Developer Pfizer, USA) Sigma Aldrich, UK
Rh Gremlin1	Human Recombinant Gremlin1 protein	Reconstituted in sterile PBS to 200µg/ml Used at 200, 500 and 600ng/ml concentrations	R&D Systems, USA
Rh BMP-4	Human Recombinant BMP-4 protein	Reconstituted in sterile 4mM HCl to 200µg/ml Used at 10ng/ml concentration	R& D Systems, USA
Sodium Orthovanadate	Competitive inhibitor for protein phosphotyrosyl phosphatases, leading to build up of phosphorylated proteins and kinase activation. Used as a positive control for phosphorylation detection in western blotting	Diluted to 10mM from 100mM stock solution. Then mixed with 10mM solution of 30% hydrogen peroxide to make Pervanadate	Sigma Aldrich, UK
Matrigel	a solubilised basement membrane preparation rich in laminin, collagen IV, heparan sulfate proteoglycans, entactin/nidogen, and growth factors.	5mg/ml stock solution	Corning, USA
Bone Matrix Extract	Proteins extracted from fresh surgical human bone samples.	Stock of 2mg/ml diluted in culture media to 0.2mg/ml concentration	In house stock produced from previous work(Davies and Jiang 2010)
DiI	1,1'-Dioctadecyl-3,3,3',3'-Tetramethylindocarbocyanine Perchlorate is a non-toxic lipophilic cell stain that fluoresces at between 550-600 nm wavelength. It is retained in daughter cells.	5mg/ml stock solution diluted in cell culture media to 100µg/ml	Thermo Fisher, UK

2.1.5 Standard reagents and solutions for protein detection

Lysis Buffer

One litre of protein lysis buffer was prepared with 8.76g of NaCl (150mM), 6.05g of Tris (50mM), 200mg Sodium azide (0.02%, w/v), 5g Sodium deoxycholate (0.5%, w/v) and 15ml Triton X-100 (1.5%, v/v) in sterile water and stored at 4°C until required. One Complete Tablets EASYpack protease inhibitor cocktail tablet (Roche Diagnostics, Mannheim, Germany) was added to a 50ml aliquot of buffer solution to ensure the blocking of protease activity during protein extraction. This was mixed in a falcon tube on a rotating wheel for 15 minutes before further aliquoting into 1ml Eppendorf tubes (Greiner Bio-One Ltd, UK) and stored at -20°C until required.

10% Ammonium Persulfate (APS)

Two grammes of ammonium persulfate was dissolved in 20ml of distilled water and stored at 4˚C until it was required.

10% Sodium Dodecyl Sulfate (SDS)

Ten grammes of SDS was dissolved in 100ml of distilled water and kept at room temperature.

Resolving gel buffer

One litre of resolving gel buffer at pH 8.8 was purchased from Bio-Rad (Bio-Rad, UK), stored at 4°C and used neat in gel preparation.

Stacking gel buffer

One litre of stacking gel buffer at pH 6.8 was purchased from Bio-Rad (Bio-Rad, UK), stored at 4°C and used neat in gel preparation.

10x Tris Buffered Saline

Ten x TBS stock solution (Sigma Aldrich, UK) was diluted 1:10 using 1L 10x solution with 9L distilled water and stored at room temperature.

Tris-Glycine-SDS running buffer

Ten x stock solution of Tris-Glycine-SDS buffer (Sigma Aldrich, UK) was diluted 1:10 using 1L 10x solution with 9L distilled water and stored at room temperature.

Tris-Glycine transfer buffer

Transfer buffer was made up using 1L 10x solution of Tris-Glycine-Buffer (Sigma Aldrich, UK), 2L of methanol (Thermo Fisher Scientific UK,) and 9L distilled water and stored at room temperature until required.

2.1.6 Standard reagents and solutions for RNA detection

Diethyl pyrocarbonate (DEPC) treated water

DEPC water was prepared by mixing 250µl diethyl pyrocarbonate (DEPC) and 4750µl of distilled water. This was autoclaved prior to use and subsequently stored at room temperature.

Tris-Boric-Acid-EDTA (TBE)

Ten x concentrated TBE buffer (Sigma Aldrich, UK) was diluted in sterile water to make a final 1x concentration of TBE. The solution was kept at room temperature.

2.1.7 Standard reagents and solutions for microbiological methods

Luria Bertani (LB) agar

Ten grammes of LB Broth low salt granulated powder (Melford Laboratories Ltd., UK) and 7.5g of agar (Sigma-Aldrich, UK) were dissolved in 500ml of distilled water, adjusted to pH value 7.0 and autoclaved. This solution when cooled to room temperature solidifies and so was heated in a microwave prior to each use.

LB broth

A solution of LB broth was made consisting of 8g LB Broth low salt granulated powder (Melford Laboratories Ltd, UK) dissolved in 400ml sterile water, adjusted to pH 7.0 and autoclaved. The solution was stored at room temperature until required.

Ampicillin

A 100mg/ml Ampicillin solution was prepared by dissolving 1g of ampicillin (Melford Laboratories Ltd, UK) in 10ml of sterile PBS. This was stored at 4°C for short term use or -20°C longer term storage.

2.2 Cell Culture

2.2.1 Cell Lines

All cells were obtained from American Type Culture Collection (ATCC), validated through short tandem repeat profiling, and utilised to less than 15 passages. Cells were grown in culture flasks, incubated at 37°C or 34°C, with 5% carbon dioxide in a humidified incubator. All cell culture work was carried out following aseptic techniques inside a class II laminar flow cabinet and autoclaved instruments were used to keep conditions sterile. Mycoplasma contamination in cell cultures was estimated using EZ-PCR Mycoplasma Test Kit (Biological Industries, Israel). Cell lines details and their culture conditions used are listed below in Table 2.4.

Table 2-4 Cell Lines

Cell Line	Tissue	Features	Culture Medium	Incubation (^{0}C)
MCF7	Breast adenocarcinoma from metastatic pleural effusion	Epithelial, retains several features of differentiated mammary epithelium.ER + Luminal A	DMEM +10% FCS	37
T47D	Breast ductal carcinoma, from metastatic pleural effusion	Epithelial, ER+, PR+ Luminal A. Calcitonin receptor present	RPMI-1640 +10% FCS	37
ZR751	Breast ductal carcinoma, from metastatic ascites	Epithelial, ER+ Luminal A	RPMI-1640 +10% FCS	37
BT474	Breast invasive ductal carcinoma from primary tumour	Epithelial, ER+, HER2+ Luminal B	RPMI-1640 +10% FCS (Phenol Red free RPMI utilised for experiments where ER signalling minimised)	37
MDA MB 361	Breast adenocarcinoma, from brain metastasis	Epithelial, ER+, PR+ Luminal A with HER2 amplification	RPMI 1640 +10% FCS	37
SKBR3	Breast adenocarcinoma from metastatic pleural effusion	Epithelial, HER2+ Over expression	McCoy's 5a +10% FCS	37
MDA MB 231	Breast adenocarcinoma from metastatic pleural effusion	Epithelial, EGFR+, KRAS mutation	DMEM +10% FCS	37
BT 549	Invasive ductal carcinoma from primary tumour	Epithelial, mucinous	RPMI- 1640 +10% FCS	37
BT 20	Breast carcinoma from primary tumour	Epithelial, ER-	DMEM +10% FCS	37
MCF 10A	From fibrocystic breast sample	Epithelial, immortalised non tumourigenic with features of normal Luminal breast cells	DMEM +10% FCS	37
A 459	Lung carcinoma	Epithelial, high expression of GREM1	DMEM +10% FCS	37
hFob1.19	Foetal Bone	Osteoblasts, differentiation to mature osteoblasts occurs at 39.5^{0}C	Ham's F12 DMEM, + 2.5 mM L-glutamine (without phenol red) + 0.3 mg/ml G418 + 10% FCS	34

All media had antibiotics added as described in section 2.1.1 unless stated otherwise. DMEM = Dulbecco's Modified Eagle's Medium, RPMI = Roswell Park Memorial Institute

2.2.2 Cell Revival

Frozen cells were removed from storage and thawed rapidly (<1 min) in a 37°C water bath. Cells were transferred to a universal container containing 10 ml of pre-warmed medium, before being centrifuged at 1400 rpm for 8 minutes to pellet the cells. Supernatant was aspirated, and the pellet resuspended in 1ml of pre-warmed medium, before being placed into a sterile 25cm^2 (T25) tissue culture flask with 10ml pre-warmed medium and incubated at 37°C (34°C for hFOB1.19), 95% humidification and 5% CO_2. The next day, cells were examined under a light microscope for sufficient viability and adherence, and the media changed to remove any dead cells.

2.2.3 Cell Maintenance

Cell lines were placed in a cell culture incubator and maintained in supplemented media as described above (Table 2.4). All media was in date and, once opened, kept at 4^{o}C and used within 4 weeks. Cells were grown to confluence in either 25cm^2 (T25) or 75cm^2 (T75) tissue culture flasks, loosely capped (Greiner Bio-One Ltd, UK), in 5% carbon dioxide and 95% humidification. Cells were washed in sterile PBS and media changed at a frequency appropriate for the health of the cells, and confluence checked regularly under a light microscope.

2.2.4 Cell Passage

At appropriate confluence (70-80%), culture medium was removed using a sterile glass pipette under vacuum, then washed with sterile PBS. Trypsin–EDTA (1-2ml) was added to the flask, incubated, and closely monitored until cell detachment occurred. This time for Trypsin EDTA to achieve detachment is dependent on the cell line and is faster under incubation than at room temperature. The detached cells were transferred to a 20ml universal container (Greiner Bio-One Ltd., UK) and an equal volume of cell media added to neutralise the trypsin. The cell suspension was then centrifuged at 1400 rpm for 8 minutes to pellet the cells. Supernatant was then discarded, and cells resuspended in the appropriate medium for experimental work, counting, reseeding in new flasks, or freezing for storage.

2.2.5 Cell Counting

A 20µl cell suspension was mixed with 20µl 0.4% Trypan blue (Sigma Aldrich, UK), a stain that is excluded from viable cells. The mixture was incubated at room

temperature for 5 minutes. Viable cell number was then determined by manual counting, using a Neubauer haemocytometer counting chamber (Mod-Fuchs Rosenthal, UK) with an Olympus CKX31 microscope, at an objective magnification of X10 (Olympus, Tokyo, Japan). The haemocytometer was cleaned between cell samples with 70% ethanol solution and counts were done in duplicate.

2.2.6 Cell Storage

After cells were cleaned and pelleted as in section 2.2.4, they were resuspended in culture medium containing Dimethylsulphoxide (DMSO) (Sigma-Aldrich, UK) at a 10% concentration as a storage medium. Resuspension in storage medium was at a concentration of 2-5 x 10^6 cells/ml. Subsequently,1ml of cells was then transferred into 1ml CRYO.STM tubes (Greiner Bio-One Ltd, UK) pre labelled with cell type, passage number and date of freezing. Tubes were wrapped in 3 layers of tissue paper and stored overnight at -80°C in a deep freezer, before long term storage in liquid nitrogen tanks.

2.2.7 Conditioned Media

Cells were grown to 80% confluence in a 6 well plate in usual growth medium. Medium was removed and cells washed x3 in sterile PBS, then replaced with serum free Optimem (Thermo Fisher Scientific, UK) medium and cells were incubated for 24 hours.

The following day the medium was collected and centrifuged at 5,000g for 10 minutes at 4^{o}C, to remove cells and debris. Conditioned medium was then siphoned off with a pipette, placed in Eppendorf tubes and either underwent protein quantification or frozen and kept at -80°C.

2.3 RNA Detection

When a gene is expressed in a cell, the deoxyribonucleic acid (DNA) coding that gene is transcribed in the nucleus into messenger ribonucleic acid (mRNA). The mRNA is then processed by the cell into the protein for that gene. Examining expression levels of mRNA in a cell reflects what gene activity may be upregulated or downregulated in certain conditions like cancer. Polymerase chain reaction (PCR) is the most well-established method of detecting these gene specific sections of RNA. It first requires lysis of the cell and separation of the RNA from the other contents of the cell (total RNA isolation). Once we have single stranded

RNA extracted from the cells, we then need to convert the single stranded RNA back into a double stranded DNA molecule (known as copy DNA or cDNA), which is more stable and can be amplified.

This utilises an enzyme called reverse transcriptase, first identified as the method by which viruses were able to convert their single stranded RNA into DNA for insertion into the host genome(Baltimore 1970). Reverse transcription utilises reverse transcriptase to build a complimentary strand of nucleosides to the single stranded RNA, producing double stranded copy DNA.

The final step is to specifically identify the cDNA relevant to the gene of interest, and amplify this so it can be detected, even if the expression within the cells was very low. This utilises primers and the polymerase chain reaction (PCR) (Figure 2.1)(Review by Garibyan and Avashia(Garibyan and Avashia 2013)).

The cDNA is heated to break the bonds between the template DNA strand and its complimentary DNA strand. Primers (also known as oligonucleotides) are short single stranded sequences of nucleic acid that are the starting point for DNA synthesis and replication. Their sequence is complimentary to the sequence of the specific target gene DNA. Each end of a DNA molecule is labelled 3’ (3 prime) or 5’ (5 prime) which refers to the number of carbon atoms at either end of the molecule and two primers are used in each PCR reaction, a forward primer and reverse primer. The forward primer attaches to the 3’ end of the template DNA strand, whilst the reverse primer attaches to the 3’ end of the complimentary DNA strand, flanking the sequence of DNA to be replicated. The primers are the start points for DNA polymerase enzyme to build new strands of DNA, duplicating the original cDNA segment relevant to the gene of interest. This process is then repeated in each cycle of denaturing, synthesising, and replicating specific sections of cDNA, exponentially amplifying the original DNA segment. In general, 20-40 cycles will produce enough DNA for analysis, any more than 40 cycles and the DNA amount plateaus as reagents deplete and polymerase activity decreases. In this thesis, initial cycles for each target gene were set at 30, 35 and 40 to determine optimal number of cycles to detect the target genes required and 35 cycles found to be optimal across all target genes.

Glyceraldehyde –3- phosphate dehydrogenase (GAPDH) is an enzyme in mammalian cells involved in glycolysis and cell metabolism, and therefore the GAPDH gene is widely and ubiquitously expressed in most cells, and a good

reference or ‘housekeeping’ gene to compare the expression of target genes to. Another widely used reference gene is βActin, which is a cell cytoskeleton gene, involved in cell structure, and again considered ubiquitous in its expression. There will of course be variability in expression of these housekeeping genes depending on the tissue type and experimental conditions, and the reference gene must be selected with care and not assumed to be stably expressed, however, in breast cancer cell lines, GAPDH and βActin have been seen to be stable reference gene expression across many different breast cancer cell lines and treatment effects(Liu et al. 2015).

The technique of PCR for detecting gene expression is highly sensitive, simple, rapid, and very well established. There are, however, some limitations and pitfalls to be aware of. The simplest error that can occur during PCR are errors in pipetting and transfer of sample materials, which can be addressed by ensuring efficiency with the least number of transfer pipetting required for each experimental set up. Due to the high sensitivity and amplification, any contamination with trace amounts of other DNA can affect results. To reduce contamination, aseptic techniques are used in cell culture and RNA/cDNA handling (bench and equipment decontamination with 70% ethanol solution, sterile pipette tips, sterile packaged plasticware, regular glove changes) and a negative control of sterile water in the reaction instead of cDNA to demonstrate uncontaminated reagents. The DNA polymerase used (Taq Polymerase) also has potential for incorporating sequence errors with incorrect nucleotides when replicating DNA. This is given by the manufacturer Promega, as approximately 1 x 10^{-5} errors/base nucleotide, which is low, but evidently the longer the DNA sequence to be replicated and the more amplification cycles required, the higher the opportunity for error, therefore, the lowest number of cycles required to amplify the PCR product to detectable level the better.

The primers used in PCR must also be specific to the target DNA sequence only. This means the target gene sequence must be known already, and the primers should not anneal in a non-specific manner to other similar DNA sequences. The primers used in this thesis had already been previously optimised and used in the laboratory and checked for specificity to the target template using Primer BLAST(NCBI). Primer BLAST is the National Center for Biotechnology Information’s (NCBI) free online platform, widely used for both designing primers,

and also for checking primers are specific to a target gene, and will not anneal to any other sequences(Ye et al. 2012).

Figure 2-1 Polymerase Chain Reaction Overview

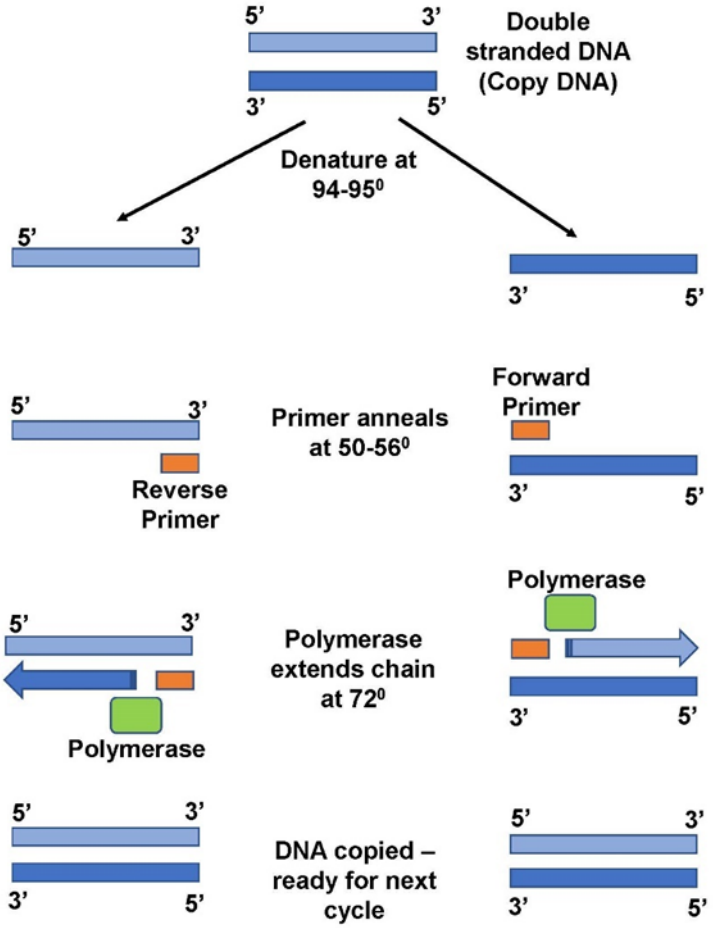

Cell samples have total RNA extracted for examination of specific gene expression. The single stranded RNA has been converted to double stranded DNA (copy DNA) using reverse transcriptase enzyme. Heating the double stranded copy DNA (cDNA) to 94-95 ^{0}C breaks the bonds between the strands, denaturing them to single strands. Primers (orange rectangle) specific to a DNA gene sequence bind to the 3' end of the sequence, with a forward and reverse primer required for the template and complimentary DNA strands respectively. A DNA polymerase (green rectangle) then binds to the primer and builds complimentary nucleotides in a chain along the DNA strand to produce a short segment of double stranded DNA specific to the gene of interest. The cycle then begins again, proportionally amplifying those specific DNA segments with each cycle(Garibyan and Avashia 2013).

After amplifying the specific PCR product representing the target DNA gene expression, gel electrophoresis is used to separate the DNA products based on the size and charge of the DNA molecules. Agarose gel is the most effective for separating DNA fragments of a wide variety of sizes. An agarose gel is made and placed in a tank with a liquid buffer solution and the PCR products placed in wells in the gel. As DNA has a negative charge, when a current is applied across the gel, conducted by the salts in the buffer, the DNA products will move towards the positive electrode. The agarose gel is a porous matrix, and the DNA molecules will move through the pores at different rates depending on their size, allowing molecules of different sizes to separate out through the gel. Smaller molecules move faster through the gel. The higher the concentration of agarose, the smaller the pore size, so to separate very small PCR products, a higher percentage agarose gel should be used. A 1% gel will resolve DNA molecules of 60 base pair size up to 10,000 base pair size, which was the range required for the PCR products in this thesis.

A stain is added to the gel that binds DNA and fluoresces under ultraviolet light, such that DNA fragments of the same size (i.e., representing the gene of interest) will accumulate at the same point in the gel as be visualised as a ‘band’. The brightness of the band under ultraviolet light is proportional to the amount of DNA visualised. A reference DNA ‘ladder’, which contains specific known sized DNA fragments is also run on the gel next to the sample PCR products, so that the equivalent size of the sample PCR products can be seen.

2.3.1 Total RNA Isolation

Cells were grown until they reached appropriate confluence (~80%). Cell medium was then aspirated, cells washed with PBS and 1ml of Sigma Total RNA Isolation (TRI) Reagent was added (Sigma-Aldrich, UK). TRI Reagent produced detachment of cells from the flask or plate and the 1ml cell suspension was then transferred into a 1.5ml Eppendorf (Greiner Bio-One Ltd, UK). To allow dissociation of nucleoprotein complexes, this was left to stand for 5 minutes at room temperature. TRI reagent solubilises DNA, RNA and denatures proteins in the cells to separate and extract them and is a widely used and well-established method. The addition of 0.1 ml of 1-bromo-3-chloropropane per 1ml of TRI Reagent was applied to cause separation of the homogenate into phases. The solution was vigorously mixed by inversion for 15 seconds before centrifugation (DJB Labcare Ltd, UK) at 12000g for 15 minutes at 4°C. The resultant homogenate formed 3 phases: a red organic phase (containing protein), an interphase (containing DNA), and a colourless upper aqueous phase (containing RNA). The upper aqueous phase containing RNA was carefully removed and transferred to a clean Eppendorf before adding 500µl of 2-propanol and mixing via inversion for 15 seconds. Samples were centrifuged for 10 minutes at 12000g at 4°C. The supernatant was removed, and the resultant RNA pellet was washed with 1ml of 75% ethanol (Fisher Scientific, UK) in DEPC water, before vortexing and centrifugation at 7500g for 5 minutes at 4°C. The supernatant was removed, and the pellet was briefly dried for 10 minutes by air-drying. The final pellet was completely resuspended in 30µl DEPC water before quantification.

2.3.2 RNA Quantification

The concentration of RNA was measured using an IMPLEN nanophotometer (Geneflow Ltd., UK) set to detect RNA in ng/µl. Measurement of samples were repeated in triplicate. The RNA samples were then used immediately for reverse transcription (RT) or stored at -80^{o}C.

2.3.3 Reverse Transcription (RT) of RNA to cDNA

Reverse transcription was carried out to generate copy DNA (cDNA) from the RNA samples using GoScript™ Reverse Transcription System (Promega, UK). A 20µl reverse transcription reaction, containing 500ng of RNA was undertaken to generate cDNA according to the manufacturer's instructions. Firstly, the following components were added to a PCR tube:

- 500ng experimental RNA (volume depends on RNA concentration) made up to 10µl with PCR water (ultra-filtered DNAse and RNAse free, Sigma Aldrich, UK)
- Add 10µl 2x RT mix, to a total volume of 20µl

Samples were then placed in the thermocycler under the following conditions:

- 25^{o}C for 10 minutes
- 37^{o}C for 120 minutes
- 85^{o}C for 5 minutes
- Samples held at 4^{o}C

The 20µl cDNA was then diluted 1:4 in sterile PCR water and then immediately utilised for PCR reactions, with primers as listed in table 2.1, or stored at -20^{o}C.

2.3.4 Polymerase Chain Reaction (PCR)

Primers were diluted in PCR water to a working concentration of 10µM for use in PCR. Individual PCR reactions were prepared in PCR plates as per the following:

- 8µl 2x PCR Master Mix Promega Green Taq (Promega, UK)
- 1µl Forward Primer
- 1µl Reverse Primer
- 5µl Sterile PCR water
- 1µl sample cDNA (or sterile PCR water as negative control)

The plate was then covered with an adhesive plate seal, centrifuged for 2 minutes, and placed into an Applied Biosystems thermocycler (Thermo Fisher Scientific, USA) with the following cycling parameters:

- 94^{o}C for 5 minutes (Initial denaturation)
- 94^{o}C for 30 seconds (Denaturation)
- 55^{o}C for 30 seconds (Annealing)
- 72^{o}C for 30 seconds (Elongation)
- 72^{o}C for 7 minutes (Final extension)
- Held at 4^{o}C

Steps 2, 3 and 4 were repeated for 35 cycles. This number of cycles was optimised by undertaking PCR for each gene of interest at 30, 35 and 40 cycles' products were then separated, and amplified target DNA identified with electrophoresis as follows.

2.3.5 Agarose Gel Electrophoresis

PCR products were separated using a 1% agarose gel. For a 50ml gel, 0.5g of agarose was placed in a flask with 50ml TBE and heated in a microwave until fully dissolved. For a 150ml gel the process was the same but with 1.5g of agarose in 150ml TBE.

The heated liquid gel was cooled and SYBER safe (Invitrogen, UK) added at a concentration of 1:10,000, which bound to and stained nucleic acids under UV or blue light. The liquid gel mixture was cast into a gel plate with combs for loading wells and left to set.

When set, the combs were removed carefully, and the gel placed in a tank with 1x TBE buffer. For each sample, 8µl was loaded into each well, with the left most well utilised for a 1Kb DNA ladder (Geneflow, UK) to allow identification of resultant band sizes. After current was used to separate the samples, bands were visualised using a U: Genius3 gel doc system (Syngene, Cambridge, UK).

2.3.6 Quantitative real time PCR (qPCR)

Quantitative real time Polymerase Chain Reaction (qPCR) was used in addition to standard PCR to confirm and quantify target gene expression. The principles of qPCR are very similar to standard PCR, utilising target gene specific primers. However, in qPCR, a fluorescent dye is included within the reagents. The fluorescent dye will only emit fluorescent signal when it is bound to the double stranded DNA as the DNA is formed during the extension phase of the PCR (Figure 2.1). This fluorescent signal is detected by the specialist qPCR machine in real time, and as the PCR products double with each cycle, the fluorescent signal increases in proportion to the quantity of target gene specific DNA.

The system optimised in our laboratory used SYBER® Green Jumpstart Taq Readymix for high throughput qPCR (Sigma Aldrich, UK). This contained SYBR® Green I fluorescent dye, JumpStart™ Taq DNA polymerase, 99% pure deoxynucleotides (dNTPs), and reaction buffer. When the thermocycler temperature reached 70^{o}C, the Taq DNA polymerase was activated to produce double stranded DNA (dsDNA) as dictated by the forward and reverse primers, incorporating the SYBER green dye which only fluoresces as part of dsDNA. Total fluorescent signal was proportional to the dsDNA, providing a quantitative method of gene expression analysis. Addition of a passive internal reference ROX (carboxyrhodamine) dye provided sample normalisation between wells. This is a passive fluorescent dye, in that its fluorescent signal is not affected by the PCR reaction, and so the ROX fluorescent signal in each well is used to normalise the PCR fluorescent signal in each well, which reduces bias in results from the variability in reaction volumes or pipetting errors between each reaction well. As with standard PCR, GAPDH expression was utilised as a control housekeeping gene for normalisation between samples.

Subsequently, 11µl reactions were set up and added to MicroAmp® Fast Optical 96-Well Reaction Plates with Barcode (Life Technologies, UK). Each reaction was set up as follows:

- Forward primer - 0.3µl (10pmol/µl)
- Reverse primer - 0.3µl (1pmol/µl)
- Q-PCR SYBER Green Master Mix -5µl
- PCR water – 1.4µl

- cDNA - 4µl

For each cDNA sample, qPCR of the target gene was repeated in triplicate. Plates were then centrifuged, and wells examined to ensure there were no bubbles present which might interfere with the reaction and detection of fluorescence. Amplification and qPCR detection was performed using Applied Biosystems® Real-Time PCR Thermocycler (Life Technologies, UK) under the following conditions:

- Initial denaturing period: 94˚C for 10 minutes.
- Denaturing step: 94˚C for 10 seconds.
- Annealing step: 55˚C for 30 seconds.
- Extension step: 72˚C for 10 seconds.

Steps 2, 3 and 4 were repeated over 100 cycles, with this number of cycles having been previously optimised in the laboratory. The thermocycler StepOnePlus™ computer software then produced a read out of the raw Cycle Threshold (Ct) for each gene expression examined across the samples. Cycle threshold is the number of cycles at which the fluorescence of the PCR products can be detected above the background (See Figure 2.2). The computer software will also flag any wells labelled as negative control that generate a fluorescent signal suggesting contamination, and automatically analyse the PCR products in each well to determine their melting temperature. If there is a single specific PCR product in the well, there will be a single peak temperature at which the PCR products ‘melt’ (the temperature at which 50% of the DNA is double stranded and 50% is single stranded). If the primers are not specific enough and there are multiple different sized DNA PCR products, there will be multiple peaks on the melt chart.

Figure 2-2 Hypothetical qPCR Amplification Curve

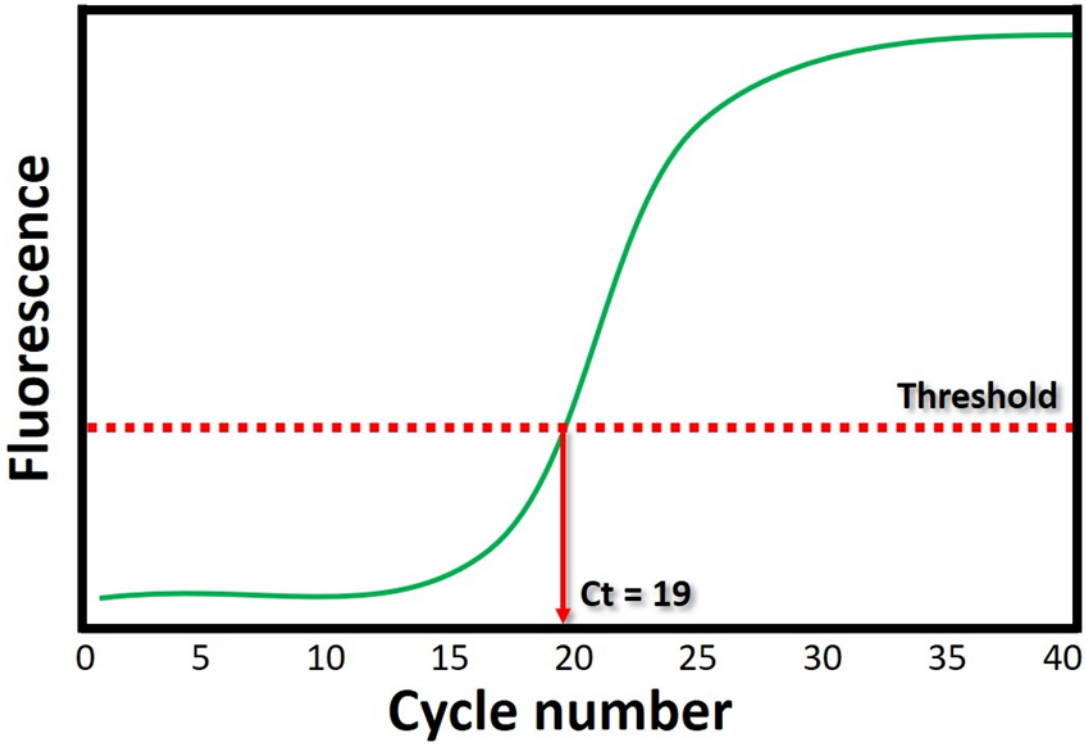

The green line represents the change in fluorescence over the number of cycles. At the start of the run, with low PCR products, the fluorescence is low and can be considered background fluorescence. As the PCR products amplify there is an exponential increase until all reagents have been used up and signal plateaus. Ct is the number of cycles for the fluorescent signal to rise above the background level. Image publicly available from www.toptipbio.com

Analysis of the raw Ct data was undertaken using the delta-delta Ct method, which gives the fold change in gene expression between a control cell sample and an experimental cell sample, for example when determining if an experimental condition has led to an increase or decrease in expression of a gene of interest, compared to control. This is otherwise known as relative quantification.

The method is outlined below:

ΔCt = Ct (gene of interest) – Ct (housekeeping gene GAPDH)

$\Delta\Delta$Ct = ΔCt (Experimental sample) – ΔCt (average of control samples)

Fold gene expression = 2^-($\Delta\Delta$Ct)

For comparing expression of genes across a panel of cell lines, where there is no specific ‘control’ to compare against, a qPCR method utilising a standard curve is

required to detect and quantify transcript copy number of target genes. This is termed absolute quantification and utilised a different qPCR method.

For this process, Precision 2X Q-PCR Mastermix (Primer Design, UK) and Amplifluor™ Uniprimer™ (Uniprobe) Universal system (Intergen company®, USA) were used, which differs to SYBR Green. The reverse primers in each reaction contain a nucleotide sequence called the Z-sequence (ACTGAACCTGACCGTACA). This is a unique sequence that is present in both the reverse primers and the Ampliflour™ probe. During the reaction, the Z sequence contained on the reverse primer becomes incorporated into the PCR product sequence over the initial rounds of amplification. Subsequently, the Ampliflour™ probe binds to the incorporated Z sequence. Ultimately, this causes extension of the Ampliflour™ probe, causing a conformational change leading to florescence which can be directly measured. This makes the fluorescent signal very much more specific to the target amplified DNA PCR product, rather than with SYBR Green, where the fluorescent probe will bind to any double stranded DNA non-specifically.

The intensity of fluorescence within each sample was compared to the fluorescence from a range of standards of known gene expression transcript copy number, which allows the calculation of transcript copy number within each sample. GAPDH copy number was also included within these samples to allow standardisation and normalisation of the samples. Each reaction was set up as follows:

- Forward primer - 0.3µl (10pmol/µl)
- Reverse primer (containing Z sequence) - 0.3µl (1pmol/µl)
- Q-PCR Master Mix -5µl
- Uniprobe – 0.3µl (10pmol/µl)
- PCR water – 3µl
- cDNA - 1µl

The same thermocycling conditions were used as listed above, for 100 cycles.

2.4 Protein Detection

Gene expression at the RNA level is useful for examining genomic influences on cellular behaviour, i.e., what RNA gene transcripts are at higher or lower levels in a cell, and how that may impact on cell activity. However, although RNA transcripts are a long-established method and used as a surrogate for protein expression, it is well known that the relationship between RNA expression (number of gene transcripts) and the final protein translated from that RNA, is not a one-to-one relationship. Difference occurs due to post transcriptional and post translational modification of proteins, and degradation of proteins(Alberts 2008).

It is therefore important to examine the presence of specific proteins within the cell, utilising the gold standard established method of western blotting for identifying and quantifying a specific protein in a complex mixture of proteins extracted from cell lysate.

As a brief overview, cells are lysed, and protein extracted. The protein amount in the lysate is quantified and denatured. Equal amounts of protein are then loaded into a gel and a current passed through the gel to separate the protein by size, similarly to agarose gel electrophoresis. Once separated, the protein bands are transferred, or ‘blotted’ onto a protein binding membrane, and an antibody specific to the protein being detected is applied, and the antibody emits a fluorescence that can then be detected(Meftahi et al. 2021).

2.4.1 Protein Extraction (cell lysis)

Cells were grown in T75 cell culture flasks until appropriate confluency (~90%) and the cell monolayer washed with PBS, before being removed from the base of the cell culture flask using a sterile disposable plastic cell scraper. Cells were transferred to a sterile 30ml universal container and centrifuged for 5 minutes at 1800rpm. The supernatant was discarded, and the pellet resuspended in 300µl cold lysis buffer. At least three cycles of cooling on ice for 5 minutes, then vortexing, was undertaken. The solution was then transferred to a1.5ml Eppendorf tube and placed on a Labinco rotating wheel (Wolf Laboratories, UK) at 25rpm, 4°C for 45 minutes. This was then centrifuged for 15 minutes at 13000rpm to pellet any insoluble proteins and the supernatant placed into a fresh Eppendorf tube before freezing at -20°C. For smaller cell flasks (T25) or 6 well plates, or where protein concentration required maximising (for example, BT474 cells form multi-layered colonies and thus do not approach confluency on light microscope

visualisation, protein yield may therefore be lower), the same procedure was performed but were resuspended in lower volumes of lysis buffer (150µl for T25, 100µl 6 well plates). Where quantification yielded very differing protein concentrations, cell lines were counted first, as per the previous protocol, and then $5x10^6$ cells used for protein extraction, as above.

2.4.2 Protein Quantification

Protein concentration of samples was determined using a Bio-Rad DC protocol (Bio-Rad laboratories, UK). This assay uses a colorimetric method to detect protein concentration following solubilisation of the proteins in the samples. To calculate protein concentration, protein samples were compared to a standard of known concentration Bovine Serum Albumin (BSA) of 100mg/ml serially diluted to 0.029mg/ml (Sigma Aldrich, UK). Samples and standards were pipetted into a 96-well plate at a volume of 5µl before adding 25µl of 'working reagent A' and 200µl of reagent B. Solutions were allowed to stand for 15 minutes to allow the colorimetric reactions to develop. Absorbance of both standards and samples were read at 620nm using an ELx800 plate reading spectrophotometer (Bio-Tek, Wolf laboratories, UK). Using the BSA known concentrations, a standard protein curve was created to establish each sample concentration. All samples were normalised to working concentrations of 2mg/ml by diluting in cell lysis buffer before further dilution in 2x Laemli buffer (Sigma-Aldrich, UK) in a 1:1(v/v) ratio. Laemli buffer improves resolution of the proteins when separated by gel electrophoresis, by reducing protein disulfide bonds, keeping the proteins linear and not 'clumped' together. It also contains a blue dye to that loading the samples into wells is easier, and migration of the protein through the gel can be visualised and tracked. Samples were boiled at 100°C for 5 minutes to denature the protein before being stored at -20°C until required.

2.4.3 SDS Page Gel Electrophoresis

In a similar method to agarose gel electrophoresis for the separation of DNA, separation of proteins uses a buffer called sodium dodecyl sulfate (SDS) within the gel and in the buffer solution, to linearise proteins and give them a universal negative charge. The SDS therefore helps proteins to move through a gel with minimised variation. Acrylamide based gel is preferred over agarose in these circumstances due to the wider range of pore size and higher resolution capability

of acrylamide gels, and the ability of the gel to withstand longer running times and higher heat than agarose.

Acrylamide resolving gels were made in house, assembled at 8-15 % concentration depending on the size of the protein being screened for (see table 2.2). Proteins in the range of 10KDa to 45KDa are resolved and separated at 15% gel concentration, as higher percentage gels will have smaller pores, resolving smaller proteins, and proteins of 25KDa to 200KDa are resolved with an 8% lower concentration gel.

The gel mixture is made and cast between two glass plates in a mould. Once this has set, a stacking gel is then placed as the topmost gel layer, with a comb to create the loading wells. For this study, 15ml of the required percentage resolving gel and 5ml of a 5% stacking gel were prepared in universal containers. The components of the resolving gels and 5% stacking gel are listed below (Table 2.5):

Table 2-5 Components of Stacking and Resolving Gels

Component	15 % Resolving gel (ml)	8% Resolving gel (ml)	5% stacking gel (ml)
Deionised Water	2.4	5.9	3.4
30% Acrylamide Mix (Sigma-Aldrich, UK)	5	5	0.83
1.0M Tris	2.5	3.8(pH 8.8)	0.63(pH 6.8)
10% SDS	0.05	0.15	0.05
10% Ammonium Persulfate	0.1	0.15	0.05
TEMED (Tetramethylethylenediamine, Sigma-Alrich, UK)	0.01	0.006	0.005

Glass plates for gel casting were cleaned thoroughly and assembled into the casting cassette. The space between the glass plates was filled with ethanol to check for leaks and then emptied and wiped free of the ethanol. Once the gels were prepared, the resolving gel was added between the glass plates using a disposable plastic pipette to a level just below where the plastic comb for well formation would sit. The solution was covered with ethanol to ensure a smooth surface left to set. Once set, the ethanol was removed, the stacking gel added, and plastic combs inserted to create the wells. Once the stacking gel had set, the loading cassettes were inserted into an electrophoresis tank and the tank was filled with 1x running buffer (see 2.1.5). The plastic combs were removed and 10µl of protein samples loaded into the wells. A molecular weight marker (Geneflow

Limited, Fradley, Staffordshire, UK) was included with the samples and loaded at a volume of 10µl.

To resolve and separate the proteins, a current is then applied. The gel electrophoresis was run at settings of 120V, 150mA and 50W for 90-120mins, until the dye front (from the Laemli buffer) was approximately 1cm from the bottom of the gel.

2.4.4 Western Blotting

Semi dry blotting technique was used to transfer the protein from gel to membrane. Polyvinylidene Difluoride (PVDF) membrane (Millipore UK, UK) was cut to the size of the gel and soaked in 100% methanol for 10-20 minutes and then in 1 x transfer buffer (see 2.1.5). Soaking in methanol and buffer hydrates the membrane and improves protein binding and transfer from the gel to the membrane. Four sheets of filter paper for each gel were also cut to size and soaked in 1 x transfer buffer until ready to use. Semi dry western blotting sandwiches the gel with the protein in it and the membrane to which we want to transfer the protein, between sheets of buffer-soaked filter paper (which act as an ion reservoir). The sandwich is then placed between two plate electrodes and a current applied which drags the negatively charged protein towards the positive electrode and on to the membrane. Semi dry transfer is rapid throughput, easy to set up and convenient. Transfer can also be done with a ‘wet’ method, whereby the gel sandwich is placed in a tank of buffer and current applied. This wet transfer method takes much longer (several hours), is more complex, but has more variation in how it can be set up depending on the conditions required. The semi dry method was therefore favoured in my laboratory, but wet transfer methods were also available.

For the semi dry transfer, two sheets of pre-soaked filter paper were placed on the positive anode graphite base. The soaked PVDF membrane was lain on top of the filter paper, and the gel then placed on top of the membrane. Finally, two further soaked filter papers were placed on top. A roller was used to gently release any air bubbles. The negative cathode cover was then placed on top and fixed in place. Electroblotting was undertaken at 15V, 500mA and 5W for 45 minutes. These settings can be adjusted to enable faster or slower transfer times and were

optimised to maximise efficiency of protein transfer. The gel should be clear of dye when transfer is complete.

The membrane was then be placed in 10ml blocking solution (10% milk, 0.1% polyoxyethylene (20) sorbitan monolaurate (Tween 20) in Tris Buffered Saline (TBS)) in a universal container and agitated for 40-60 minutes at room temperature (or overnight at 4^{o}C) prior to antibody staining. The blocking solution is important for saturating any free binding sites on the membrane, such that when a specific antibody is applied, it prevents the antibodies from binding non-specifically. This then improves the sensitivity of the specific antibody binding.

Non-fat milk powder is most used for blocking as it is cheap and widely available, however, Bovine Serum Albumin (BSA) at 5% in TBS and Tween 20, which is more expensive, was utilised as blocking solution when detecting phosphorylated proteins, as milk contains abundant casein, which is a phosphoprotein and would cause high background signal and nonspecific antibody binding.

The 10% blocking solution was then poured off the membrane and 5ml of 5% (5% milk or BSA, 0.1%Tween 20 in TBS) blocking solution with the primary antibody added at the dilution stated in Table 2.2. This was agitated on a roller at room temperature for 1 hour. The primary antibody is targeted specifically to the protein you are trying to detect and will bind to that protein. Primary antibody concentration was initially at the manufacturer's recommendation, and then adjusted upwards if unsuccessful to higher concentration in increments until successful.

The membrane was then washed to remove any unbound primary antibody with buffer (0.2% Tween 20 in 30ml TBS) in agitation for 30 minutes, with buffer changed every 10 minutes. After washing, a secondary antibody is added. The secondary antibody is directed at binding the primary antibody and has Horse Radish Peroxidase (HRP) conjugated to it. The HRP is an enzyme label, that can be visualised as it catalyses the conversion of a chromogenic or chemiluminescent substrate to produce a colour or luminescent signal.

The HRP secondary antibody was added to the 5% blocking solution at 1:1000 dilution (listed in Table 2.2) and the membrane incubated in the secondary antibody solution with agitation for 1 hour at room temperature.

Finally, the membrane was washed again in buffer (0.2% Tween 20 in 30ml TBS) twice, for 15 minutes each time and then the membrane kept in TBS until ready for chemiluminescent detection, using EZ-ECL protein detection reagent (GeneFlow Ltd., UK) before visualising on a G: BOX Chemi XRQ protein detection system (Syngene, UK).

2.4.5 Tissue Microarray Immunohistochemistry

Tissue microarray (TMA) is a method of examining expression of DNA, mRNA, and protein in multiple tissue samples at the same time. Small representative pieces of tissue, such as breast cancer samples from many different patients are embedded in a single paraffin block, with defined co-ordinates such that the details relevant to each small sample can be correlated. It allows the analysis of many samples all in one tissue slide, with maximal preservation of limited and irreplaceable tissue samples. These are commercially produced, which removes the need for costly and lengthy prospective collection of patient tissue, or the use of banked tissue, and guarantees quality control and validation of the samples. Tissue microarray is therefore seen as extremely cost and time effective, and microarray assessment of biological markers and proteins has been shown to be equivalent to whole tissue assessment(Milanes-Yearsley et al. 2002).

To examine protein expression in a tissue microarray, immunohistochemistry is used. This is the technique of antibody binding to proteins in tissues rather than extracting the protein by lysing cells. It allows examination of protein expression within the architecture of the tissue

A Tissue Microarray BR1505d was purchased to explore Gremlin1 expression in breast cancer tissue (invasive ductal carcinoma) of different grades, stages, and receptor status. This was purchased from US Biomax (US Biomax, Inc., Rockville, USA) and tissues were collected under HIPAA (Health Insurance Portability and Accountability Act, USA) approved protocols by the manufacturer. Every tissue block is collected, checked, and arranged by pathologists employed by the company and validated for antigens in the tissue to assure the tissue is properly fixed and processed.

TMAs were stored and logged according to local HTA (Human Tissue Act) regulations with double locking under restricted access. This TMA consisted of 75 patients, with two core biopsy samples for each patient, totalling 150 samples, with a control Pheochromocytoma adrenal gland sample. From the information

provided by the company, US Biomax, the core sample size is 1.5mm in diameter, which is well above the minimum size thought to be representative of the whole tissue sample(0.6mm). Each 10^{th} section of the microarray is stained with H&E and reviewed by two pathologists to ensure each core has correct pathological material and matches adjacent serial sections. Table 2.6 lists details of the TMA samples. The process of Gremlin1 immunohistochemistry for this TMA was undertaken under the supervision of Ms Fiona Ruge, our laboratory research technician, who has a wide experience of laboratory methodology and specialises in immunohistochemistry.

Table 2-6 TMA BR1505a Sample Data

A1	48	Invasive ductal Carcinoma	T2N0M0	1	2+, 50%	1+, 3%	2+
A2	42	Invasive ductal Carcinoma	T3N0M0	1	0	0	3+
A3	57	Invasive ductal Carcinoma	T2N0M0	1	3+	3+, 95%	3+
A4	57	Invasive ductal Carcinoma	T2N0M0	2	3+	0	1+
A5	66	Invasive ductal Carcinoma	T2N2M0	2	0	0	3+
A6	48	Invasive ductal Carcinoma	T2N0M0	-	2+, 60%	2+, 60%	0
A7	48	Invasive ductal Carcinoma	T2N0M0	2	3+, 80%	2+, 70%	1+
A8	48	Invasive ductal Carcinoma	T3N1M0	2	3+, 80%	0	1+
A9	46	Invasive ductal Carcinoma	T2N0M0	2	3+, 80%	3+, 80%	0
A10	58	Invasive ductal Carcinoma	T2N0M0	2	3+, 95%	3+, 90%	2+
A11	38	Invasive ductal Carcinoma	T3N0M0	2	3+, 95%	2+, 70%	0
A12	59	Invasive ductal Carcinoma	T2N0M0	3	3+, 95%	0	0
A13	50	Invasive ductal Carcinoma	T3N0M0	2	1+, 40%	0	3+
A14	66	Invasive ductal Carcinoma	T3N0M0	2	0	1+, 20%	3+
A15	39	Invasive ductal Carcinoma	T2N0M0	2	1+, 10%	1+, 3%	0
B1	48	Invasive ductal Carcinoma	T2N0M0	1	1+, 20%	0	2+
B2	42	Invasive ductal Carcinoma	T3N0M0	-	0	0	3+
B3	57	Invasive ductal Carcinoma	T2N0M0	2	3+, 95%	3+, 95%	2+
B4	57	Invasive ductal Carcinoma	T2N0M0	-	3+, 95%	1+, 3%	1+
B5	66	Invasive ductal Carcinoma	T2N2M0	-	0	0	3+
B6	48	Invasive ductal Carcinoma	T2N0M0	-	2+, 30%	1+, 5%	0
B7	48	Invasive ductal Carcinoma	T2N0M0	2	3+, 95%	3+, 90%	2+
B8	48	Invasive ductal Carcinoma	T3N1M0	2	3+, 95%	1+, 2%	1+
B9	46	Invasive ductal Carcinoma	T2N0M0	2	3+, 95%	3+, 90%	0
B10	58	Invasive ductal	T2N0M0	2	3+, 95%	3+, 90%	1+

		Carcinoma					
B11	38	Invasive ductal Carcinoma	T3N0M0	2	3+, 95%	2+, 80%	0
B12	59	Invasive ductal Carcinoma	T2N0M0	3	0	0	0
B13	50	Invasive ductal Carcinoma	T3N0M0	2	1+, 60%	0	3+
B14	66	Invasive ductal Carcinoma	T3N0M0	2	0	1+, 5%	3+
B15	39	Invasive ductal Carcinoma	T2N0M0	2	2+, 60%	1+, 5%	0
C1	46	Invasive ductal Carcinoma	T2N0M0	2	0	0	3+
C2	48	Invasive ductal Carcinoma	T3N0M0	2	3+, 95%	3+, 80%	0
C3	59	Invasive ductal Carcinoma	T2N0M0	2	0	0	3+
C4	40	Invasive ductal Carcinoma	T3N1M0	2	0	0	2+
C5	47	Invasive ductal Carcinoma	T4N0M0	2	0	0	0
C6	60	Invasive ductal Carcinoma	T4N0M0	2	n/a	0	3+
C7	58	Invasive ductal Carcinoma	T3N2M1	2	1+, 30%	0	0
C8	45	Invasive ductal Carcinoma	T3N1M0	2	0	0	0
C9	62	Invasive ductal Carcinoma	T1N0M0	-	3+, 80%	2+, 70%	0
C10	49	Invasive ductal Carcinoma	T4N0M0	2	3+, 90%	3+, 80%	0
C11	50	Invasive ductal Carcinoma	T2N0M0	2	0	0	0
C12	45	Invasive ductal Carcinoma	T3N1M1	2	1+, 20%	0	3+
C13	46	Invasive ductal Carcinoma	T2N1M0	2	0	0	3+
C14	53	Invasive ductal Carcinoma	T2N0M0	2	0	0	3+
C15	35	Invasive ductal Carcinoma	T4N1M0	2	0	0	3+
D1	46	Invasive ductal Carcinoma	T2N0M0	-	0	0	3+
D2	48	Invasive ductal Carcinoma	T3N0M0	2	3+, 95%	3+, 95%	0
D3	59	Invasive ductal Carcinoma	T2N0M0	2	0	0	3+
D4	40	Invasive ductal Carcinoma	T3N1M0	2	0	0	3+
D5	47	Invasive ductal Carcinoma	T4N0M0	2	1+, 20%	1+, 3%	0
D6	60	Invasive ductal	T4N0M0	2	0	0	3+

		Carcinoma					
D7	58	Invasive ductal Carcinoma	T3N2M1	2	0	1+, 3%	0
D8	45	Invasive ductal Carcinoma	T3N1M0	2	0	0	0
D9	62	Invasive ductal Carcinoma	T1N0M0	-	3+, 70%	1+, 40%	0
D10	49	Invasive ductal Carcinoma	T4N0M0	2	3+, 70%	2+, 70%	0
D11	50	Invasive ductal Carcinoma	T2N0M0	2	0	0	0
D12	45	Invasive ductal Carcinoma	T3N1M1	2	1+, 20%	0	3+
D13	46	Invasive ductal Carcinoma	T2N1M0	2	0	0	3+
D14	53	Invasive ductal Carcinoma	T2N0M0	2	0	0	3+
D15	35	Invasive ductal Carcinoma	T4N1M0	2	0	0	0
E1	35	Invasive ductal Carcinoma	T2N0M0	2	3+, 90%	2+, 80%	0
E2	67	Invasive ductal Carcinoma	T3N0M0	2	3+, 90%	1+, 10%	1+
E3	42	Invasive ductal Carcinoma	T3N0M0	2	1+, 5%	2+, 5%	3+
E4	44	Invasive ductal Carcinoma	T3N0M0	2	1+, 10%	0	3+
E5	62	Invasive ductal Carcinoma	T2N0M0	2	1+, 10%	0	3+
E6	44	Invasive ductal Carcinoma	T2N0M0	2	3+, 90%	2+, 70%	0
E7	61	Invasive ductal Carcinoma	T3N1M0	-	0	0	3+
E8	42	Invasive ductal Carcinoma	T3N0M0	-	2+, 80%	3+, 90%	0
E9	54	Invasive ductal Carcinoma	T3N0M0	2	0	0	3+
E10	43	Invasive ductal Carcinoma	T2N0M0	2	2+, 90%	3+, 90%	0
E11	63	Invasive ductal Carcinoma	T2N0M0	2	3+, 100%	1+, 5%	1+
E12	53	Invasive ductal Carcinoma	T2N0M0	2	1+, 20%	2+, 40%	0
E13	58	Invasive ductal Carcinoma	T2N0M0	2	1+, 20%	0	3+
E14	51	Invasive ductal Carcinoma	T4N1M0	2	1+, 10%	2+, 60%	3+
E15	67	Invasive ductal Carcinoma	T2N0M0	2	3+, 100%	2+, 60%	0
F1	35	Invasive ductal Carcinoma	T2N0M0	2	3+, 90%	3+, 90%	0
F2	67	Invasive ductal	T3N0M0	2	3+, 90%	0	1+

		Carcinoma					
F3	42	Invasive ductal Carcinoma	T3N0M0	2	1+, 10%	2+, 0%	3+
F4	44	Invasive ductal Carcinoma	T3N0M0	2	0	0	2+
F5	62	Invasive ductal Carcinoma	T2N0M0	2	1+, 10%	0	3+
F6	44	Invasive ductal Carcinoma	T2N0M0	2	3+, 90%	2+, 60%	0
F7	61	Invasive ductal Carcinoma	T3N1M0	2	1+, 3%	0	3+
F8	42	Invasive ductal Carcinoma	T3N0M0	2	1+, 5%	0	0
F9	54	Invasive ductal Carcinoma	T3N0M0	2	0	0	3+
F10	43	Invasive ductal Carcinoma	T2N0M0	2	2+, 70%	3+, 80%	0
F11	63	Invasive ductal Carcinoma	T2N0M0	2	3+, 90%	1+, 10%	1+
F12	53	Invasive ductal Carcinoma	T2N0M0	2	3+, 100%	3+, 100%	0
F13	58	Invasive ductal Carcinoma	T2N0M0	2	1+, 10%	0	3+
F14	51	Invasive ductal Carcinoma	T4N1M0	2	0	2+, 60%	3+
F15	67	Invasive ductal Carcinoma	T2N0M0	2	3+, 100%	2+, 60%	0
G1	65	Invasive ductal Carcinoma	T1N2M0	2	0	0	0
G2	63	Invasive ductal Carcinoma	T2N0M0	2	1+, 5%	1+, 60%	3+
G3	52	Invasive ductal Carcinoma	T2N0M0	2	0	0	3+
G4	40	Invasive ductal Carcinoma	T2N0M0	2	0	1+, 3%	0
G5	67	Invasive ductal Carcinoma	T2N0M0	2	0	0	3+
G6	45	Invasive ductal Carcinoma	T2N0M0	3	0	0	0
G7	49	Invasive ductal Carcinoma	T2N0M0	3	3+, 90%	3+, 95%	0
G8	60	Invasive ductal Carcinoma	T4bN1M0	3	0	0	3+
G9	46	Invasive ductal Carcinoma	T3N0M0	3	3+, 90%	3+, 95%	3+
G10	64	Invasive ductal Carcinoma	T2N0M0	3	0	0	0
G11	40	Invasive ductal Carcinoma	T2N1M0	3	0	0	3+
G12	43	Invasive ductal Carcinoma	T2N0M0	3	3+, 80%	3+, 80%	0
G13	75	Invasive ductal	T2N1M0	3	0	0	0

		Carcinoma					
G14	50	Invasive ductal Carcinoma	T2N0M0	-	1+, 2%	2+,5%	0
G15	40	Invasive ductal Carcinoma	T2N0M0	3	2+, 60%	0	0
H1	65	Invasive ductal Carcinoma	T1N2M0	2	n/a	0	n/a
H2	63	Invasive ductal Carcinoma	T2N0M0	2	1+, 10%	1+,30%	3+
H3	52	Invasive ductal Carcinoma	T2N0M0	2	0	0	3+
H4	40	Invasive ductal Carcinoma	T2N0M0	2	0	1+,5%	0
H5	67	Invasive ductal Carcinoma	T2N0M0	2	0	0	1+
H6	45	Invasive ductal Carcinoma	T2N0M0	3	0	0	0
H7	49	Invasive ductal Carcinoma	T2N0M0	3	3+, 90%	3+,80%	0
H8	60	Invasive ductal Carcinoma	T4bN1M0	3	0	0	3+
H9	46	Invasive ductal Carcinoma	T3N0M0	3	3+, 90%	3+,90%	3+
H10	64	Invasive ductal Carcinoma	T2N0M0	3	0	0	0
H11	40	Invasive ductal Carcinoma	T2N1M0	3	0	0	3+
H12	43	Invasive ductal Carcinoma	T2N0M0	3	3+, 90%	3+,80%	0
H13	75	Invasive ductal Carcinoma	T2N1M0	3	0	0	0
H14	50	Invasive ductal Carcinoma	T2N0M0	-	3+, 90%	1+,5%	3+
H15	40	Invasive ductal Carcinoma	T2N0M0	3	1+, 20%	0	0
I1	50	Invasive ductal Carcinoma	T2N0M0	3	3+, 90%	0	0
I2	37	Invasive ductal Carcinoma	T3N0M0	3	1+, 70%	0	0
I3	66	Invasive ductal Carcinoma	T2N0M0	3	3+, 90%	0	3+
I4	33	Invasive ductal Carcinoma	T2N0M0	3	0	0	3+
I5	49	Invasive ductal Carcinoma	T4N2M0	-	0	0	3+
I6	49	Invasive ductal Carcinoma	T2N2M0	3	0	0	3+
I7	40	Invasive ductal Carcinoma	T3N2M0	3	0	0	0
I8	53	Invasive ductal Carcinoma	T4bN1M0	3	3+, 90%	3+, 90%	0
I9	54	Invasive ductal	T2N0M0	3	0	0	0

		Carcinoma					
I10	51	Invasive ductal Carcinoma	T2N0M0	3	0	0	0
I11	68	Invasive ductal Carcinoma	T2N0M0	3	0	0	0
I12	33	Invasive ductal Carcinoma	T2N0M0	3	3+, 90%	3+,80%	0
I13	50	Invasive ductal Carcinoma	T2N0M0	3	0	0	3+
I14	53	Invasive ductal Carcinoma	T2N0M0	3	0	0	0
I15	34	Invasive ductal Carcinoma	T2N0M0	3	2+, 60%	3+,80%	0
J1	50	Invasive ductal Carcinoma	T2N0M0	3	3+, 90%	0	0
J2	37	Invasive ductal Carcinoma	T3N0M0	3	1+, 20%	0	0
J3	66	Invasive ductal Carcinoma	T2N0M0	3	3+, 90%	0	3+
J4	33	Invasive ductal Carcinoma	T2N0M0	3	0	0	3+
J5	49	Invasive ductal Carcinoma	T4N2M0	3	0	0	3+
J6	49	Invasive ductal Carcinoma	T2N2M0	3	0	0	3+
J7	40	Invasive ductal Carcinoma	T3N2M0	3	0	0	0
J8	53	Invasive ductal Carcinoma	T4bN1M0	3	3+, 90%	3+,80%	0
J9	54	Invasive ductal Carcinoma	T2N0M0	3	0	0	0
J10	51	Invasive ductal Carcinoma	T2N0M0	3	0	0	0
J11	68	Invasive ductal Carcinoma	T2N0M0	3	0	0	1+
J12	33	Invasive ductal Carcinoma	T2N0M0	3	3+, 90%	3+, 90%	0
J13	50	Invasive ductal Carcinoma	T2N0M0	3	0	0	3+
J14	53	Invasive ductal Carcinoma	T2N0M0	3	0	0	0
J15	34	Invasive ductal Carcinoma	T2N0M0	3	2+, 80%	3+,50%	0
-	42	Adrenal Phaeochromocytoma	-	-	-	-	-

The slide was placed in an oven set at 45°C for 48 hours to aid the sections adherence. Following this, the slide was de-waxed and re-hydrated by immersing in the following solutions for 5 minutes each: 100% xylene (x2), 50% xylene/50% ethanol, 100% ethanol (x2), 90% ethanol, 70% ethanol, 50% ethanol, distilled water, and PBS (Phosphate buffered saline) buffer. After rehydration, antigen protein binding sites need to be retrieved. The previous process of fixing the tissues with Formalin can cause protein cross linking, which would inhibit the binding of antibodies to their specific protein antigen. The cross linking therefore needs to be broken using a buffer solution and heat in a process called antigen retrieval.

An antigen retrieval buffer was made during the last immersion step using 1mM EDTA (Ethylenediaminetetraacetic acid) buffer (0.37g EDTA in 1000ml dH2O, pH 8). Antigen retrieval was performed by placing the slide in a plastic container and covering with the EDTA buffer. This was microwaved on full power for 20 minutes, shaking the slide at 10 minutes to disperse bubbles. After cooling, the slide was washed for 10 minutes using tap water.

Following antigen retrieval and washing, excess fluid was removed from the sections and a ring of wax applied to keep all applied solutions on the slide. The microarray slide was then incubated with blocking solution (10% horse serum/0.1% Bovine Serum Albumin/PBS) for at least 90 minutes. The process of blocking, like western blot, is to reduce nonspecific antibody binding. Following the blocking incubation, the solution was removed and the TMA section was covered with the Gremlin1 primary antibody and incubated overnight at 4^{o}C. The primary antibody used was the same as for Western blotting, Gremlin1 (Santa Cruz Biotechnology, USA) and was prepared to a final concentration of 2µg/ml in the blocking solution.

The following day, the TMA section was washed three times for five minutes each in PBS buffer and then a Vectastain Universal Elite ABC Kit (PK-6200) (Vector Laboratories Ltd, UK) was used for detection of the Gremlin1 antibody.

Avidin-Biotin Complex (ABC) based detection is a widely used technique in immunohistochemistry. After binding of the primary antibody to the target protein, a secondary antibody targeted to the primary antibody is applied. The secondary antibody has the small molecule Biotin conjugated to it. In this method, two drops of the Vectastain secondary reagent (Horse anti-mouse IgG with biotin

conjugated) are added to 5ml of the blocking solution, placed on the slide and incubated for 30 minutes. The TMA slide is then washed again 3 times for 5 minutes with PBS buffer.

The next step is to add 2 drops of the molecule Avidin (Reagent A in Vectastain kit), into 5ml blocking solution. Further to this, 2 drops of Biotin bound to Horse Radish Peroxidase (HRP) (Reagent B in Vectastain kit) is then added to the 5ml blocking solution and this solution must stand for 15-30 minutes. Avidin binds the biotinylated HRP with very high affinity to make HRP conjugated Avidin Biotin Complexes (ABC reagent).

The ABC reagent in the 5 ml blocking solution is added to the TMA slide for 30 minutes. The Avidin - Biotin complexes with HRP in the ABC reagent bind to the biotin on the secondary antibody, labelling it with HRP.

Three more wash steps were made prior to development with DAB (diaminobenzidine) substrate (D5637) (Sigma-Aldrich, Dorset, UK) for 10 minutes. Diaminobenzidine is a chromogen, and HRP catalyses hydrogen peroxide oxidating DAB. Oxidised DAB forms an insoluble brown precipitate at the location of the HRP, thus visualising the Gremlin1 protein via avidin-biotin complexes.

Diaminobenzidine was prepared in 5ml PBS (final concentration 1mg/ml) and 6µl hydrogen peroxide was added immediately before use, adding the DAB to the slide, and allowing the brown stain to develop. Slides were washed briefly with water before counterstaining the nuclei with Gill's Haematoxylin (Vector Laboratories Ltd, UK) for 2 minutes, and then washed with water for 5 minutes. Sections were then dehydrated for five minutes in each 50% ethanol, 70% ethanol, 90% ethanol, 100% ethanol (x2), 50% ethanol/50% xylene and cleared in xylene (x2). Finally, sections were mounted with glass coverslip and left to dry prior to analysis. The slide was scanned for digital photography at high resolution using EVOS FL Auto Imaging (Invitrogen, ThermoFisher Scientific Ltd, UK).

As the TMA already has pathologist confirmation of the cancer tissues on the slide as part of company controls, pathologist verification of the tissues has already ben complete. For analysis of the intensity of Gremlin1 staining, MIPAR image analysis software (Ohio, USA) was utilised to threshold images of the samples in greyscale to determine percentage depth of staining. Digital image analysis for immunohistochemistry quantification is being increasingly used and has

demonstrated good correlation to analysis by pathologists(Rizzardi et al. 2012; Martinez-Morilla et al. 2020) .

The background, or acellular areas were determined at a greyscale threshold of 190-255, low stain at 90-189, moderate at 40-89 and high as 0-39. The software then provided the pixel number and percentage of the image at each threshold for each picture of each sample and a score from 1-4 was given depending on which greyscale threshold group had the highest percentage, with 1 as no stain, 2 = low, 3 = moderate and 4 = high. This semi quantitative assessment was then correlated with the sample clinical parameters.

2.4.6 Gremlin1 Sandwich Enzyme Linked Immunosorbent Assay (ELISA)

Another method of protein detection is the Enzyme Linked Immunosorbent Assay (ELISA). This method is designed for detecting proteins in solution, and is relevant to Gremlin1, as this is a protein that is found both within cells and at the cell membrane, but also secreted into the extracellular matrix. In this ELISA a Gremlin1 specific antibody is coated onto the surface of a 96 well plate. When a sample solution is added to the wells, the antibody will specifically bind the protein. A secondary antibody specific to the target protein and conjugated with an enzyme such as HRP is then added and ‘sandwiches’ the protein between the two antibodies. A reagent that produces a colorimetric or chemiluminescent change on exposure to the enzyme can then be used to visualise the amount of target specific protein in the well. The intensity of the colorimetric or chemiluminescent change in test samples can then be compared to a set of known standard concentrations to calculate the concentration of the target protein in solution. Sandwich ELISA is a very sensitive method for detecting proteins in serum, plasma, conditioned media, and other biological fluids and can detect proteins even at very low concentrations of picomoles/ml.

To confirm Gremlin1 protein secretion into conditioned media, across samples of cells where Gremlin1 was knocked down or overexpressed, a sample of a Human Gremlin1 ELISA kit was provided by Abbexa (abx351709, Abbexa, Cambridge, UK). This was a 48 well sample plate for a limited run of samples and repeats.

An antibody specific to human Gremlin1 was pre-coated onto the wells of the plate, and was used to detect Gremlin1 concentrations in the range 0.156 ng/ml - 10 ng/ml. It was therefore useful for low concentration protein detection.

Firstly, ELISA wash buffer was diluted 1:25 with distilled water. Standards of known Gremlin1 concentration were then prepared no more than 15 minutes prior to experiment. The standard was reconstituted at 10ng/ml and then serially diluted in diluent buffer to concentrations of 5ng/ml,2.5ng/ml, 1.25ng/ml, 0.625ng/ml, 0.3125ng/ml and 0.15625 ng/ml.

Duplicates of 100µl of each Standard, test sample and negative control (diluent buffer alone) were placed into the wells. The plate was covered and incubated at 37^0C for 90 minutes. After incubation the liquid was removed from the wells and 100µl biotin conjugated antibody working solution added to each well without touching the side walls of the well. The plate was covered and incubated at 37^0C for 60 minutes.

The biotin conjugated antibody solution was then removed, and the wells washed three times with 300 µl each time of 1x Wash Buffer to each well, allowing 1-2 minutes of soaking for each wash and complete removal of buffer at each wash. After the third wash cycle, all liquid was removed, and the plate inverted and blotted against absorbent paper towels. This was followed by the addition of100 µl of HRP (Horse Radish Peroxidase) working solution to each well and incubation at 37^0C for 30 minutes. After incubation the solution was discarded and the wells washed again five times, with wash buffer as described above.

TMB (3,3′,5,5′-Tetramethylbenzidine) substrate was used to visualize HRP activity as TMB is catalysed by HRP to produce a blue colour product that changes into yellow after adding stop solution. The intensity of the yellow colour is proportional to the Gremlin1 amount bound on the plate. Then 90 µl of TMB was added to each well, the plate was covered in foil and incubated in the dark at 37^0C for 20 minutes until a gradient appeared in the standard wells. 50 µl of stop solution was then added to each well to terminate the reaction and the plate was tapped to ensure thorough mixing and no bubbles. Absorbance was then measured on a microplate reader (Glomax multi-detection system, Promega, UK) at 450nm. Concentration of Gremlin1 was then calculated as follows:

Relative absorbance = absorbance of standards/samples – absorbance of negative control well

A standard curve was then plotted with the relative absorbance of each standard solution(Y) against the respective Log concentration of each standard (X) and a line fitted with trendline equation used to determine Gremlin1 concentrations of

samples (See Appendix). Percentage change in Gremlin1 concentrations between control and experimental cell lines were then determined using the following:

$$\text{Change in Gremlin1 concentration (\%)} = \frac{\text{Concentration of Gremlin1 (experimental)}}{\text{Concentration of Gremlin1 (control)}} \times 100$$

2.5 Plasmid Cloning

Plasmid cloning is one of the most common methods in molecular biology research. Plasmids are a small circular double stranded DNA molecule, found most often in bacteria where in nature the plasmid carries genes that benefit the survival of the organism. In the laboratory, artificial plasmids can be made that contain a gene of interest and then are inserted into host cells and confer a genetic change in those cells.

To build a stock of plasmids for use in genetic knockdown or overexpression experiments, the plasmid of interest can be cloned, or replicated. Bacterial cells, such as *Escherichia Coli* are used to host and replicate the plasmid of interest. This is because it is easy to introduce the plasmid into the bacterial cell, after which the bacterial cell will very efficiently start replicating and assembling copies of the plasmid vector, which can then be purified, stored, and used to introduce particular genetic information into mammalian cells.

Plasmid cloning was undertaken to replicate and build stock of plasmid vectors described in subsequent sections, utilising the Oneshot ®TOP10 chemically competent *Escherichia Coli* system (ThermoFisher, UK). This system has chemically competent *E.Coli* bacterial cells that are treated with calcium chloride and this facilitates attachment of the plasmid DNA to the E.coli cell membrane. On rapidly heating the competent *E.Coli* cells, this opens the pores of the cell membrane, allowing entry of the plasmid DNA into the *E.Coli* cells.

Oneshot® *E. Coli* were removed from the deep freezer and allowed to thaw on ice. 2µl of the plasmid vector was added to 20µl *E. Coli* and mixed gently by stirring with the pipette tip. The suspension was then placed on ice for 30 minutes before a heat shock at 42°C in a pre-heated water bath for 30 seconds. This was then immediately transferred back to ice for 5 minutes. Following this, 200µl of pre-warmed S.O.C. medium (cell recovery medium) was added and incubated for 1 hour at 37°C on rotation. This media contains nutrients and helps the *E.Coli*

recover from the process of transformation (i.e., introducing the plasmid into the bacteria).

After incubation, the *E. coli* mix was spread onto agar plates (containing 100µg/ml ampicillin) at high volume and low volume to allow suitable colony proliferation overnight at 37°C in an incubator. Once colonies had propagated, a fine pipette tip was used to remove a bacterial colony and placed in 15ml lysogeny broth (LB) with appropriate concentration selection antibiotic (as per plasmid manufacturer's instruction) and placed on rotation overnight in an incubator at 37°C. This media, LB, contains nutrients to support bacterial growth. The plasmid contains an antibiotic resistance gene, such that bacteria that have incorporated the plasmid will continue to propagate and replicate the plasmid, whereas those cells that do not have the plasmid with the resistance gene will die. This purifies the bacterial colony to only those bacterial cells with the plasmid in them. After propagation of the plasmid containing *E.Coli,* we need to extract the replicated DNA plasmid from the bacterial cells. This is done by lysing the bacterial cells, precipitating the DNA plasmids with ethanol, and filtering out the plasmids from the cellular debris.

For extraction and purification of the cloned DNA plasmid I used Sigma GenElute Plasmid MiniPrep Kit (Sigma-Aldrich, UK), according to the provided protocol. Colony cultures were removed from the incubator and centrifuged at 3000 rpm for 10 minutes to pellet the bacteria. The supernatant was discarded, and the pellet resuspended in 200µl of Resuspension Solution (containing RNAase A, this is to degrade and RNA, as we do not want RNA contaminating our DNA plasmid). This was followed by the addition of 200µl of Lysis Solution to lyse the cells which was mixed 6-8 times by inversion, followed immediately by adding 350µl Neutralisation/Binding Solution and then centrifuged at 12,000g for 10 minutes in a micro centrifuge. Mini Spin Columns were then prepared by adding 500µl Column Preparation Solution and centrifuging at 12,000g for 30 seconds. The cell lysate was then transferred into prepared Mini Spin Columns and centrifuged at 12,000g for 1 minute. The flow-through containing cell debris and protein was discarded and 750µl Wash Solution added to the column before centrifuging at 12,000g for 1 minute. Wash solution was discarded, and an additional spin was carried out to remove excess. The Mini Spin Column was then transferred to a clean collection tube and the plasmid DNA within the mini spin column was eluted in 100µl Elution Solution by centrifugation at 12,000g for 1 minute. The plasmid DNA was then run on a 1% agarose gel electrophoresis to check both plasmid purity and product

size. Plasmid concentration was quantified using the IMPLEN nanophotometer (Geneflow Ltd., UK) set to detect dsDNA in µg/ml. Plasmids were then utilised as vectors to produce lentiviral particles, or induce overexpression in mammalian cell lines, as described below.

2.6 Generation of Lentiviral Knockdown shRNA Model

Short hairpin RNA (shRNA) is a type of RNA interference, used to silence expression of a target gene. Lentiviral shRNA is delivered by packaging the shRNA sequence into lentiviral particles, which are then transduced into the cell. The lentiviral vector integrates the shRNA sequence into the cell's genome, such that daughter cells will inherit the targeted genomic silencing.

Lentiviral plasmid vectors containing either a *GREM1* shRNA (CTGAAGCGAGACTGGTGCAAA) sequence, HER2 shRNA (GAGATCACAGGTTACCTATAC) sequence, or a dummy Scram, le control shRNA sequence (CCTAAGGTTAAGTCGCCCTCG) was obtained from Vector Builder (USA). These *GREM1* shRNA, HER2 shRNA and scramble shRNA plasmid vectors also carry Green Fluorescent Protein (GFP) and resistance to neomycin as a selection marker. Lentiviral particles were produced using HEK (Human Embryonic Kidney) 293T cells transduced with the packaging plasmid vectors pMD2G and pSPAX2 and either the shRNA vector, or scramble vector. The HEK 293T cell is widely used in cell biology, as they can robustly undergo transfection with plasmid vectors and grow rapidly and reliably, cloning the plasmid vector easily, in a similar manner to *E.Coli* .Whereas the E.Coli are good for reproducing double stranded DNA plasmids only, the HEK 293T cells are more suited to replicating DNA plasmids, translating the DNA into protein, and assembling the proteins that the plasmids code for, into viral particles that have the ability to transfect mammalian cells, but not be pathogenic. Effectively, are using the HEK 293T cells to produce viral particles that can enter a mammalian cell in culture, integrate the target gene of choice into the host cell's DNA, such that that gene will then be stably expressed in the host cell. The viral particle will also contain an antibiotic resistance gene, so that only cells that have integrated the particles DNA will survive selection when grown in media containing that antibiotic.

Approximately 24 hr before transfection, HEK 293T cells were seeded onto a 6 well plate and incubated at 37°C, 5% CO_2 overnight. The cells were at 70% confluence at the time of transfection.

Cells were transfected with the shRNA plasmid vectors and the viral particle packaging plasmid vectors using 1mg/ml stock of PEI (Polyethylenemine, Sigma-Aldrich, UK), in the biological agents and genetically modified micro-organisms facility (GM room with separate cell culture cabinet). PEI condenses DNA plasmids into positively charged particles that bind to the cell surface and are then endocytosed, releasing the plasmid vector into the cytoplasm and is a commonly used method of successful transfection.

On the day of transfection, the HEK 293T cells are washed with PBS and 2.5ml fresh DMEM / 5% FCS medium was added to each well. For each plasmid, 3µg plasmid DNA was diluted in 150µl Optimem (serum free medium) and 9µg PEI diluted in 150µl Optimem. The diluted plasmid DNA and diluted PEI were then added together and gently stirred with a pipette tip and left to incubate at room temperature for 30 minutes. The mix was then carefully pipetted down the side of the well onto the cells and the plate returned to the incubator overnight. The media was then changed the following day and the cells checked for GFP expression with fluorescent microscopy to demonstrate successful transfection of the plasmids.

The HEK 293T cells then produced packaged lentiviral particles carrying the shRNA and secretes these particles into the medium. Culture medium containing the particles was harvested at 48 hours, centrifuged at 500g for 5 minutes to pellet cell debris and then the supernatant passed through a 0.45µm filter. This viral supernatant was then snap frozen and stored at -80^{o}C until required for experimental use.

To produce GREM1 shRNA knockdown, HER2 shRNA knockdown, or Scramble shRNA control in mammalian cells, cell lines were grown to 80% confluence in 6 well plates. Fresh medium containing 8µg/ml polybrene, used to increase the transfection efficiency, was added with 0.1-0.5ml Lentiviral particle solution (0.5ml for a high multiplicity of infection (MOI), and 0.1ml for a low MOI, as effectiveness of viral transfection can differ depending on how high or low the viral particle load is, so two different amounts were utilised to optimise for each cell line being transfected) and the cells were incubated at 37^{o}C and 5% CO2 overnight.

Polybrene is a cationic polymer which neutralises the charge repulsion between the viral particles and the cell surface, increasing the efficiency of the viral particles ability to infect the cells. It can however at higher concentrations cause cellular death, so if it was found the cells were not surviving transfection, the polybrene concentration was lowered, and if the transfection efficiency was not good enough the concentration of polybrene was increased. This was optimised as far as possible for each cell line transfected, but balance was required between transfection efficiency and cell death, and 8μg/ml polybrene was the optimal concentration for this balance in most cell lines.

Transfected cells were then cultured in media with G418 (Neomycin) added at 500μg/ml for selection of transduced clones and GFP expression in the cells examined with fluorescent microscopy for 14 days to ensure continued selection of successfully transduced cells. Thereafter, cells were maintained with 100μg/ml G418 in standard media. Knockdown efficiency for each cell line was determined with both PCR, qPCR, and western blot as described above.

2.7 Generation of cDNA plasmid overexpression Model

The full-length human GREM1 coding sequence had previously been amplified from a cDNA library derived from normal prostate tissue and subsequently cloned by the laboratory into a pEF6/V5 - His TOPO TA DNA plasmid vector (Invitrogen Ltd., UK) (see Figure 2.2).

Figure 2-3 PEF6/V5 His TOPO Vector Map

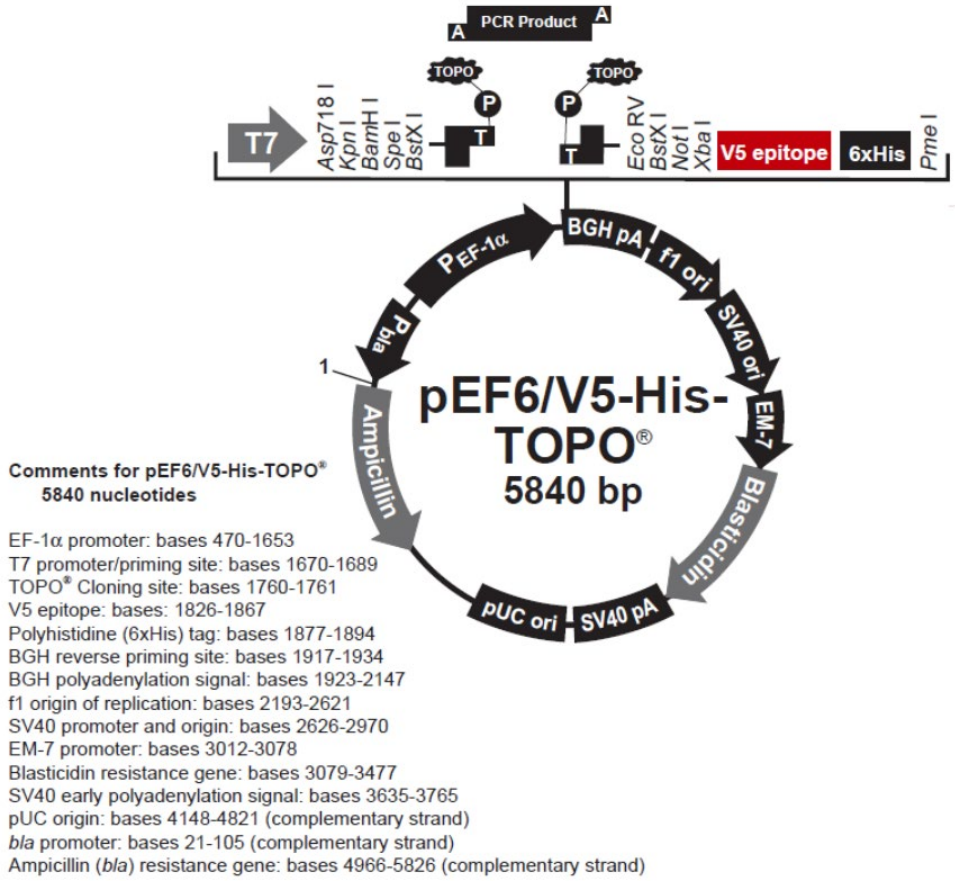

The one step cloning process to produce the plasmid vector takes the amplified PCR product for GREM1 and uses a DNA topoisomerase to insert the sequence for GREM1 between the TOPO cloning sites of the plasmid vector. The plasmid can then be cloned using the Oneshot®TOPO E.Coli cloning system, plasmid purified as described in section 2.5 and then transduced into cells to create overexpression of GREM1 in the target cells.

Following purification and quantification of plasmids (as described in section 2.5), 10µg of GREM1 overexpression plasmid, and 5µg control empty pEF plasmid, was used to transfect mammalian cell lines using electroporation. MCF7, MDA MB 231 and BT474 were grown to confluence and then washed with PBS, detached from cell flasks using trypsin EDTA, pelleted, resuspended, and counted as described above. Following this, 1x 10^6 cells in 1ml media were placed in a 4mm sterile electroporation cuvette with the plasmid added. The cuvette was loaded into a Cell Pulser Xcell™ Total System (BioRad, Hertfordshire, UK) and was pulsed with electricity (see Table 2.7 below for electroporation conditions).

Table 2-7 Electroporation conditions for cell lines

Cell line	Voltage	Capacitance(μF)
MCF 7	290	1000
MDA MB 231	310	1500
BT474	290	1000

The electrical pulse causes cell membrane disruption, and the current flow allows the plasmid to enter the cell, with resultant integration of plasmid DNA. Cells were immediately transferred into 5ml of prewarmed media in a T25 flask and placed in an incubator under standard incubation conditions overnight. Cells were selected the following morning for 14 days in appropriate cell line media containing 5μg/ml Blasticidin S (Melford, Suffolk, UK). Cells were subsequently maintained in 0.5μg/ml Blasticidin, and once at sufficient confluence, RNA and protein was extracted as above for determination of overexpression of GREM1 compared to control vector. These GREM1 overexpressing cells were then used in further experiments and maintained at low passage numbers.

2.8 Cell Function Assays

Cell function assays are a simple way of examining how cells respond to alterations in gene expression, or their environment, or response to treatments. Assays can be done to examine the effect of these factors on many different aspects of cell function such as cell growth, proliferation, cell death, metabolism, motility, invasiveness, and cell cycle. Culturing cells in 2D, with an adherent monolayer is simple, low cost and is how most functional assays for *in vitro* cell work have been developed. However, 2D culture does not represent how cells within a tumour mass interact in terms of cell to cell and cell to extracellular environment. These kinds of interactions can influence the cellular functions. In 2D culture the cells have access to all the ingredients and nutrients of the media, which is good for a more regulated and less variable cellular response, but this again does not represent the natural architecture of a tumour mass, which will have variation in the availability of nutrients and oxygen(Kapalczynska et al. 2018).

To try and culture cells in 3D as spheres rather than as a monolayer may better represent morphology, polarity, and cell to cell interactions, although, these approaches are less well established than 2D culture assays. The use of a non-adherent round bottomed culture well reduces the interaction of the cells with the plate, and instead encourages the cells to form into spheroids. Spheroids have been shown to have more cell to cell contact, more contact with extracellular matrix components (if the spheroid is cultured in a scaffold of extracellular matrix proteins) and has a diffusion gradient of nutrients, waste, oxygen and drugs(Bialkowska et al. 2020). In addition, demonstrating functional effects on cancer cells in different ways can add to the robustness of the experimental findings, so both methods were utilised in function assays.

2.8.1 Growth Assay (2D and 3D)

Cell growth of control and experimental cell lines was measured using an *in vitro* tumour proliferation assay. Approximately, 3,000 cells per well were seeded into a 96-well plate (Nunc, Fisher Scientific, UK) with 200µl of cell medium and placed in standard cell culture conditions. In total, three plates were seeded to obtain proliferation readings at time points of Day 1, Day 3, and Day 5. Plates were seeded approximately 24 hours prior to the start of the first time point (Day 1). Cell proliferation at Day 3 and Day 5 time points were compared to the control (Day 1). For each experiment, samples were run in triplicate. After each incubation period (Day 1, 3 or 5), cells were fixed in 4% formalin for 10 minutes before staining for 10 minutes with 0.5% (w/v) crystal violet in distilled water. The plates were washed with water and the cells lysed using 200µl 10% acetic acid (v/v) to release the crystal violet stain. Absorbance was measured at a wavelength of 540nm on an ELx800 plate reading spectrophotometer (Bio-Tek, Wolf laboratories, UK).

The percentage of cell proliferation was determined using the following equation:

$$\text{Percent Growth Increase} = \frac{\text{Absorbance Day x} - \text{Average day 1 absorbance}}{\text{Average day 1 absorbance}} \times 100$$

For 3D growth assay 3,000 cells were seeded into a 96 Ultra low attachment round bottomed well plate (Corning, USA) in 140µl culture media and incubated in standard cell culture conditions, after centrifuge of the plate at 300g for 3 minutes to centralise the cells in spheroid formation. Spheroids were examined 24 hours after seeding and photographed at x10 magnification. Spheroids were then

imaged at the same magnification every 48 hours for up to 14 days (depending on cell line) and media carefully exchanged every 4 days. Experiments were repeated in triplicate.

The images were processed using Image J software to calculate spheroid area and percentage change in spheroid volume compared to Day1 as follows:

$$\text{Percent change in spheroid area} = \frac{\text{Area on Day x} - \text{Average area day 1}}{\text{Average area day 1}} \times 100$$

2.8.2 MTT Assay

The MTT assay is a colorimetric assay that measures cell metabolic activity, and therefore its purpose is different, but complimentary to the cell growth assay described above. The MTT assay measures viable cell activity and metabolism, rather than proliferation per say. Viable cells with active metabolism convert MTT (3-(4,5-dimethylthiazol-2-yl)-2,5-diphenyltetrazolium bromide) into a purple-coloured formazan precipitate. When cells die, they lose the ability to do this and so the purple colour formazan serves as a marker of only viable cells. The formazan must be solubilised to take a colorimetric reading.

In a 96 well plate (Nunc, Fisher Scientific, UK) 3,000 cells were seeded in 100µl culture media and incubated for 24 hours in standard conditions After 24 hours 10µl of MTT(3-(4,5-dimethylthiazol-2-yl)-2,5-diphenyltetrazolium bromide, Sigma Aldrich, UK) to a final concentration of 0.5mg/ml, was added to each well, and incubated for 3 hours. The culture medium was removed and 150µl of MTT solvent (Sigma Aldrich, UK) was added. The plate was wrapped in foil and placed on a shaker for 15 minutes. Finally, absorbance was read on a ELx800 plate reading spectrophotometer (Bio-Tek, Wolf laboratories, UK) at 590nm.

2.8.3 Invasion Assay (2D and 3D)

An important cancer cell function is that of invasiveness, as a marker of cancer metastasis. To reflect this *in vitro,* a transwell invasion assay quantitates the degree to which cancer cells can penetrate a barrier of basement membrane and extracellular matrix components, in response to the chemoattractant properties of the growth factors in culture media with serum.

This invasion assay utilises a chamber, or insert, the bottom of which has a porous membrane through which cells can pass. The bottom of the chamber is lined with

commercially available extracellular matrix extract called Matrigel (Table 2.3). This is an extracellular matrix extract from a mouse sarcoma that is enriched in basement membrane components such as laminin and collagen. At low temperatures it is in liquid form, which allows its dilution in serum free media and coating of the inserts, but then will precipitate into a gel at temperatures above 8^0C. More invasive cells will invade into the gel and through the porous membrane of the insert, to sit on the underside of the insert. At the end of the assay, any non-invaded cells and Matrigel is removed from the inside of the insert and the cells on the underside fixed and stained to determine the proportion of cells that have invaded.

For the assay,8µm pore transwell inserts (FALCON®, pore size 8.0µm, 24 well format, Greiner Bio one, Germany) were placed into wells of a 24 well plate (NUNC™, Greiner Bio one, Germany), in sterile conditions to prevent contamination.

Each insert was coated with 100µl of serum free media containing 50µg Matrigel (stock concentration 0.5µg /µl) and left to dry for 2 hours at 55°C. The Matrigel was then rehydrated with 200µl sterile water at room temperature for 45 minutes. After aspirating and discarding any remnant water, 20,000 cells, in 200µl serum free medium, were seeded into each insert, with 600µl of medium with FCS then added to the bottom chamber of each well. A control well for each cell line without the insert, but with 20,000 cells in the same volume and composition of culture medium, was also seeded to account for baseline cellular proliferation. The cells were incubated for 72 hours, with 5% CO2 at 37°C.

After 72 hours incubation, the Matrigel layer and the non-invasive cells were then removed from the inside of the insert using a cotton bud. This left just the cells that had invaded through the Matrigel and pores of the insert and established on the underside of the insert. These cells, along with those cells in the control wells, were then fixed with 4% formalin for 10-20 minutes and then stained with 0.5% crystal violet for 10 minutes. The crystal violet was then washed off and the plate was left to airdry. The stained cells were subsequently counted and photographed under the microscope before extraction with 200µl 10% acetic acid (v/v). Absorbance was measured at a wavelength of 540nm on an ELx800 plate reading spectrophotometer (Bio-Tek, Wolf laboratories, UK).

Invasion could then be compared as follows:

$$\text{Percentage Invasion} = \frac{\text{Absorbance invaded cells}}{\text{Absorbance control well cells}} \times 100$$

As with the growth assay, to add to the robustness of results and to further examine how tumour cells might behave *in vivo*, a 3D invasion assay was also performed. This is undertaken by first creating a spheroid with the cells in a round bottom non adherent well plate, and once the spheroid is established, replacing the culture media with Matrigel around the spheroid. This allows us to establish invasion of cancer cells into the Matrigel in 3D. However, this must also be done in conjunction with the proliferation and growth assays, as proliferation rather than invasion can contribute to spheroid volume.

For 3D invasion assay 3,000 cells were seeded into a 96 Ultra low attachment round bottomed well plate (Corning, USA), in 140µl standard culture medium and incubated in standard cell culture conditions, after centrifuge of the plate at 300g for 3 minutes, to centralise the cells in spheroid formation. Spheroids were grown for 3 days, at which point 50µl of culture medium was aspirated gently from each well and replaced with 50µl Matrigel. Each well was checked to ensure no disruption of the spheroid and the plate centrifuged at 300g for 3 minutes to centralise the spheroid again. The plate was incubated for 1 hour at 37^{o}C to allow the Matrigel to solidify. The well was then topped up with 60µl culture media. Spheroids were photographed at x10 magnification the following day, as Day 1, and then photographed every 48 hours for up to 14 days. Every 4 days, 60µl of culture medium was carefully aspirated off and replaced. Experiments were repeated in triplicate.

The images were processed using Image J software to calculate spheroid area and percentage change in spheroid area compared to Day 1 as follows:

$$\text{Percent change in spheroid area} = \frac{\text{Area on Day x} - \text{Average area day 1}}{\text{Average day 1 area}} \times 100$$

2.8.4 Migration Assay

For migration assays, the same principles apply as the invasion assay, except there is no basement membrane Matrigel in the well inserts, and this assay purely looks at the motility of the cells, their ability to move through the porous membrane. This was chosen above a ‘wound scratch’ assay. In a wound scratch assay cells are grown to near confluence in a 6 or 24 well plate and a pipette tip

dragged manually in a line down the centre of the well, to create a gap in the cells that is then monitored for how rapidly the cells close this gap. This approach whilst simple and widely used can have variation introduced by inconsistencies in the wound scratch formation and that the cells may fill the wound gap by proliferation rather than migration. The use of a porous membrane however through which the cells must migrate is more consistent, and a control well without the membrane to account for cell proliferation addresses the issue of the cells merely proliferating once they have migrated through the membrane.

For this assay 8µm pore transwell inserts (FALCON®, pore size 8.0µm, 24 well format, Greiner Bio one, Germany) were placed into wells of a 24 well plate (NUNC™, Greiner Bio one, Germany), in sterile conditions to prevent contamination. Each insert was seeded with 20,000 cells, in 200µl serum free medium, with 600µl medium with FCS then added to the bottom chamber of each well. A control well for each cell line without the insert, but with 20,000 cells in the same volume and composition of culture media, was also seeded to account for baseline cellular proliferation. The cells were incubated for 72 hours, with 5% CO_2 at 37^{o}C.

After 72 hours incubation, non-migrated cells were removed from the inside of the insert using a cotton bud. This left just the cells that had migrated on the underside of the insert and in the bottom of the well. These cells, along with those cells in the control wells, were then fixed with 4% formalin for 10-20 minutes and then stained with 0.5% crystal violet for 10 minutes. The crystal violet was then washed off and the plate was left to airdry. The stained cells were subsequently counted and photographed under the microscope before extraction with 200µl 10% acetic acid (v/v). Absorbance was measured at a wavelength of 540nm on an ELx800 plate reading spectrophotometer (Bio-Tek, Wolf laboratories, UK).

Migration could then be compared as follows:

$$\text{Percentage Migration} = \frac{\text{Absorbance migrated cells}}{\text{Absorbance control well cells}} \times 100$$

2.8.5 Colony Forming Assay

This is an *in vitro* cell survival assay, based on how capable a single tumour cell is at unlimited replication, to form a colony of cells from a single parent cell and reflects cell survival.

For each cell line tested, cells were resuspended in culture media after trypsinisation, pelleting, washing, and counting, at a quantity of 200 cells per ml. One ml of cells was then dispersed in a further 2ml of culture medium per well on a 6 well plate. The plate was incubated at the appropriate conditions for the cell line for two weeks, or until countable colonies had formed. The medium was then aspirated, the cells gently washed to remove non adherent cells and debris, then fixed for 10 minutes with 4% Formalin, and stained with 0.5% crystal violet for 10 minutes. The crystal violet was washed away with water and the plate left to air dry. Colonies were then counted.

2.9 In Vitro Bone Model Assays

2.9.1 Bone Matrix Extract (BME)

BME was used in tumour functional assays to replicate a bone like microenvironment in tumour cell functional assays (See Table 2.3). This extract is the extracellular matrix of natural human bone containing collagens, proteins, minerals, growth factors and osteogenic substances that are an essential part of the bone environment. In this setting, BME is used to analyse whether its presence enhances or inhibits the migration and invasion of breast cancer cells, reflecting the ability of the breast cancer cells to establish within the bone environment.

BME had previously been prepared by the laboratory using fresh human bone tissue, obtained with consent during hip replacement surgery. The tissue was crushed at ice cold temperature prior to processing using a Bone Mill (Splerings Orthopaedics B.V., The Netherlands) and subsequently a BioRuptor (Wolf Laboratories, York, UK) to solubilise and extract matrix proteins in PBS buffer. For use in the following assays an aliquot of stock BME (at concentration 2mg/ml) was removed from the freezer and allowed to thaw at room temperature. BME was then diluted in cell culture medium to a working concentration of 100µg/ml.

2.9.2 Co-Culture Adhesion Model

To examine how BT474 tumour cells might locate to a bone microenvironment, a co culture model was undertaken to examine adhesion of DiI labelled BT474 cells (both control and GREM1 overexpressing) to a layer of hFob (human foetal Osteoblast) cells. DiI (or tetramethylindocarbocyanine perchlorate) is a lipophilic membrane stain that is only weakly fluorescent until incorporated into membranes, when it will maximally fluoresce orange red at a light wavelength of 549nm. It is a very stable and long-lasting fluorescent dye.

The day before the adhesion experiment 8,000 hFob cells were seeded per well on a 96 well plate and incubated overnight at 34^{o}C to make a monolayer of osteoblast cells. To stain the cancer cells with DiI, first 2 x10^{5} tumour cells were pelleted in a 4^{o}C centrifuge at 5,000g for 5 minutes. The pellet was washed with PBS and centrifuged again to pellet. The cells were then re suspended in 1ml of culture medium, with 20µl of stock DiI (at 5mg/ml concentration) added to the cells which were incubated for 40 minutes at 37^{o}C. After incubation the cells were centrifuged at 5000g for 5 minutes to pellet and then washed with PBS and centrifuged a further two times. This resulted in a pink coloured pellet which was then resuspended in culture medium. Twenty thousand stained tumour cells were then added to the wells containing hFob cells and this was returned to the incubator at 37^{o}C for 6 hours. The controls comprised tumour cells added to wells without any hFob cells to demonstrate adhesion without the presence of osteoblasts, and hFob wells with no tumour cells added to demonstrate no background staining or fluorescence of hFob cells.

After incubation the medium was removed from the wells and the wells were washed once with PBS to remove non adherent cells. The cells were then fixed in 100µl 4% Formalin per well. Each well was imaged with fluorescent microscopy in 3 random fields for cell counting of the DiI labelled tumour cells, with 6 repeats per cell line and experimental repeat in triplicate. The average number of adherent tumour cells could then be compared between control BT474^{PEF} and GREM1 overexpressing BT474^{GREM1}.

2.9.3 Co-Culture Migration and Invasion Assay

As described above, to examine how tumour cells may be influenced by the bone environment, tumour cell migration and invasion were examined in the presence of either osteoblast cells(hFob), or bone matrix extract (BME).

The day before the experiment, 40,000 hFob cells were seeded into 6 wells of a 24 well plate (NUNC™, Greiner Bio one, Germany). The following day 8µm pore transwell inserts (FALCON®, pore size 8.0µm, 24 well format, Greiner Bio one, Germany) were placed in 18 of the wells in sterile conditions to prevent contamination. For invasion assay the insert had a membrane of Matrigel at the base, as described in section 2.8.2 above.

Each insert was seeded with 20,000 cells, either $BT474^{PEF}$ or $BT474^{GREM1}$ in 200µl serum free medium, with either hFob cells in 600µl culture medium on the bottom chamber of each well, or 600µl normal culture medium with 100µg/ml BME, or 600µl normal culture medium with nil addition (see Figure 2.3). A control well for each cell line without the insert, but with 20,000 cells in the same volume and composition of culture medium, was also seeded to account for baseline cellular proliferation. The cells were incubated for 72 hours, with 5% CO2 at 37ºC.

Figure 2-4 24 Well Plate set up for co-culture migration and invasion assays

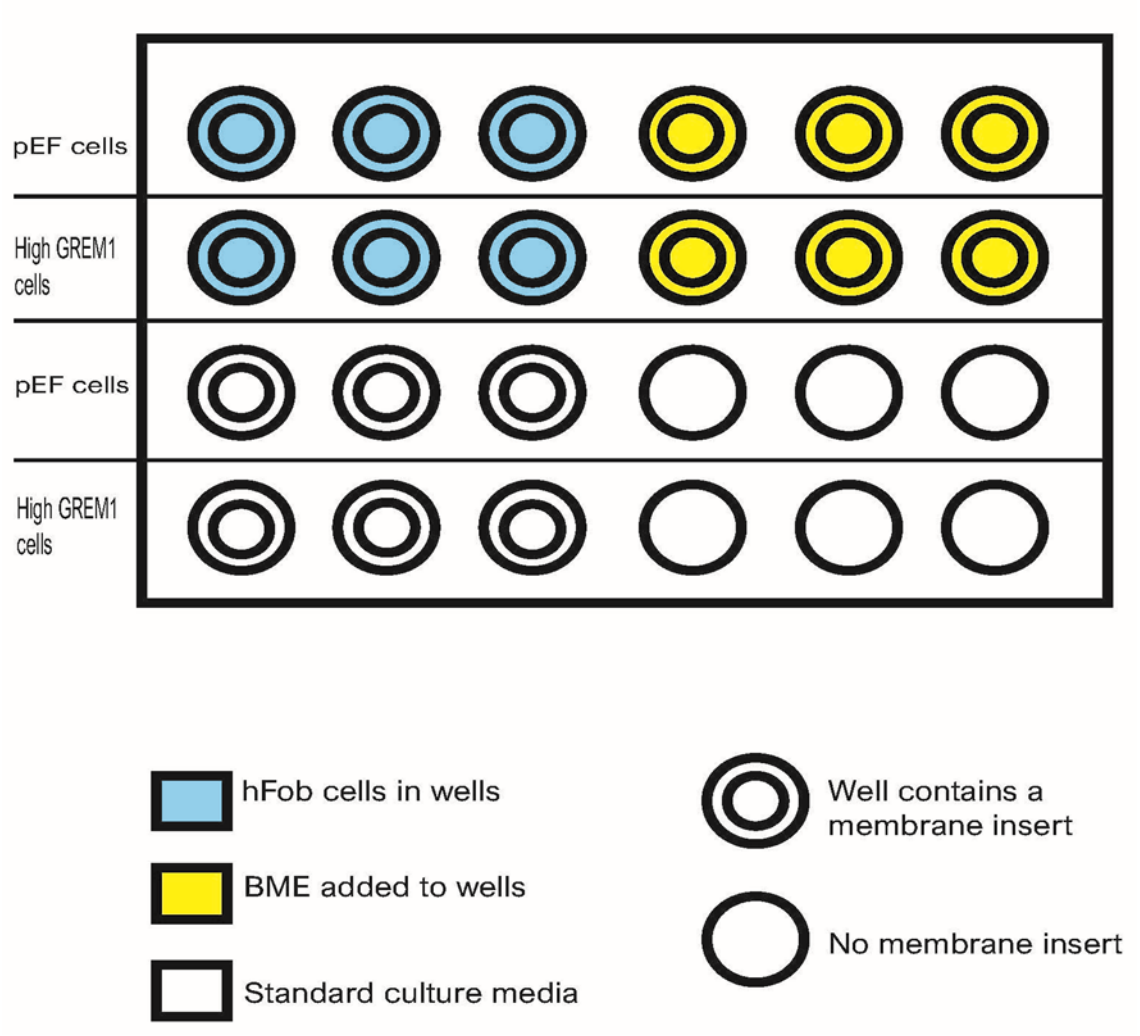

After 72 hours incubation, as per the previous migration and invasion assays described above, non-migrated/invaded cells were removed from the inside of the insert using a cotton bud. This left just the cells that had migrated/invaded on the underside of the insert. These cells, along with those cells in the control wells, were then fixed with 4% formalin for 10-20 minutes and then stained with 0.5% crystal violet for 10 minutes. The crystal violet was then washed off and the plate was left to airdry. The stained cells were subsequently counted and photographed under the microscope before extraction with 200µl 10% acetic acid (v/v). Absorbance was measured at a wavelength of 540nm on an ELx800 plate reading spectrophotometer (Bio-Tek, Wolf laboratories, UK). Experiments were repeated in triplicate. Migration/Invasion could then be compared as follows:

$$\text{Percentage Migration/Invasion} = \frac{\text{Absorbance migrated/invaded cells}}{\text{Absorbance control well cells}} \times 100$$

2.10 Cell Treatment Assays

2.10.1 HER2 Inhibitor CP724714 Assay

Approximately, 2 x 10^6 cells were seeded in each well of a 6 well plate. The following day, cells were washed with PBS and media was replaced with Phenol red free RPMI media, with charcoal stripped FCS. Phenol red in culture media has been found to act as a weak oestrogen, and FCS in its usual form has oestrogens within it. Removal of Phenol red and stripping of oestrogen from FCS is necessary for assays where we want to minimise the impact of the oestrogen receptor pathway signalling. As BT474 are known to strongly express ER (Al-Bader et al. 2011; Ford et al. 2011), we have removed ER stimulus when examining the HER2 pathways. The HER2 selective small molecule tyrosine kinase inhibitor CP724714 (developed by Pfizer, obtained from Sigma Aldrich, UK) was selected as a potent and selective inhibitor of HER2, with an IC50 of 10nM. It is 640 times more selective for HER2 than EGFR. A highly specific HER2 inhibitor was favoured above the clinically used HER2 inhibitors Trastuzumab and Pertuzumab, as these medications have off target effects that could not be controlled for and would confound experimental findings.

CP724714 was added to wells at a concentration of 40nM in Phenol red free RPMI with charcoal stripped FCS media, with treatment times of 4 hours and 24 hours. These times were selected as a 4-hour treatment is long enough to see effects on changes in gene expression and protein production, and 24 hours should demonstrate the resolution of the effect as the small molecule inhibitor is used up and the cells compensate for the temporary HER2 inhibition. A treatment time course can be done to fine tune this process if necessary. The control was media vehicle with no inhibitor added. Treated cells were then harvested as described in previous sections for RNA and protein extraction.

2.10.2 Treatment with recombinant Gremlin1

Approximately, 2 x 10^6 cells were seeded onto 6 well plates the day prior to experiment. Recombinant (Rh) Gremlin1 has an IC50 for inhibiting BMP-2 induced luciferase activity at 34 ng/ml, and in other experimental work demonstrated inhibition of BMP-4 activity at 100-200ng/ml and BMP-7 activity at 400ng/ml (Church et al. 2015; Laulan and St-Pierre 2015; Kišonaitė et al. 2016). As Gremlin1 preferentially affects BMP-2 and 4, effect dose of 200ng/ml was chosen as a basic treatment dose for BMP inhibition, and 600ng/ml as a high dose, to

reflect high Gremlin1 concentration environment. The day of the experiment, cells were washed with PBS and medium refreshed with either 200ng/ml or 600ng/ml RhGremlin1 and treated for 6 hours based on the methodology of published work(Laulan and St-Pierre 2015), before cells were harvested for RNA extraction.

2.10.3 BMP and Gremlin1 treatment for signalling pathway activation

To examine the influence of Gremlin1 on signalling pathways in BT474 cells, 2 x 10^6 cells were seeded into a 6 well plate. The following day cells were placed in serum free, Phenol red free RPMI media and serum starved for 2 hours.

Based on prior literature and the supplier's technical data(Calpe et al. 2015; Church et al. 2015; Laulan and St-Pierre 2015), 150ng/ml RhGremlin1 will inhibit cellular proliferation induced by 30ng/ml RhBMP-4, and 500ng/ml RhGremlin1 will inhibit 10ng/ml RhBMP-4 activation of an ID1 luciferase reporter. In order to find the peak activity time for signalling pathways 10ng/ml RhBMP-4 was selected to treat the cells for a time trial period of 15 minutes, 30 minutes, 1 hour, 2 hours and 4 hours, harvesting the cells for protein extraction at these time points to analyse with Western blot for phosphorylated(p) smad1/5/8, pAKT and pERK (as per technique section 2.4 and using antibodies listed in Table 2.2).The control used was βActin. This failed to show significant activity after three repeats. BMP-4 concentration was then increased to 40ng/ml with successful activity.

Following this primary time trial, 2 x 10^6 BT474 cells, after starvation for 2 hours, were treated for 1 hour with plain vehicle medium (negative control), or 40ng/ml RhBMP-4, or 500ng/ml RhGremlin 1, or 40ng/ml RhBMP-4 followed after 30 minutes by 500ng/ml RhGremlin 1, or 10mM Pervanadate (positive control). Protein was then extracted for Western blot analysis of pSmad 1/5/8, pERK and pAKT with antibodies and concentrations as listed in Table 2.2.

2.11 *In Vivo* Mouse Models

To produce *in* vivo mouse models, 28 balb/c nude female mice aged 4-6 weeks were purchased from Charles River Laboratories (Charles River Laboratories International, Inc., Kent, England, UK) and settled for 2 weeks before use. For successful engraftment of human cells, the mice must be immunocompromised. Balb/c nude mice lack a thymus, and are therefore immune deficient, which allows human cells to be engrafted and grow tumours. There are prior successful experiments using this mouse type with BT474 cell lines(Khalili et al. 2005; Wang et al. 2005; Chen et al. 2017).Balb/c mice have an advantage over the more

expensive and more immune compromised NSG(NOD SCID Gamma) mice as Balb/c mice are less prone to thymic lymphoma and are nude, which makes measurement of primary tumour engraftments easier. Balb/c mice also have the advantage over the more commonly used athymic nude mice, as they do not require oestrogen supplementation to force tumour growth, and the laboratory had recent difficulty with athymic nude mice not being fully hairless from the supplier. The Balb/c mouse was therefore felt to be the best experimental option.

Experiments were conducted under Home Office Project licence (PPL: PE944FC2, held by the laboratory at Cardiff University in an online format) and I was trained and granted a personal licence (PIL) for A and B level procedures in mice (PIL number: I503919EB – see Appendix V). I undertook all experimental work, with supervision for intracardiac injection by Dr Lin Ye, who has significant experience in this procedure.

All mice were kept in filter-topped isolation cages and all procedures were carried out in a class-II cabinet. One mouse was terminated prior to any experimental work due to a cystic growth (Figure 2.5):

Figure 2-5 Cystic Growth in Mouse

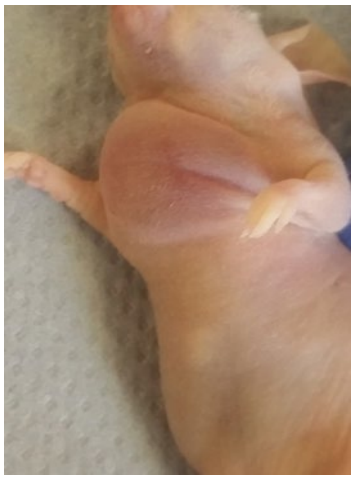

$BT474^{PEF}$ and $BT474^{GREM1}$ cells were washed and counted as described in section 2.2.5. On the day of injection, 40 x 10^6 cells of each were diluted in PBS to 2.5 x 10^6 /50µl and an equal volume of 5mg/ml Matrigel was added, with final concentration of 2.5 x 10^6 cells/100µl solution for injection into each 4th mammary fat pad. This model recreates primary breast tumour development by placing the cells in the breast environment, which is preferable rather than a standard subcutaneous placement of tumour cells. All mice were weighed and examined for tumour growth on a twice weekly basis for twelve weeks, with tumours measured

by digital callipers in width and length. At the end of the experiment mice were culled and the mammary fat pads excised and fixed in 4% formalin.

Tumour volume(mm^3) was calculated as = (Length x Width x Width)/2.

For a model of metastatic breast cancer, injection of the cells into the arterial circulation via a cardiac injection gives a more widespread metastasis, but particularly favours bone metastasis, as is the focus of this thesis. Injection into the venous circulation via the tail vein would give predominantly lung metastasis, so, although tail vein injection is easier and has less risk of procedural complication, it would not be the optimal model(Gomez-Cuadrado et al. 2017).

For intracardiac injection 150,000 cells were suspended per 150µl PBS, using a fine needle to prevent clumping (any clumping of cells can produce embolic or stroke events when injected into the mice), and kept on ice. Mice were given inhaled anaesthesia (3% isoflurane/100% O_2 in an induction chamber) and maintained with isoflurane and O_2 via a nose cone. Anaesthesia was confirmed when no withdrawal reflex was observed with toe pinch and the mouse taped in position on a foam pad to maintain body temperature. A 22G needle was used to draw up 150µl containing 150,000 cells and the tip aimed at the left ventricle of the heart. A flashback of arterial colour blood was expected to confirm correct placement before slow injection of the cells. This procedure was undertaken with Dr Lin Ye, as an experienced user of this model. One mouse had periprocedural arrest and one mouse developed symptoms of stroke the following day requiring termination. Mice were weighed twice weekly and examined for signs of metastatic malignancy for 12 weeks.

To determine metastasis of the tumour cells Positron Emission Tomography (PET) computed tomography (CT) imaging was chosen as a very sensitive method that we are fortunate to have access to at Cardiff University. A PET scan uses a radioactive tracer combined with glucose molecules, which is taken up on injection by rapidly metabolising cells in tumours, emitting a radioactive signal that is detected by the PET scanner. A CT is undertaken at the same time to image the body such that the radioactive signal can be co-located. This method of imaging can detect tumour deposits as small as 1mm and is used clinically in oncology for the staging of certain cancers(Koba et al. 2013).

Mice that had undergone intracardiac injection were examined with PET CT for evidence of metastasis after 12 weeks from injection. They were housed in filter

top cages in The Wales Research and Diagnostic Positron Emission Tomography Imaging Centre (PETIC) with injection/scan protocol devised and administered by Dr Stephen Paisey. I assisted with anaesthesia of the mice and injection of the mouse tail vein.

Mice were anaesthetised after 12 hours starvation (starvation reduces the metabolism of the tissues and thus reduces background tracer signal) with 3–3.5% isoflurane/100% O2 via nose cone and placed on the heating pad, then 10MBq (Megabecquerel) of the radioactive tracer 18F- Fluorodeoxyglucose(18F-FDG) was intravenously injected at the tail vein using 22G insulin syringes. Mice were placed prone in the scanner in a 2-mouse animal bed (Mediso, Budapest, Hungary), and 1.5–2%/100% O2 isoflurane anaesthesia was maintained via nose cone. PET imaging, followed by CT, was performed using PET/CT Preclinical Imaging System (nanoScan122S PET/CT Mediso, Budapest, Hungary). Respiration was monitored with pressure pad during PET/CT examination. PET scans were performed 1 h after injection and emission data collected for 20 minutes, followed by CT scan. Images were reconstructed using in house Matlab® software (Mathworks, USA). PET CT ‘hotspots’ were then identified by me and Dr Paisey, and these areas targeted for dissection after culling of the mice.

2.12 Statistical Analysis

Statistical analysis was performed using GraphPad Prism (GraphPad Software, California, USA). Each experimental protocol was performed at least three times (unless stated otherwise) and data obtained were presented as the mean of the repeats with standard error of the mean (SEM). Comparison between test groups was performed for normally distributed data using a two sample, two tailed t-test paired or unpaired. For non-normally distributed data a Mann Whitney U test was used for 2 independent data groups and Wilcoxon Signed Rank test for dependent groups. Comparison of more than two groups used ANOVA or Kruskall- Wallis depending on data normality. To assess the strength of a liner association between two variables, the Pearson’s correlation co-efficient was utilised. P value of ≤ 0.05 was statistically significant.

Image J is an open source, image processing toolkit available in the public domain, developed by the National Institutes of Health and the Laboratory for Optical and Computational Instrumentation (USA). This was used for densitometry comparisons for PCR and Western blot analysis.

3 The expression and clinical relevance of Gremlin1 in Breast Cancer

3.1 Introduction

Gremlin1 is a secreted protein antagonist of BMPs -2, -4 and -7, which exerts its antagonist effect by directly binding to BMPs and preventing ligand-receptor interaction (Namkoong et al. 2006). Gremlin1 has been shown to have greater affinity binding with BMP-2 and -4 than BMP-7 (Church et al. 2015). Previous studies demonstrating primary breast tumour expression of BMP -2, -4 and -7 are small and used varying methodologies. Bobinac et al examined 15 breast carcinomas (all patients had confirmed bone metastases) using IHC and compared to 5 normal breast samples. BMP-7 was highly expressed in the breast carcinoma, but not BMP-2 or -4 (Bobinac et al. 2005). In a study with 39 primary breast tumours, RNA expression was studied and showed 85% expressed BMP-2 whilst 100% expressed BMP-4 and -7 (Alarmo et al. 2007). In the largest study, 120 breast cancer samples and 32 background samples were examined at both RNA and protein level. BMPs-2 and -7 appeared lower on IHC staining in breast cancers compared to normal tissue, with weak BMP-4 staining in normal and cancer tissues. The RNA expression of BMP-2 and -4 was lower in breast cancers and BMP-7 was higher, but results did not reach statistical significance (Davies et al. 2008). Definitive evidence of up or down regulation of Gremlin1 ligands in breast cancer remains elusive.

There is little available literature regarding the expression of Gremlin1 in breast cancers. Laurila et al examined a tissue microarray of several normal tissues and several different solid cancers. This included 3 normal breast samples and 16 breast cancer samples and Gremlin1 staining was found to be weak in normal breast, and weak to moderate in breast carcinoma. However, this was not quantitatively assessed or statistically compared (Laurila et al. 2013). Schuetz et al took 9 tumours, with both invasive and in situ disease, and sampled cells with laser capture microdissection to compare differentially expressed genes between DCIS and invasive ductal carcinoma (IDC). GREM1 mRNA was found to be more highly expressed in IDC than DCIS (Schuetz et al. 2006).

To determine the role for Gremlin1 in breast cancer, it is important to expand on the available data and attempt to define more clearly any up or downregulation of Gremlin1 expression (and that of its BMP ligands) in breast cancers, and whether this can be linked to the disease.

3.2 Methods

3.2.1 Clinical Cohort Immunohistochemistry

Previous work was performed by Dr Lin Ye on a cohort of 82 Breast cancer tissues and 24 normal background tissues. The methods described below were performed and completed by Dr Ye before the initiation of this PhD, were not part of my general methods, and the results provided to me for interpretation. Tissue samples were collected immediately after surgery and stored at -80^{o}C until use. The presence of tumour cells in the collected tissues was verified by a consultant pathologist, who examined stained frozen sections and confirmed the pathology results.

A small number of frozen sections of breast tumours, DCIS and background tissues were cut at a thickness of 6µm and mounted on a SuperFrost Plus™ (ThermoFisher Scientific Ltd, UK) microscope slide. The sections were air dried and fixed in a mixture of 50% Acetone and 50% methanol. The sections were then placed in "Optimax" wash buffer for 20 minutes to rehydrate. Sections were incubated for 20 minutes in a 0.6% BSA blocking solution and probed with goat polyclonal antibody against human Gremlin1 (Santa Cruz Biotechnology, Inc., CA, USA, SC-18274) for 1 hour at room temperature. Following extensive washings, sections were incubated for 30 minutes in the secondary biotinylated antibody (Multilink Swine anti-goat/mouse/rabbit immunoglobulin, Dako Inc.). Following washing, Avidin Biotin Complex (Vector Laboratories) was then applied to the sections followed by extensive washings. Diamino benzidine chromogen (Vector Labs) was then added to the sections, which were incubated in the dark for 5 minutes. Sections were then counter stained in Gill's Haematoxylin and dehydrated in ascending grades of methanol, before clearing in xylene and mounting under a cover slip. Photographs at different magnifications were then taken.

3.2.2 RT-qPCR from Clinical Cohort

Dr Ye also performed real-time quantitative PCR on homogenised tissue samples, based on the Amplifluor™ technology. Sequences for GREM1 were 5'-CTGCTGAAGGGAAAAAGAA for forward primer and 5'-**ACTGAACCTGACCGTACA**CGACTGAGTCTGCTCTGAGT for reverse primer (Z sequence in bold). The reaction, which used different reagents and methods at that time, was carried out using the following: Hot-start Q-master mix (Abgene),

10pmol of specific forward primer, 1pmol reverse primer with Z sequence, 10pmol of FAM-tagged probe (Intergen Inc.) and cDNA from 50ng of RNA. The reaction was carried out using IcyclerIQ (Bio-Rad, Surrey, England, UK), which is equipped with an optic unit that allows real-time detection of 96 reactions, under the following conditions: 94^{o}C for 12 minutes and 80 cycles of 94^{o}C for 15 seconds, 55^{o}C for 40 seconds, and 72^{o}C for 20 seconds. The levels of the GREM1 transcript were given as number of the transcript copies per 50ng RNA, generated from an internal standard, Podoplanin (PDPL) that was simultaneously amplified during the same quantitative real time PCR. Cytokeratin-19 (CK19) was used as the housekeeping gene against which to normalise. Forward and Reverse primers for CK19 were 5'-CAGGTCCGAGGTTACTGAC and 5'-**ACTGAACCTGACCGTACA**CACTTTCTGCCAGTGTGTCTTC, respectively.

3.2.3 Use of publicly available RNA expression databases

High throughput gene expression arrays allow significant amounts of gene expression and sequencing data to be generated. Researchers can upload their array data from clinical tissue cohorts to various repositories which hold hundreds of thousands of arrays from multiple species. Users can explore these databases for specific cell line or tissue cohorts and can examine genes of interest that may not have been the specific focus of the original researchers' work but were present on the array performed at the time of the experiment. One of the most used and wide-ranging databases is the Gene Expression Omnibus (GEO; www.ncbi.nih.gov/geo/) as well as Array Express, which imports all the data from GEO and has directly added data (www.ebi.ac.uk/Databases/microarray.html). Both sites provide all original data for download and analysis.

A search of the GEO database was performed for all experiments with the keywords 'breast cancer' and 'GREM1' and/or 'Gremlin1'. This returned 251 experiments that had GREM1 expression data for breast cancer cell lines or tissues under different experimental circumstances. Each of the 251 datasets was examined for relevance to comparable cohorts of normal breast tissues with breast cancer tissues, or cohorts with staging and clinical outcomes information. A total of 11 out of 251 were deemed suitable for initial analysis. Six were then excluded based on experimental methodology and low sample numbers, leaving 5 datasets for in depth analysis (Table 3.1).

Table 3-1 Experimental datasets examined

Dataset (Reference)	Protocol summary	Array used	GREM1 Probe ID	BMP-2 Probe ID	BMP-4 Probe ID	BMP7 Probe ID
GSE70951 (Subset 70905) (Quigley et al. 2017)	43 normal reduction mammoplasties 47paired tumours and adjacent normal breast tissue ***Total =137*** RNA preserved at time of surgery. Whole cell lysate	Agilent-014850 Whole Human Genome Microarray 4x44K G4112F	28118	30308	27400	10756
GSE70951 (Subset 70947) (Quigley et al. 2017)	148 paired breast tumours and adjacent normal tissue ***Total = 296*** Method as above	Agilent-028004 Sure Print G3 Human GE 8x60K Microarray	61098	n/a	n/a	n/a
GSE20685 (Kao et al. 2011)	***Total = 327*** breast tumours. Fresh frozen tissue and whole cell lysate	Affymetrix U133 plus 2.0	218469_at	205289_at	211518_s_at	209590_at
GDS3324 (Casey et al. 2009)	25 breast tumours and 5 normal reduction mammoplasty samples. ***Total = 30*** Laser capture microdissection of stromal and epithelial cells	Affymetrix Human Genome U133A 2.0 Array	218469_at	205289_at	211518_s_at	209590_at
GDS3853 (Kretschmer et al. 2011)	5 reduction mammoplasty samples 9 DCIS samples 5 IDC samples ***Total = 19*** Fresh frozen whole cell lysate.	Affymetrix U133 plus 2.0	218469_at	205289_at	211518_s_at	209590_at
GDS4761 (Kimbung et al. 2014)	***Total = 91*** Fine needle aspiration samples of breast cancer metastases from different metastatic sites	Human RSTA Custom Affymetrix 2.0 microarray [HuRSTA-2a520709]	218469_at	205289_at	211518_s_at	209590_at

3.2.4 Survival data from Kaplan Meier (KM) Plotter

KM plotter is a manually curated database of 5,143 breast cancer patients. This database is updated biannually. Gene expression data and relapse free and overall survival information are downloaded from GEO (Affymetrix microarrays only), European Genome-phenome Archive (EGA) and The Cancer Genome Atlas (TCGA).

The gene of interest's most validated array probe was selected, and the median selected as the cut off for high/low expression. The two patient cohorts were compared by a Kaplan-Meier survival plot, and the hazard ratio with 95% confidence intervals and log rank P value were calculated. The two groups of high or low gene expression could then be compared for overall survival (OS), relapse free survival (RFS) and distant metastasis free survival (DMFS). Length of follow up was chosen. Analysis was divided by ER status, PR status, HER2 status, lymph node status, tumour grade, intrinsic molecular subtype and patient treatment regimes. An overall readout was also given of median and inter-quartile expression values for any gene probe in the whole cohort of breast cancer and normal breast tissues.

For this analysis the Affymetrix best probe for GREM1, 218469_at, was selected. OS, RFS and DMFS Kaplan Meier plots were then calculated using KMplot to examine survival outcomes between those with high or low expression of GREM1 in their primary tumours. The longest survival timeframe was 300 months. No other sub-analyses were chosen at this stage.

3.3 Results

3.3.1 Aberrant expression of GREM1 and its BMP ligands in normal breast and carcinoma

The initial breast cohort examined by Dr Ye contained 82 breast carcinoma tissues and 24 normal breast tissues. When comparing the mean qPCR transcript copy numbers for GREM1 RNA expression in these tissues it appeared that, although the mean copy number was higher in breast carcinoma tissue compared to normal, this did not reach statistical significance (p = 0.19, Table 3.2).

Table 3-2 GREM1 expression in a cohort of Breast Cancer tissues

	Sample Number (n)	**Mean GREM1 transcripts** (Copies/50ngRNA +/- SE mean)	
Breast Carcinoma	82	118184±42394 (95% CI 35,100 to 201,000)	
Normal mammary tissue	24	56493±20950 (95% CI 15,400 to 97,600)	P = 0.19
Histological type			
Ductal	59	91530±38431	
Lobular	11	64187±61105	P = 0.082
Histological grade			
Grade 1	12	263178±172452	
Grade 2	31	60502±31852	P = 0.27
Grade 3	5	2795±1645	P = 0.16
TNM staging			
TNM1	2	650±350	
TNM2	25	35382±15626	**P = 0.036**
TNM3	5	2795±1645	P = 0.27
TNM4	4	652696±631500	P = 0.38

This cohort was also an historic cohort collected and processed prior to this thesis, of which I was given the data to analyse. Had this cohort been undertaken as a core part of this thesis, a larger cohort sample, or use of tissue banks, with more even numbers of the normal and carcinoma tissues, and the different grades and stages would have been beneficial and may have shown statistical significance of increased GREM1 expression in carcinoma compared to normal tissue. To use external tissue bank samples for RNA extraction in large numbers would have been prohibitively expensive, and to prospectively collect larger numbers of clinical samples, particularly of normal comparative tissues locally would have taken prohibitive length of time. Normal breast tissue for the purpose of comparative expression studies should be collected from those undergoing breast reduction surgery with no personal or family history of breast cancer, and there are restrictions within the national health service in Wales regarding clinical qualification for this type of surgery that would reduce the availability of this tissue.

An alternative that has become possible with the advent of high throughput DNA microarrays is to examine gene expression utilising data from published experimental work that is available in public data repositories. A DNA microarray can examine the expression of many genes in a sample in one experiment. To publish any work that involves microarray results, it is mandatory to deposit all the raw data and experimental conditions according to worldwide accepted guidelines. There are now several databases that collate this data of guideline compliant microarrays, such that researchers have public access to large amounts of expression data that can be utilised to support their research projects.

Publicly available data from KMplot was used to look at RNA expression levels of GREM1 and its ligands in 6547 breast tumour samples and 76 normal breast samples. (Table 3.3) This demonstrated significantly higher expression of GREM1 and significantly lower expression of BMP-2 in breast cancers compared to normal tissue ($p < 0.0001$). BMP-4 was lower, and BMP-7 higher compared to normal breast tissues, although this only just reached significance ($p = 0.05$).

Table 3-3 KM Plot expression of GREM1 and BMP ligands in Breast Cancer samples and normal breast tissue

Gene (Array ID)	Normal breast median expression (IQR) N=76	Breast carcinoma median expression (IQR) N=6547	P value
GREM1 (218469_at)	242(65-429)	633(351-1093)	<0.0001
BMP-2 (205289_at)	168(31-285)	50(27-84)	<0.0001
BMP-4 (211518_s_at)	44(13-346)	28(15-102)	0.05
BMP-7 (209590_at)	111(75-203)	140(73-241)	0.05

One of the limitations with utilising a large, pooled database is that although strict data compliance requirements are met, there is variation of the methodologies and patient populations in the studies pooled, which can potentially skew the findings. Using the GEO database, individual studies comparing normal and breast cancer tissues can be examined more selectively to answer more specific questions. However, many of the studies that had data on GREM1 expression in normal breast tissue and breast cancer tissue, were of small size (5-10 tumours), unpaired samples, and of mixed or undefined tumour type.

The largest tissue cohort in the GEO database that was found was GSE70951. This had gene expression data for 47 paired samples of breast tumours and tumour associated stroma, compared to 43 normal specimens from reduction mammoplasties, from which RNA was extracted and

examined with a multi gene expression microarray(Quigley et al. 2017). Interestingly in contrast to the pooled gene expression data from KMplot, this single cohort showed GREM1 expression was lower in tumour compared to normal breast ($p = 0.005$, Figure 3.1A), which is likely due to the smaller sample numbers than the pooled database, and different methodology.

What this cohort has that the pooled databases such as KMplot do not is matched tumour adjacent stroma. With whole tissue lysate databases, it will not be clear as to whether the increased GREM1 expression in the tumour samples are from tumour cells, or increased GREM1 expression in the stroma. In the matched tumour and tumour associated stroma samples for GSE70951, GREM1 expression was reduced in the tumour adjacent stroma compared to normal tissue ($p =0.002$ Figure 3.1A), but GREM1 expression levels in the tumour and tumour adjacent stroma were not different ($p = 0.71$, Figure 3.1A). This is important as it indicates GREM1 and possibly BMPs expression alter within the stroma as well as the tumour cells, which could have an impact on the observed expression levels if the methods of tissue sampling do not exclude stromal cells.

The IHC performed by Dr Ye for Gremlin1 protein (Figure 3.1B), although not quantifiable in the same way as the expression microarray data, supports the appearance that in normal breast tissue Gremlin1 protein was seen strongly mainly in the ductal epithelial cells rather than stroma, and as disease progressed from *in situ* to invasive disease, Gremlin1 staining appeared to be more evenly distributed throughout the tissue.

Figure 3-1 GREM1 expression in normal and Breast Cancer tissues

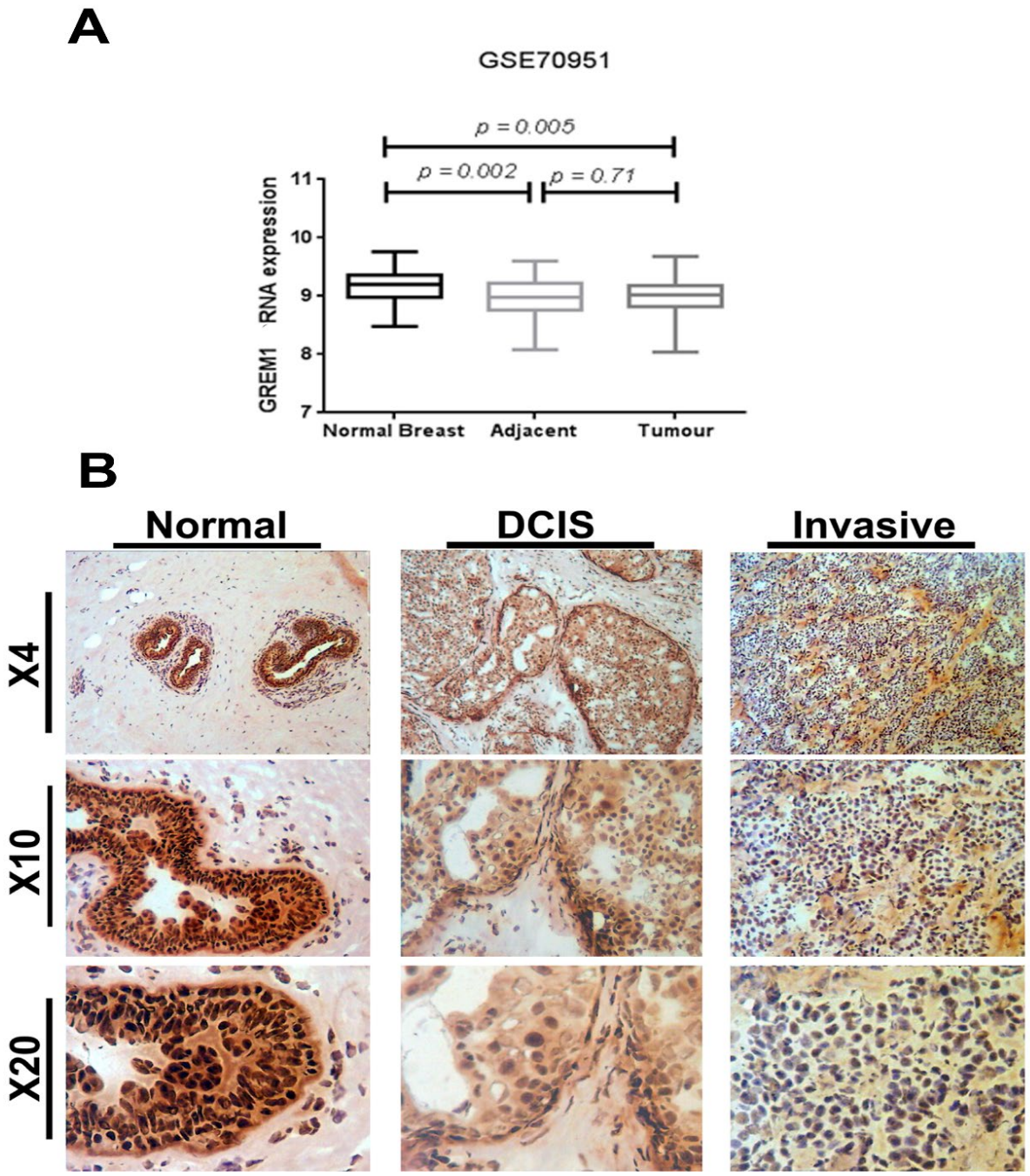

A) Boxplot of mean (+/-SEM) GREM1 expression value in 47 breast tumours with paired tumour adjacent stroma compared to 43 samples of normal breast. Data extracted from publicly available gene expression microarray dataset GSE70951.Expression of GREM1 is higher in normal reduction mammoplasty tissue compared to breast tumours (p = 0.005, unpaired t test) and tumour adjacent tissue (p = 0.002, unpaired t test). Expression of GREM1 is equivalent between paired tumour and tumour adjacent tissue (p = 0.71, paired t test with Welch's correction)

B) IHC staining for Gremlin1 in normal breast, DCIS, and invasive breast carcinoma at x4, x10 and x20 magnification. Gremlin1 can be seen in ductal epithelial cells in normal breast tissue and DCIS, becoming more diffuse in invasive cancer.

To remove the potential bias of whole tissue lysate and stromal cell expression on total gene expression levels, in a much smaller sample set than GSE70951, GDS3324(Casey et al. 2009) used laser capture microdissection to collect epithelial and matched stromal cells from 25 breast tumours and 5 normal breast samples. Microarray data shows GREM1 RNA was higher in the epithelial cells of tumour compared to normal breast (Figure 3.2 A, $p = 0.02$) and was also higher in tumour adjacent stromal cells compared to normal stromal cells (Figure 3.2 B, $p = 0.01$). There was no difference in GREM1 expression when comparing normal epithelial and stromal cells ($p = 0.8$, see Appendix 9.2.1), or between invasive epithelial and cancer associated stromal cells ($p = 0.2$, see Appendix 9.2.1).

The use of selecting cells with laser capture microdissection seems to indicate that in contrast to the whole tissue lysate samples in GSE70951, where GREM1 expression was lower in tumour compared to normal, GREM1 expression specifically in breast cancer epithelial and stromal cells was higher than in normal breast cells. This demonstrates how differences in methodology and sample size can return completely opposite results and highlights the difficulties in definitively addressing whether GREM1 expression increases or decreases in breast cancer.

Although GREM1 expression was higher in tumour compared to normal tissue in this laser capture microdissection cohort, the GREM1 expression in cancer epithelial and cancer stromal cells was equivalent (Appendix 9.2.1), which is the same finding as in GSE70951(Figure 3.1A), i.e., there is no expression gradient of GREM1 between tumour cells themselves and the surrounding tumour associated stroma/microenvironment. It is therefore interesting to consider whether Gremlin1's BMP ligands demonstrate similar expression patterns.

Figure 3-2 GREM1 expression in laser capture microdissection cells from breast cancer and normal breast tissues

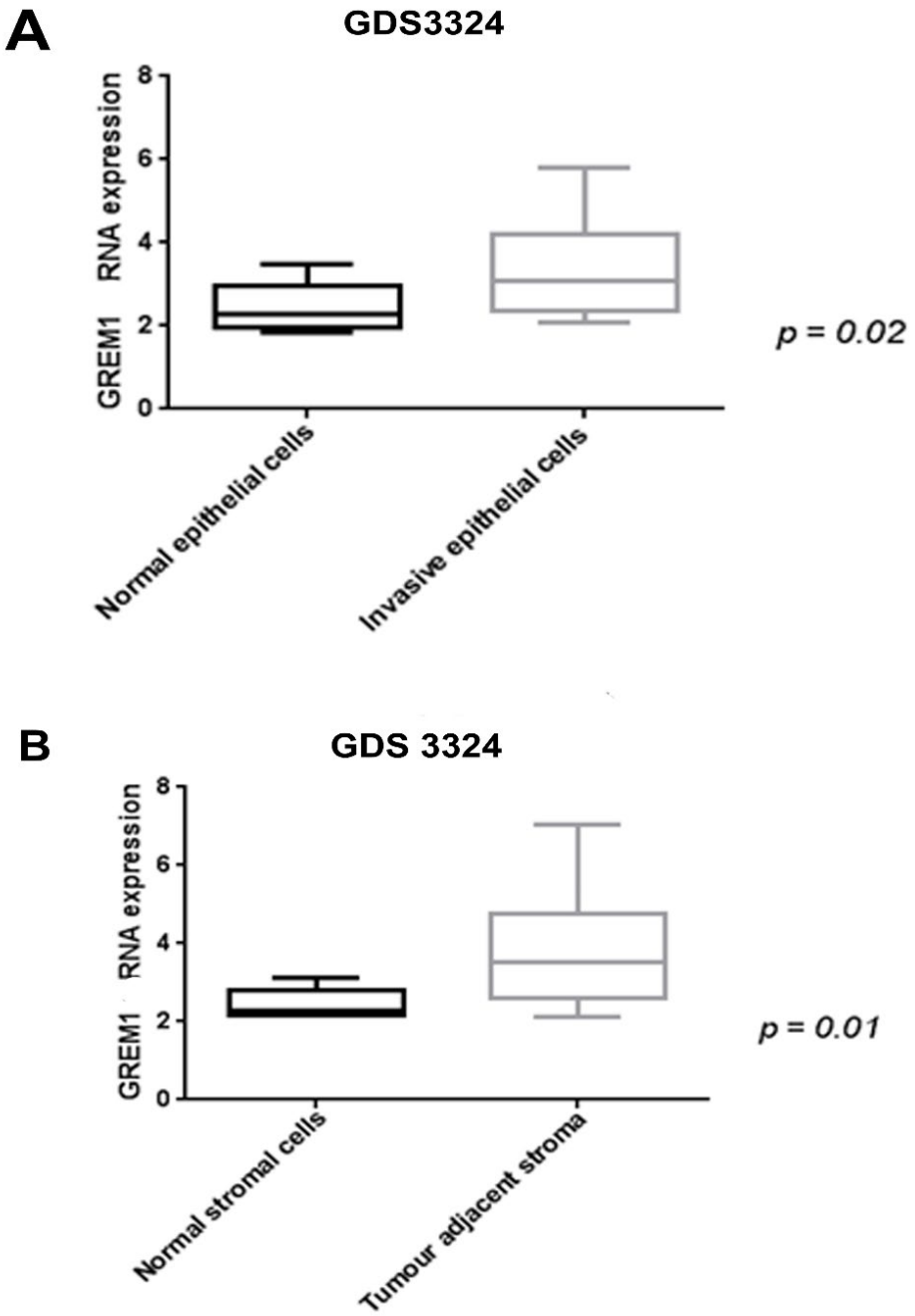

A) Geodata set (GDS) 3324 boxplots of mean (+/-SEM) GREM1 expression value in laser capture microdissected epithelial cells from 25 breast tumours and 5 normal breast samples. This specifically looks at gene expression in epithelial cells and excludes stromal cells. Expression of GREM1 is higher in invasive cancer epithelial cells compared to normal breast epithelial cells (p = 0.02, Mann Whitney test)

B) The same GDS3324 samples as in A, comparing GREM1 expression in microdissected stromal cells from normal breast tissue and from the adjacent stroma of the 25 tumours shows higher GREM1 expression in breast cancer stromal cells compared to normal breast stromal cells (p=0.01, Mann Whitney test)

Interestingly, equilibrium between tumour and surrounding tumour adjacent tissue was not seen when examining RNA expression levels of Gremlin1's ligands, BMP-2, -4 and-7, in the GSE70951 cohort. There was differential expression between the tumour and the tumour adjacent tissue, with BMP-2 and -4 expressed significantly higher in tumour compared to adjacent tumour tissue and BMP-7 significantly lower in tumour compared to adjacent tissue (Figure 3.3A, B and C, $p < 0.0001$, $p = 0.003$ and $p < 0.0001$ respectively). BMP-2 and -4 were significantly increased in breast tumour compared to normal tissue (Figure 3.3A and B, $p < 0.0001$ and $p = 0.0002$ respectively), which would suggest a reciprocal increase in ligand as antagonist decreases. However, BMP-7 was not significantly different in tumour compared to normal breast (Figure 3.3C, $p=0.06$). As Gremlin1 is known to have less affinity for BMP-7 than BMPs -2 and -4(Church et al. 2015), this may result in changes in Gremlin1 expression level as less likely to impact BMP-7 expression.

Overall, when examining RNA expression of these BMP ligands in a cohort of 327 breast tumours (GSE20685 (Kao et al. 2011)) BMP-7 was more highly expressed than BMP-2, and BMP-4 had the lowest expression(Figure 3.4), which was also seen in the median expression data from the 6547 patients analysed by KMplot (Table 3.2).As the largest individual cohort of primary breast tumours that has microarray data for the expression of GREM1 and its BMP ligands, it adds weight to the pooled data from KMplot, that demonstrates high GREM1 expression in breast cancers, with reciprocal low expression of its main target ligands BMP-2 and -4. It must be remembered with caution however that these BMPs expression may also be influenced by other BMP antagonists, and the expression and role of BMPs in cancer has often been found to be contradictory(Alarmo and Kallioniemi 2010; Ouahoud et al. 2020).

Figure 3-3 GREM1 ligand RNA expression in breast tumour and matched tumour adjacent tissue compared to normal breast tissue

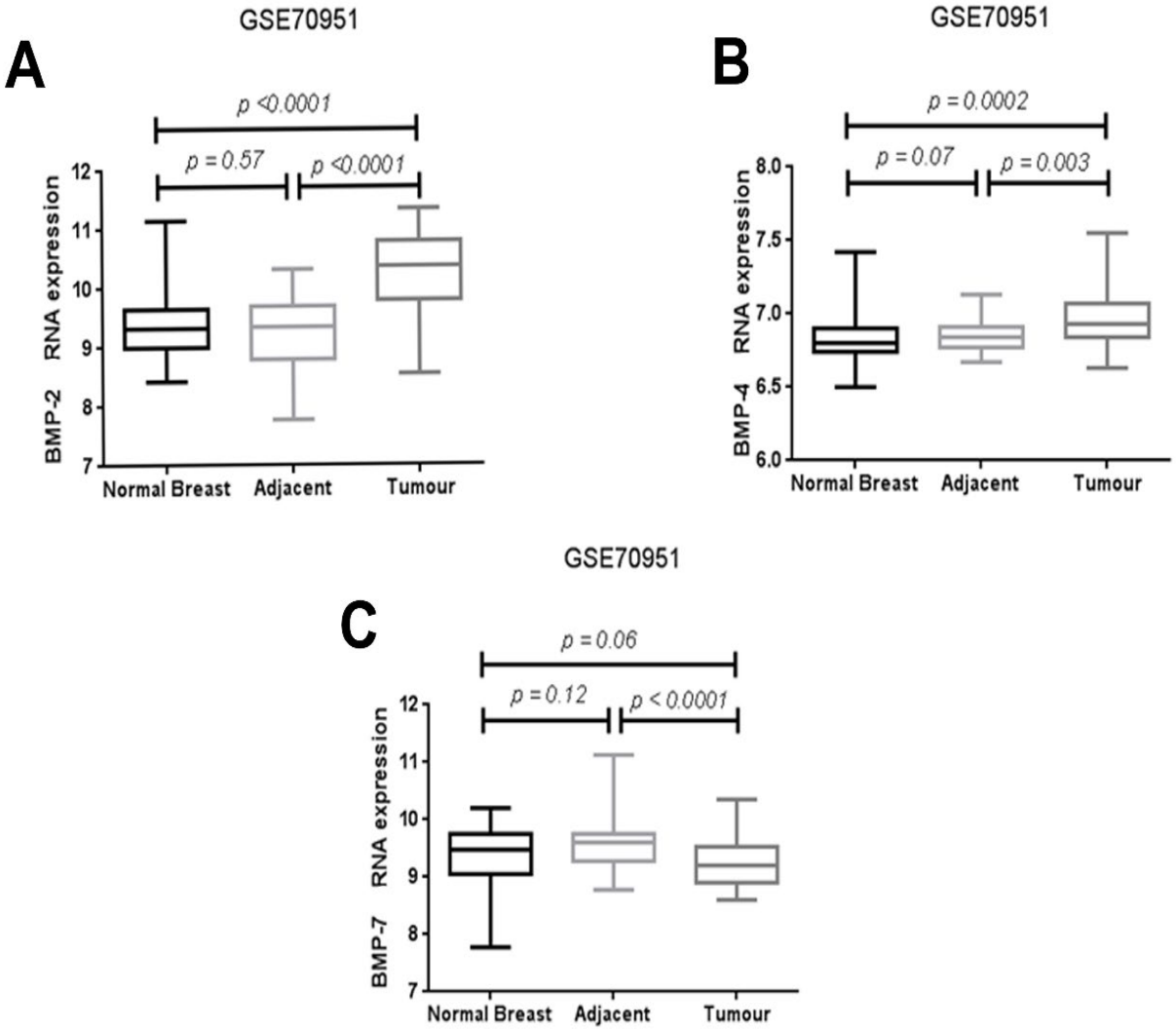

A) BMP-2 expression (gene array ID 205290_s_at) in 47 breast tumours with paired tumour adjacent stroma compared to 43 samples of normal breast. Data extracted from GSE70951, a publicly available gene expression microarray dataset. Expression of BMP-2 is higher in breast tumours compared to tumour adjacent tissue ($p<0.0001$, paired t test with Welch's correction), and compared to reduction mammoplasty tissue ($p<0.0001$, Mann Whitney test)

B) BMP-4 expression (gene array ID 211518_s_at) in the same GSE70951 cohort as A shows higher BMP-4 expression in breast tumour tissue compared to normal breast tissue ($p=0.0002$, Mann Whitney test) and compared to tumour adjacent tissue ($p = 0.003$, paired t test with Welch's correction)

C) BMP-7 expression (gene array ID 209590_at) in the same GSE70951 cohort as A shows lower BMP-7 expression in breast tumour compared to matched tumour adjacent tissue ($p<0.0001$ paired t test with Welch's correction). Expression of BMP-7 is not statistically significantly lower in tumour compared to normal breast tissue ($p=0.06$, Mann Whitney test)

Figure 3-4 Expression level of GREM1 ligands in 327 primary tumours

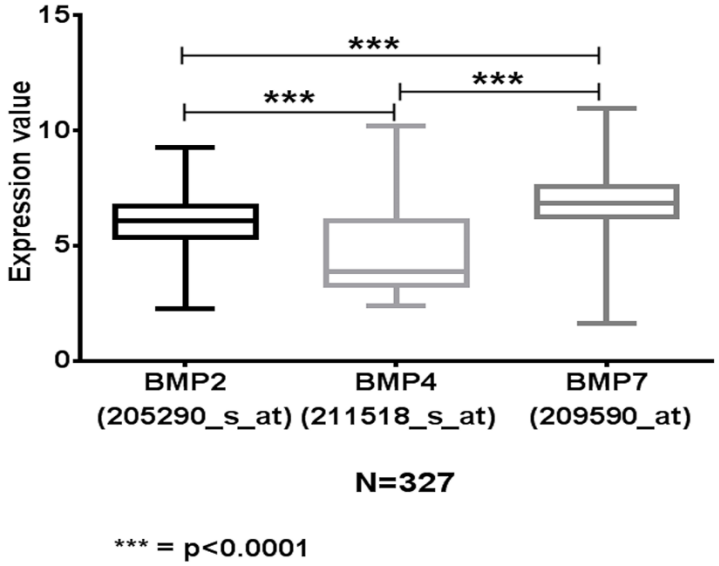

Comparative whole tissue RNA expression levels of Gremlin1's ligands BMP-2, -4 and -7 in a cohort of 327 primary breast tumours from publicly available microarray data GSE20685. The highest expression is seen in BMP-7 (p <0.0001, Mann Whitney test) compared to BMPs -2 and -4, with BMP-4 having the lowest tumour expression out of the three. Although this may be because higher levels of Gremlin1 in breast tumours antagonise and reduce the expression of BMPs -2 and -4 to a greater extent than BMP-7, it cannot be excluded that there will be other antagonists and regulatory pathways that could influence the expression of BMPs in breast tumours(Alarmo and Kallioniemi 2010; Ouahoud et al. 2020)

3.3.2 Deregulated GREM1 expression in tumourigenesis and local invasion

The evolution of normal breast tissue into an *in situ* malignancy requires genetic aberrations and deregulation of certain cellular functions. Further alterations are then required for the tumour cells to acquire an invasive phenotype and become an invasive carcinoma. It is useful to examine expression in invasive tumours in comparison to the *in-situ* stage as a reflection of genetic alterations that may be key to an invasive phenotype.

There are only very limited available tissue cohorts that have microarray data for expression of GREM1 that include DCIS samples. A large prospective collection of DCIS samples, or tissue bank samples would be required for more robust data. GDS3853 is a small cohort of 5 normal breast samples,10 DCIS and 5 IDC that used whole tissue lysate for RNA extraction and

microarray analysis. GREM1 RNA expression appeared to increase in DCIS compared to normal breast tissue then reduced in IDC compared to DCIS (Figure 3.5A). This result is limited by the very small sample size, and interpretation should be cautious, but it is possible that the balance of Gremlin1 and its BMP ligands alters as breast tumour cells undergo progression from an *in situ* to invasive phenotype. This would require an expression profile of a larger number of DCIS and IDC samples.

Further evidence of the putative influence of Gremlin1 in tumour progression may be indirectly observed by correlating Gremlin1 expression with the TNM (Tumour size, Nodal status, Metastatic disease) staging. A patient with stage 1 disease will have small tumours with no progression beyond local disease in the breast, whereas a stage 4 patient will have larger tumours with lymphovascular invasion and progression to local and distal metastases. Using the largest available public cohort with patient staging data (GSE20685, n=327) it appears that the only significant difference in GREM1 RNA expression by overall disease stage (Figure 3.5B) is that stage 3 disease has higher GREM1 primary tumour expression than stage 1 disease(p=0.01).This could not be seen with the most advanced stage 4 disease compared to stage 1, although the number of patients with stage 4 disease was only 8, and had there been more patients in the stage 4 group the findings might have been different. When stage 1 and 2 disease was grouped, and compared to stage 3 and 4 disease grouped, there was significantly higher GREM1 expression in stage 3 and 4 compared to stage 1 and 2 disease (see appendix 9.2.3, p=0.01).

Another clinicopathological parameter that indirectly reflects progression and invasive potential is the histopathological grade of the tumour, with Grade 1 tumours having low mitotic index and proliferation and Grade 3 the highest proliferation and poorly differentiated features. In the cohort of 82 tumours previously examined by Dr Ye there was a trend that with increasing tumour grade, the GREM1 expression reduced, although this did not reach statistical significance, and again, had there been larger cohort numbers, particularly in the grade 3 group, these findings would be less prone to type 2 error (Figure 3.5C).

Taken together, the expression data reflects that increased GREM1 expression may be required in initial proliferative stages such as DCIS, and then with tumour progression, dedifferentiation, and a more invasive phenotype, although the available data is unfortunately from small sample cohorts.

Figure 3-5 GREM1 expression in relation to disease progression

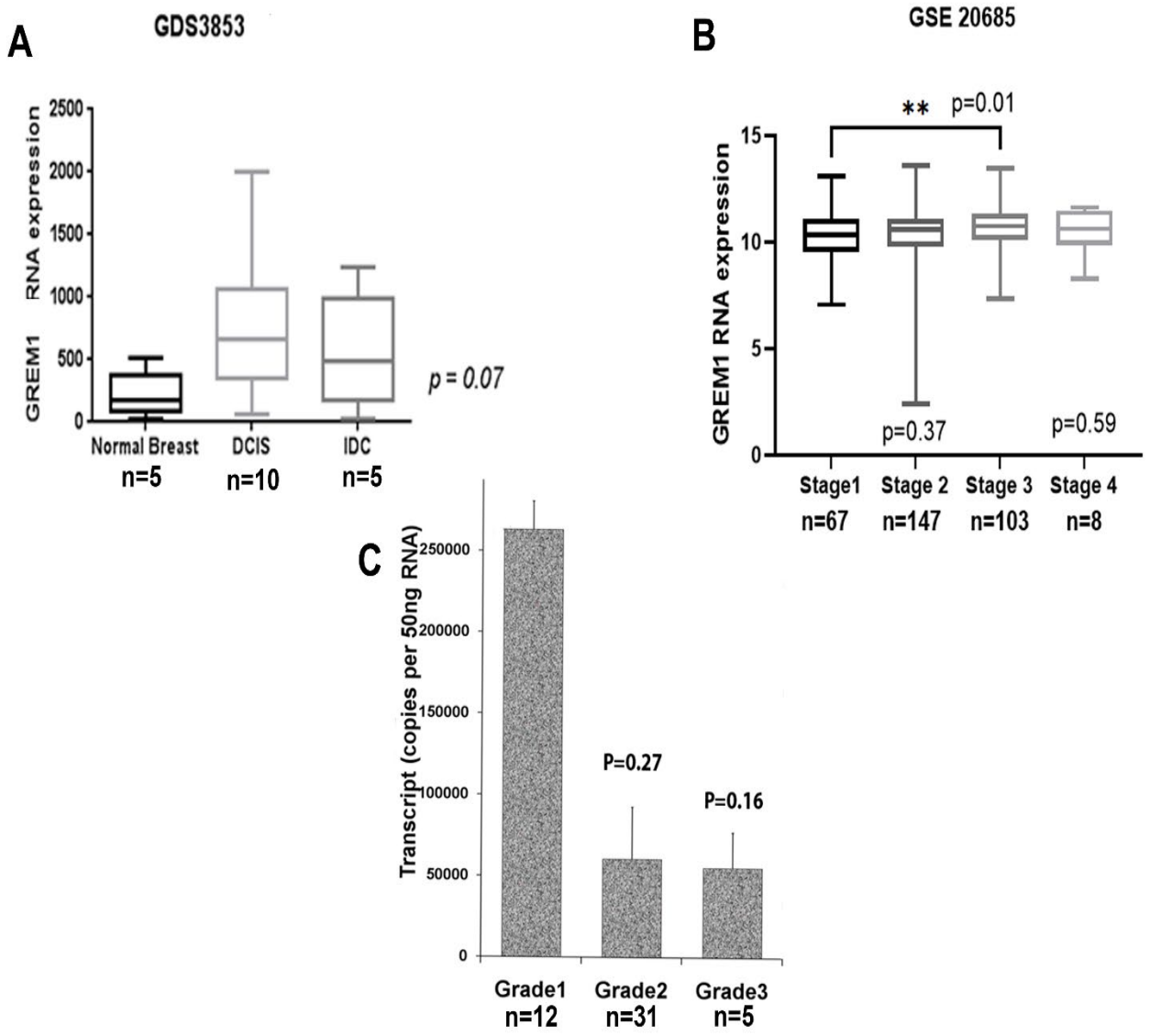

A) GREM1 RNA expression level in cohort GDS3853 comparing three unmatched groups of 5 normal breast samples, 10 DCIS samples and 5 IDC samples. There is a trend towards higher GREM1 expression in DCIS compared to normal and IDC tissues, however this does not reach significance (p = 0.07 Kruskal Wallis test of variance between 2 or more independent sample groups)

B) GSE20685 cohort of tissue samples from 327 primary breast tumours showing GREM1 RNA expression by different clinical staging of the patients, with stage 1 being lowest stage of progression and stage 4 most advanced disease. Compared to stage 1 disease, stage 2 did not have higher GREM1 expression (p=0.37, Mann Whitney test), stage 3 did have higher GREM1 expression (p=0.01 Mann Whitney test), and stage 4 did not (p=0.59 Mann Whitney test)

C) Cohort of 82 patients comparing GREM1 expression in transcript copy number relative to housekeeping gene CK19 in different histopathological tumour grades. Grade 2 and 3 tumours show a lower mean GREM1 expression compared to Grade 1 tumours, (copy number for Grade1 = 263178±172452, Grade 2 = 60502±31852 and Grade 3 = 2795±1645) but this is not statistically significant (p = 0.27 and p = 0.16 respectively, Mann Whitney test)

3.3.3 Deregulated GREM1 expression in nodal and distant metastases

In our prior local cohort of 82 patients, it appears that those with metastases had a lower mean GREM1 RNA expression level compared to those patients that remained disease free, although this did not reach statistical significance due to the low number of patients in the cohort with metastasis(n=4) (Figure 3.6 A, p = 0.087). A mean lower GREM1 expression was also seen in those patients with positive locoregional lymph nodes, but again this did not reach significance (see appendix 9.2.2 Table 9.1, p = 0.082. Node negative n =40, node positive n =38). There was significantly lower mean GREM1 expression in patients with disease recurrence and those who died from breast cancer compared to those who remained disease free (Figure 3.6A, p = 0.017 and p=0.016 respectively). These results should be interpreted with caution as the numbers in the groups are small. Larger patient cohorts with longer follow up data would reduce the possibility of type 2 statistical error.

Interestingly, a subgroup of this cohort with bone metastases was found to have significantly reduced GREM1 expression, compared to those remaining disease free, although again, the numbers were small (Figure 3.6 B p = 0.032).

Figure 3-6 GREM1 expression in tissue cohort by metastasis and clinical outcome

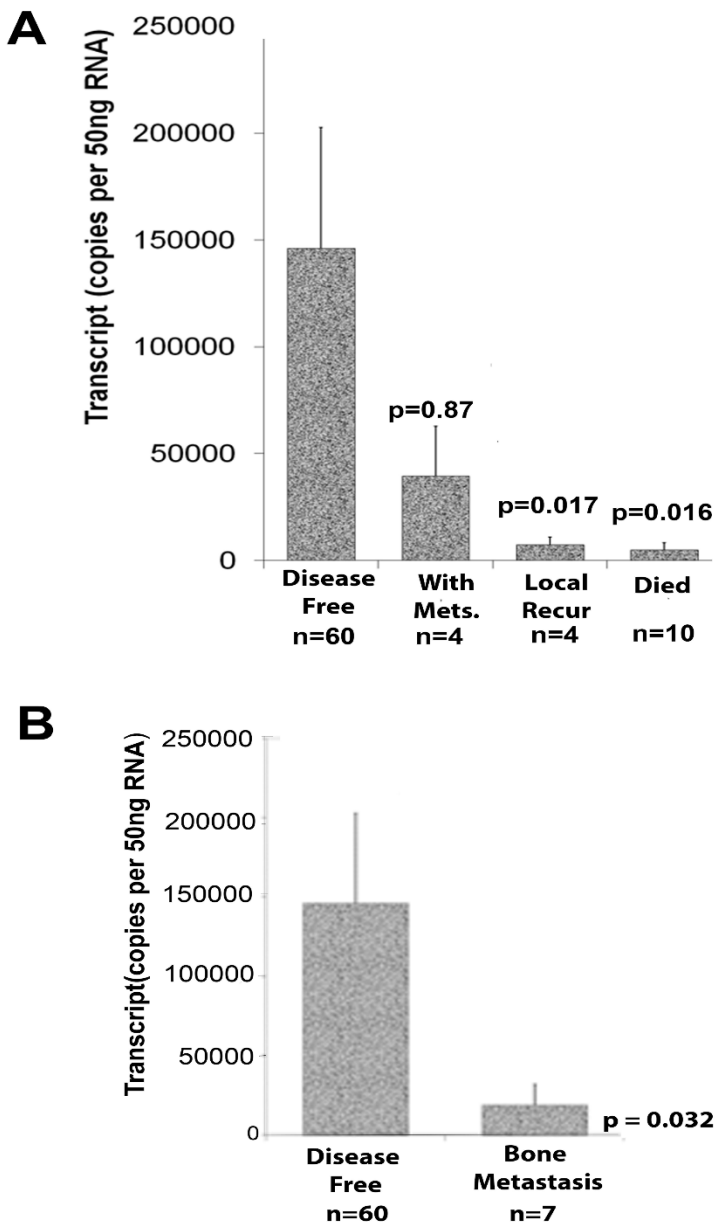

A) Mean GREM1 RNA transcript copy number (standardised against expression of CK19, +/-SEM) from qPCR within a cohort of 82 tumours when grouped by clinical outcome. GREM1 copy number was lower in primary tumours of patients with metastases (p = 0.087), local recurrence (p = 0.017) or who died from breast cancer (p = 0.016) compared to those who remained disease free (Mann Whitney test)

B) From the same cohort as A, those patients with bone metastasis had significantly lower GREM1 transcript copy number in primary tumour compared to those patients remaining disease free (p = 0.032, Mann Whitney test)

A larger cohort of patients with available DNA microarray data was therefore examined. The GEO cohort GSE20685 had gene expression microarray data from 327 patients, along with clinicopathological data. When analysing the cohort GSE20685 by nodal status, those with more positive axillary nodes (N2 and N3 stage) had higher GREM1 expression compared to those with negative axillary nodes (N0 stage) (Figure 3.7 A, p=0.01), implying higher GREM1 expression in the primary breast tumour is associated with higher volume of axillary lymph node metastasis. It can be further derived that those with more axillary lymph node involvement will have a higher likelihood of distant metastasis.

Whilst data on lymph node metastasis is readily available, as most patients that undergo surgery for breast cancer will have some form of axillary excision of local lymph node tissue, it is far less common to obtain direct tissue from breast metastasis to distant organs, as most diagnoses of distant metastasis are made radiologically without the need for tissue sampling of the metastatic tissue. Trying to determine, therefore if GREM1 expression is different in samples of metastatic tissue compared to primary tumour is more challenging. The GEO data cohort GDS4761 consisted of 304 women with metastatic breast cancer who were enrolled in a randomized phase III trial, conducted between 2002 and 2007 in Sweden (Hatschek et al. 2012). This trial was comparing chemotherapies and excluded patients with brain metastases, HER2 amplified tumours, or other malignancies diagnosed within five years of enrolment. Previous hormone therapy was accepted, but samples of metastasis were taken before commencement of chemotherapies. Samples of 91 breast cancer metastases from 6 specific anatomical sites were obtained with fine needle aspirates containing at least 50% tumour cells, and microarray performed. Using the data from this microarray the GREM1 RNA expression profile of 5 bone metastases, 16 liver metastases, 17 skin metastases and 39 unspecified lymph node metastases were compared, and a mean lower GREM1 expression in the bone metastases and liver metastases, with higher levels seen in lymph node and skin metastases (Figure 3.7 B, p=0.02). This could suggest that low or high GREM1 expression level may result in a higher likelihood of

successful establishment of metastases in specific metastatic niches, in particular the liver and bone environment. Unfortunately, these samples of breast cancer metastatic material did not have matched paired samples of the primary tumours, which would have been a useful comparison.

We have already seen that lymph node metastases themselves have higher GREM1 expression compared to other metastases, and those with higher burden of axillary lymph node metastasis have higher GREM1 expression in their primary tumours. To see if this translates to more distant metastasis, the cohort GSE20685, with 327 patient tumour samples and clinicopathological outcomes was examined comparing the GREM1 expression level in those patients with distant metastasis to those without. Those with metastases in this group had higher GREM1 expression than those without (Figure 3.7 C, $p = 0.005$), although no data was available for this cohort as to the specific metastatic site(s). This has some relevance, as it may be that the expression level of GREM1, and its' ligands in the primary tumour, influences which metastatic sites are more likely and not all metastases are equal in terms of prognosis. As an example, if GREM1 expression associates with tendency to bone metastasis, which a patient may continue to live with for longer, clinical outcomes would be better compared to brain metastasis for example, which have a very poor prognosis. If GREM1 expression resulted in tendency to brain metastases, this would have the effect of associating GREM1 expression with breast cancer death, as those with brain metastases or multiple metastatic sites will have a poorer survival than those with bone metastases in isolation. What would be required, is a database of banked tissue from primary tumours, with paired tissue from the metastatic sites and clinicopathological parameters for every patient, with long follow up. This would enable us to differentiate and compare the expression profiles of primary tumours and their specific metastases, which would allow better understanding of the metastatic process, prognostic, and predictive markers and preventative or improved treatments and surveillance.

Figure 3-7 GREM1 expression in local and distant metastasis

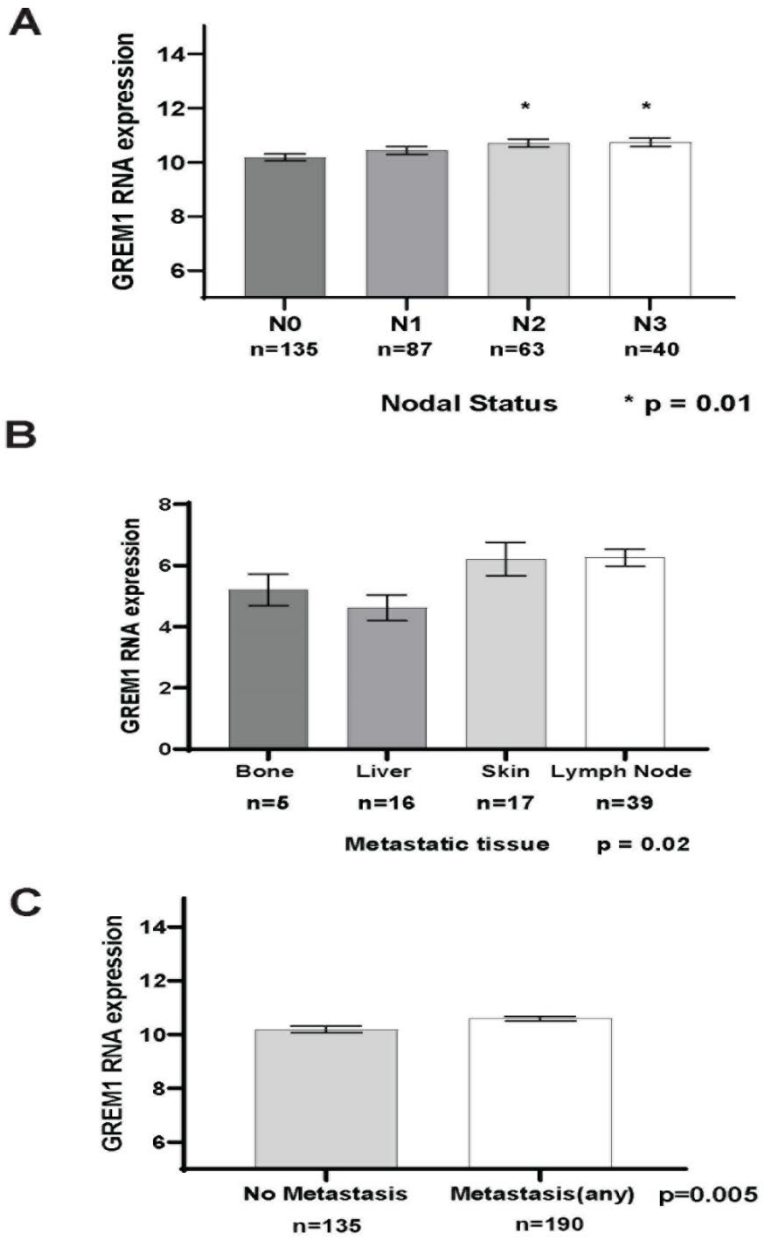

A) Mean GREM1 RNA expression(+/-SEM) of cohort GSE20685 in 327 breast tumour patients by lymph node status. Those with the most lymph nodes positive for breast cancer deposits (Stage N2 and 3) had higher Gremlin1 expression in their primary tumour compared to those with no lymph nodes(N0) (p = 0.01, Mann Whitney test)

B) Cohort GDS4761, mean GREM1 RNA expression value (+/- SEM) from fine needle aspirates of metastatic tissue from various sites. Expression of GREM1 was lower in bone and liver metastasis (p = 0.02 Kruskall-Wallis test for variance between two or more independent group samples).

C) In the same cohort as A (total n = 327), those patients with metastases of any kind had a higher GREM1 expression in their primary tumour than those that did not have metastases (p = 0.005, Mann Whitney test)

3.3.4 GREM1 expression in Breast Cancer outcomes and survival

When the patients in our local cohort were grouped by their Nottingham Prognostic Index (NPI), those with NPI 3 (i.e., poorest prognosis) had significantly lower primary tumour GREM1 RNA expression levels compared to those with NPI1 (good prognosis) disease (Figure 3.8 A). This outcome is what might be expected within this cohort, as we have already seen for this group of tumours that those with higher histopathological grade, positive lymph nodes and breast cancer death or recurrence i.e., those with a poor prognosis or features thereof, had a mean lower GREM1 expression.

When examining survival of breast cancer patients on a wider scale with larger cohort numbers however, KMplot readings show that those patients with above median (i.e., higher) RNA expression of GREM1 in their primary tumour, had a poorer overall survival (OS, $p = 0.015$), relapse free survival (RFS, $p < 0.0001$) and distant metastasis free survival (DMFS, $p < 0.0001$) compared to those with below median GREM1 expression (Figure 3.8 B, C and D). This would seem to be contrary to the local cohort data, for which there could be several reasons. As already mentioned, the cohort is smaller, but uses a single reliable methodology. It does potentially mean the results are only applicable to the cohorts' population. The online data repositories coalesce information from thousands of patients, and thus potentially can provide a far greater overview, with a better chance of reducing statistical error, but they are however an amalgamation of data from many different groups, with greater methodological and patient population variability, and thus greater variation in breast cancer treatments, surveillance, assessment, and sampling which could impact on the survival results seen. In addition, consideration must be given to the fact that different molecular subtypes of breast cancer, reflected clinically as tumours with different receptor status, will behave differently and will receive different treatments and have different prognosis. These subtypes must therefore be considered individually.

Figure 3-8 GREM1 expression and prognosis/survival

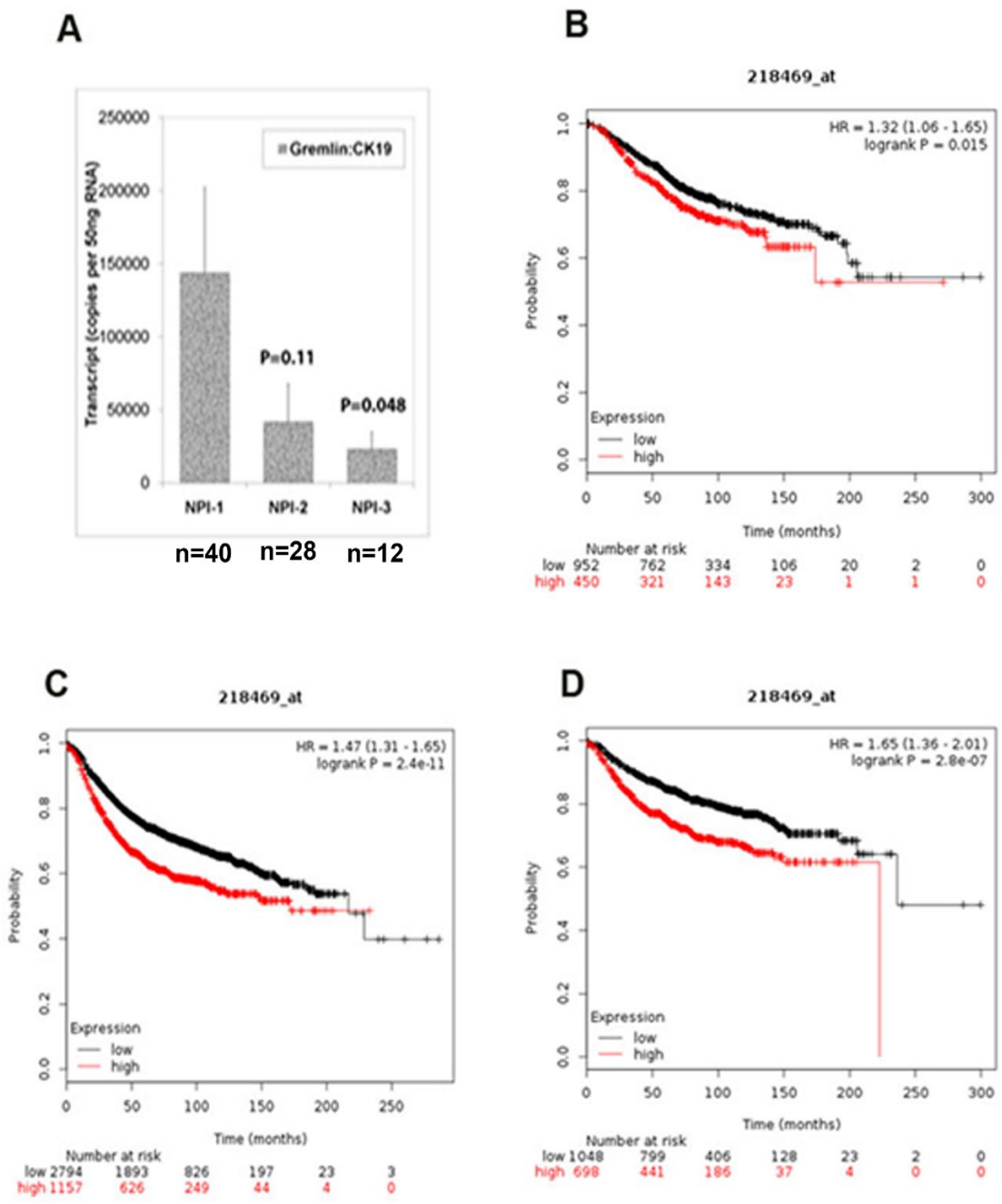

A) In our cohort of 82 breast cancers grouped by the patient's Nottingham Prognostic Index (NPI), those with poor prognosis NPI 3 disease had significantly lower mean primary tumour GREM1 RNA transcript copy numbers compared to patients who had good prognosis NPI 1 disease (p = 0.048, Mann Whitney test).

B) Kaplan Meier overall survival plot of breast cancer patients whose tumour had GREM1 RNA expression above the median showing poorer survival than those whose GREM1 expression was below the median, p = 0.015. Data was obtained from KMplot website, a public access database of microarray data and survival outcomes.

C) From the same data as in B, relapse free survival was also poorer for patients with above median GREM1 expression(p<0.0001), as was

D) Distant Metastasis Free Survival (p<0.0001)

3.4 Discussion

BMPs have been examined in clinical breast cancer samples previously, with some conflicting results. Decreased mRNA expression of GREM1 ligands BMP-2 and BMP-7, has been seen in breast cancer tissues and associated with poor clinical outcomes (Reinholz et al. 2002; Buijs et al. 2007; Davies et al. 2008). Conversely, BMP-2, BMP-4, and BMP-7 expression has been reported as elevated in breast tumours, and the latter two associated with poor prognosis (Bobinac et al. 2005; Raida et al. 2005; Alarmo et al. 2006; Alarmo et al. 2007; Davies et al. 2008) Whether these BMP ligands are up or downregulated in breast cancer therefore remains controversial, and even less is known regarding aberrant GREM1 in breast cancers. To determine a possible role for GREM1 and its ligands in breast cancer, the expression patterns and correlation to clinical disease outcomes needed clarification. No previous studies have compared GREM1 RNA expression in breast cancer to normal tissues. Expression of GREM1 RNA in our clinical cohort was higher in breast tumours vs normal breast tissue. This, however, did not reach statistical significance, and the sample size may yet be too small to detect significant differences.

The KMplot database has expression data for GREM1 and its ligands in 6547 tumours and concurred that GREM1 is expressed overall more highly in breast tumours compared to normal breast tissues. It also demonstrated a reduced expression of the main Gremlin1 BMP ligands (2 and 4) in tumours versus normal tissue and that BMP-7, for which Gremlin1 has less affinity, expression was higher compared to normal tissue (Table 3.3). The microarray data for cohort GSE20685 also concurs that in 327 breast tumours, BMP-2 and -4 are expressed at a lower level than BMP-7 (although this did not compare to normal breast tissue samples). This reflects the findings of Davies et al, who examined RNA expression of BMPs in 120 breast cancers and 32 normal breast tissues and found BMP-2 and -4 were lower in breast cancers and BMP-7 was higher, compared to normal tissue, although not statistically significantly so (Davies et al. 2008). However, they did not examine GREM1 expression. The higher BMP-7 levels in breast cancers is in keeping with a more recent study by Neckmann et al (Neckmann et al. 2019), who used 960 patient breast cancer samples from TGCA and analysed them for genetic alterations using cBioportal, and found higher rates of BMP-7 amplification

than BMP-2 or -4, but that elevated BMP-2,-4 or -7 expression did not correlate with worse survival, whereas elevated GREM1 did.

When scrutinising the method of comparing GREM1 expression in breast tumours versus normal breast tissue, we can see KMplot holds the expression profiles of huge numbers of breast tumours, but only 76 normal unmatched breast tissues. High throughput profiling of tumour transcriptomes, using microarray platforms, has provided a wealth of data and permits us to examine a large overall patient cohort, such that we might identify gene signatures or biomarkers applicable to our general population of breast cancer patients. Indeed, this approach has already informed the production of several prognostic gene signature tools in clinical use, such as MammaPrint and Oncotype Dx. However, there are limitations to use of gene expression repositories that pool experimental results. The KMplot analysis of expression in 6547 tumours and 76 normal breast tissues comes from several different studies pooled into a large series. Studies are performed by different researchers, with different methodologies and patients will have undergone different treatment regimens and sample handling. To mitigate somewhat, KMplot will only merge data from the same array platform, but this will not resolve the bias that experimental or trial design could significantly influence the overall outcome, and in merging so many different experiments we lose the specific applicability of the results to what is a heterogeneous disease.

Keeping this in mind, smaller but more specific individual experiments were analysed for GREM1 expression. Many of the experiments initially examined used either unpaired samples, or a very small number of samples, and were therefore discounted. The largest experiment examined (GSE70951) took 47 samples of histopathologically determined breast tumour and paired tumour associated stroma and compared this to 43 non-cancerous reduction mammoplasty specimens for RNA expression. Although this had less tumour samples than our clinical cohort, there is a more evenly matched number of normal breast samples for comparison, which gives these results an advantage. GREM1 RNA expression was significantly lower in both tumour adjacent tissue and the tumour itself, compared to reduction mammoplasty tissue. This result is statistically significant, whereas the local clinical cohort result implying greater GREM1 expression in breast tumours versus normal tissue was not. It demonstrates that it is not uncommon to find that different cohorts of patient tissue may have contrary results, and that there are multiple aspects of bias that in small tissue cohorts will

result in type 2 statistical error. Further confirmation would be preferable with a larger prospectively collected and analysed cohort of breast tumours and reduction mammoplasties to examine GREM1 expression both at RNA and protein level. This could be achieved via a tissue bank, or tissue microarray.

It was important that the cohort GSE70951 differentiated expression in tumour and paired adjacent stroma, as interactions between tumour cells and the surrounding stromal microenvironment can play a critical role in tumour growth and development (Pickup et al. 2015; Bussard et al. 2016). The paracrine nature of BMP signalling means that at a cellular level, expression of BMPs and antagonists may well be different between stroma and tumour cells and may skew gene expression results, if analysed together as a whole tissue. Combining laser capture microdissection (LCM) of individual cells with microarray expression profiling provides more cell specific expression profiles (Ma et al. 2003).

Ma et al used LCM and microarray to analyse 14 patient matched samples of normal stroma and epithelium, and tumour stroma and epithelium. GREM1 was one of the top genes differentially expressed/upregulated in tumour associated stroma compared to normal stroma. The authors hypothesise that the upregulation in the stroma could be due to the role of BMPs and BMP antagonists in blocking cellular differentiation, thus maintaining a population of self-renewing stem cells within the tumour microenvironment (Ma et al. 2009). Ma et al's microarray data is not held within the public repositories but interestingly, in the same year, Casey et al (Casey et al. 2009) performed a similar analysis, using LCM for matched epithelial and stromal cells, in 28 breast cancer tumours and 5 unmatched normal breast samples. GREM1 did not appear as a top differentially expressed gene in this study, but when analysing the microarray data myself (GDS3324), like the findings of Ma et al, GREM1 was upregulated in tumour stroma compared to (unmatched) normal stroma (Figure 3.2B).

In contrast, the larger GSE70951 cohort of paired adjacent tissue/tumour tissue and unmatched normal breast tissue showed lower GREM1 expression in tumour adjacent tissue compared to normal (Figure 3.1A). This cohort did not use LCM, and therefore may not be as specific as the results of Ma et al and Casey et al. Microdissection is more targeted to the specific microenvironment cellular relationships but is only reflective of a small snapshot in one tumour, and therefore should be seen as complimentary to the whole tissue samples.

Another reason for the contrast in results between these studies is the difference in study patient characteristics. For example, tumour receptor status appears to influence the effect of BMP signalling in breast cancer, including influences such as the epigenetic effects of oestrogen receptor signalling on BMP promoter regions (Zhang et al. 2005).

Carcinomas of different pathological types and different stages of disease, or histopathological 'aggressiveness', may also exhibit different expression profiles. Of the 14 tumours in the study by Ma et al, 40% were HER2 positive, 79% were ER positive, all were ductal carcinomas and 21% were lymph node negative. Compared to Casey et al where HER2 status was not given, 73% were ER positive, 10% were lobular carcinomas and 60% were lymph node negative. The GSE70951 cohort had 26% HER2 positive, 79% ER positive, the type of carcinoma was not stated and 27% were lymph node negative. Therefore, in addition to sample size and methodology, the patient/tumour characteristics may also account for whether GREM1 is found to be up or downregulated in tumour compared to normal breast tissues. There is also a disadvantage of using reduction mammoplasty samples as controls. These patients are on average much younger than women with non-familial breast cancer and are more likely to be overweight or obese. Obesity is linked to breast cancer risk (Picon-Ruiz et al. 2017), so the use of reduction mammoplasty specimens as 'normal' breast tissue may not be representative of a true 'normal'.

When using GSE70951 to compare expression of GREM1 and BMP ligands in the adjacent stroma with the tumour tissue itself, rather than comparing to normal breast tissue, the BMP ligands appear similarly expressed in normal breast and tumour adjacent stroma, but interestingly in the tumour itself, BMP-2 and -4 expressions significantly increased compared to stroma, and BMP-7 decreased (GSE70951 Fig 3.3). As previously discussed, BMP signalling can influence the tumour microenvironment, for example, stimulation of fibroblasts by BMP signalling promotes breast tumour cell invasion and increased inflammatory cytokine production (Owens et al. 2012). An analog of dorsomorphin (DMH1), a small molecule BMP inhibitor, can attenuate the pro-tumour microenvironment by altering expression of certain genes (such as ID-1 and MMPs) in fibroblasts, lymphatic vessels, and macrophages in a mouse model. (Owens et al. 2015). In addition, BMP-2 induces the extracellular matrix glycoprotein Tenascin-W in breast tumour associated stroma, promoting invasion and migration of cancer cells

through an interaction with α8 integrin (Scherberich et al. 2005). A similar effect to BMP-2 on stromal cells appears to be true with BMP-4 treatment in mammary stromal fibroblasts. Fibroblasts stimulated with BMP-4 enhanced MCF-7 cell invasion, and these effects were inhibited by DMH1. BMP-4 increased Matrix Metalloprotease-3 and the cytokine IL-6 in conditioned medium from treated mammary fibroblasts, suggesting BMP-4 can influence the tumour microenvironment to promote breast cancer invasion (Owens et al. 2013). These raised levels of BMP-2 and -4 expression in the tumours of cohort GSE70951, compared to the stroma, may demonstrate how the tumour is influencing its microenvironment to promote ongoing tumour cell survival and invasion. GREM1 expression on the other hand was similar in both tumour and tumour adjacent tissue, in keeping with the analysis of matched tumour stroma and tumour epithelial cells from GDS3324, which also had similar GREM1 expression levels. So, although it seems we have conflicting results as to whether GREM1 expression increases or decreases in tumour associated stroma compared to normal breast tissues, there may not be a significant differential GREM1 expression between the tumour and its adjacent tissue. This loss of Gremlin1 'gradient', and increased ligand expression differential between tumour and stroma, may be reflecting stochastic mechanisms that result in the up-regulation of BMP-2 and -4 expression within the tumour, in the same way that stochastic mechanisms and lateral inhibition occur to determine cell fate (Lim et al. 2015).

Overall, the question of whether GREM1 is more highly expressed in breast cancer has conflicting evidence – individual studies with small numbers show opposing outcomes. This is perhaps not a surprise considering conflicting evidence for BMP expression in breast cancer is also well documented(Alarmo and Kallioniemi 2010). However, large, pooled expression databases, which are not without their own limitations, show that GREM1 is more highly expressed in breast cancer compared to normal breast tissue, and this should be confirmed with large prospective tissue collection or tissue banks.

The question regarding whether dysregulation in GREM1 and its BMP ligands influences progression from *in situ* disease through to invasive carcinoma is challenging to answer, as there are only studies with small numbers of samples of DCIS and IDC in which GREM1 has been assessed. In the cohort examined (GDS3853 (Kretschmer et al. 2011)), consisting of whole lysate from 5 normal breast tissues, 10 DCIS tissues and 5 non matched IDC samples, it was

interesting to find that mean GREM1 RNA expression increased in DCIS, but then dropped in IDC. This trend did not reach statistical significance however, and the low sample numbers and use of whole tissue lysate, rather than microdissection, means interpretation should be cautious. Scheutz et al performed LCM of tumour epithelial cells in 9 tumours that had both DCIS and IDC components. They found, in matched samples, that GREM1 was upregulated in IDC compared to DCIS in both microarray and RT-PCR (Schuetz et al. 2006). Larger tissue cohorts are required to determine whether alterations in GREM1 expression in DCIS (either in the stroma or epithelium) contribute to progression from *in situ* to invasive disease. *In vitro* cell function tests, of growth and invasion with altered GREM1 expression levels, may also help to decipher further the influence GREM1 has in this respect and will be examined in later chapters.

The influence of Gremlin1 on disease progression and clinical outcomes can also be considered by comparing RNA expression values in the primary tumours of patients who have smaller, low grade localised tumours compared to those with more aggressive, high grade or advanced disease. GSE20685 was the largest cohort of patients with microarray GREM1 expression data (n=327), clinical data including disease stage at diagnosis (both TNM and American Joint Committee on Cancer (AJCC) staging) and outcome events such as metastasis.

In GSE20685, GREM1 primary tumour expression value was only significantly higher in AJCC stage 3 patients compared to stage 1(Figure 3.5B, $p = 0.01$). Patients in this cohort with higher GREM1 expression in the primary tumour also had higher N stage/positive lymph nodes and distant metastasis (Figure 3.7 A and C). KMplot also demonstrated that those with a primary tumour that had GREM1 expression above the median, had a poorer overall survival, relapse free survival and metastasis free survival (Figure 3.8 B, C and D). This implies higher GREM1 expression in primary tumour is a poor prognostic indicator.

In our smaller local clinical cohort, there was lower mean GREM1 copy numbers in patients with local recurrence and death, and poor prognosis disease as assessed by NPI (Figures 3.6A and 3.8A). This contrasts to the GSE20685 cohort, and as already discussed, the reasons for these discrepancies fall mainly to methodological differences, and the possibility that the small sample size in our cohort does not give adequate power to the findings. Both the GSE20685 cohort and KMplot, although larger numbers of patients, suffer from an 'unselected' population, that will consist of tumours with varying clinical receptor status and

thus different neoadjuvant and adjuvant treatment regimens which may skew metastasis and survival outcomes. To better understand the role of Gremlin1 in metastasis and clinical outcomes, *in vitro* cell function tests of migration and invasion in cells with high or low GREM1 expression will help to examine this seeming disparity, as would *in vivo* metastasis models. A larger prospective cohort of patients with clinicopathological data and followed for metastatic relapse or death correlated to the primary tumour GREM1 expression, would provide further clarity with consistent methodology. Subgroup analysis, by clinical receptor status and treatment regime, could then be performed. The possibility that BMP signalling and aberrant Gremlin1 may have different roles in different molecular subtypes of breast cancer will be considered in subsequent chapters.

Of interest, given the nature of BMPs role in regulating bone metabolism, is the role of Gremlin1 in the bone metastatic niche. The current data in our cohort demonstrated that GREM1 was expressed at lower levels in primary tumours of patients with bone metastasis, and the cohort of metastatic tissue (GDS4761) although small numbers, showed GREM1 expression was lower in bone and liver metastatic tissue compared to skin or lymph node metastases. Obtaining tissue from metastatic sites, matched to a patient's primary tumour, would provide very interesting data on how BMP antagonism and signalling might have very different roles within the primary tumour, compared to how circulating cancer cells establish themselves in a particular metastatic niche like bone, or maintain self-renewing cells within that niche in a quiescent state, leading to subsequent relapse in disease. Some studies suggest BMPs could induce stem cell quiescence, which would have important implications for disease relapse. Gao et al demonstrated that paracrine BMP signalling suppresses cancer stem cell traits, and that BMP antagonist Coco (part of the same DAN family of antagonists as Gremlin1) reactivates dormant metastatic breast cancer cells in the lungs. Coco induced a self-renewing stem cell-like phenotype in the metastatic cells by blocking the BMP-induced repression of core stem cell transcription factors (Gao et al. 2012). In breast cancers, the influence of BMP signalling and antagonism on stem cell populations and the metastatic niche is not yet clear. A BMP-2/7 heterodimer applied to provoke BMP signalling, strongly reduced the size of a breast cancer stem cell population *in vitro,* and *in vivo* when cells were pre-treated with the BMP heterodimer, bone metastases were also reduced (Buijs et al. 2012). Conversely Katsuno et al found BMP induced transcriptional pathways are very much active in

breast cancer bone metastatic lesions *in vivo,* and xenografts with dominant negative BMP receptors had reduced bone metastases *in vivo* (Katsuno et al. 2008). Tan et al showed that breast cancer cells with induced epithelial to mesenchymal transition (EMT) exhibited an elevated level of bone related genes (BRGs) and osteoblast like features in an exposure to BMP-2. Breast cancer cells expressing these BRGs preferentially metastasise and survive in bone. It also interestingly made cells more resistant to chemotherapy. These effects were reversed with application of BMP antagonist Noggin (Alarmo and Kallioniemi 2010; Carreira et al. 2014; Tan et al. 2016). As a BMP antagonist, Gremlin1 may have a significant currently undefined role in breast cancer bone metastasis, suggested by these initial GREM1 expression results, which will be examined in further chapters.

In conclusion, the expression profile of GREM1 and its BMP ligands, is aberrant between normal breast tissue compared to breast tumour tissue and its associated stroma. Large data cohorts suggest GREM1 expression is increased in breast cancers compared to normal breast tissue, but methodological limitations make this difficult to be certain. Likewise, the same large patient cohorts (with the same limitations) suggest Gremlin1 as a poor prognostic factor in breast cancer. It is unclear how Gremlin1 aberrations may influence local tumour growth and invasion, but there appears to be a link between aberrant GREM1 expression in primary breast tumours and grade of the tumour, lymph node metastasis, distant and bone metastasis and prognosis that warrants a more detailed evaluation, particularly in respect of the influence of the molecular subtypes of breast cancer, and this will be explored in following chapters.

4 The expression of Gremlin1 in Breast Cancer cell lines and effect on cellular functions

4.1 Introduction

Differential gene expression and dysregulation has long been examined in molecular cancer biology, to identify key drivers of tumourigenesis and disease progression. We have already established that there are aberrations in Gremlin1 expression, at both the RNA and protein levels in breast carcinomas, (See Chapter 3) which could play an important role in breast cancer progression, as high GREM1 expression in primary breast tumours appears to be significantly associated with poorer survival outcomes for breast cancer patients.

There are very few *in vitro* studies of how Gremlin1 might influence cellular functions in cancer. Guan et al examined Gremlin 1 in the carcinogenesis of glioma using ShRNA transfection of U87-MG cells. Knockdown of GREM1 reduced cell viability, suppressed migration, invasion, and markers of EMT. Interestingly, GREM1 knockdown cells demonstrated abolition of TGFβ1-mediated Smad signalling, which may have contributed to the suppression of EMT. This study suggests Gremlin1 as potentially important for supporting EMT processes in Glioma (Guan et al. 2017b). Liu et al found ShRNA knockdown of GREM1 in colorectal cancer (CRC) cell lines significantly inhibited cellular proliferation, migration, angiogenesis and EMT (Liu et al. 2019). In lung cancers, when GREM1 is overexpressed in lung fibroblasts and epithelial cells, it induces significantly increased cellular proliferation (Mulvihill et al. 2012). On ShRNA Gremlin1 knockdown in mesothelioma cells lines, cellular proliferation was greatly reduced (Wang et al. 2012) and, in a second study, GREM1 silencing inhibited mesothelioma cell invasion *in vitro*, with downregulation of the EMT transcription factor SNAI2 (Yin et al. 2017).

Thus, for other cancers, the indication appears to be that Gemlin1 may promote cellular proliferation, EMT and invasion. As there were no prior publications or *in vitro* models regarding Gremlin1 in breast cancers at the time of this study, this chapter attempts to establish the expression profile of GREM1 in breast cancer cell lines and describes the subsequent development of in *vitro* models in the most utilised and characterised breast cancer cell lines, MCF7 and MDA MB 231.

4.2 Methods

4.2.1 Cell lines and culture

The breast cancer cell lines MCF-7, T47D, ZR751, BT474, MDA MB 361, SKBR3, MDA MB 231, BT549, BT20 and MCF10A were cultured for this study. The culture media used, standard incubation conditions and passage methods are described in Chapter 2.2.

4.2.2 RT-PCR and RT-qPCR

RNA extraction was performed using the TRI reagent RNA extraction protocol (SigmaAldrich, Dorset, UK). RT of 500ng RNA was then carried out using GoScript™ Reverse Transcription System (Promega, UK), as described in Chapter 2.3.

cDNA from the cell lines MCF7, T47D, ZR751, BT474, MDA MB 361, SKBR3, MDA MB 231, BT549, BT20 and MCF10A was used for both PCR and qPCR.

PCR was performed according to the protocols in Chapter 2.3, for 35 cycles, utilising GoTaq Green Master mix and primers from Sigma (Sigma-Aldrich, Dorset, UK) as listed in Table 2.1. Housekeeping gene GAPDH was utilised as an internal control and sterile water as the negative cDNA control. Image J software was used to provide densitometry readings and semi-quantification.

For comparative qPCR of the breast cancer cell lines, Precision Q-PCR 2X qPCR Mastermix (Primer Design, UK) and a PDPL standard curve were used, according to protocols and conditions as described in Chapter 2.3, with primers listed in Table 2.1. When confirming knockdown or overexpression of GREM1, SYBERgreen JumpStart Taq Ready Mix^{TM} and SYBRgreen primers were utilised in a comparative $C_T(\Delta\Delta C_T)$ analysis as described in Chapter 2.3. Quantitative PCR data were analysed and normalised to the housekeeping gene, GAPDH, with a sterile water negative control.

4.2.3 Western Blot

Protein expression was established using SDS-PAGE and Western blotting. Western blotting used PDVF membranes and a semi-dry transfer method. A full protocol is found in Chapter 2.4, including the antibodies used (Table 2.2). Housekeeping protein β Actin was the internal control. Semi quantification densitometry was performed using Image J software.

4.2.4 ELISA

A sample of a Human Gremlin1 ELISA kit was provided by Abbexa (abx351709, Abbexa, Cambridge, UK). This was a 48 well sample plate for a limited run of samples and repeats. A run of ELISA standards (5ng/ml,2.5ng/ml, 1.25ng/ml, 0.625ng/ml, 0.3125ng/ml and 0.15625 ng/ml) in duplicate, and conditioned media samples from $MCF7^{Scr}$, $MCF7^{SH2}$, MDA MB 231^{Scr}, MDA MB 231^{SH2}, $BT474^{PEF}$, and $BT474^{GREM1}$ were plated in triplicate, with diluent buffer as the negative control. ELISA protocol was according to manufacturer's instruction as described in Chapter 2.4.6.

4.2.5 GREM1 Lentiviral Knockdown

U6 Promoter Lentiviral particle vectors (Cyagen, USA) containing shRNA targeting GREM1(SH1 and SH2), or scramble shRNA (Scr) were produced and then used to transfect MCF7 and MDA MB 231 cells using polybrene (See Chapter 2.6 for full protocol). After selection for up to 14 days using 500µg/ml G418(Geneticin, Melford, Suffolk, UK) in standard culture medium, cells were further maintained in the same medium supplemented with between 100µg-300 µg /ml G418, depending on the tolerance of the cell line. The SH1 knockdown shRNA did not appear as successful as the SH2 knockdown therefore, for all further experiments, SH2 knockdown was utilised. In addition, GREM1 knockdown was also attempted with SKBR3 cell line, but transfection and selection were poorly tolerated, such that stable knockdown was not conducive to cell survival, even with removal of antibiotic selection. This cell line was therefore subsequently removed from ongoing experiments.

4.2.6 GREM1 Plasmid Overexpression

pEF6/V5-HIS TOPO TA vector containing GREM1 overexpression plasmid or empty pEF6/V5-HIS TOPO TA vector were used to transfect MCF7 and MDA MB 231 cells ($MCF7^{PEF}$/MDA MB 231^{PEF}, MCF7/MDA MB 231^{GREM1}). Transfection was achieved by electroporation (Chapter 2.7). Following transfection, cells were selected for up to 14 days in relevant cell culture medium with Blasticidin S (Melford, Suffolk, UK) at 5µg/ml and further maintained in 0.5µg/ml Blasticidin S.

4.2.7 Growth Function Assay

For standard growth assay, 3,000 transfected MCF7 or MDA MB 231 cells were seeded into 200µl medium in three 96-well plates, and incubated for 1, 3, and 5

days respectively. After incubation, cells were gently washed with PBS, fixed with 4% Formalin, and stained with crystal violet. Following this, 100 µl Acetic acid (10% v/v) was then applied and the absorbance was determined at a wavelength of 540nm using a spectrophotometer. Measurements were recorded as % Growth, whereby the absorbance at days 3 and 5 are comparative to the reading at day 1. For spheroid growth assay, 3,000 cells were seeded into a 96 Ultra low attachment, round bottomed well plate in 140µl culture media and centrifuged to centralise the cells in spheroid formation. Spheroids were examined 24 hours after seeding and photographed at x10 magnification at day 1, 4, 6 and 8. Images were processed with Image J to determine spheroid area and calculate % growth compared to day 1. All growth assays were performed with internal triplicate and repeated three times.

4.2.8 Proliferation Function Assay

For proliferation assay, 3,000 MCF7 or MDA MB 231 cells were seeded into a 96 well plate, incubated for 24 hours and MTT assay undertaken as per protocol in Chapter 2.8.2. Absorbance was read at 590nm, reading for experimental cells compared to control cells.

4.2.9 Invasion Function Assay

For invasion assay (Chapter 2.8.3 for full protocol), 20,000 MCF7or MDA MB 231 cells were seeded in 200 µl serum free medium within an 8µm pore well insert that had been previously coated with a Matrigel membrane. Normal medium with serum (10% FCS) was placed in the underlying well. Control wells, to account for proliferation effects over 72hrs, had 20,000 cells seeded with no inserts. After 72 hours incubation, any remaining cells within the insert, and the Matrigel membrane were removed. Cells were then fixed with 4% Formalin and stained with crystal violet. Three field views of the insert with invaded cells, and the control wells were photographed. Stained cells were dissolved with 300 µl acetic acid (10% v/v) and plated into a 96 well plate for reading of absorbance at wavelength of 540nm. Percentage invasion was calculated as Absorbance of invaded cells/Absorbance of control cells x 100. For 3D spheroid invasion, 3,000 cells were seeded into a U bottom 96 well plate and grown for 3 days, before a mix of Matrigel and medium was added. After a further 24 hours incubation, spheroids were photographed as day 1, and then at day 4, 6 and 8. Images were processed with Image J to

determine Spheroid area and calculate % growth compared to day 1. Experiments were conducted with internal triplicate and repeated three times.

4.2.10 Transwell Migration Assay

As per the 2D invasion assay above, the experimental protocol remained the same (full protocol Chapter 2.8.4), but the 8µm inserts did not contain a Matrigel layer. Migrated cells after 72 hours were fixed with Formalin and stained with crystal violet, dissolved in acetic acid and absorbance read at 540nm. % Migration was calculated as Absorbance of migrated cells/Absorbance of control cells x 100.

4.4 Results

4.4.1 Gremlin1 expression in breast cancer cell lines

A wide selection of breast cancer cell lines readily available in our cell bank were chosen, and expression of GREM1 was examined in these cell lines using PCR, RT-qPCR and at the protein level by Western blotting. It became evident that the expression of GREM1 was variable by breast cancer cell line, as one might expect (Figure 4.1 A and C). The cell lines chosen span the various molecular subtypes of breast cancer and are thought to adequately represent the receptor profiles (Holliday and Speirs 2011a; Dai et al. 2017) .

GREM1 was not abundantly overexpressed in any of the cell lines, with PCR and qPCR often requiring a threshold of around 35 cycles to generate significant signal. In the Luminal A subtype (MCF7, T47D and ZR751), MCF7 appears to demonstrate the highest GREM1 expression, with no expression seen in T47D or ZR751.Similarly, in the 'triple negative' cell lines, MDA MB 231 had higher expression, with low expression in BT20 and none in BT549. Interestingly those cell lines with HER2 expression, namely the Luminal Bs and HER2 enriched (BT474, MDA MB 361 and SKBR3 respectively) all had relatively prominent GREM1 expression, with MDA MB 361 demonstrating the highest. MCF10A cells are derived from proliferative breast tissue and are an immortalised non tumourigenic cell line, often used to represent ‘normal’ breast cells although, they do not express ER or HER2 and have a triple negative basal like phenotype(Qu et al. 2015), again, appearing to express GREM1 at low levels.

With regards to the expression of Gremlin1 BMP ligands, the expression of BMP-2, -4 and -7 are also variable across the breast cancer cell lines (Figure 4.1 B). BMP-2 expression appears more prominent in the triple negative subtype cell lines, particularly MDA MB 231 and BT549, and MCF10A but not in the Luminal A, B or HER2 enriched. BMP-4 shows most expression in cell lines with ER expression, namely T47D, ZR751 and BT474, but not MCF-7. BMP-7 expression is most marked in BT474 and SKBR3, both HER2 expressing cell lines, but also in BT20, a molecular TNBC subtype.

At the protein level, it was difficult to obtain an adequate Western blot (Figure 4.2A) of total cell lysate, with large variability in the housekeeping protein βActin, and poorly defined bands at 21kDa, the product size for Gremlin1. The image displayed was the best obtained after several months of optimisation attempts

(detailed in Section 9.3, Appendix III) of a technique that was new to me at the time, and of which I improved my technique for over the three-year research period. At the time this initial western blot process was undertaken, relative densitometry was performed to account for the variability in housekeeping expression. This appeared to show that the Luminal A type cells, MCF7 and ZR751 and the TNBC type BT549, had relatively higher cellular levels of Gremlin1 than the Luminal B types BT474 and MDA MB 361, HER2 enriched SKBR3 and TNBC type MDA MB 231 and BT20. It appears that the expression of GREM1 at the RNA level may not consistently correlate with the production of Gremlin1 at the protein level, although this cannot be interpreted due to the inadequacy of the Western blot results.

Figure 4-1 Expression of GREM1 and BMPs at RNA level in a panel of Breast Cancer cell lines

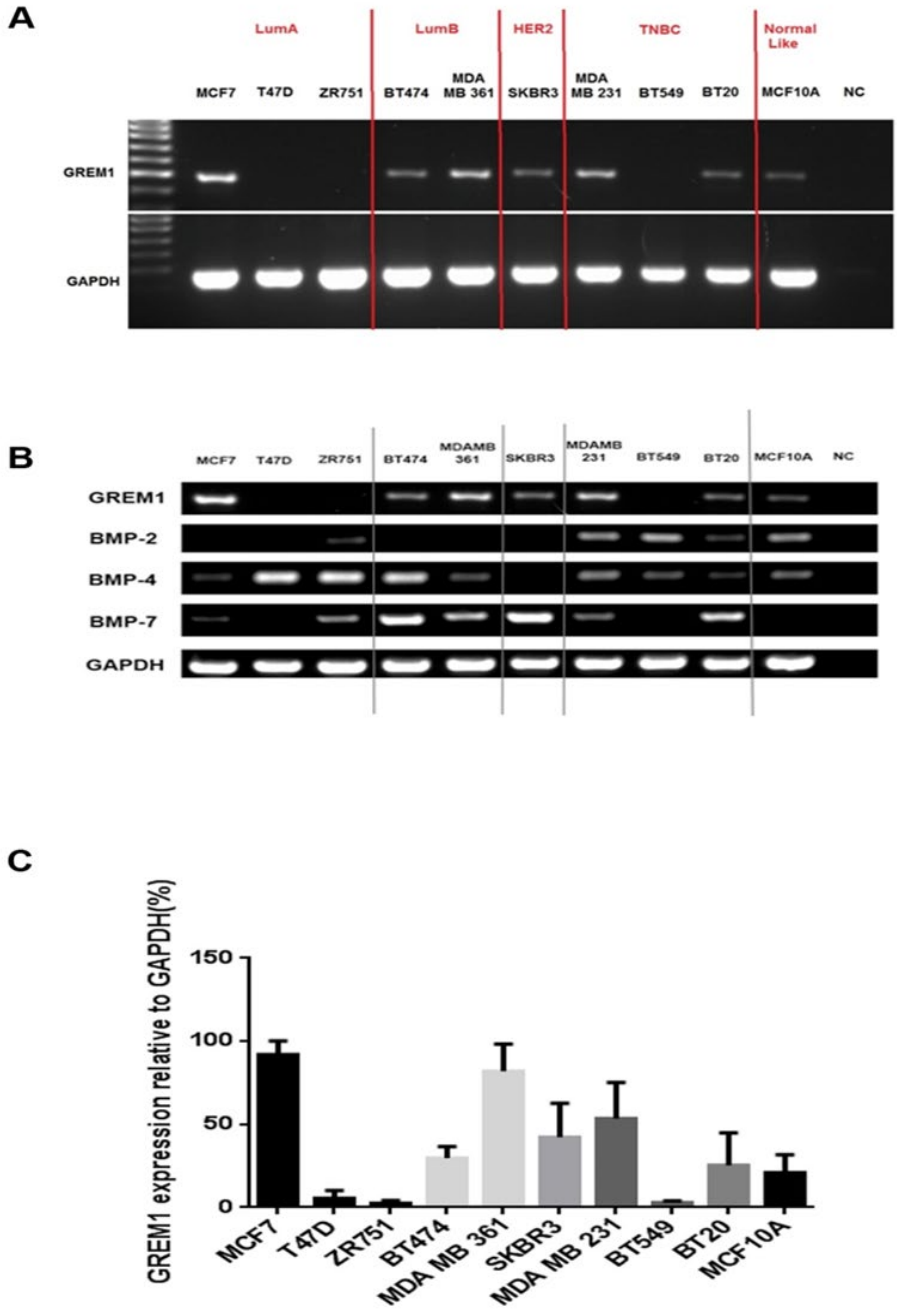

A) PCR of GREM1 expression across a panel of breast cancer cell lines divided by section into representatives of the different molecular clinical breast cancer subtypes. GREM1 demonstrates variable expression across the cell lines. The selected internal control is GAPDH

B) With the same panel of cell lines as in 4.1A, the expression of the Gremlin1 BMP ligands (BMP-2, -4 and -7) is also shown, again divided by molecular clinical subtype

C) GREM1 expression relative to GAPDH in the panel of breast cancer cell lines from A. This semi quantified based on the intensity of the GREM1 expression PCR band signal relative to intensity of the GAPDH signal for each sample, using ImageJ software

Figure 4-2 Whole cell lysate protein expression of Gremlin1

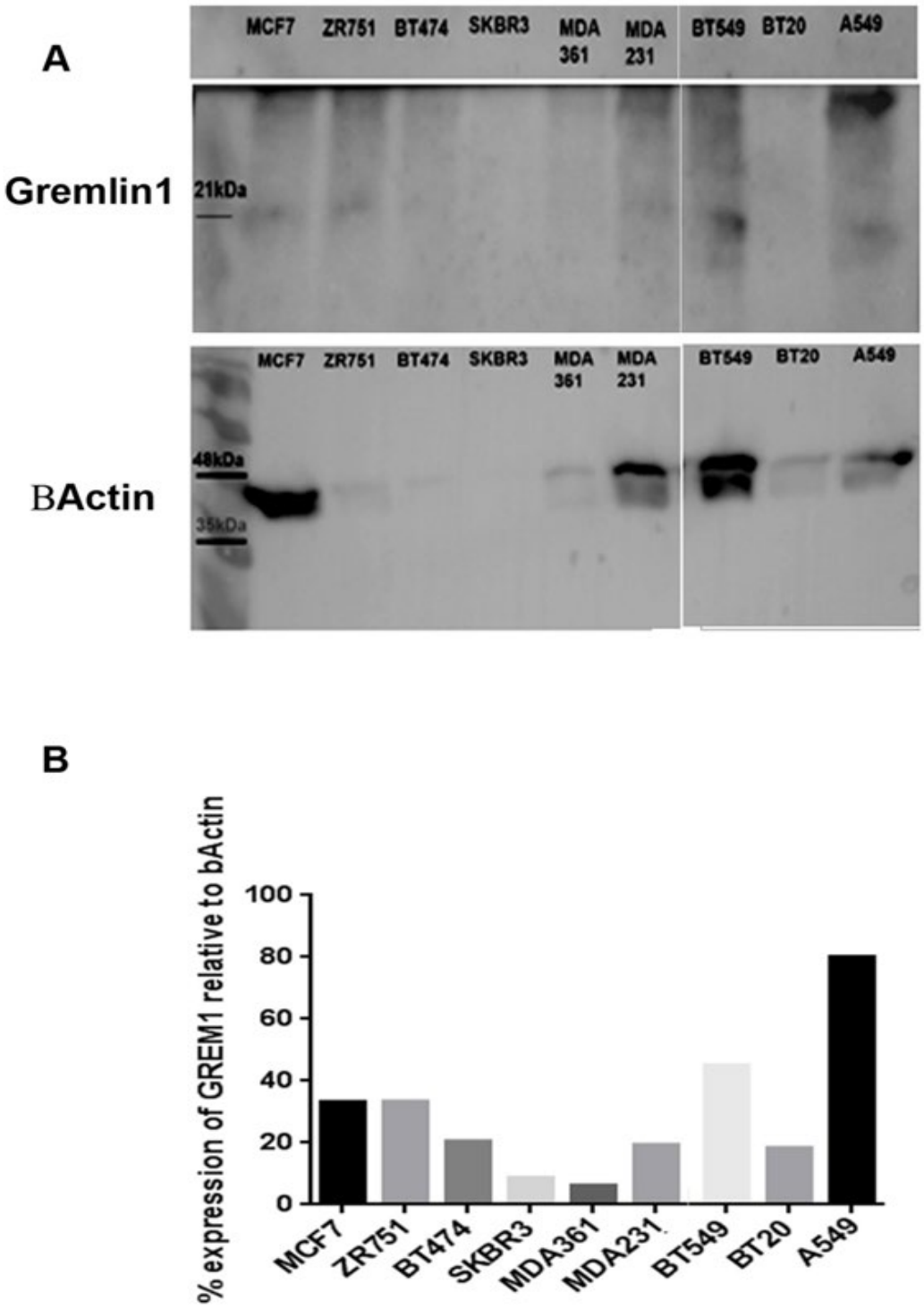

A) Western blot of panel of Breast Cancer cell lines using whole cell lysate to examine the expression of Gremlin1 protein(21kDa). The housekeeping protein βActin(42kDa) is the internal control, and the positive control is whole cell lysate from A549 cells

B) Gremlin1 protein expression relative to βActin using ImageJ processing of the western blot in A, which semi quantifies the intensity of the gremlin1 band relative to the βActin band for each cell line protein sample

4.4.2 GREM1 Knockdown in MCF7 and MDA MB 231 cells

As MCF7 and MDA MB 231 had moderate GREM1 expression on PCR and qPCR and are well characterised breast cancer cell lines that are most used in breast cancer research, these lines were selected for initial lentiviral knockdown of GREM1. As can be seen, the SH2 lentiviral construct produced a greater knockdown initially at the mRNA level in MCF7 cells (Figure 4.3 A and B) and was therefore subsequently utilised as the main knockdown construct in all further experiments. Confirmation of Gremlin1 knockdown at mRNA and protein level is seen in Figure 4.3 A-D, in the MCF7 cell lines and Figure 4.4 A-D in MDA MB 231 cell lines. A Gremlin1 ELISA sample kit was also procured (Abbexa, Cambridge, UK) and conditioned media from the control and knockdown cell lines examined for secreted Gremlin1. This demonstrated a non-significant reduction in Gremlin1 secretion (see also appendix 9.3) (Figure 4.5 A-C). This was a free sample kit that I had obtained from the manufacturer, as the only manufacturer producing Gremlin1 ELISA kits at the time. Due to budget constraints full and further ELISA kits could not be purchased, and so with only one small kit, the ELISA experiment could not be broadened to more samples or repeated for optimisation.

Figure 4-3 GREM1 knockdown in MCF7 cells

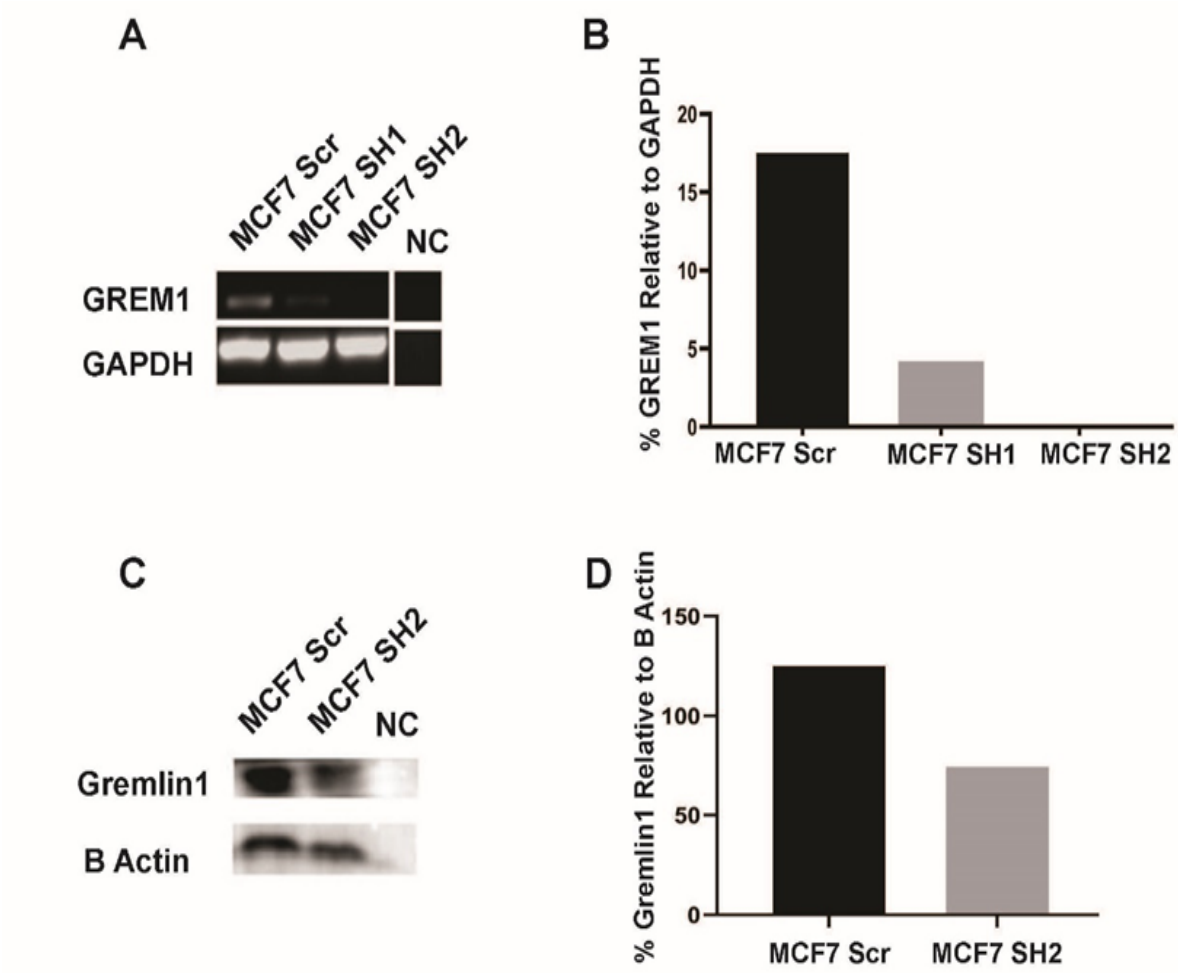

A) PCR of GREM1 expression and housekeeping gene GAPDH, in MCF7 GREM1 lentiviral knockdown cells showing Scramble control (Scr), SH1 lentiviral construct and SH2 lentiviral construct. The lentivirus particles integrate a short hairpin DNA sequence into the cells genome, resulting in production of short hairpin (SH) RNA that targets the GREM1 gene and prevents transcription and translation of GREM1.Two different short hairpin RNA sequences were trialled, with SH2 providing the better knockdown of GREM1. NC = Negative control (sterile water)

B) The PCR in A underwent semi quantitative densitometry, whereby intensity of the GREM1 PCR bands in each sample is normalised relative to the intensity of the GAPDH bands, with GREM1 expression displayed as percentage of GAPDH. SH2 knockdown construct was most successful and therefore utilised for the rest of the knockdowns.

C) Western blot of Gremlin1 protein in whole cell lysate of MCF7 scramble and SH2 knockdown cells in comparison to housekeeping protein, β Actin. NC = Negative Control (Laemli buffer)

The western blot in C underwent semi quantitative densitometry, with intensity of Gremlin1 bands normalised to β Actin bands for each sample and displayed as a percentage of β Actin. MCF7 SH2 shows less Gremlin1 than MCF7 Scr control.

Figure 4-4 GREM1 knockdown in MDA MB 231 cells

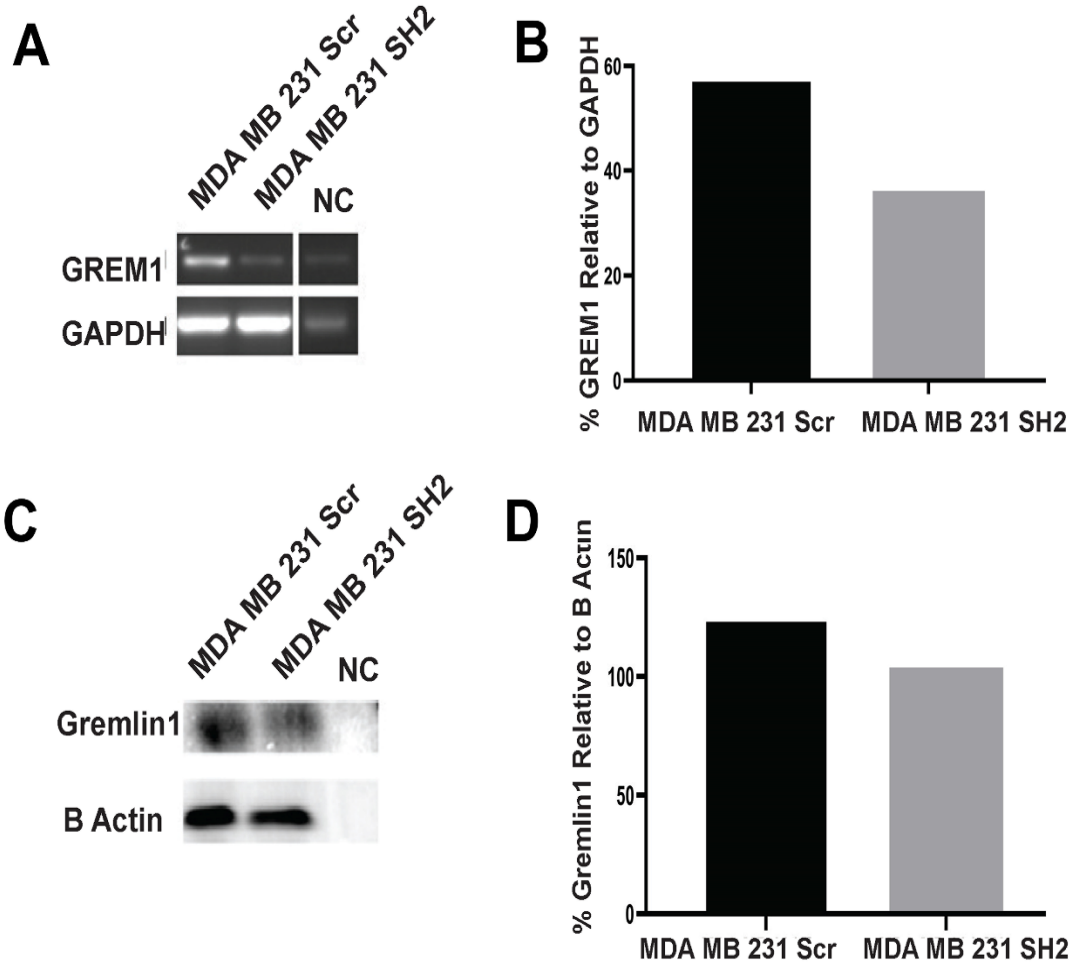

A) PCR of GREM1 expression and housekeeping gene GAPDH, in MDA MB 231 GREM1 lentiviral knockdown cells showing Scramble control (Scr) which contains a 'nonsense' DNA sequence, and SH2 lentiviral construct containing a GREM1 targeted DNA sequence for a short hairpin RNA that will interfere with GREM1 transcription and translation. The SH2 knockdown has reduced GREM1 expression compared to Scr control.NC = Negative control (sterile water)

B) Densitometry of A, GREM1 expression relative to GAPDH whereby intensity of the GREM1 PCR bands in each sample is normalised relative to the intensity of the GAPDH bands, with GREM1 expression displayed as percentage of GAPDH

C) Western blot of Gremlin1 protein in whole cell lysate of MDA MB 231 scramble and SH2 knockdown cells in comparison to housekeeping protein, β Actin.NC = Negative control (Laemli buffer)

D) The western blot in C underwent semi quantitative densitometry, with intensity of Gremlin1 bands normalised to β Actin bands for each sample and displayed as a percentage of β Actin. MDA MB 231 SH2 shows less Gremlin1 than Scr control.

Figure 4-5 Secreted Gremlin1 in conditioned media assessed by ELISA

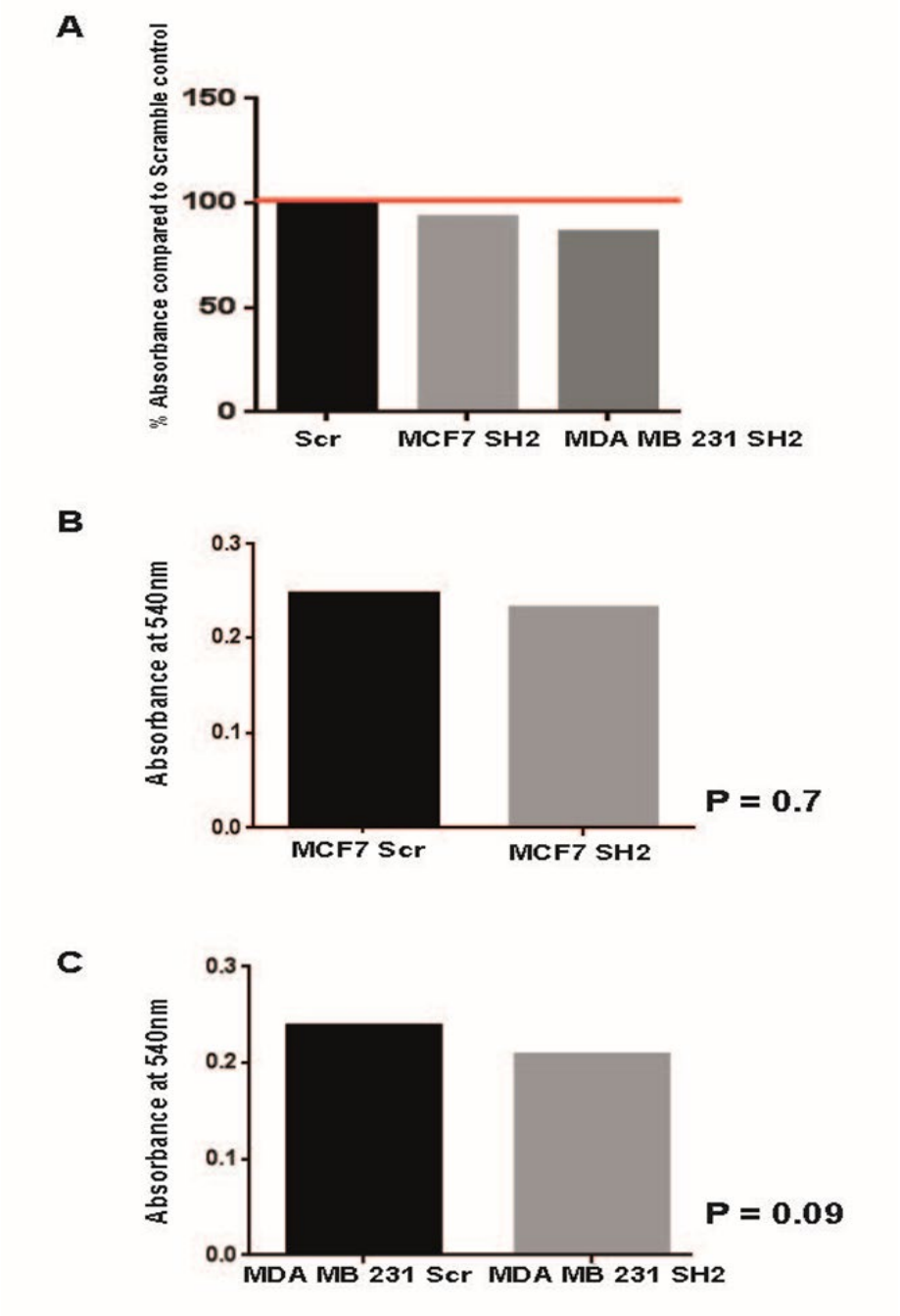

A) Secreted Gremlin1 from culture media of MCF7 ^{SH2} GREM1 knockdown cells and MDA MB 231^{SH2} GREM1 knockdown cells compared to the respective Scramble (Scr) control cells as a percentage if the control is set at 100%. Secreted Gremlin1 from the control or knockdown cells is captured by a sandwich ELISA, and a colorimetric assay shows a change in colour intensity (absorbance) relative to the amount of Gremlin1 in solution. The knockdown cells (SH2) secrete less Gremlin1 compared to control cells (Scr).

B) Mean ELISA absorbance reading for MCF7^{SH2} GREM1 knockdown compared to MCF7^{Scr}, in triplicate, with a non-significant reduction in Gremlin1 secreted. (p = 0.7, Mann Whitney test)

C) Mean ELISA absorbance reading for MDA MB 231^{SH2} GREM1 knockdown compared to MDA MB 231^{Scr}, in triplicate, with non-significant reduction in Gremlin1 secreted. (p = 0.09 Mann Whitney test)

4.4.3 Effect of GREM1 Knockdown on cell function in MDA MB 231 cells

In MDA MB 231 ^{SH2} there was significant increase in cellular growth at 3 and 5 days compared to MDA MB 231 ^{Scr} (Figure 4.6 A, $p < 0.0001$). This was also reflected in an MTT assay (Figure 4.6 B). MTT, a yellow tetrazole, is reduced to purple formazan in living cells. The degree of spectrophotometer light absorption is dependent on the degree of formazan concentration accumulated inside the cell and on the cell surface. The greater the formazan concentration, the greater the metabolism and cellular proliferation of the cells, and the more viable cells present. MDA MB 231 ^{SH2} cells displayed significantly greater formazan production ($p < 0.001$) compared to control, reflecting the increased proliferation. This was not reflected in a 3D growth assay, where there was no significant difference in growth of spheroids over 8 days (Figure 4.6 C, $p = 0.76$ see appendix 9.3.2), although, this did not assess spheroid density, and the spheroids do appear to become denser over time, implying that there could be cellular growth in a tight cluster, without showing radial growth.

Invasion of MDA MB 231 ^{SH2} through a Matrigel membrane was significantly increased compared to control (Figure 4.7 A, $p < 0.001$), but transwell migration without the Matrigel layer was not (Figure 4.7 B, $p = 0.54$). The finding of increased invasiveness with GREM1 knockdown was supported by the 3D Spheroid invasion assay (Figure 4.7 C, $p = 0.03$ see appendix 9.3.2), whereby the GREM1 knockdown cells were seen to be spreading through the Matrigel in a looser conformation in all directions, compared to control.

Figure 4-6 Effect of GREM1 knockdown on MDA MB 231 growth cellular functions

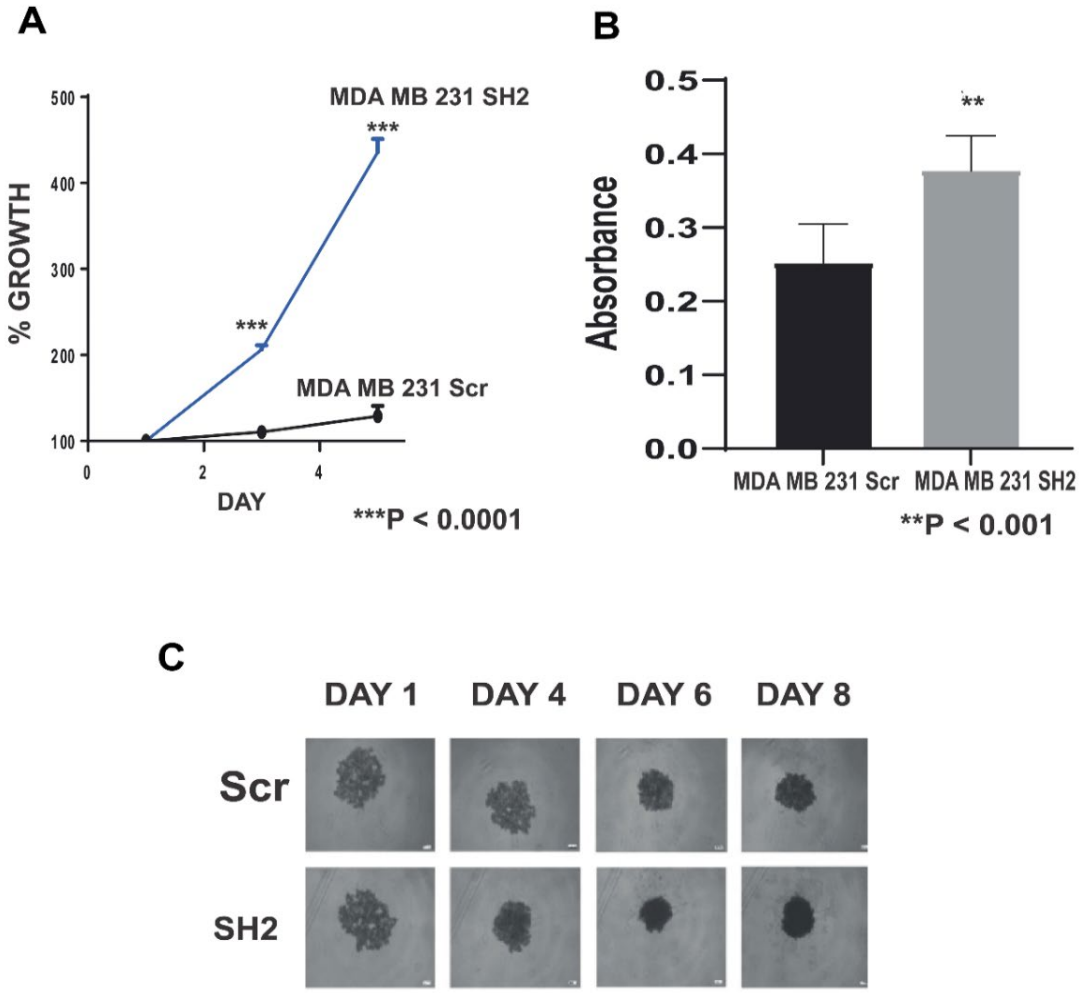

A) Growth assay over 5 days from day 1 baseline, comparing % growth of MDA MB 231^{Scr} to MDA MB 231^{SH2}. At time points day 1, day 3 and day 5 cells are fixed and stained with crystal violet. The intensity of staining at each time point is determined by an absorbance reader. Results over time are displayed as relative percentage of staining at day1. GREM1 knockdown resulted in significantly increased growth at day 3 and 5, ***p < 0.0001(Mann Whitney test, experiment repeated in triplicate, displayed mean percentage increase +/- Standard error of mean (SEM))

B) MTT proliferation assay demonstrated increased cellular division and metabolism in MDA MB 231^{SH2} compared to control ** p < 0.001(Mann Whitney test). MTT is a colorimetric assay that uses metabolism of a chemical into formazan, which precipitates as a yellow colour, intensity of which is proportional to metabolism and proliferation of viable cells. Repeated in triplicate and displayed as mean +/- SEM (error bar)

C) MDA MB 231^{Scr} and MDA MB 231^{SH2} cells were grown in 3D on special U bottomed non adherent plates as a cluster, or spheroid of cells.3D Spheroid growth was measured using ImageJ software for each spheroid over 8 days. MDA MB 231^{Scr} and MDA MB 231^{SH2} had no difference in radial growth, p = 0.76(See appendix 9.3.2 for growth chart)

Figure 4-7 Effect of GREM1 knockdown on MDA MB 231 cells invasion and migration

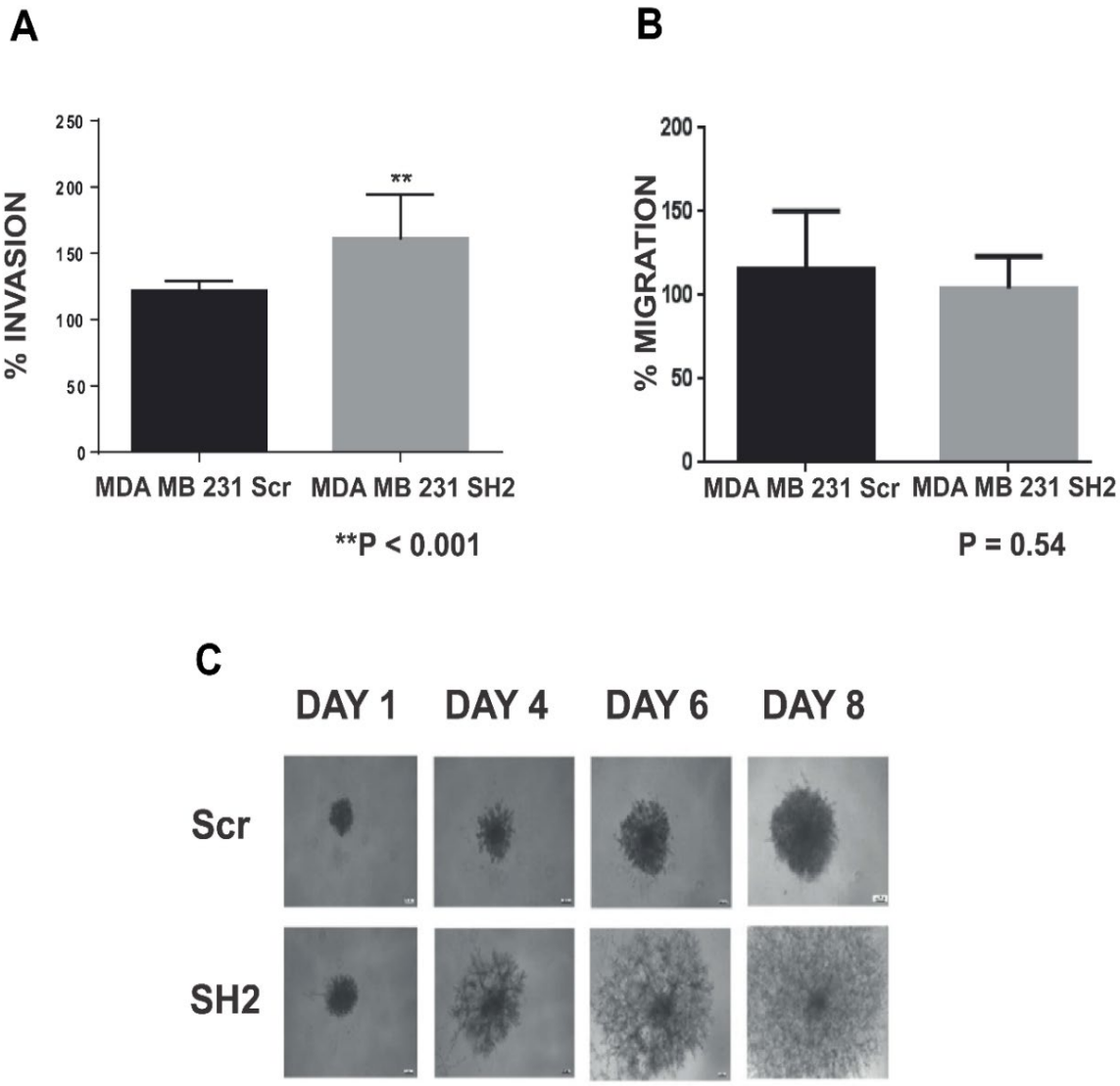

A) Invasion of cells was assessed by how many cells invaded through a porous membrane coated with extracellular matrix (Matrigel) over 72 hours. Cells that invaded through the membrane were fixed and stained and intensity of stain measured. A well of cells with no membrane was used as control to account for different rates of proliferation which might spuriously increase the number of cells. MDA MB 231^{SH2} cells have greater invasion through a transwell Matrigel membrane over 3 days than control (p < 0.001 Mann Whitney test, repeated in triplicate and presented as Mean +/- SEM)**

B) Migration of cells was assessed as in the invasion assay, excepting the porous membrane is not coated with extracellular matrix (Matrigel), instead the cells must migrate through the pores of the membrane. MDA MB 231^{SH2} cells did not show any significant difference in percentage migration through a transwell membrane compared to MDA MB 231^{Scr} (p = 0.54, Mann Whitney test, repeated in triplicate and presented as Mean +/- SEM).

C) MDA MB 231^{Scr} and MDA MB 231^{SH2} cells were grown in 3D on special U bottomed non adherent plates as a spheroid of cells which is then surrounded by Matrigel. Invasion of spheroid into the Matrigel was measured using ImageJ software for each spheroid over 8 days. Increased invasion of MDA MB 231^{SH2} in a loose formation is clearly seen compared to MDA MB 231^{Scr} control (p = 0.03. See appendix 9.3.2 for invasion measurement chart)

4.4.4 Effect of GREM1 Knockdown on cell function in MCF7 cells

In contrast to MDA MB 231 cells, the effect of GREM1 knockdown in MCF7 cells was less apparent. Mean growth and proliferation appeared slightly increased in $MCF7^{SH2}$ compared to control (Figure 4.8 A and B, $p > 0.05$ and $p = 0.13$ respectively), but this was not statistically significant, and the effect considered negligible. The growth also decreased after 3 days following initial high increase, which may indicate both initial rapid growth and then rapid cell death. Spheroid growth was also no different between $MCF7^{Scr}$ and $MCF7^{SH2}$ (Figure 4.8 C, $p = 0.08$, see appendix 9.3.3) although, as with the MDA MB 231 cells, the experimental and control spheroids both appeared to get smaller in circumference, and size measurement did not reflect the density of the spheroid.

Likewise, invasion of $MCF7^{SH2}$ cells through a Matrigel membrane, or within spheroid formation, was not significantly different to control (Figure 4.9 A and C $p = 0.09$ and 0.7 respectively) and invasion of cells concentrically outwards from the spheroid did not seem to occur in MCF7 cells, as they did in MDA MB 231 cells. Migration through a transwell membrane was also no different in $MCF7^{SH2}$ compared to control (Figure 4.9 B, $p = 0.52$).

Figure 4-8 Effect of GREM1 knockdown on MCF7 growth cellular functions

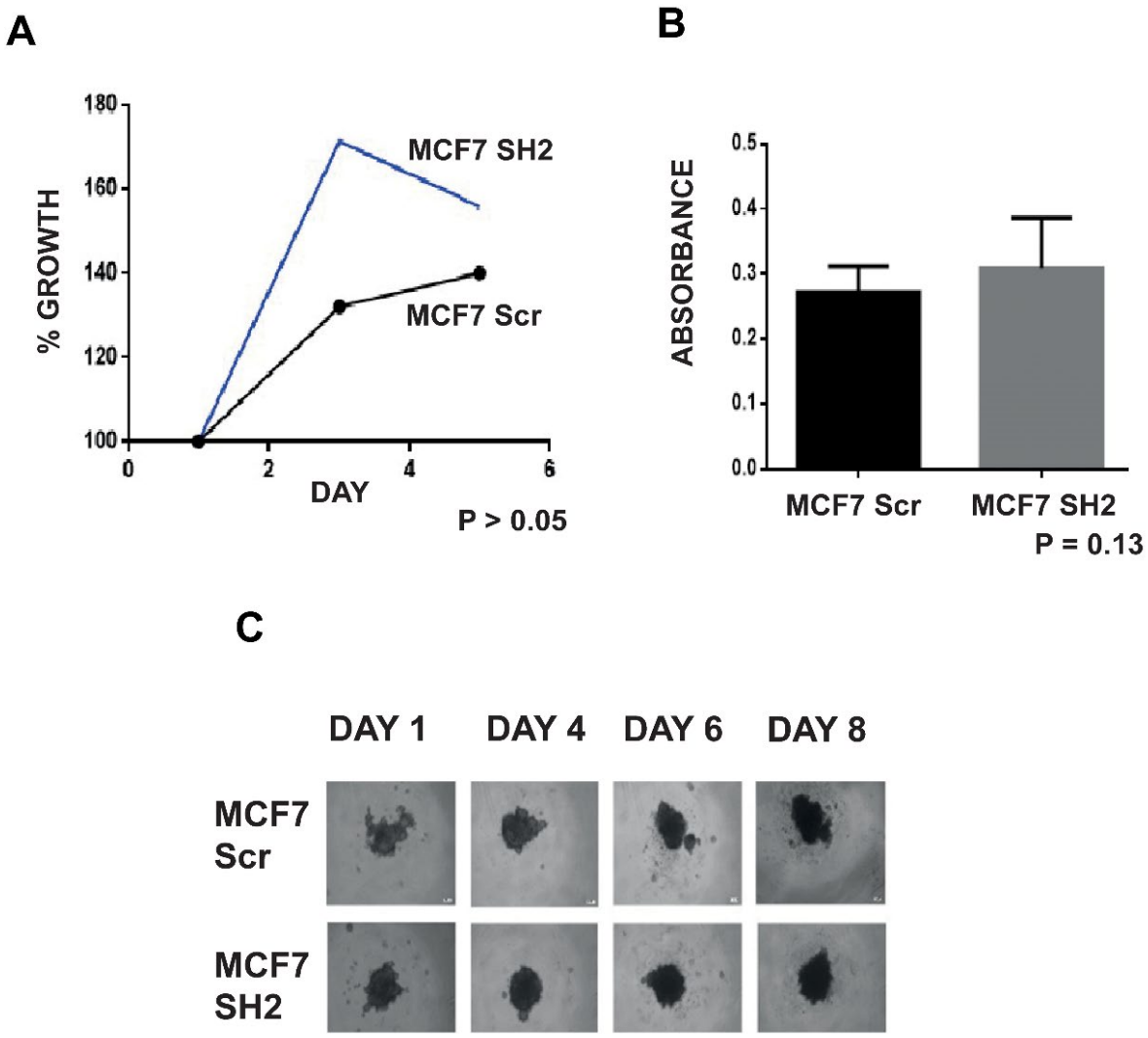

A) Growth assay over 5 days from day 1 baseline, comparing % growth of $MCF7^{Scr}$ to $MCF7^{SH2}$. At time points day 1, day 3 and day 5 cells are fixed and stained with crystal violet. The intensity of staining at each time point is determined by an absorbance reader. Results over time are displayed as relative percentage of staining at day 1. GREM1 knockdown resulted in non-significant increased growth at day 3 with a decline at day 5, possibly due to rapid growth and cell death, p>0.05(Mann Whitney test, experiment repeated in triplicate, displayed mean percentage increase +/- Standard error of mean (SEM))

B) MTT is a colorimetric assay that uses metabolism of a chemical into formazan, which precipitates as a yellow colour, intensity of which is proportional to metabolism and proliferation of viable cells. MTT proliferation assay demonstrated no significant increased cellular division and metabolism in $MCF7^{SH2}$ compared to control (p = 0.13, Mann Whitney test, repeated in triplicate and displayed as mean +/- SEM (error bar)

C) $MCF7^{Scr}$ and $MCF7^{SH2}$cells were grown in 3D on special U bottomed non adherent plates as a cluster, or spheroid of cells. Spheroid growth was measured using ImageJ software for each spheroid over 8 days. GREM1 knockdown in MCF7 cells showed no difference in radial growth of spheroid, p = 0.08. (See appendix 9.3.3 for growth chart)

Figure 4-9 Effect of GREM1 knockdown on MCF7 cells invasion and migration

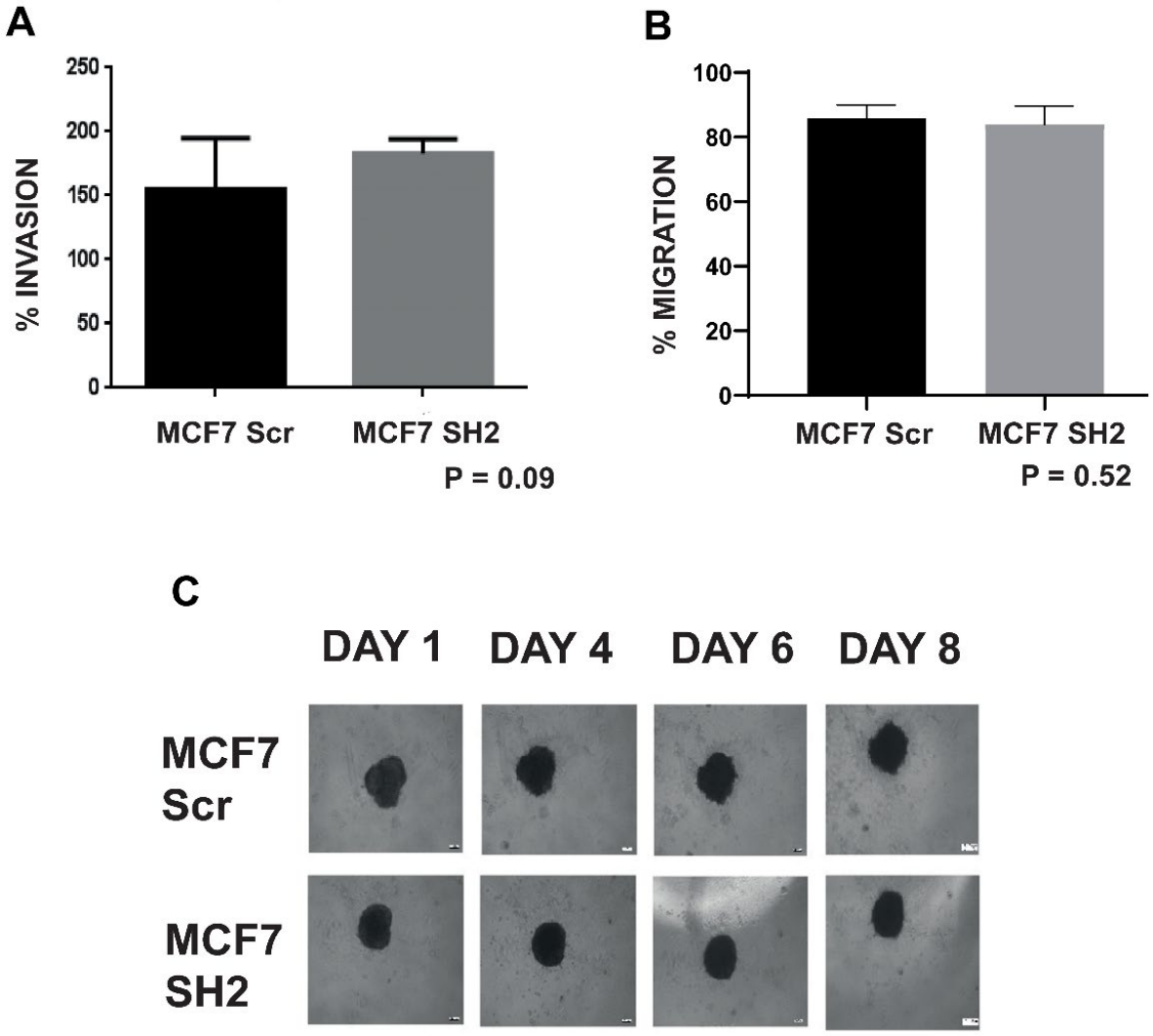

A) Invasion of cells was assessed by how many cells invaded through a porous membrane coated with extracellular matrix (Matrigel) over 72 hours. Cells that invaded through the membrane were fixed and stained and intensity of stain measured. A well of cells with no membrane was used as control to account for different rates of proliferation which might spuriously increase the staining. MCF7^{SH2} cells did not show significant difference in invasion through a transwell Matrigel membrane than control (p =0.09, Mann Whitney test, repeated in triplicate and presented as Mean +/- SEM)

B) Migration of cells was assessed by how many cells migrated through a porous membrane over 72 hours. Cells that migrated were fixed and stained and intensity of stain measured. A well of cells with no membrane was used as control to account for different rates of proliferation which might spuriously increase staining. MCF7^{SH2} cells did not show any significant difference in migration through a transwell membrane compared to control (p = 0.52, Mann Whitney test, repeated in triplicate and presented as Mean +/- SEM)

C) Cells were grown in 3D on special U bottomed non adherent plates as a spheroid of cells which is then surrounded by Matrigel. Invasion of spheroid into the Matrigel was measured using ImageJ software for each spheroid over 8 days.3D Spheroid invasion assay in Matrigel demonstrates no difference of invasion of MCF7^{SH2} compared to control, p = 0.7 (See appendix 9.3.3 for invasion chart)

4.4.5 GREM1 Overexpression in MCF7 and MDA MB 231 cells

Having examined the effect on GREM1 knockdown on cellular function, the same breast cancer cell lines underwent forced overexpression of GREM1, utilising a plasmid vector previously characterised in the laboratory. Other breast cancer cell lines such as BT474 also underwent successful GREM1 overexpression with this plasmid vector, confirmed with PCR, Western blot, and ELISA, and will be discussed in later chapters. As the ELISA was a sample only, there was not enough to undertake confirmation of Gremlin1 over secretion, specifically in MDA MB 231 and MCF7 cell lines however, the PCR and qPCR evaluation of GREM1 overexpression in both cell lines was convincing, compared to controls (Figure 4.10 A – C, $p = 0.03$ in MDA MB 231 and Figure 4.11 A-C $p = 0.001$ in MCF7). The PCR of GREM1 overexpression in MCF7 cells (Figure 4.11 A) does have a slightly stronger GAPDH band signal in $MCF7^{GREM1}$ compared to $MCF7^{PEF,}$ which might imply that the GREM1 expression is only greater on PCR because more sample has been loaded onto the gel, or more RNA was reverse transcribed in that sample. This is overcome using densitometry, which gives a semi quantitative measure of the GREM1 bands relative to their own control GAPDH band, accounting for variances in sample loading. The use of qPCR with the same samples also utilises a second method of confirming GREM1 overexpression.

Figure 4-10 GREM1 overexpression in MDA MB 231 cells

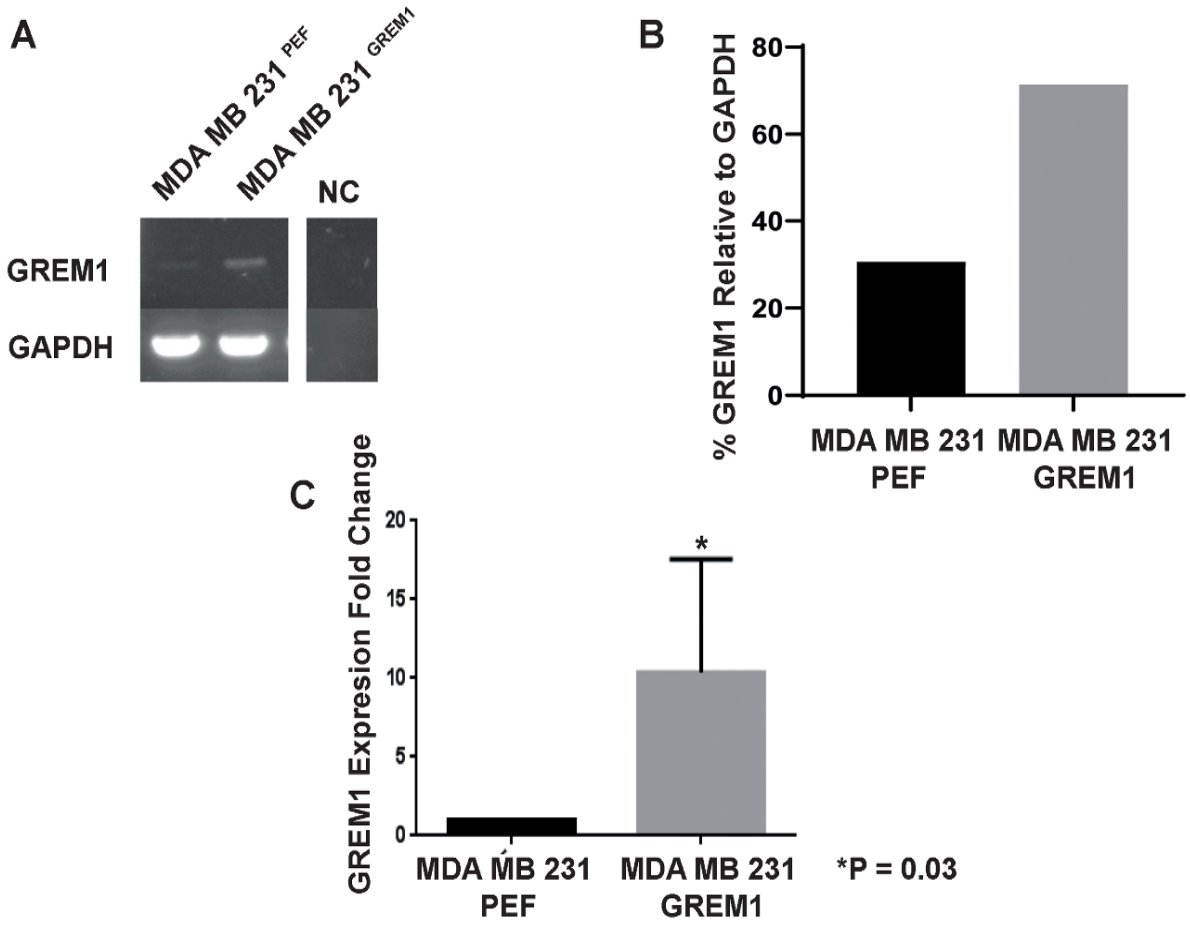

A) Polymerase chain reaction (PCR) at 35 cycles of GREM1 expression and expression of housekeeping gene GAPDH, in MDA MB 231^{GREM1} cells compared to control MDA MB 231$^{PEF.}$ GREM1 has been forcibly overexpressed using a DNA plasmid vector carrying GREM1 or a control nonsense DNA sequence (PEF).NC = negative control (sterile water)

B) Semi quantitative representative of A using image J analysis of the PCR gel, by comparing the intensity of the GREM1 PCR bands as a percentage relative to the intensity of the GAPDH band in each sample, such that sample loading differences are accounted for. The GREM1 expression band in MDA MB 231^{GREM1} cells is stronger than in MDA MB 231^{PEF}.

C) qPCR (quantitative PCR) chart shows the increased fold change in GREM1 expression in MDA MB 231^{GREM1} compared to control, normalised relative to the expression of GAPDH in each sample. Chart representative of combined 3 experimental repeats, presented as mean fold change +SEM (error bar)

Figure 4-11 GREM1 overexpression in MCF7 cells

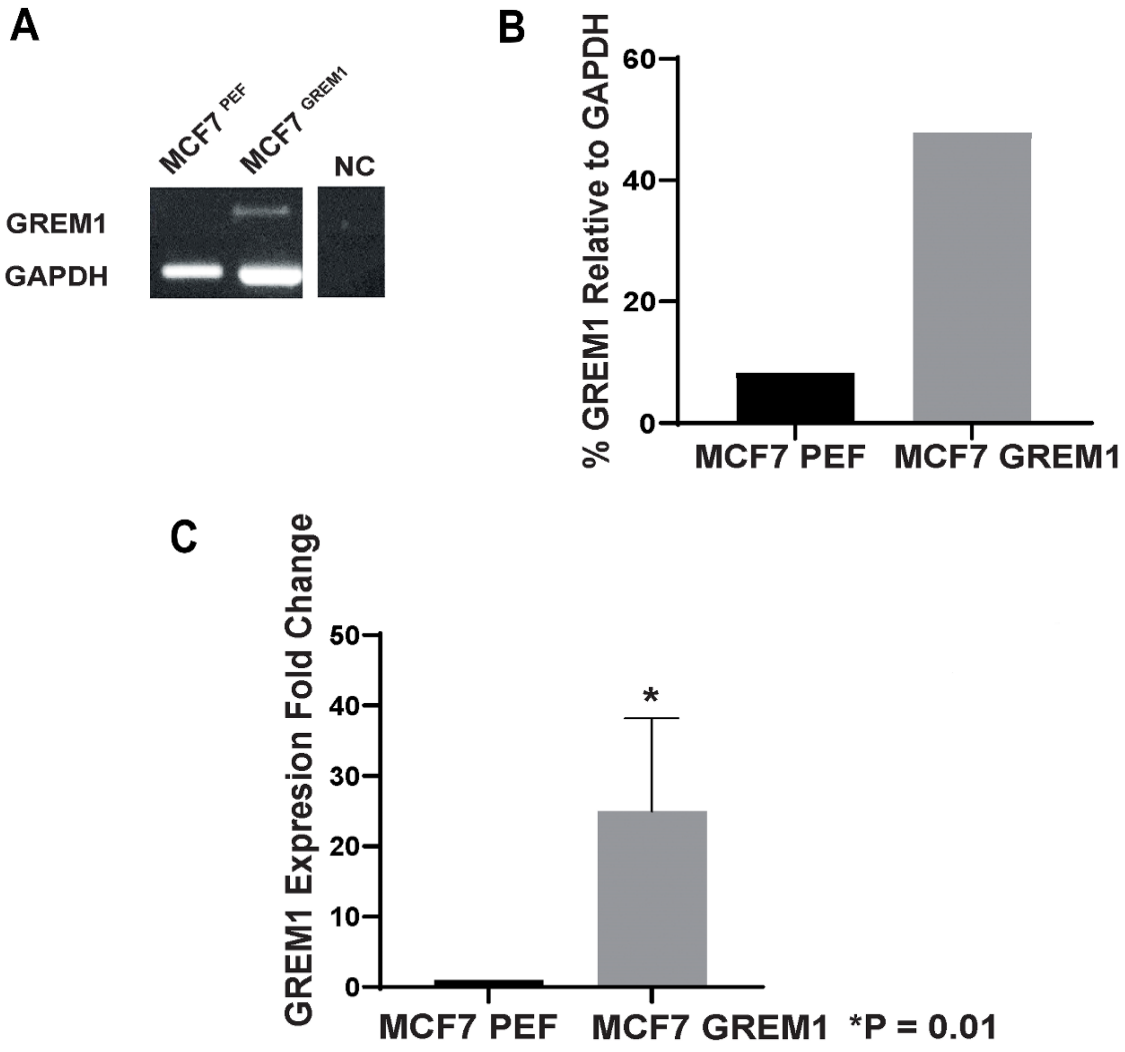

A) PCR at 35 cycles. GREM1 expression and expression of housekeeping gene GAPDH, in $MCF7^{GREM1}$ cells compared to control $MCF7^{PEF}$. GREM1 has been forcibly overexpressed using a DNA plasmid vector carrying GREM1 or a control nonsense DNA sequence (PEF). NC = negative control (sterile water)

B) Densitometry of the PCR from A using image J analysis of the PCR gel, by comparing the intensity of the GREM1 PCR bands as a percentage relative to the intensity of the GAPDH band in each sample, such that sample loading differences are accounted for. The GREM1 expression band in $MCF7^{GREM1}$ cells is stronger than in $MCF7^{PEF}$.

C) qPCR with fold change in GREM1 expression in $MCF7^{GREM1}$ cells compared to control, normalised relative to GAPDH. Chart representative of combined 3 experimental repeats, presented as mean fold change +SEM (error bar)

4.4.6 Effect of GREM1 overexpression in MDA MB 231 cells

In direct contrast to GREM1 knockdown in this cell line, growth in MDA MB 231^{GREM1} was reduced compared to control (Figure 4.12 A p = 0.002 at day 5), however, this was not seen in the MTT proliferation assay or the 3D spheroid growth assay (Figure 4.12 B and C, p = 0.94 for both, see appendix 9.3.4 for spheroid growth chart). As with GREM1 knockdown, there was no significant difference in migration with GREM1 overexpression (Figure 4.13 B, p = 0.06), suggesting GREM1 may not have a significant role in cellular migration at all for this cell line. MDA MB 231^{GREM1} cells had an average reduced invasion compared to control cells, although the error bars were wide and this did not reach significance due to the experimental variability (Figure 4.13 A, p = 0.82). This contrasts with GREM1 knockdown in MDA MB 231^{SH2} cells which had significantly increased invasion. The 3D spheroid invasion model did not show any significant impact of GREM1 overexpression on invasion (Figure 4.13 C p = 0.84 see appendix 9.3.4 for spheroid invasion chart). These comparative results would suggest, in MDA MB 231 cells, that the loss or reduction of GREM1 expression has more impact on cellular function than GREM1 overexpression, and that GREM1 reduction results in more aggressive growth and invasion.

Figure 4-12 Effect of GREM1 overexpression on MDA MB 231 cellular growth functions

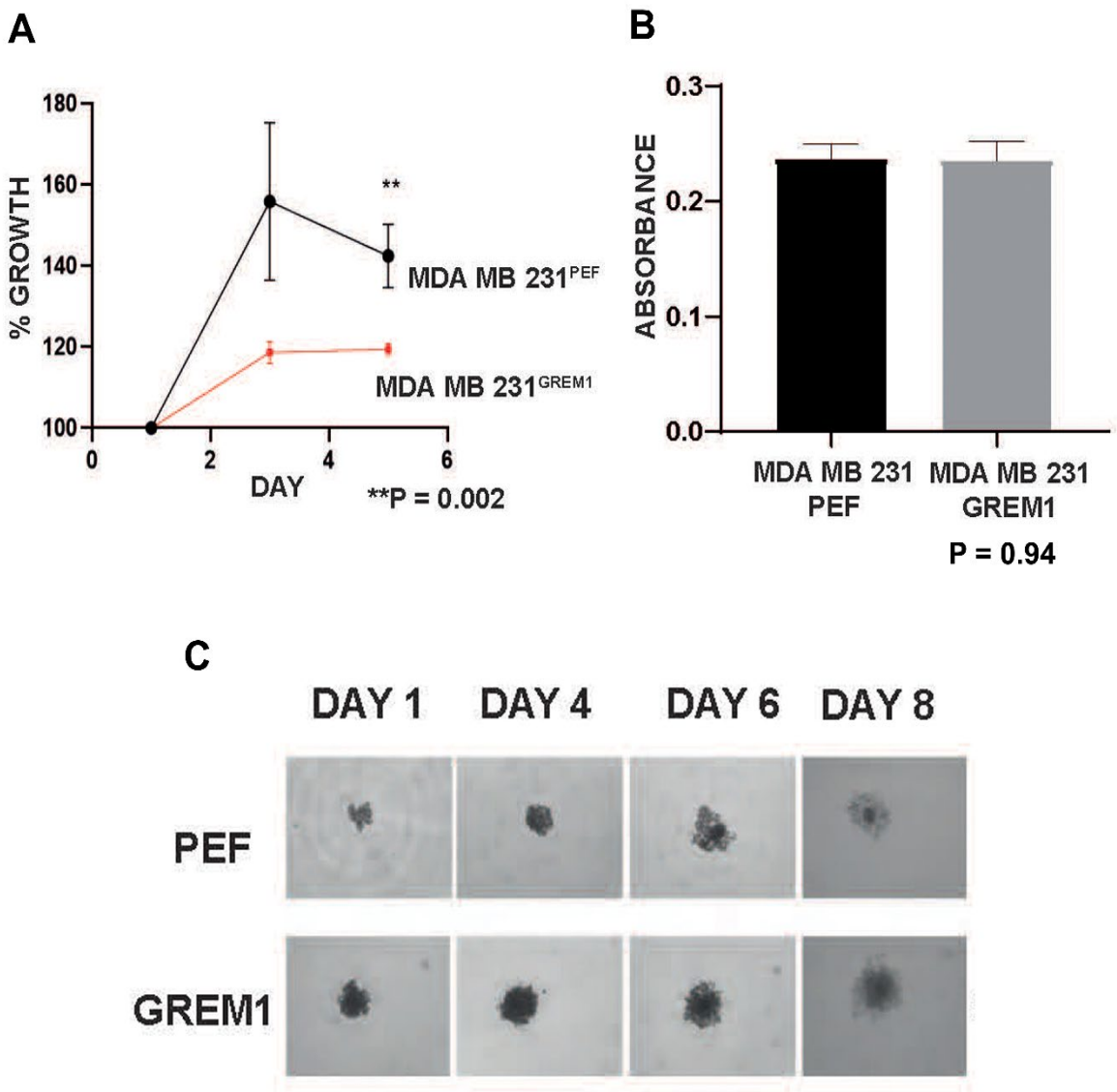

A) **Growth assay over 5 days comparing percentage growth of MDA MB 231^{PEF}to MDA MB 231^{GREM1}. At time points day 1, day 3 and day 5 cells are fixed and stained with crystal violet. The intensity of staining at each time point is determined by an absorbance reader. Results over time are displayed as relative percentage of staining at day1. GREM1 overexpression (red line) resulted in reduced growth at day 3 and significantly reduced at day 5, p = 0.002(Mann Whitney test, experiment repeated in triplicate, displayed mean percentage increase +/- Standard error of mean (SEM))**

B) **MTT is a colorimetric assay that uses metabolism of a chemical into formazan, which precipitates as a yellow colour, intensity of which(absorbance) is proportional to metabolism and proliferation of viable cells. MTT proliferation assay demonstrated no different proliferation and cellular metabolism in MDA MB 231^{GREM1}compared to MDA MB 231^{PEF} (p = 0.94 Mann Whitney test, repeated in triplicate and displayed as mean +/- SEM)**

C) **Cells were grown in 3D on special U bottomed non adherent plates as a cluster, or spheroid of cells. Spheroid growth was measured using ImageJ software for each spheroid over 8 days. MDA MB 231^{GREM1} cells do not have significantly different growth compared to control p = 0.94 (See appendix 9.3.4 for 3D Spheroid growth graphs)**

Figure 4-13 Effect of GREM1 overexpression on MDA MB 231 cells invasion and migration

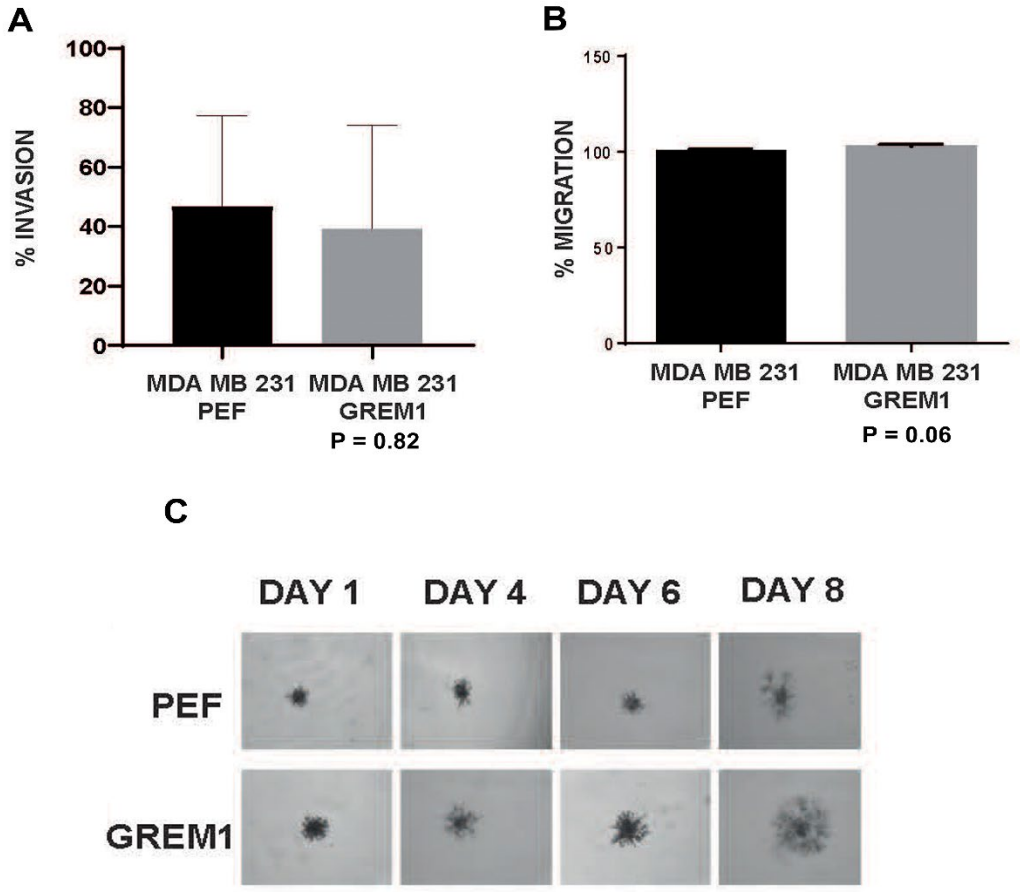

A) Invasion of cells was assessed by how many cells invaded through a porous membrane coated with extracellular matrix (Matrigel) over 72 hours. Cells that invaded through the membrane were fixed and stained and intensity of stain measured. A well of cells with no membrane was used as control to account for different rates of proliferation which might spuriously increase the staining. MDA MB 231^{GREM1} cells did not show significant difference in invasion through a transwell Matrigel membrane than control MDA MB 231^{PEF} (p =0.82, Mann Whitney test, repeated in triplicate and presented as Mean +/- SEM)

B) Migration of cells was assessed by how many cells migrated through a porous membrane over 72 hours. Cells that migrated were fixed and stained and intensity of stain measured. A well of cells with no membrane was used as control to account for different rates of proliferation which might spuriously increase staining. MDA MB 231^{GREM1} cells did not show any significant difference in migration through a transwell membrane compared to control (p = 0.06, Mann Whitney test, repeated in triplicate and presented as Mean +/- SEM)

C) Cells were grown in 3D on special U bottomed non adherent plates as a spheroid of cells which is then surrounded by Matrigel extracellular matrix. Invasion of spheroid into the Matrigel was measured using ImageJ software for each spheroid over 8 days. There was no difference in 3D invasion between MDA MB 231^{GREM1} and control cells p = 0.84 respectively (See appendix 9.3.4 for 3D Spheroid invasion graphs).

4.4.7 Effect of GREM1 Overexpression in MCF7 cells

In keeping with the effects seen in MDA MB 231 GREM1 overexpression, and in contrast to GREM1 knockdown, growth was significantly reduced in MCF7^{GREM1} cells compared to control at day 3 and 5 (Figure 4.14 A, $p < 0.001$). However, this was not seen in the proliferation MTT assay, whereby MCF7^{GREM1} cells had a non-significant, slight increase in proliferation (Figure 4.14 B, $p = 0.17$). When assessing 3D growth, there was a non-significant reduction in growth of MCF7^{GREM1} cells compared to control (Figure 4.14 C, $p = 0.42$, see appendix 9.3.5 for 3D growth graph).

Again, in keeping with the previous findings, MCF7^{GREM1} cells display significantly reduced invasion compared to control in transwell invasion assay (Figure 4.15 A, $p = 0.03$), although, as with MDA MB 231^{GREM1} cells, there was no significant difference seen in 3D spheroid invasion (Figure 4.15 C, $p = 0.50$, see appendix 9.3.5 for invasion graph).

As in all prior cellular function experiments, GREM1 overexpression in MCF7 cells had no discernible effect on transwell migration (Figure 4.15 B, $p = 0.61$).

Figure 4-14 Effect of GREM1 overexpression on MCF7 cellular growth functions

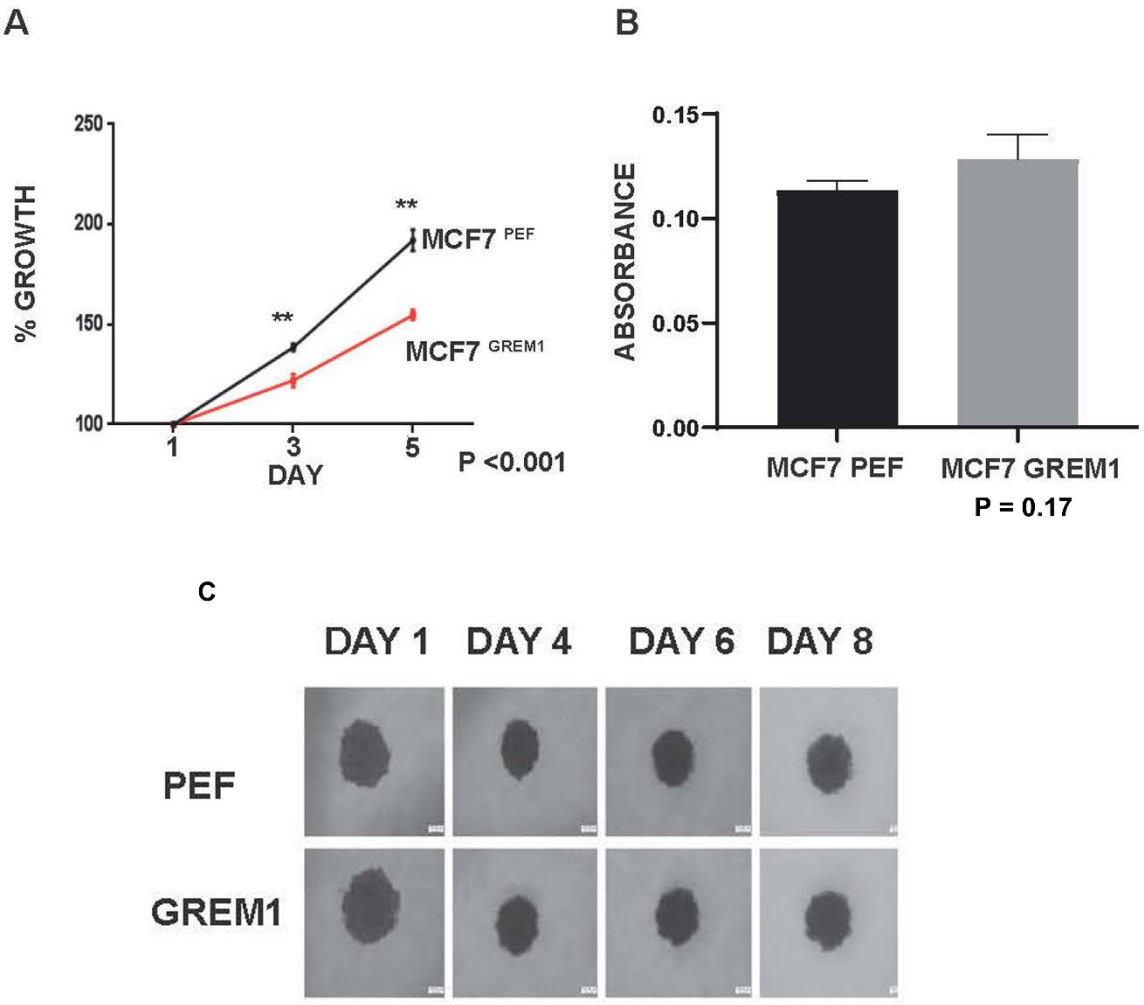

A) Growth assay over 5 days comparing % growth of $MCF7^{PEF}$ to $MCF7^{GREM1}$. At time points day 1, day 3 and day 5 cells are fixed and stained with crystal violet. The intensity of staining at each time point is determined by an absorbance reader. Results over time are displayed as relative percentage of staining at day1. GREM1 overexpression (red line) resulted in significantly reduced growth at day 3 and day 5, P < 0.001 (Mann Whitney test, experiment repeated in triplicate, displayed mean percentage increase +/- Standard error of mean (SEM))

B) MTT proliferation assay, in which the cells metabolise a chemical into formazan, which precipitates into a yellow colour in proportion to viable and proliferating cells, and absorbance of the colour intensity is read. This demonstrated no difference in proliferation of $MCF7^{GREM1}$ compared to control, p = 0.17 (Mann Whitney test, repeated in triplicate and displayed as mean +/- SEM)

C) Cells grown in 3D on special U bottomed non adherent plates as a cluster, or spheroid of cells. Spheroid growth was measured using ImageJ software for each spheroid over 8 days. $MCF7^{GREM1}$ cells did not have different spheroid growth compared to control, p = 0.42(See appendix 9.3.5 for 3D Spheroid growth graphs)

Figure 4-15 Effect of GREM1 overexpression on MCF7 cells invasion and migration

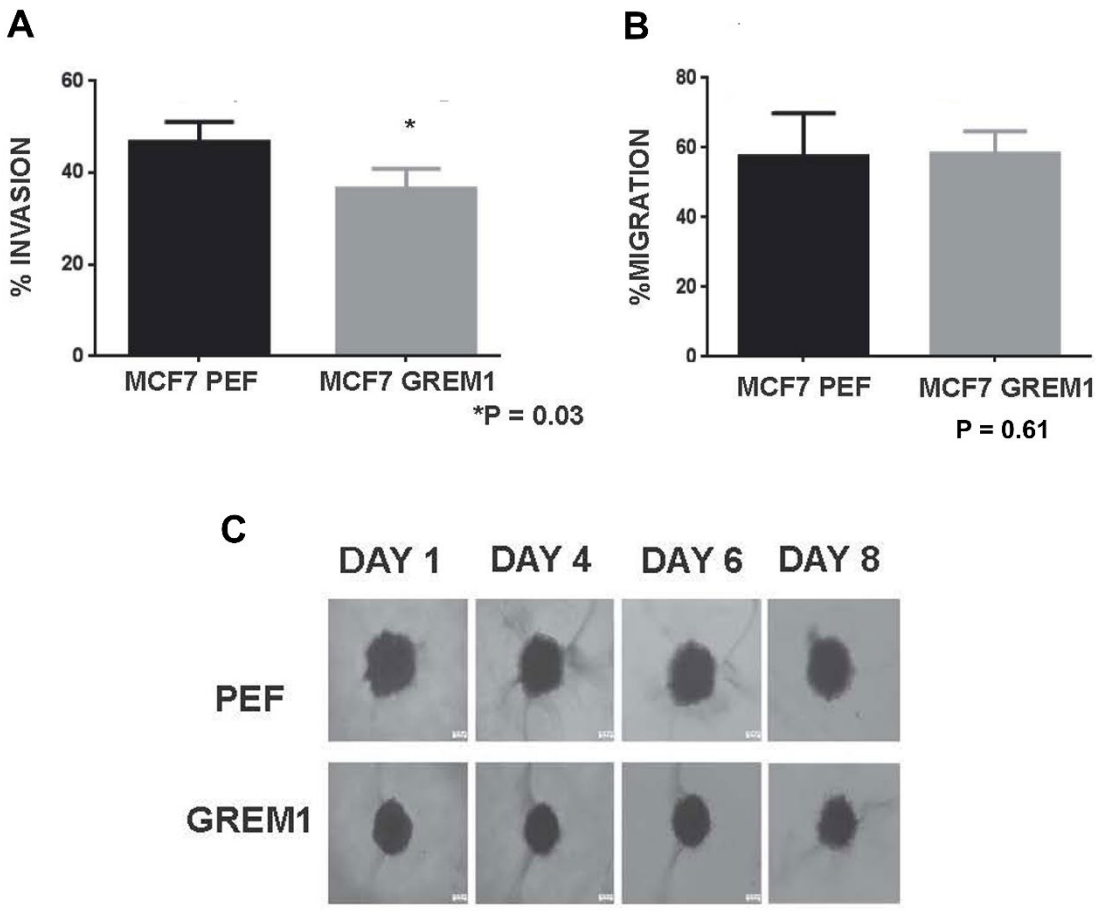

A) Invasion of cells was assessed by percentage of cells invaded through a porous membrane coated with extracellular matrix (Matrigel) over 72 hours. Cells that invaded through the membrane were fixed and stained and intensity of stain measured. A well of cells with no membrane was used as control to account for different rates of proliferation which might spuriously increase the staining. MCF7^{GREM1} cells have significantly reduced invasion through a Matrigel membrane compared to control, p = 0.03 (Mann Whitney test, repeated in triplicate and presented as Mean +/- SEM)

B) Migration assay was undertaken with the same method as the invasion assay, but instead the membrane was not coated with Matrigel, and cells migrated through the porous membrane only. MCF7^{GREM1} cells did not show any significant difference in migration through a transwell membrane compared to control, p = 0.61(Mann Whitney test, repeated in triplicate and presented as Mean +/- SEM)

C) For a 3D invasion assay cells were grown in non-adherent u bottomed wells to create spheroids that were then surrounded by Matrigel and invasion into the Matrigel monitored over 8 days, with Image J software used to quantify radial invasion. There was no significant difference in spheroid invasion between MCF7^{GREM1} and control cells, p = 0.50 (See appendix 9.3.5 for 3D Spheroid invasion graphs)

4.5 Discussion

GREM1 and the relevant BMP ligands BMP-2, -4 and -7, showed very variable expression across a panel of breast cancer cell lines. Although GREM1 seemed to be most consistently expressed in cell lines expressing HER2, it was also expressed in MCF7 (which are ER+/PR+ cells) and MDA MB 231 cells (which have neither HER2, PR or ER expressed). Regulation of GREM1 expression remains largely unknown. Studies in limb development suggest BMP-2 has a concentration dependent effect on GREM1 expression, with BMP-2 inducing upregulation of GREM1, unless at very high concentrations, whereby downregulation occurs (Nissim et al. 2006). In the expression panel of multiple cell lines and GREM1/BMP ligands, there did not appear to be any consistent correlations between level of GREM1 expression and expression of BMP-2, -4 and -7. For example, SKBR3 and MDA MB 231 cell lines had relatively similar GREM1 expression, but SKBR3 only expressed BMP-7 and at high levels, whereas MDA MB 231 cells expressed moderate amounts of all three ligands (Figure 4.1B). This is likely to reflect the unknown multivariable influences on the expression of GREM1, via several different cell signalling and regulatory pathways, and the many ways dysregulation of gene expression can occur in breast cancers.

This also demonstrates the limitations of studies which undertake cellular function tests in only one cell line, as representative of breast cancer and, therefore, three cell lines were selected for cell function testing to examine how generalisable the findings might be. MCF7 and MDA MB 231 were initially selected as these are the most well characterised and utilised breast cancer cell lines therefore, any results are more comparative to current literature. These cell lines also had a reasonable GREM1 expression and thus could be manipulated both with knockdown and overexpression of GREM1. In addition, BT474 and SKBR3 were selected as HER2+ cell lines, as GREM1 appeared to be more consistently expressed in HER2+ cell lines. The association between GREM1 in HER2+ breast cancers are the subject of further experimental work in subsequent chapters. SKBR3 cells proved to be challenging to manipulate GREM1 expression without causing cell death. This may reflect the sensitivity of SKBR3 cell lines to surviving the method of lentiviral particle transfection and selection, although SKBR3^{SH2} cells did not survive, even when selection antibiotics were removed. It could also reflect that GREM1 may be a vital component of cell survival or apoptosis pathways for this cell line. In a recent study published since the completion of this thesis work, Park

et al undertook GREM1 knockdown in MDA MB 453, MDA MB 468 and SKBR3 cells and found cell viability was significantly reduced compared to control (Park et al. 2020).

Park et al also noted in this study that ER negative cell lines had higher GREM1 expression than ER positive cell lines. This was not consistently seen in the above expression panel (Figure 4.1 and 4.2), although this utilised MDA MB 231, BT20 and BT549 as more representative triple negative cell lines, whereas Park et al utilised MDA MB 468, MDA MB 453 and SKBR3 which are only ER negative rather than truly triple negative. In fact, the three ER negative cell lines in the Park et al study have HER2 expression, and this thesis found GREM1 to be more consistently expressed in HER2 positive cell lines. SKBR3 is well known as having amplified HER2 expression on IHC, as does MDA MB 453, but to a lesser degree, and MDA MB 468 has been shown to have overexpression of $pHER2^{Y877}$, indicating that although HER2 is not amplified, it is activated in this line (Burguin et al. 2020).

Gremlin knockdown resulted in significant increases in growth and invasion in TNBC MDA MB 231 cells, but this was not seen in the ER+ MCF7 cell line. There was a slight trend towards increased growth and invasion in $MCF7^{SH2}$ cells although this was not statistically significant and overall, GREM1 knockdown in MCF7 cells did not appear to impact any of the cellular function assays significantly. This may be because, although knockdown in MCF7 cells appeared significant at the mRNA level, the ELISA showed the secreted Gremlin1 was only reduced by a small amount (Figure 4.5). This reduction may not have been enough to alter cell function in MCF7 cells in culture.

Interestingly, although MDA MB 231^{SH2} had increased growth and invasion, MDA MB 231^{GREM1} did show a decreased growth, but no other significant effect on cellular function. It may be that in this cell line, Gremlin1 has more of a tumour suppressor role than in MCF7 cells, and the reduced GREM1 expression in MDA MB 231 allowed aberrant BMP and MAPK signalling pathways to promote growth and invasion. Subsequent GREM1 overexpression in MDA MB 231 cells may not have had much of an impact on cellular function, because GREM1 was already expressed at sufficient levels and may not have been overexpressed at a high enough level to impact cellular function significantly. The tumour suppressive effects were however seen in MCF7 cells instead, whereby GREM1 overexpression resulted in reduced growth and invasion.

In further experiments of the effect of Gremlin1, MCF7 cells were treated with human recombinant Gremlin1 at high concentration (see appendix 9.3.6), and expression levels of markers of EMT examined with qPCR, which supported the $MCF7^{GREM1}$ findings, markers of invasiveness such as Snail, Slug and Vimentin decreased, and E- Cadherin increased. A cohort of cell function tests in the presence of high concentrations of recombinant Gremlin1 would be a further useful method of investigating Gremlin1's effect on breast cancer cell function.

In conclusion of this chapter, within the limitations described, it would appear GREM1 affects breast cancer cellular functions depending on the cell line studied. The triple negative MDA MB 231 cells increased their invasiveness, growth, and proliferation with GREM1 knockdown, but GREM1 overexpression in this cell line had no real functional effect, excepting a decrease in growth. In the ER+ MCF7 cell line GREM1 knockdown had no effect on cell functions at all, but GREM1 overexpression resulted in decreased growth and invasion. This highlights the issue of taking results of *in vitro* cell function studies from a single cell line as representative of the disease, and the characteristics of each cell line will influence the effect of GREM1 knockdown or overexpression. Further to this, a study published after the completion of the work for this thesis, undertook knockdown and overexpression of GREM1 in MDA MB 231 cells, and found GREM1 knockdown decreased cellular proliferation on MTT assay, and decreased motility on a wound scratch assay, with the converse found on GREM1 overexpression (Sung et al. 2020b). These findings by Sung et al fit more with the large database findings in Chapter 3, whereby higher GREM1 is associated with more metastasis and poor clinical outcomes, whereas my in vitro function findings fit more with the local clinical cohort data, whereby lower GREM1 associated with poorer prognosis. Different methodology was utilised and may explain the difference in findings. Sung et al also did not present any growth, invasion, or spheroid assays, with which to compare.

The extent to which single cell lines reflect clinical tumours is evidently limited. In particular, the clinical subtype and molecular phenotype of breast cancers is increasingly important in clinical practice, and I have identified in this chapter that not all cell lines or breast cancer phenotypes may be affected by aberrant GREM1 in the same way. The associated GREM1 expression in HER2+ breast cancer cell lines are of interest, and thus, Gremlin1 in breast cancer subtypes is examined more closely in the following chapters.

5 Aberrant Gremlin1 expression has a role specific to HER2+ Breast Cancer

5.1 Introduction

It is well recognised that breast cancers of different phenotype and genotype require different treatment approaches and have different outcomes. Gene expression profiling of breast cancers (e.g., Oncotype Dx, MammaPrint, Endopredict and Prosigna (PAM50)) is becoming increasingly utilised clinically for prognostic information and treatment decisions, such as how much benefit those with early-stage breast cancer may get from certain adjuvant treatments.

HER2 overexpression is seen in 20-25% of invasive breast cancers and denotes poor prognosis and chemo-resistance (Ren et al. 2014a; Dai et al. 2015; Adamczyk et al. 2017). HER2 (ErbB2) is one of four cell surface receptors of the HER/ErbB receptor tyrosine kinase family, and is unique amongst its family in that there is not yet an identified ligand, and thus its action is postulated to be via dimerisation with other HER/ErbB receptors (Valabrega et al. 2007). On receptor dimerization, transphosphorylation of the intracellular kinase domains occurs, resulting in downstream intracellular signalling cascades such as PI3K/AKT/mTOR and Ras/Raf/MAPK. This controls cellular proliferation, motility and apoptosis and is consequently oncogenic.

Patients demonstrating an overexpression of HER2 are treated with Trastuzumab, a humanised monoclonal antibody directed against the extracellular portion of HER2. Approximately 15-30% of HER2 positive cancers respond to Trastuzumab as monotherapy and this can be increased to up to 80% when combined with chemotherapy however, up to a quarter of these patients will relapse, with the greatest risk in the 12 months following cessation of Trastuzumab (Valabrega et al. 2007; Adamczyk et al. 2017). For those with HER2 positive breast cancers resistant to, or progressive after this treatment, it appears therapeutic success may be greatest if other related pathways are targeted. For example, the CLEOPATRA study (Baselga and Swain 2010) added pertuzumab (a monoclonal antibody which blocks HER2 dimerisation with EGFR, HER3 and HER4) to trastuzumab and docetaxel, improving the response to therapy by a median of nearly 8 months.

There is evidence from *in vitro* studies that BMP signalling interacts with the clinically important EGF/ErbB(HER) signalling pathways in breast cancer (Zabkiewicz et al. 2017). In this chapter we further examined the association of Gremlin1 expression with breast cancers of the different molecular subtypes and

receptor status, with reference to HER2+ breast cancers. GREM1 expression in HER2 positive breast cancer cell line BT474 was then manipulated to assess the effect on cellular functions.

5.2 Methods

5.2.1 Examination of publicly available expression database Gene-Expression Miner

bc-GenExMiner v4.1 (breast cancer Gene-Expression Miner v4.1) is a statistical mining tool of published annotated genomic data. The database comprises 36 breast cancer studies for which annotated genomic data is available. The patient cohorts in these studies range in size from 41-401 patients, with a total of 5861 patient tumours examined using a variety of microarray platforms, the most common being Affymetrix. The population data can then be used to examine targeted gene expression against clinical criteria and molecular subtype.

Patients were pooled according to their molecular subtypes based on Sorlie's, Hu's and PAM50 classifications, only patients with concordant molecular subtype assignment were kept. Univariate Cox proportional analysis was performed for the chosen gene for each of the different molecular subtype populations. Geneminer performed statistical analyses to assess the significance of the difference in gene distributions between the different subtypes, either a Welch's test or Dunnett-Tukey-Kramer's tests when appropriate.

5.2.2 Examination of GEO dataset GSE20685

GSE20685 is one of the largest breast cancer datasets available for analysis. The gene expression profiles of 327 breast cancer samples were determined using total RNA and Affymetrix U133 plus 2.0 arrays. On many Affymetrix gene expression microarrays, a given gene may be detected by multiple probe sets, which may deliver inconsistent or even contradictory measurements. The 'Jetset'(Li et al. 2011) best correlated probes were selected for determining gene expression measures in this cohort and are as follows:

Gene	Affymetrix best probe(s)
GREM1	218469_at (218468_s_at, second line)
ESR1(ER-α)	211235_s_at ***or*** 211234_x_at
PGR(PR)	228554_at
HER2	234354_x_at

Patients within the cohort were grouped by receptor status using an expression cut-off value calculated by the authors for ESR1, PGR and HER2. GREM1 expression could then be compared between these groups using unpaired t test with significance at $p < 0.05$. Pearson's correlation co-efficient was also calculated between GREM1 and receptor gene expression, with significance at $p < 0.05$. The receptor status could then also be correlated to available clinical outcome parameters.

5.2.3 KMplot survival analysis

For this analysis the Affymetrix Jetset best probe for GREM1, 218469_at, was selected. OS, RFS and DMFS Kaplan Meier plots were then calculated using KMplot to examine survival outcomes between those with high or low expression of GREM1 in their primary tumours by different molecular subtypes of breast cancer. Molecular subtypes were based on the 2013 St. Gallen criteria (Senkus et al. 2013).

5.2.4 Tissue Microarray

The tissue microarray Br1505d (BIOMAX, USA) contained 150 x 1mm diameter core biopsies (dual cores) from 75 cases of confirmed invasive ductal carcinoma. Case information also included patient age, TNM, Stage, Grade, ER/PR status (by IHC and percentage staining) and HER2 status (by IHC). Full TMA specifications, processing, IHC and analysis details can be found in Chapter 2.4.5.

In brief, the slide underwent de-paraffinisation, antigen retrieval and then IHC with Gremlin1 antibody at 1:250 dilution (C7, Santa Cruz biotechnology, USA). On completion of IHC the slide was photographed using high definition EVOS imaging system (Thermofisher, UK). Images were processed using MIPAR^{TM} image analysis software (Sosa et al. 2014), each core could then be assessed for proportion of the core at each staining intensity, and a grade from 1 (low proportion stain/background) to 5 (majority of core high intensity stain).

5.2.5 BT474 GREM1 Overexpression

pEF6/V5-HIS TOPO TA vectors containing GREM1 overexpression plasmid or empty pEF6/V5-HIS TOPO TA vector were used to transfect BT474 cells, as per Chapter 2.7. Following transfection, cells were selected for up to 14 days in culture medium with Blasticidin S (Melford, Suffolk, UK) at 5µg/ml and further maintained in 0.5µg/ml Blasticidin S. PCR and RT-qPCR of cDNA from BT474^{GREM1}

overexpressing and BT474^{pEF} control cells was used to confirm stable overexpression. Overexpression of secreted protein by 21.5% was also confirmed with ELISA (See protocol Chapter 2.4.6 and appendix 9.3.1).

5.2.6 PCR and qPCR

Protocols and cycling conditions for RNA extraction, RT, PCR, qPCR, and analysis are found in Chapter 2.3. PCR and qPCR for GREM1, HER2 and GAPDH (internal control) utilised the SYBRgreen primers listed in Table 2.1. For expression markers of cell cycle and EMT, Precision Q-PCR 2X qPCR Mastermix (Primer Design, UK) and primers from Sigma (Sigma Aldrich, Inc., Dorset, UK) were used for qPCR of GREM1, P27, P21, CyclinD, ID1, Snail, Slug, E- Cadherin, Vimentin and GAPDH (See Primer Table 2.1).

QPCR data were analysed and normalised to the housekeeping gene, GAPDH, with a sterile water negative control, and comparative $C_T(\Delta\Delta C_T)$ analysis as described in Chapter 2.3.

5.2.7 Western Blotting

Protein expression for Gremlin1, HER2 and β Actin was established using SDS-PAGE and Western blotting. Western blotting used PDVF membranes and a semi-dry transfer method. A full protocol is found in Chapter 2.4, including the antibodies used (Table 2.2). Housekeeping protein β Actin was the internal control. Semi quantification densitometry was performed using Image J software.

5.2.8 Growth Function Assays

BT474^{GREM1} or BT474^{pEF} cells were seeded at 3,000 per well into 200µl medium (RPMI Phenol red free, with 10% charcoal stripped FCS to reduce oestrogenic and growth hormone stimulus) in three 96-well plates, and incubated for 1, 3, and 5 days respectively. Full protocol as per Chapter 2.8.1. with fixation and staining of cells with crystal violet, and absorbance measured. Results are displayed as % growth, whereby the absorbance at days 3 and 5 are comparative to the reading at day 1. A 3D Spheroid growth assay was also undertaken with BT474^{GREM1} and BT474^{pEF} cells as per protocol in Chapter 2.8.1, photographed at the same magnification on days 1, 4, 6 and 8 and then analysed using ImageJ software for Spheroid area and % growth comparative to day 1.

5.2.9 Invasion Function Assays

Twenty thousand BT474^{GREM1} or BT474^{pEF} cells were seeded in 200 µl Serum free RPMI Phenol Red free medium, within an 8µm pore well insert that had been previously coated with a Matrigel membrane (see Chapter 2.8.3). Medium with serum (10% charcoal stripped FCS) was placed in the underlying well. Control wells to account for proliferation effects over 72hrs had 20,000 cells seeded with no inserts. After 72 hours incubation the cells invaded to the underside of the insert, and the cells in the control wells were fixed and stained with crystal violet. Three field views of the insert with invaded cells, and the control wells were photographed. Stained cells were dissolved with 300 µl acetic acid (10% v/v) and plated into a 96 well plate for reading of absorbance at wavelength of 540nm. Percentage Invasion was calculated as Absorbance of invaded cells/Absorbance of control cells x 100. Spheroid invasion assay was also undertaken with 3,000 BT474^{GREM1} or BT474^{pEF} as per protocol in Chapter 2.8.3, however, very little change was seen in the spheroids over at least 8 days, and results are instead available in appendix 9.4.1

5.2.10 Migration Function Assay

As per the invasion assay above and Chapter 2.8.4, the experimental protocol remained the same, but the 8µm inserts did not contain a Matrigel layer. Migrated cells after 72 hours were fixed with Formalin and stained with crystal violet, dissolved in acetic acid and absorbance read at 540nm. Percentage migration was calculated as Absorbance of migrated cells/Absorbance of control cells x 100.

5.2.11 Colony Formation Assay

BT474^{GREM1} or BT474^{pEF} cells were placed in suspension and counted (method as described in Chapter 2). One hundred cells per well were plated onto a 6 well plate, using a fine gauge (30G) needle and syringe to avoid cell clumps, and to scatter the cells as single cell suspension. Cells were then cultured under standard conditions for two weeks, gently washed with PBS, then fixed with formalin and stained with crystal violet. A count was then done of the number of colonies formed.

5.3 Results

5.3.1 GREM1 expression varies by molecular subtype and receptor status of Breast Cancer

GREM1 expression was highest in breast tumours classified solely as HER2 + in comparison to Luminal A, Luminal B and Basal/TNBC. This remained true whatever the molecular subtype classification tool used, be it PAM50, Sorlie's, Hu's or combining the three (Figure 5.1A, includes only those samples for which the molecular subtype agrees across all three classification systems).

In a cohort of 327 patients from the GEOdata set GSE20685, GREM1 expression did not significantly differ between clinically ER positive and ER negative, or PR positive and PR negative patients, but there was significantly higher GREM1 expression in HER2 positive patients compared to HER2 negative patients (Figure 5.1 B $p = 0.004$). Table 5.1 shows the Pearson's correlation co-efficient in the cohort GSE20685 for the association between GREM1 RNA expression and the RNA expression of ER, PR and HER2. This demonstrated a statistically significant negative correlation between GREM1 and ER expression on both microarray probe sets (Table 5.1 $p = 0.00122$ and 0.00564). GREM1 and PR were also negatively correlated to statistical significance on one GREM1 probe set but not to significance with the Jetset 'best' GREM1 probe 218469_at. GREM1 was significantly positively correlated with HER2 expression at RNA level in this cohort (Table 5.1, $p = 0.0304$), in keeping with the IHC clinical receptor status in Figure 5.1B. Figure 5.2 A, B and C show the correlation in graph form comparing ER, PR and HER2 expression with GREM1 Jetset 'best' microarray probes.

Figure 5-1 Correlating GREM1 expression with clinical receptors and molecular subtypes

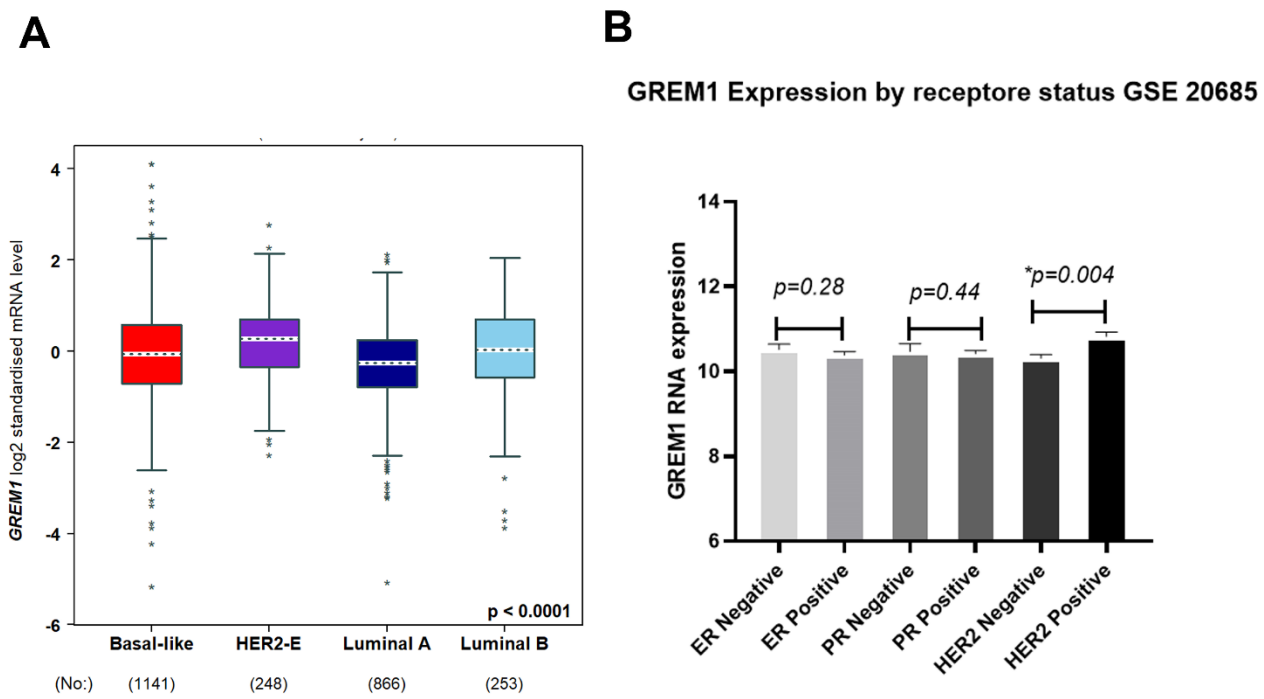

A) 2,192 breast cancer samples analysed in GenExMiner online pooled microarray data repository for GREM1 expression by molecular subtype of Breast Cancer.GREM1 expression is highest in HER2 enriched tumours and lowest in Luminal A tumours. P < 0.0001 Dunnett-Tukey-Kramer test of multiple pairwise comparisons, and Welch's t tests between the four groups, as provided by the online statistical software(Jezequel et al. 2021)

B) Geodata cohort GSE20685 (n = 327) shows no significant difference in GREM1 expression between clinical immunohistochemistry ER or PR positive and negative patients (p = 0.28 and 0.44 respectively, Mann Whitney test). There is significant increased expression of GREM1 in HER2 positive patients compared to HER2 negative (p = 0.004 Mann Whitney test). Displayed as Mean, with standard error of the mean (SEM) error bar.

Figure 5-2 Correlation of GREM1 expression in breast cancers with clinical receptor expression

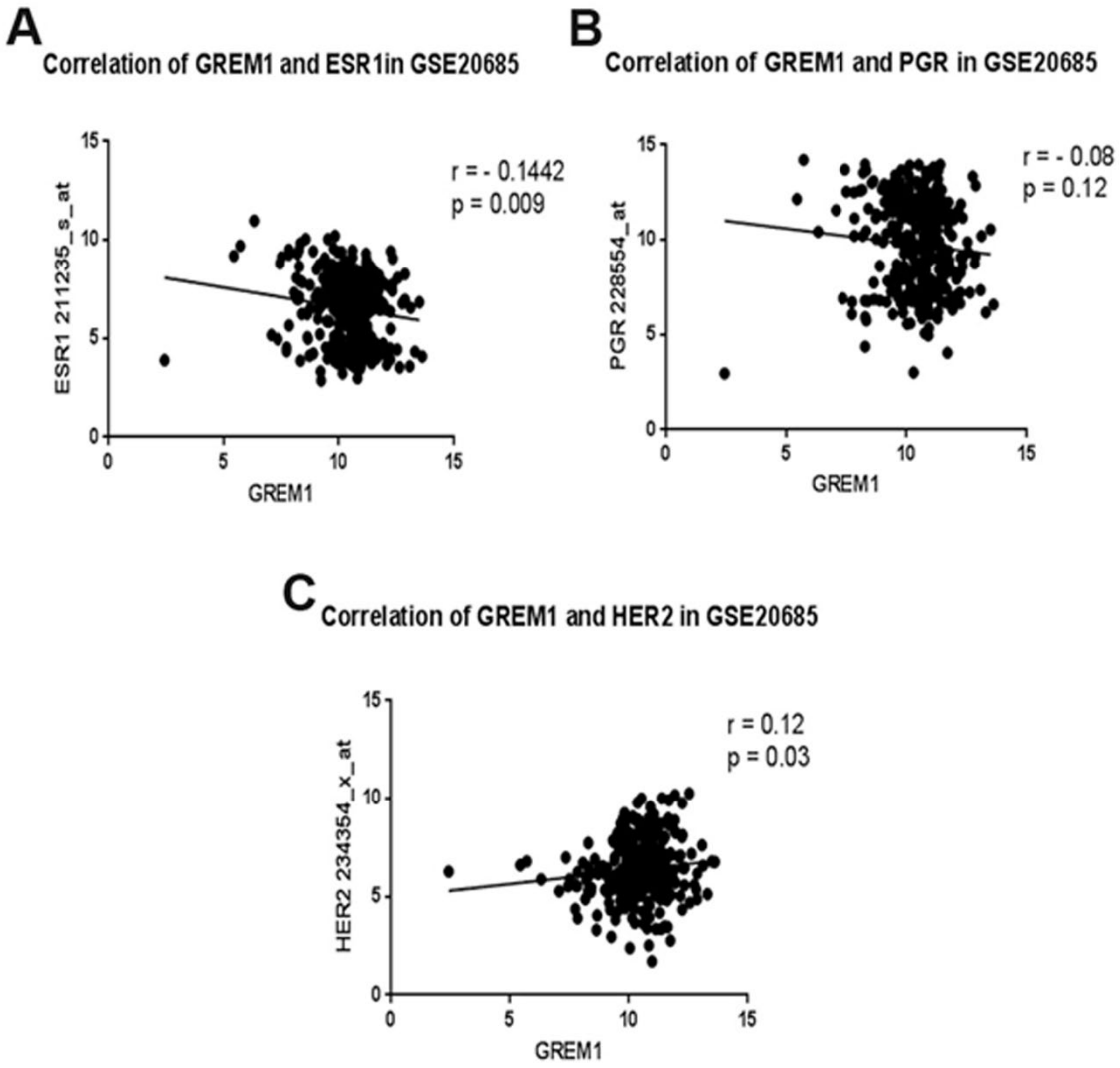

A) In a cohort of 327 primary breast tumours with publicly available DNA microarray data(Jezequel et al. 2013), GREM1 expression could be correlated with oestrogen receptor (ESR1) expression. Graphical representation of Pearson's correlation in cohort GSE20685 between GREM1 and ESR1 expression (statistically significant mild negative correlation p = 0.009, r = -0.14). ESR1 expression is at the DNA level, whereas when clinically assessed, ER is assessed by immunohistochemistry at the protein level.

B) As in the same cohort as A, Progesterone receptor (PgR) and GREM1 expression correlation in a cohort of 327 primary breast tumours (not statistically significant with Pearson's correlation p = 0.12, r = -0.08)

C) For the same cohort in A, GREM1 and HER2 expression correlation (Pearson's correlation statistically significant with mildly positive correlation p = 0.03, r = 0.12).

Table 5-1 Pearson's correlation of GREM1 RNA expression and receptor RNA expression

	GREM1(218468_s_at)	GREM1(218469_at)
ER-α (211234_x_at)	r = -0.178	r = -0.153
	p = 0.00122	p = 0.00564
ER-α (211235_s_at)	r = -0.171	r = -0.144
	p = 0.00194	p = 0.00902
PR (228554_at)	r = -0.153	r = -0.0858
	p = 0.00546	p = 0.121
HER2 (234354_x_at)	r = 0.145	r = 0.12
	p = 0.00852	p = 0.0304

Due to the interesting link between GREM1 expression at the RNA level, and receptor status, a tissue microarray (TMA) of invasive ductal breast cancer samples was stained via IHC for Gremlin1 (Figure 5.3 A and B) and staining intensity then correlated to patient clinical receptor status (Figure 5.4 A, B, C and D). Gremlin1 staining was seen in all breast cancer samples on the TMA (Figure.5.3 A). In some samples Gremlin1 appeared to stain strongly throughout most cells (Figure 5.3 B left hand picture) and in others there were still some ductal structures (Figure 5.3 B central picture) whereby Gremlin1 stained strongly in the epithelial cells, but not the stroma. The overall intensity of staining of the core samples was thus dependant on the ratio of epithelial cancer cells and stromal cells present. Computer software was utilised to threshold certain intensities of stain and then calculated the percentage of each core at each staining intensity, so that each cores' score from 1-4 was a combination of how intense Gremlin1 staining was and in what proportions in each core. This is the same approach used in digital pathology assessment of IHC for breast cancer

receptor scoring and has been shown to be as reliable as dual pathologist reporting(Nam et al. 2020).

In keeping with the Table 5.1, in the TMA, Gremlin1 staining was significantly lower in ER positive tumours compared to ER negative (Figure 5.4 A, p = 0.02). There was no statistically significant difference in Gremlin1 staining between PR positive or negative patients, or between HER2 positive or negative patients (Figure 5.4 B and C, p = 0.07 and 0.7 respectively). When patient profiles were subdivided (Figure.5.4 D), based on clinical receptor status, into groups representing the molecular subtypes, those patients with TNBC tumours had significantly higher Gremlin1 staining that those that were ER positive only (p = 0.02). Those that were HER2 + only showed similar Gremlin1 staining to the triple negative tumours, being stronger staining than ER positive/HER2-, but this did not reach statistical significance (p = 0.06). After TNBC and HER2+ tumours with the strongest Gremlin1 staining, the next strongest was the ER+/HER2+, followed by the weakest staining in ER+/HER2-. This implies the more proliferative and aggressive breast cancers, i.e., triple negative and HER2+ have higher Gremlin1 expression compared to the ER+ tumours.

Figure 5-3 Gremlin1 staining in TMA and correlation with clinical receptor status

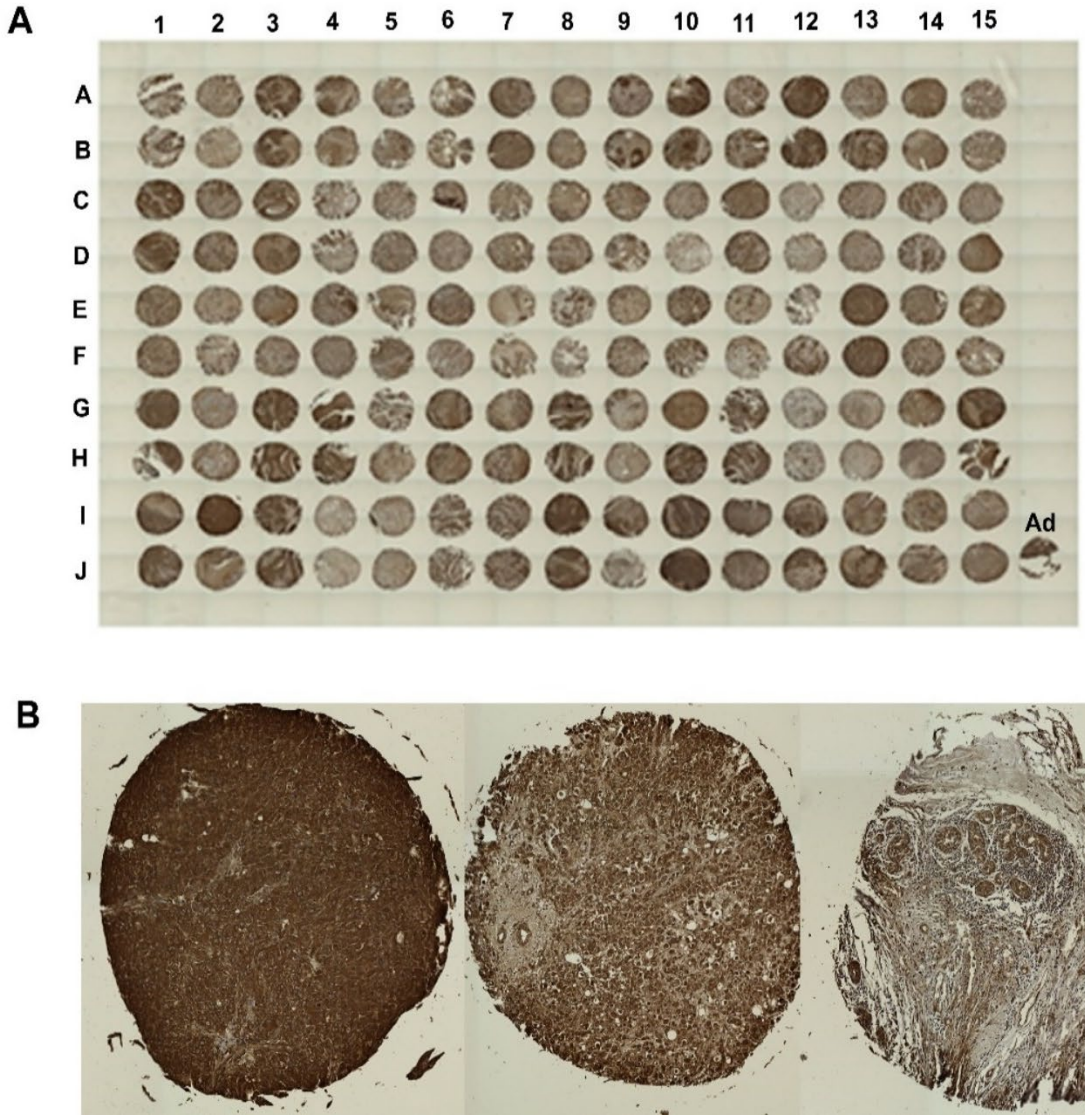

A) Gremlin1 immunohistochemistry staining in tissue microarray Br1505d (BIOMAX, USA). There are 150 core samples from primary breast cancers, all tissue microarray slides are quality controlled by the company, with 2 pathologists ratifying the cores every 10th section to ensure each of the cores demonstrates breast tumour. There is a variety of different Gremlin1 staining in the different cores. Ad =adrenal phaeochromocytoma tissue marker.

B) More magnified views of high Gremlin1 staining in core I2(Left hand picture), moderate Gremlin1 staining in A14(central picture) and low Gremlin1 staining in J9(Right hand picture)

Figure 5-4 Tissue microarray Gremlin1 staining intensity correlated to clinical receptor status

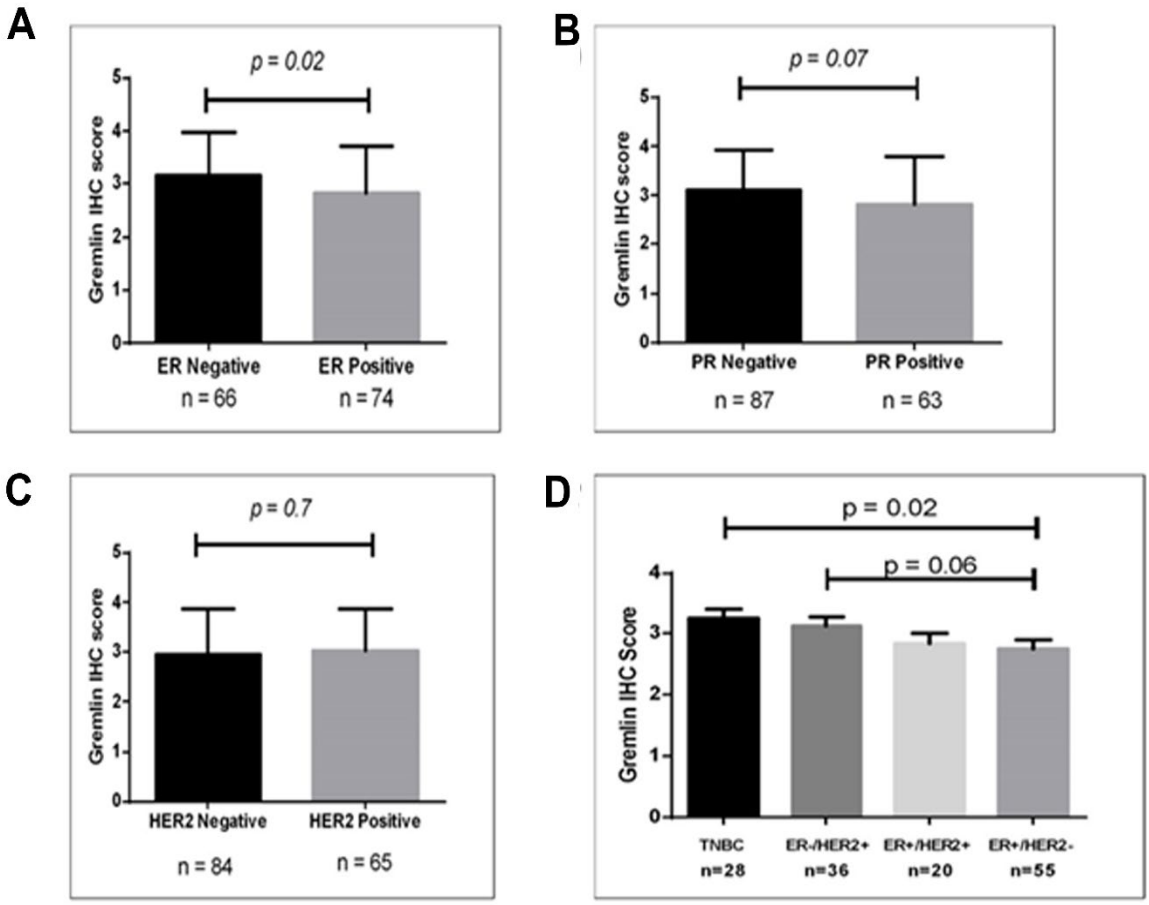

A) Each core of the tissue microarray was assessed and scored for staining utilising MIPAR software, which thresholds staining intensity and then determines the percentage area of each staining intensity on each core. The combination results in a score for Gremlin1 immunohistochemistry, with 1 being low presence of Gremlin1, and 4 being high presence of Gremlin1.Bar graph A displays Gremlin1 IHC staining score in ER positive and negative samples, with ER negative samples having higher Gremlin1 score (p = 0.02, Mann Whitney test),

B) Bar graph using the same methodology as in A but for PR positive and negative samples, with no difference in Gremlin1 score (p = 0.07 Mann Whitney test)

C) When examining HER2 positive and negative samples, there was no difference in Gremlin1 score (p = 0.7 Mann Whitney test).

D) Gremlin1 IHC staining by subdivision of samples into representative subtypes. When the core samples are put into groups representing the different molecular subtypes, the triple negative samples (TNBC) have significantly higher Gremlin1 staining compared to ER+/HER2-, as did the ER-/HER2+ samples (p = 0.02 and p = 0.06 respectively, Mann Whitney test)

Bar charts are representative mean and SEM (error bar)

5.3.2 GREM1 expression and clinical outcomes by Breast Cancer subtype

It is interesting that the tissue microarray implies higher Gremlin1 in the more aggressive subtypes of breast cancer – the triple negative and ER-/HER2 +, as GREM1 expression was also highest in the equivalent molecular subtypes, basal and HER2 enriched when examining expression in a large cohort database of breast cancers (Figure 5.1 A). It is therefore interesting to explore whether GREM1 expression in the molecular subtypes correlates to clinical outcomes.

The online microarray database tool KMplot takes gene expression data from the main microarray databases such as Gene Expression Omnibus (GEO) and The Cancer Genome Atlas (TCGA) and splits the patients into two groups (High or Low expression) based on quantile analysis of the target gene of interest. The software will then plot a Kaplan Meier survival plot and calculate a hazard ratio with confidence intervals and a log rank P value to analyse whether the target gene of interest at high or low value expression, results in an effect on patient survival.

In all subtypes of breast cancer, distant metastasis free survival (DMFS) was poorer in patients with a higher than median GREM1 expression in their primary tumour (Figure 5.5 A-D). This was statistically significant for Luminal A (p= 0.00012), HER2 enriched ($p < 0.0001$) and basal ($p = 0.027$) subtypes, but not Luminal B subtype ($p = 0.21$). The effect on DMFS was most significant in HER2 enriched subtype.

In terms of median survival in months (Table 5.2), high GREM1 expression in Luminal A subtype had lower overall survival (OS), but this did not reach statistical significance ($p = 0.09$). For Luminal A subtype high GREM1 expression patients had significantly worse relapse free survival (RFS) and distant metastasis free survival (DMFS) ($p = 0.0004$ and $p = 0.0001$ respectively). However, the median DMFS for low GREM1 expressing Luminal A tumours was 236 months, with 223 months for high GREM1 expressing tumours. This is a DMFS of nearly 20 years in both high and low GREM1 Luminal A tumours, reflecting the generally good prognosis of Luminal A disease, and the longer time to metastasis.

Luminal B subtype had statistically significantly worse OS and RFS in tumours with high GREM1 compared to low GREM1 ($p = 0.0001$ and 0.009 respectively). Median DMFS was 75 months in low GREM1 tumours and 47 months in high GREM1 tumours, but this did not reach statistical significance ($p = 0.21$). Overall

survival, whether GREM1 high or low, was similar in median months to Luminal A (174-198 months Luminal B,169-121 months Luminal A), however, the RFS and DMFS were shorter than in Luminal A (Table 5.2). This implies Luminal B disease progresses in a shorter timeframe than Luminal A, but that these patients live with their progressed or metastatic disease for long periods before death.

In basal tumours, high GREM1 tumours had statistically significantly worse RFS and DMFS than low GREM1 tumours ($p = 0.02$ and 0.03 respectively). Median OS was shorter in high GREM1 tumours, but this did not reach statistical significance ($p = 0.15$). As expected, median survivals were worse than Luminal A or B subtypes regardless of GREM1 status (Table 5.2). There were fewer numbers of HER2 enriched patients to compare in this analysis. No statistically significant difference was seen in OS between GREM1 high or low tumours ($p = 0.17$), with median survival in GREM1 high tumours at 41 months and in GREM1 low tumours 55 months. RFS was significantly worse in GREM1 high tumours ($p = 0.03$), demonstrating similar median survival to the basal subtype. The most significant result was in DMFS of HER2 enriched tumours, with a median survival for GREM1 low tumours at 98 months, and significantly worse in GREM1 high tumours at just 15 months ($p < 0.0001$). This implies GREM1 high HER2 enriched tumours are more likely to rapidly metastasise.

Figure 5-5 Subtype and GREM1 expression correlates with survival and metastasis

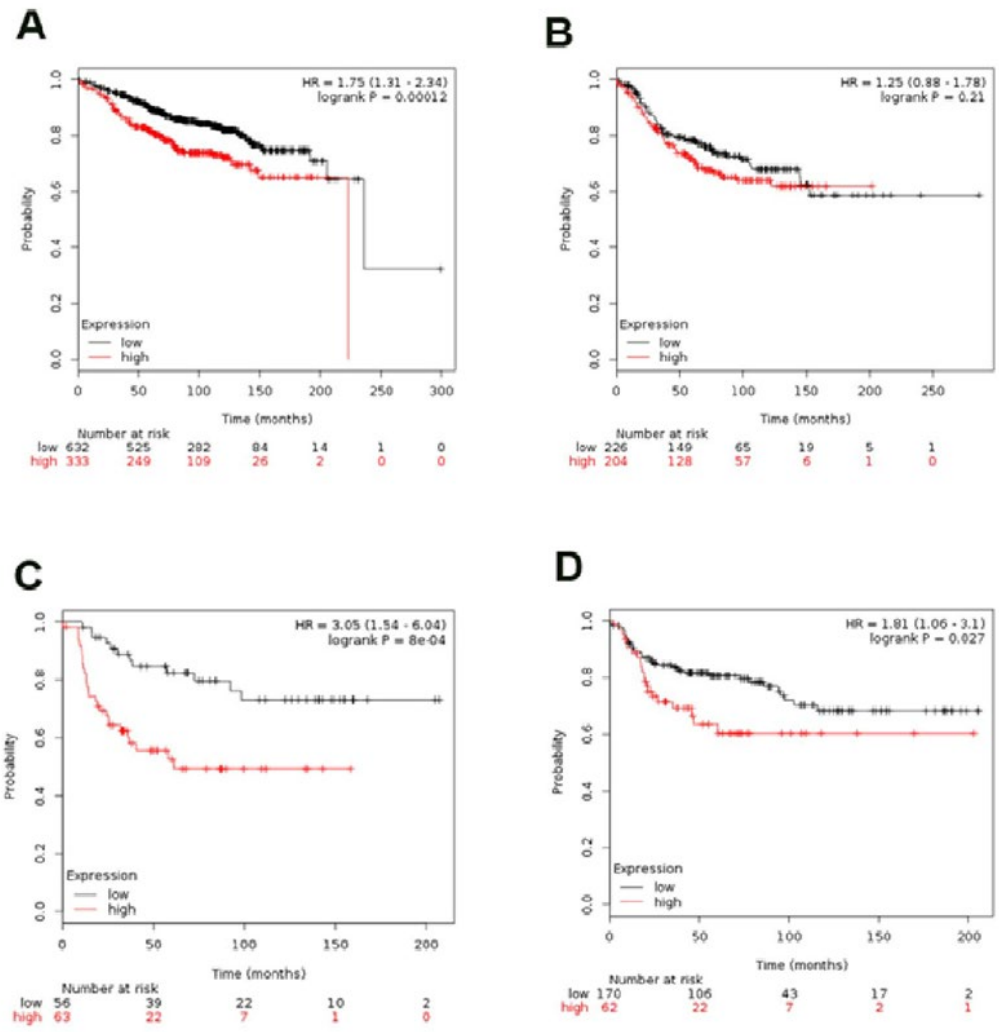

A) Kaplan Meier survival plots showing poorer distant metastasis free survival (DMFS) in patients with higher than median GREM1 expression(red) vs. lower than median GREM1 expression(black) in Luminal A primary cancers (p = 0.00012). KMplot uses gene expression data and survival information from the main microarray databases (GEO, TCGA). Patient samples are split into two groups according to quantile expressions of GREM1. The two patient cohorts are compared by a Kaplan-Meier survival plot, and the hazard ratio with 95% confidence intervals and log rank P value are calculated.

B) KMplot data shows no difference in DMFS for Luminal B tumours with High or Lower GREM1 expression (p = 0.21),

C) There was significantly poorer DMFS in HER2 enriched tumours with higher GREM1 expression compared to lower GREM1 expression on KMplot (p < 0.0001)

D) In triple negative breast cancers, higher GREM1 expression resulted in poorer DMFS compared to lower GREM1 expression (p = 0.027)

Table 5-2 Median survival(months) in low or high GREM1 expressing Breast Cancer by molecular subtype

OS = Overall Survival, RFS = Relapse Free Survival, DMFS = Distant Metastasis Free Survival.

Molecular subtype	Low expression median survival (months)	Low expression patient numbers	High expression median survival (months)	High expression patient numbers	P value
Luminal A					
OS	169	428	121	183	0.09
RFS	95	1242	58	691	0.0004
DMFS	236	632	223	333	0.0001
Luminal B					
OS	198	156	174	277	0.0001
RFS	47	860	31	289	0.009
DMFS	75	226	47	204	0.21
Basal					
OS	81	180	53	61	0.15
RFS	25	401	18	217	0.02
DMFS	95	170	24	62	0.03
Her2+					
OS	55	64	41	53	0.17
RFS	23	120	15	131	0.03
DMFS	**98**	56	**15**	63	**< 0.0001**

Most statistically significant result is highlighted in bold

In addition to the data from KMplot to further support the findings of poor survival in HER2+ GREM1 highly expressing tumours, and the significant reduction in distant metastasis free survival in this group, a cohort of HER2 positive cancers was examined for GREM1 expression in those HER2+ patients with metastasis and those without metastasis (Figure 5.6, total n = 65). GREM1 expression was significantly higher in the primary tumours of those patients that had metastasis at diagnosis, compared to those that did not (p = 0.04).

Figure 5-6 GREM1 expression in HER2+ patients that have metastasis

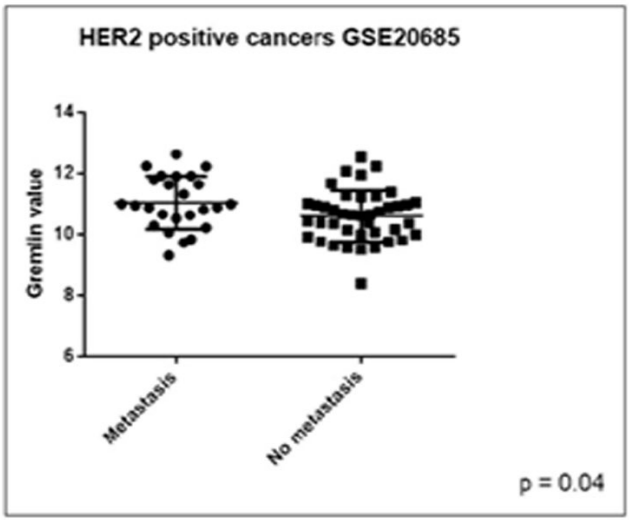

From cohort GSE20685, GREM1 expression in HER2 positive breast cancer patients with metastasis (n = 25) vs no metastasis (n = 40) at diagnosis. GREM1 is significantly higher in those with metastasis, p = 0.04(Mann Whitney test)

5.3.3 GREM1 Overexpression in HER2+ BT474 cell line

As determined in chapter 3, GREM1 expression was consistently higher in HER2+ breast cancer cell lines. There is evidently a strong correlation between GREM1 and HER+ breast cancers and poor clinical outcomes, which warranted further investigation. SKBR3 cells are recognised as representative of the HER2 enriched subtype (Holliday and Speirs 2011b; Dai et al. 2017) and were the original choice for the planned experimental work. However, manipulation of GREM1 or HER2 proved challenging in this cell line. Problems encountered included difficulties in efficient vector transfection, and poor cellular growth or high cellular apoptosis, particularly on manipulation of HER2 itself. This may be because the cell line is dependent on HER2 and/or BMP signalling for cellular growth and survival that manipulation has a catastrophic result on cellular function. BT474 was selected as an alternative HER2+ cell line and GREM1 was successfully stably over expressed with confirmation of overexpression performed using PCR and densitometry (Figure 5.7 A and B), qPCR (Figure 5.7 C) and western blotting with densitometry (Figure 5.9 A and B).

Interestingly, in the same samples, the HER2 expression was also seen to increase on GREM1 overexpression (Figure 5.8 A, B, C and Figure 5.9 A and C). This supports the positive expression correlation seen in clinical tumour samples.

Figure 5-7 GREM1 Overexpression in BT474 cells

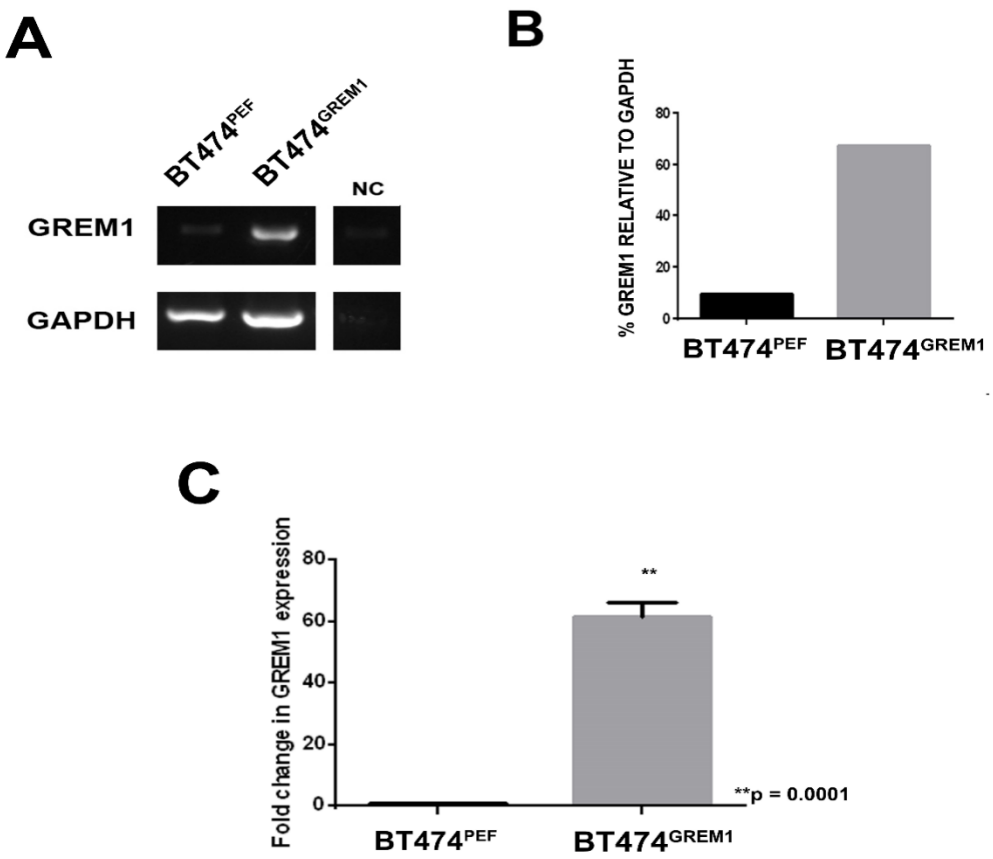

A) A GREM1 plasmid vector was introduced into BT474 cells (BT474^{GREM1}) to forcibly overexpress GREM1. A control plasmid was also introduced into BT474 cells (BT474^{PEF}). cDNA from cell samples was run for 35 cycles of PCR targeting GREM1 and GAPDH was the target housekeeping gene. Displayed is a 1% gel electrophoresis of BT474^{GREM1} and BT474^{PEF}with GREM1 overexpression confirmed in the BT474^{GREM1} cell line compared to control.NC=negative control (sterile water)

B) Densitometry of the PCR from A using image J analysis of the PCR gel, by comparing the intensity of the GREM1 PCR bands as a percentage relative to the intensity of the GAPDH band in each sample, such that sample loading differences are accounted for. GREM1 overexpression is confirmed in the BT474^{GREM1} cell line compared to BT474^{PEF}control.

C) qPCR with fold change in GREM1 expression in BT474^{GREM1} cells compared to control, normalised relative to GAPDH. Chart representative of combined 3 experimental repeats, presented as mean fold change +SEM (error bar)

Figure 5-8 HER2 expression in GREM1 overexpressing BT474 cells

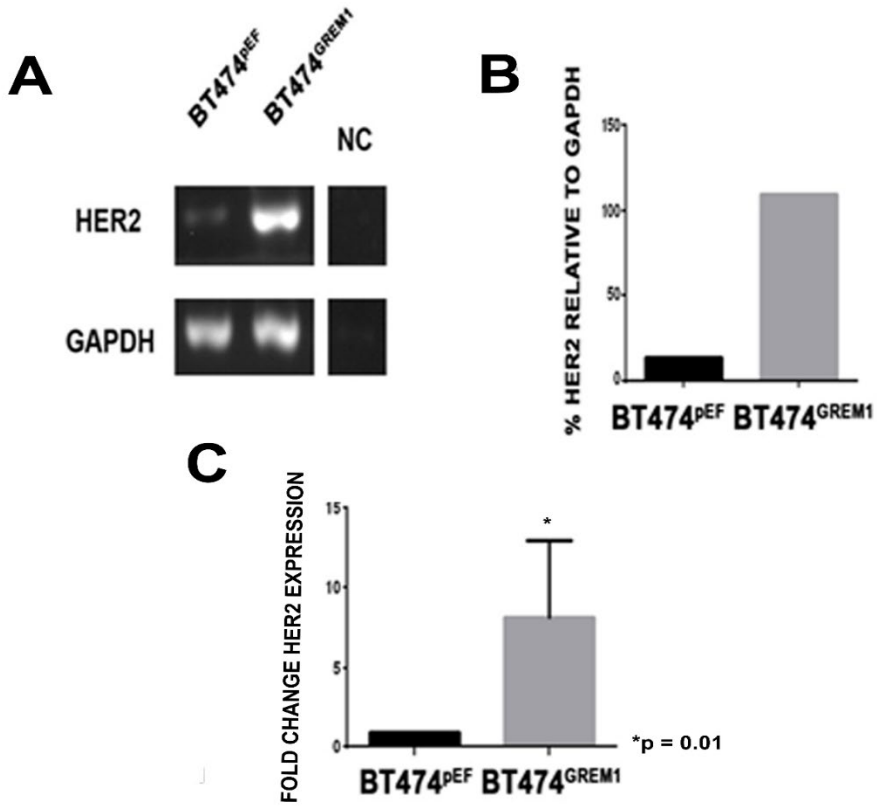

A) In Figure 5.7 GREM1 overexpression has been undertaken and confirmed on PCR. The same samples with control BT474^{PEF} and GREM1 overexpression BT474^{GREM1} were examined with PCR at 35 cycles for HER2 expression and run on a 2% gel electrophoresis. HER2 expression appears increased in GREM1 overexpressing BT474 cells.

B) Densitometry of the PCR from A using image J analysis of the PCR gel, by comparing the intensity of the HER2 PCR bands as a percentage relative to the intensity of the GAPDH band in each sample, such that sample loading differences are accounted for. Increased HER2 expression is seen in the BT474^{GREM1} cell line compared to BT474^{PEF}control.

C) qPCR with fold change in HER2 expression in BT474^{GREM1} cells compared to control, normalised relative to GAPDH. Chart representative of combined 3 experimental repeats, presented as mean fold change +SEM (error bar)

Figure 5-9 Western blot for Gremlin1 and HER2 protein in GREM1 overexpressing BT474 cells

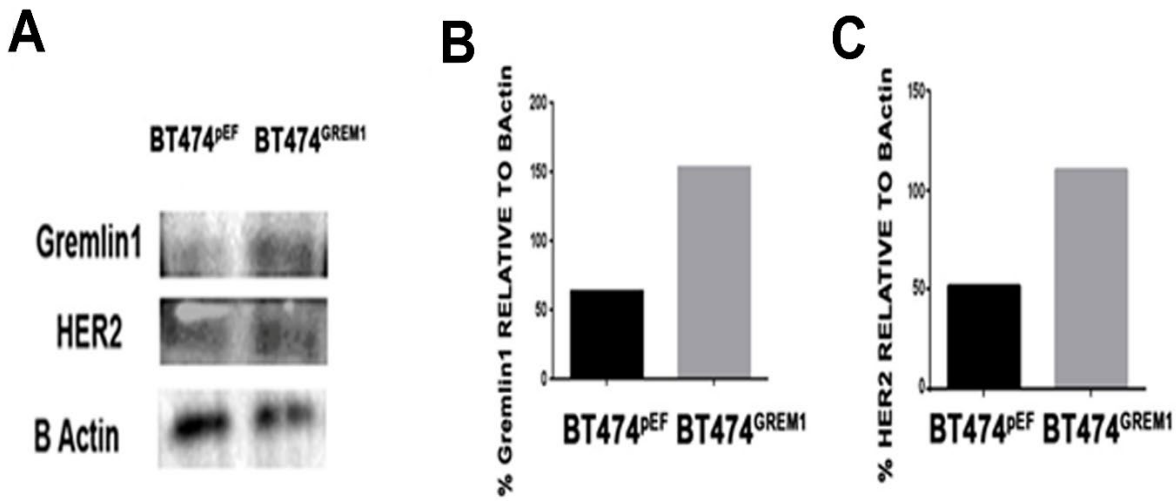

A) **Western blot of Gremlin1 and HER2 protein in whole cell lysate of BT474^{PEF} and BT474^{GREM1} cells in comparison to housekeeping protein, β Actin. Gremlin1 was separated on at 15% gel, whilst HER2 and β Actin being larger proteins were separated on an 8% gel.**

B) **The western blot in A underwent semi quantitative densitometry, with intensity of Gremlin1 bands normalised to β Actin bands for each sample and displayed as a percentage of β Actin. Gremlin1 was higher in the GREM1 overexpressing cells compared to control.**

C) **Further semi quantitative densitometry of the western blot in A, with intensity of HER2 bands normalised to β Actin bands for each sample and displayed as a percentage of β Actin. Her2 protein also seems relatively increased in GREM1 overexpressing cells.**

5.3.4 Cellular functions in GREM1 overexpressing HER2+ cells

$BT474^{GREM1}$ demonstrated significantly increased cellular growth compared to $BT474^{pEF}$, both at 3 days growth and 5 days growth (Figure 5.10 A, $p < 0.05$). This was confirmed on spheroid growth with significant increase in growth on day 4 and 6 (Figure 5.10 C and D, $p = 0.002$ and 0.004). In support of this an MTT assay also showed $BT474^{GREM1}$ had significantly increased proliferation (See appendix 9.4.1, $p = 0.002$). Transwell migration was also significantly increased in $BT474^{GREM1}$ compared to $BT474^{pEF}$ (Figure 5.10 B, $p < 0.0001$).

Interestingly, the morphology of $BT474^{GREM1}$ cells appeared altered (Figure 5.11 A) in comparison to control cells, having a more 'spindled' appearance, and growing in culture in a more diffuse 'sheet' like manner, rather than the clumps or 'island' like growth of control cells.

Transwell Matrigel invasion assays did not demonstrate any significant difference in invasive capability between $BT474^{GREM1}$ and $BT474^{pEF}$ (Figure 5.11 B, $p > 0.05$), also found in 3D Spheroid assays (see appendix 9.4.2). There was also no significant difference in colony formation (Figure 5.11 C and D, $p = 0.9$).

These results imply raised GREM1 expression in HER2+ tumours may result in more aggressive growth and migration, but not necessarily an increased ability to easily form metastasis.

Figure 5-10 Growth and Migration cellular function in GREM1 overexpressing HER2+ cells

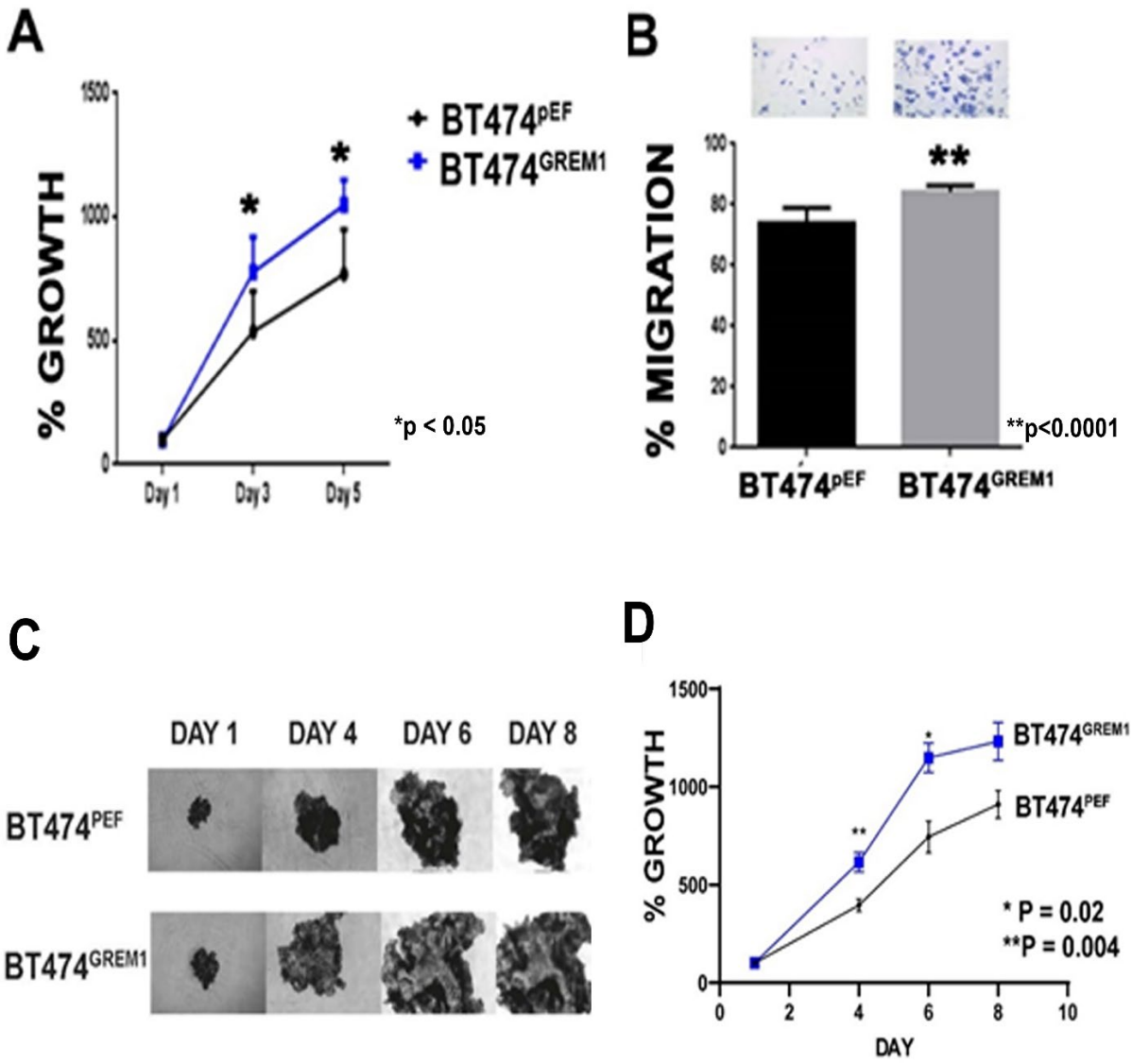

A) Growth assay comparing % growth of BT474^{PEF}to BT474^{GREM1}. At day 1, day 3 and day 5, cells are fixed and stained with crystal violet. The intensity of staining at each time point is determined by an absorbance reader. Results are displayed as relative percentage of staining at day1. GREM1 overexpression (blue line) resulted in significantly increased growth at day 3 and day 5, P < 0.05 (Mann Whitney test, experiment repeated in triplicate, displayed mean percentage increase +/- Standard error of mean (SEM))

B) Cell migration was assessed by how many cells migrated through a porous membrane over 72 hours. Migrated cells were stained, and intensity of stain measured. A well of cells with no membrane was a control to account for different rates of proliferation. BT474^{GREM1} cells had significantly increased migration through a transwell membrane compared to control (p = 0<0.0001 Mann Whitney test, repeated in triplicate and presented as Mean +/- SEM). Representative micrograph picture of increased migrated cells above bar chart.

C) Cells grown in 3D on l U bottomed non adherent plates as a spheroid of cells. Spheroid growth was measured using ImageJ software for each spheroid over 8 days. Representative pictures showing BT474^{GREM1} spheroid with increased growth compared to control

D) Growth chart of ImageJ measurements of spheroid growth as a percentage of size on day1.BT474^{GREM1} had significantly increased growth (blue line) compared to control at day 4(p = 0.004) and day 6(p=0.02) (Mann Whitney test, repeated in triplicate and presented as Mean +/- SEM)

Figure 5-11 Invasion and colony formation in GREM1 overexpressing HER2+ cells

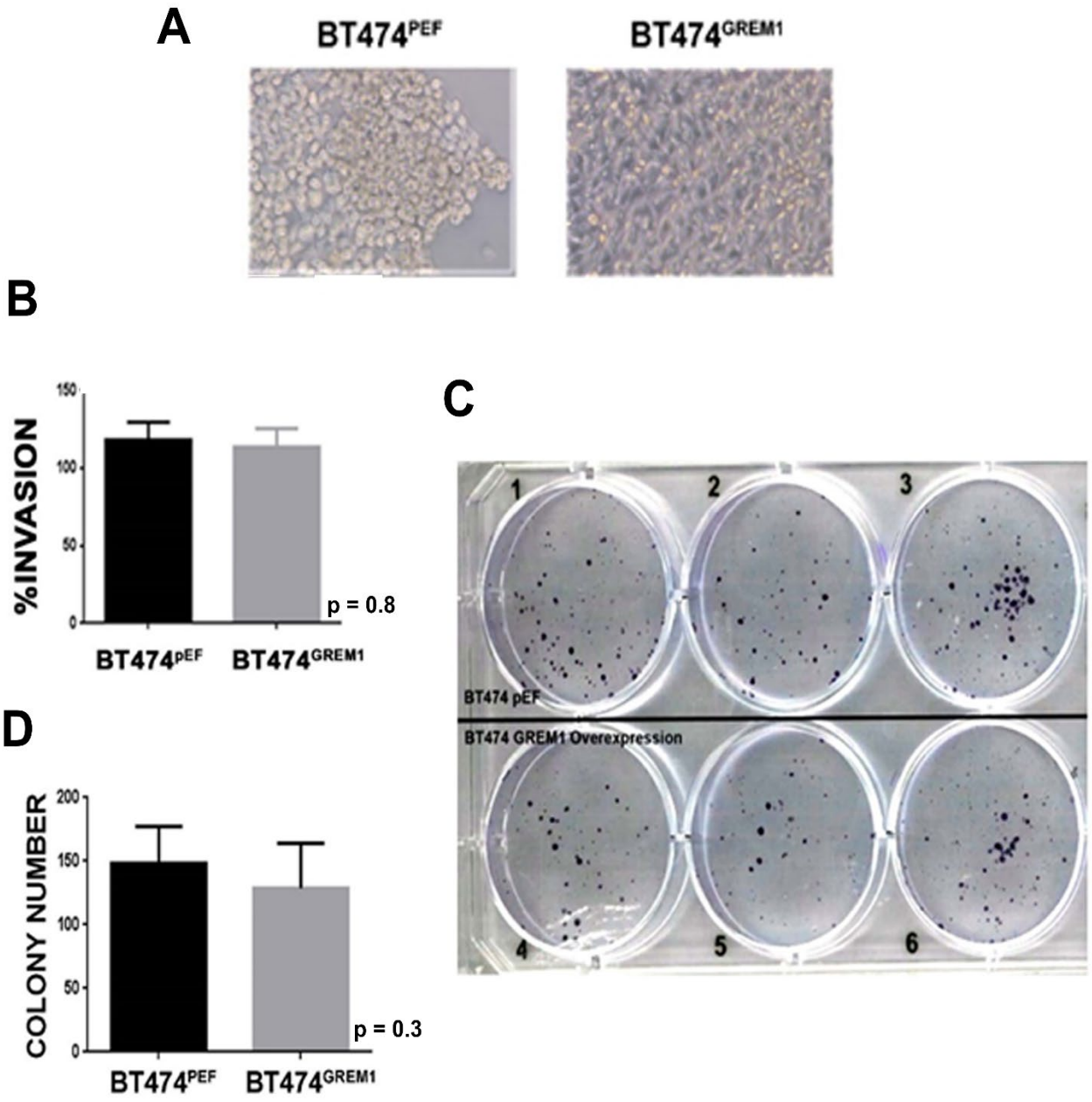

A) Microscopy image of BT474^{GREM1} and BT474^{pEF} at x20 magnification demonstrating differences in morphology, with BT474^{GREM1} being more 'spindle like' and forming sheets of cells rather than clusters, which is more typical of BT474 cells. This morphology is more reflective of a mesenchymal phenotype.

B) Invasion of cells was assessed by percentage of cells invaded through a porous membrane coated with extracellular matrix (Matrigel) over 72 hours. Cells that invaded through the membrane were fixed and stained and intensity of stain measured. A well of cells with no membrane was used as control to account for different rates of proliferation which might spuriously increase the staining. There was no difference in percentage invasion p = 0.8 (Mann Whitney test, repeated in triplicate and presented as Mean +/- SEM)

C) To reflect lone cell survival necessary for establishing metastasis, a low number (200) of cells were seeded into each well. Representative image of colony formation assay after 14 days comparing BT474^{GREM1} and BT474^{pEF}.

D) Bar Graph of colony counts from colony formation assay in C comparing BT474^{GREM1} and BT474^{pEF}.There was no significant difference (p =0.3, Mann Whitney test, repeated in triplicate and presented as Mean +/- SEM)

5.3.5 Markers of cell cycle and EMT in GREM1 overexpressing HER2+ cells

To explore the increased proliferation further, qPCR for markers of cell cycle were performed (Figure 5.12 A, B and C). P27 was seen to be increased in expression in BT474^{GREM1} compared to BT474^{PEF}, by a mean fold increase of 1.3 although this did not reach statistical significance (p = 0.46). CyclinD1 was decreased in expression, but again this did not reach statistical significance (p = 0.12). P21 decreased in expression which neared, but did not reach, statistical significance (p = 0.07).

GREM1 overexpression was confirmed in all BT474^{GREM1} samples compared to BT474^{PEF}samples used in RT-qPCR analysis (Figure 5.12 D, p = 0.001). Interestingly, ID1, which is a major downstream transcriptional target of BMP signalling, was decreased in expression, which did not quite reach statistical significance (Figure 5.12 E, p = 0.06). This could be extrapolated, that because of an increased BMP antagonism with GREM1 overexpression, then the downstream target of BMP signalling would be expected to decrease. As there was also a significant increase in migratory capacity of BT474^{GREM1} cells in comparison to control, it was of interest to see how gene expression markers of this process may also have changed with GREM1 overexpression. In terms of EMT markers (Figure 5.12. E-H) the decrease in mesenchymal marker Vimentin was statistically significant (Figure 5.12 F, p = 0.02). Vimentin expression typically reflects a mesenchymal cellular phenotype; thus, it is unusual that the expression would be decreased in BT474^{GREM1} cells that have greater migratory capacity. However, vimentin also has roles within apoptosis and invasion, and may not be relevant to the migration in BT474^{GREM1} cells (Strouhalova et al. 2020; Chen et al. 2021). Conversely, the epithelial marker E- Cadherin's expression in BT474^{GREM1} significantly reduced (Figure 5.12 G, p = 0.01). This would be expected in more migratory cells. Snail (SNAI1), which promotes repression of E- Cadherin, demonstrated a mean 4-fold increase in expression in BT474^{GREM1} compared to BT474^{PEF}.This was not quite statistically significant (Figure 5.12 I, p = 0.05). Slug (SNAI2) is known to have a similar function to Snail in the repression of E-Cadherin and was seen to have an average 42-fold increase in expression in BT474 compared to BT474^{PEF}, although the range was wide (1.89- fold to 118 – fold), which likely accounts for this comparison not reaching statistical significance (Figure 5.12 H, p = 0.12).

Figure 5-12 qPCR for expression of cell cycle and EMT markers in GREM1 overexpressing HER2+ cells

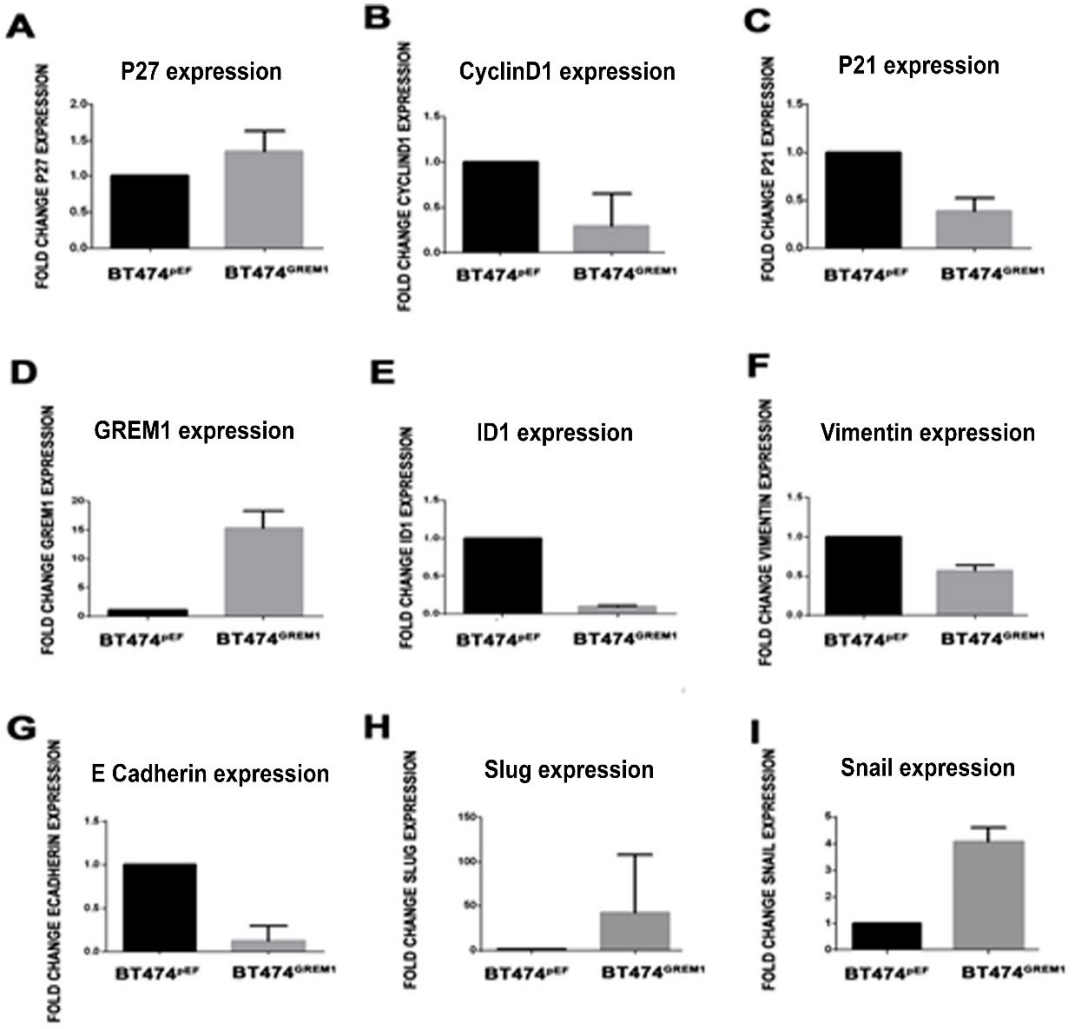

A) Quantitative polymerase chain reaction(qPCR) of cDNA from BT474^{GREM1} compared to BT474^{pEF}, displayed as fold change in expression. There was no difference in expression of cell cycle regulator P27 (p = 0.46). Fold change displayed as mean + SEM (error bar)

B) qPCR of the same samples as in A for expression of cell cycle regulator CyclinD1 showed no significant difference (p = 0.12),

C) qPCR of the same samples as in A for expression of cell cycle regulator P21 showed no significant difference in expression (p = 0.07),

D) qPCR of the same samples as in A for expression of GREM1 confirmed plasmid GREM1 overexpression was successful and present in these samples (p = 0.001),

E) qPCR of the same samples as in A for expression of epithelial to mesenchymal transition (EMT) marker ID1, showed no significant difference (p = 0.06)

F) qPCR of the same samples as in A for expression of EMT marker Vimentin shows vimentin expression is significantly reduced in BT474^{GREM1} cells (p = 0.02.

G) qPCR of the same samples as in A for expression of EMT marker E- Cadherin, which is significantly reduced in BT474^{GREM1} cells (p = 0.01), implying these cells have more migratory capacity

H) qPCR of the same samples as in A for expression of EMT marker Slug showed no difference in expression (p = 0.12)

I) qPCR of the same samples as in A for expression of EMT marker Snail showed significantly increased expression in BT474^{GREM1} cells (p = 0.05), implying a more mesenchymal migratory and invasive phenotype.

5.4 Discussion

Traditionally and historically, the receptor status of the patient's tumour has been utilised to guide treatment strategy, with therapeutics targeted towards these receptors, such as endocrine therapy and anti-HER2 treatments.ER, PR and HER2 are assessed at diagnosis using standardised immunohistochemistry techniques (or *in situ* hybridisation for gene amplification if HER2 IHC is equivocal) (Senkus et al. 2013). Further developments in high throughput microarray technology and the dawn of the genomic era, made it possible to classify breast cancers on a molecular phenotype basis (Perou et al. 2000; Wesolowski and Ramaswamy 2011). Due to the costly nature of this technology, clinical application turned to utilising already available pathological tests, such as IHC for certain markers, that could be deemed representative of these expression array subtypes. In clinical guidelines, in addition to hormone receptors and HER2, the proliferative marker Ki67, and basal markers such as cytokeratins can also be assessed and combined with receptor status to give a 'proxy' intrinsic molecular subtype (Schnitt 2010).

Given the variability in GREM1 expression seen in different breast cancer cell lines and cohort samples (See chapters 3 and 4), the sometimes-conflicting data regarding BMP signalling and antagonism in breast cancer (See chapter 1 and review (Zabkiewicz et al. 2017)), and the recognised signalling crosstalk between BMP signalling and both ER signalling and EGFR/HER2 signalling, it is a valid question to consider whether the effects and role of Gremlin1 in breast cancer may have links to the receptor status of the tumour.

It is apparent from large and small cohort DNA microarray data that GREM1 expression positively correlates with HER2 expression, and negatively correlates with ER/PR expression (section 5.3.1.) At the protein level, there is data from the TMA that supports the negative correlation between Gremlin1 and the ER receptor status, but the correlation between Gremlin1 and HER2 is not strong statistically. ER positive tumours make up most invasive ductal carcinomas, and thus it is possible to analyse correlation with ER in larger patient groups. As HER2+ tumours account for around 20% of breast cancers, it may be that the numbers in the TMA cohort were simply not enough to demonstrate a statistically significant result. One limitation to TMA is the core samples provided are only a small sample of the whole tumour, and thus does not represent what Gremlin1 expression might be in the tumour overall. An approach to obtain a more definitive result at the

protein level would be the prospective collection of a large cohort (several hundred patients) of tumour tissue for whole tissue IHC of Gremlin1. However, this is unlikely to be feasible on a practical level, as tissue use in breast cancer patients must first be prioritised for histopathological diagnosis, making it less available for large sample use in research, and on a large scale would be expensive and time consuming. This is where TMA has some advantage, in being a more efficient method of processing many samples under the same conditions. Previous studies have found TMA to be a fair representation of whole tumours, but this becomes less valid if the core samples are restricted in size to 0.6mm (Camp et al. 2000; Alkushi 2009). The TMAs used in this study were 1mm in size, and thus, exceeds the minimum required area thought to be a valid representative of the tumour. In addition, every 10th section of the TMA was stained with H&E and reviewed by two pathologists to ensure the pathology diagnosis was current and matched to the adjacent serial sections. Therefore, although TMA has its limitations in representing a large cohort of breast tumours, this has been mitigated for as much as is possible.

When examining the implications of GREM1 for clinical outcomes, in the different molecular subtypes of breast cancer, it appears that, although high GREM1 in the primary tumour leads to poorer survival in all subtypes (Figure 5.3), the most significant result statistically and clinically, was in distant metastasis free survival in HER2+ patients. This dropped from a median of 98 months in GREM1 low HER2+ tumours, to just 15 months in GREM1 high HER2+ tumours (Table 5.2). Those HER2+ patients in GEO cohort GSE20685 also had higher GREM1 expression in patients with metastatic disease than those without metastases. This implies GREM1 could be of clinical importance for HER2+ patient outcome.

To further examine this concept, GREM1 was overexpressed in a HER2+ cell line to see what effect it had on HER2+ cellular function. Stable GREM1 overexpression was achieved in BT474 cells, which are representative of Luminal B HER2+ cells (ER+/HER2+). Further culture and assays were performed in Phenol Red free medium, with charcoal stripped FCS to reduce any oestrogen effects and better represent a more specifically HER2 enriched tumour. Of note, and again in support of the positive correlation between HER2 and GREM1 in clinical samples, when GREM1 was overexpressed, HER2 expression also appeared to increase.

GREM1 overexpressing cells had increased growth and motility, but not invasion or colony formation. This might indicate that high Gremlin1 is most advantageous to the HER2 positive tumour early on in tumourigenesis and progression, but that other mechanisms might then be required for invasion and metastatic dissemination to occur.

Growth and proliferation in BT474^{GREM1} cells were briefly examined with expression of certain cell cycle markers. The cell cycle is a tightly regulated process involving Cyclins, Cyclin Dependant Kinases (CDKs) and Cyclin Dependant Kinase Inhibitors (CDKIs), that control progression of cell division through defined phases (G_0: cell cycle arrest, G1: Cell growth and chromosomal duplication, S: DNA Synthesis, G2: protein synthesis and error checks, M: Cell division). Dysregulation of these critical genes has been demonstrated in many different cancers, including breast cancer (Abukhdeir and Park 2008; Finn et al. 2016). Cyclin D1 is one of the most well characterised cyclins and is vital for regulating progression from G1 to S phase via influence on CDKs (particularly CDK 4 and 6) and promotes cellular proliferation and division. Cyclin D1 overexpression has been reported in breast carcinomas and linked to poor clinical outcomes (Alao 2007; Yang et al. 2007; Mohammadizadeh et al. 2013).

In GREM1 overexpressing HER2+ cells, which have increased growth compared to control cells, the expression level of Cyclin D1 was reduced, but not to statistical significance. Of course, the difficulty with interpretation of cell cycle gene expression, is that the RNA extraction is performed on a group of cells, some of which may be at slightly differing stages of the cell cycle, even when in log phase growth. In addition, Cyclin D1 level rises early in G1 phase of the cell cycle but rapidly falls on entrance to the S phase (Yang et al. 2006) thus, the above expression result, with low CyclinD1 in GREM1 overexpressing cells, could still reflect relatively more cells in S phase. As a further layer of complication, CyclinD1 is also an intermediary molecule in other signalling pathways, such as the Nf$\kappa\beta$ pathway (Hinz et al. 1999; Ouyang et al. 2005), which has also been implicated as having crosstalk downstream of BMP signalling (Fong et al. 2008; Cao et al. 2014). Thus, the alteration in CyclinD1 expression in GREM1 overexpression may be due to a yet uncharacterised link between BMP signalling and other signalling pathways that involve Cyclin D1.

P21 and p27 are both inhibitors of cyclins and CDKs. CDKIs are important as checkpoints to halt cell cycle and allow DNA damage to be repaired, or initiate cell

death if damage is irreparable. They can both inhibit Cyclin D1, although in certain cell types have been seen to have paradoxical effects, such as facilitating the interaction between Cyclin D1 and CDK4/6 (Abukhdeir and Park 2008). P21 inhibits cell cycle such that DNA repair can occur, and its expression positively correlates with suppression of genes responsible for cell cycle progression. It can inhibit cell cycle both directly through its actions on CDKs, and indirectly via other avenues such as mediating the tumour suppressive activity of p53. P53 can also instigate p21 transcription, thus a reduction or loss of p53 would result in low p21 expression (Abukhdeir and Park 2008; Abbas and Dutta 2009). In GREM1 overexpressing BT474 cells, p21 expression is reduced compared to control, which may support the finding of increased cellular growth. Further study on expression of p53 in these cells would also be interesting.

P27 has generally been viewed as a tumour suppressor, with low levels associated with poor clinical outcomes. P27 opposes cell cycle progression by inhibiting certain Cyclin/CDKs, but can also promote assembly of CyclinD/CDKs, and thus has the potential for opposing functions (Chiarle et al. 2001; Alkarain et al. 2004; Abukhdeir and Park 2008). Interestingly, recent studies have shown that outside of its nuclear role, an accumulation of cytoplasmic p27 protein can have an effect on RhoA and results in increased cell motility (Larrea et al. 2009).The expression changes showing increase in p27 expression for GREM1 overexpressing cells may therefore have more to do with the increased cellular motility, than cellular growth.

As part of future studies on the increased proliferation and growth of GREM1 overexpressing HER2+ breast cancer cells, it would be intended that cell cycle flow cytometry studies of cell phase be undertaken, and Western blotting or immunostaining of nuclear and cytoplasmic cell cycle proteins, particularly p27, be carried out to better characterise the cell cycle effects. Single cell analysis may also help to reduce the ‘noise’ created in analysing cell populations.

In addition to sustained cellular proliferation, a further hallmark of cancer is the ability of cancer cells to become more motile, as a step in the process towards invasion and metastasis. The cellular shape alters and attachment to adjacent cells or extracellular matrix loosens. The most well characterised event is the loss of E- Cadherin, a key cell-cell adhesion molecule that is not only vital for cell-cell adherens junctions, but also maintaining quiescence in epithelial cells. Reduction or loss of E- Cadherin is commonly seen in carcinomas and is associated with an

invasive phenotype (Hanahan and Weinberg 2011). In the GREM1 overexpressing BT474 cells, E- Cadherin expression was significantly reduced, in keeping with the increased motility seen in the cellular function tests.

Snail and Slug (SNAI1 and SNAI2 respectively) are both transcription factors well recognised for their role in promotion of EMT, including direct repression of E-Cadherin expression, increased motility, and invasiveness. In our GREM1 overexpressing BT474 cells both Snail and Slug expression were upregulated, although did not quite reach statistical significance. Western blotting, although requiring further optimisation of EMT markers, did however confirm an increased expression of Snail at the protein level (see appendix 9.4.3). Upregulation of these transcription factors would be in keeping with the observed downregulation of E-Cadherin and the increased cellular motility. There are multiple possibilities as to the mechanism of increased GREM1 resulting in EMT, for example, the increased expression of HER2 in GREM1 overexpressing cells may drive EMT (Ingthorsson et al. 2016), or the suppression of BMP signalling, by increased Gremlin1, might then allow TGFβ induced EMT to become more prominent. The exact mechanism by which Gremlin1 overexpression may elicit these changes is not clear and would require further study.

In this chapter I have explored a previously undetermined area of breast cancer and BMP antagonist biology. It is apparent that Gremlin1 has different expression levels dependent on molecular subtype of breast cancer and is strongly positively correlated with HER2 expression and HER2+ receptor status, with clinically poorer outcomes in GREM1 high, HER2+ primary tumours. This may provide an interesting patient risk stratifier, or therapeutic target, as even with anti HER2 treatment such as Trastuzumab, a significant proportion of patients will relapse with metastatic disease. Gremlin1 overexpression appears to increase cellular growth and motility, both important functions for tumour progression. Further chapters will explore the relationship between GREM1 and HER2, the effects *in vivo,* and within the most common breast cancer metastatic site, the bone environment.

6 Mechanisms and signalling interactions of Gremlin1 in HER2+ Breast Cancer

6.1 Introduction

GREM1 expression is strongly correlated with HER2+ breast cancers, and high GREM1 expression in HER2+ tumours correlates, in clinical cohorts, with increased metastasis and poor clinical outcomes. High GREM1 expression in HER2+ cells *in vitro* appeared to increase growth and migration, with a reduction in E- cadherin and increase in Slug and Snail as markers of increased EMT (see chapter 5).

There is no current published data on Gremlin1 and its interaction with HER2 in breast cancer, but there are previous studies on Gremlin1s role in EMT of relevance. There is already evidence of the influence of Gremlin1 on EMT related to renal and pulmonary fibrosis, mediated via interactions with TGFβ signalling, as described in Chapter 1. In colon cancer cells, Gremlin1 induced EMT with loss of E- Cadherin and upregulation of Snail (Karagiannis et al. 2015). In glioma cells, migration and invasion mediated by TGFβ/Smad signalling was abolished by GREM1 knockdown (Guan et al. 2017a). Most recently in MDA MB 453 breast cancer cells, treatment with recombinant Gremlin1 induced expression of Vimentin and Slug, and TGFβ induced migration was suppressed by GREM1 knockdown (Sung et al. 2020a).

Both BMP and HER2 signalling are known to induce EMT in breast cancer cells (Ingthorsson et al. 2016; Frey et al. 2020), and both can induce activity in the MAPK pathways (PI3K/AKT/mTOR, JNK, ERK) that lead to proliferation, migration, and invasion. This chapter examines how Gremlin1 and HER2 may interact, resulting in the increased EMT and functional changes of HER2+ cells seen in previous chapters.

6.2 Methods

6.2.1 Treatment with HER2 small molecule inhibitor

BT474 cells were plated to 80% confluency in 6 well plates. Cells were placed for 12 hours in serum free, phenol red free RPMI (as this contains no proteins, lipids, or growth factors such as Oestrogens). Cells were then treated with either vehicle control (serum free, phenol red free RPMI) or irreversible HER2 small molecule inhibitor CP724714, at 40nM concentration for 4 and 24 hours. RNA was then extracted for further evaluation as per protocol in Chapter 2.3.

6.2.2 Lentiviral HER2 Knockdown

U6 Promoter Lentiviral particle vectors (Vectorbuilder, USA), containing shRNA targeting HER2/ErBb2(shRNA5/SH5 and shRNA12/SH12) or scramble shRNA, were produced and then used to transfect BT474 and SKBR3 cells using polybrene (See Chapter 2 for full protocol). After selection for up to 14 days using 500µg/ml G418 (Geneticin, Melford, Suffolk, UK) in standard culture medium, cells were further maintained in the same medium supplemented with between 100µg-300 µg /ml G418, depending on the tolerance of the cell line. RNA and protein were extracted to confirm HER2 knockdown and examine GREM1 expression. SKBR3 cells did not produce a verifiable HER knockdown and were not used further in this study.

6.2.3 BT474^{GREM1} spheroid growth assay with CP724714

Spheroid growth assay was undertaken with 3,000 BT474^{PEF} or BT474^{GREM1} cells, as per the protocol in chapter 2.8.2, in u bottom 96 well plates, and photographed at x10 magnification on day 1, 4, 6 and 8. Cells were grown in either normal medium, Phenol red free RPMI with 10% charcoal stripped FCS, or with the addition of CP724714 in the medium to a concentration of 40nM. Spheroid area was calculated using Image J software and presented as percentage growth in relation to spheroid area on day 1.

6.2.4 BT474^{GREM1} migration assay with CP724714

Transwell migration assay with BT474^{PEF} and BT474^{GREM1} was undertaken in accordance with the protocol in chapter 2.8.4. Twenty thousand cells were seeded in serum and Phenol red free RPMI into a well insert with a membrane, with or without the addition of CP724714 at 40nM concentration. Phenol red free RPMI and 10% charcoal stripped FCS was placed in the well below the insert and

migration through the membrane assessed at 72 hours. The control well contained 20,000 cells without the membrane insert, with or without the addition of CP724714. Migrated cells were fixed and stained with crystal violet, then dissolved with acetic acid and absorbance measured. Data was presented as percentage migration, with or without CP724714.

6.2.5 Cell treatment for signalling pathway phosphorylation

For the full protocol see Chapter 2.10.2. Wild type BT474 cells were seeded at 2 x 10^6 cells into a 6 well plate, then after 24 hours they were serum starved for 2 hours in Phenol red free RPMI only. Cells were then treated with 40ng/ml RhBMP-4 for time intervals of 15 minutes, 30 minutes, 1 hour, 2 hours or 4 hours. Protein was extracted for Western blot analysis of Gremlin1, phosphorylated smad1/5/8, phosphorylated ERK, phosphorylated AKT and βActin as the housekeeping control.

Subsequently, cells were plated, and serum starved as before, and then treated for 1 hour with 500ng/ml RhGremlin1 or 40ng/ml RhBMP-4, or both, 30 minutes apart. Na Orthovanadate was the positive control and Phenol red free RPMI medium was the negative control. Protein was then extracted to examine with Western blot for phosphorylated smad1/5/8, AKT and ERK, with βActin as internal control. Antibodies and concentrations for Western blot are listed in Table 2.2 and the protocol for western blot in Chapter 2.4.

6.3 Results

6.3.1 Treatment with HER2 inhibitor CP724714 reduces GREM1 expression

CP724714 is a reversible small molecule kinase inhibitor specific to HER2, which was originally developed as a potential oral delivery alternative to Trastuzumab, with an IC50 of 32nM. It has been shown to inhibit growth and induce apoptosis in BT474 cells both *in vitro* and *in vivo*, as well as decreasing HER2 specific phosphorylation and downstream MAPK/AKT signalling (Jani et al. 2007).

Treatment of BT474 cells with CP724714 at 40nM showed a decrease in HER2 and GREM1 expression with treatment for 4 hours on PCR (Figure 6.1 A and B). In Jani et al's original studies, onset of HER2 inhibition with CP724714 was rapid, within 10 minutes, and effects decreased with decreasing plasma concentration over 4 hours. This may well explain why the expression level of GREM1 and HER2 return towards control levels at 24 hours (Figure 6.1 A and B), as the effect of the small molecule inhibitor has diminished. The same effect was seen with qPCR (Figure 6.1 C and D), although this was not statistically significant ($p > 0.05$).

Figure 6-1 BT474 cells treated with CP724714

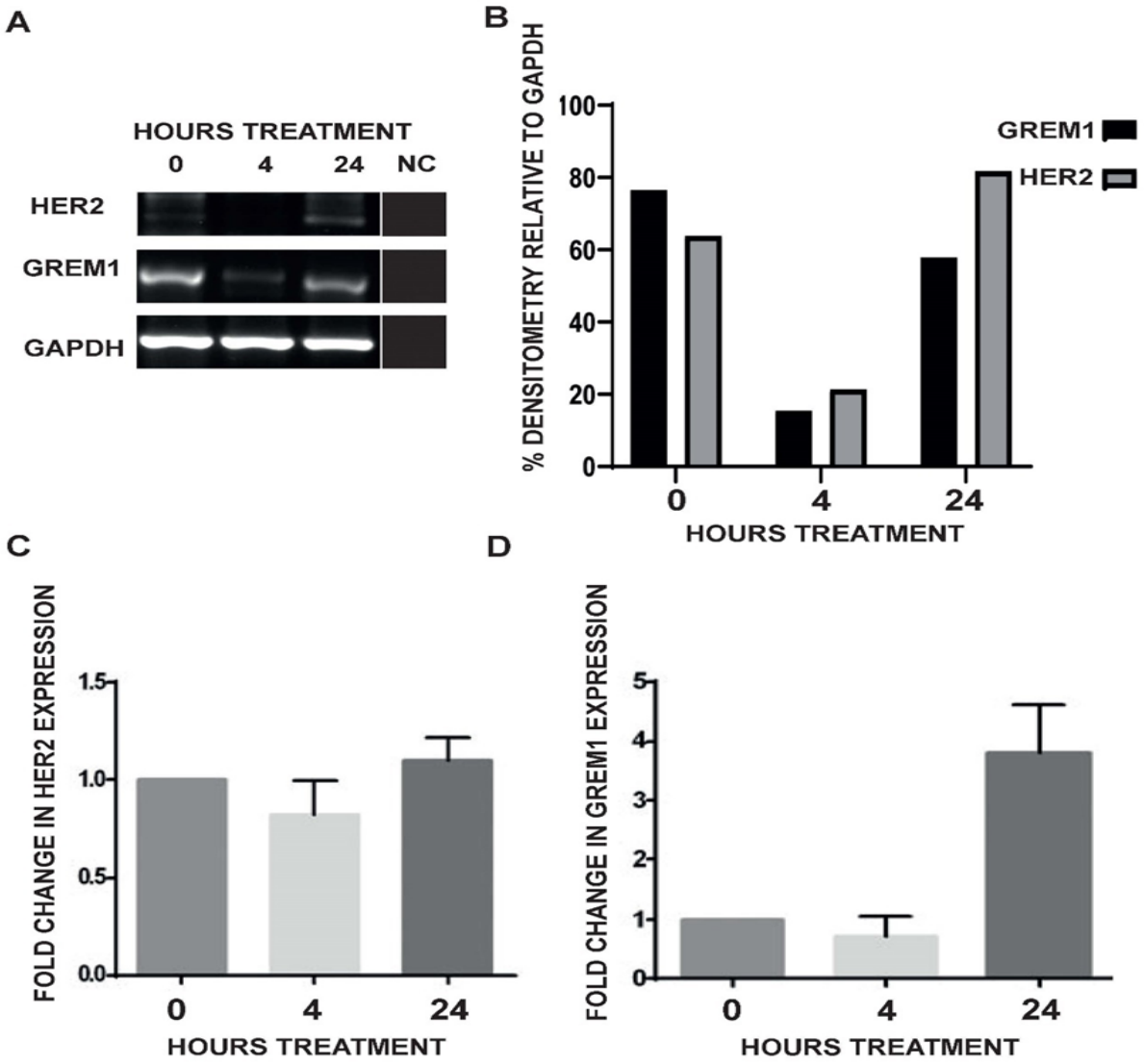

A) PCR at 35 cycles, of GREM1 and HER2 expression when BT474 cells are treated with small molecule HER2 inhibitor CP724714 at 4 and 24 hours compared to control vehicle (0 hours). The GREM1 and HER2 expression seem to decrease after 4 hours treatment with HER2 inhibitor, and then recover at 24 hours.NC = Negative Control (sterile water)

B) Densitometry of the PCR from A using image J analysis of the PCR gel, by comparing the intensity of the GREM1 and HER2 PCR bands as a percentage relative to the intensity of the GAPDH band in each sample, such that sample loading differences are accounted for. This shows the same expression reduction pattern as in A

C) qPCR of the same samples as A showing fold change expression of HER2 at 4 and 24 hours of treatment with CP724714 compared to control (0 hours). Although there is a decrease of HER2 expression at 4 hours treatment like that seen in B, this was not significant ($p > 0.05$)

D) qPCR showing fold change expression of GREM1 at 4 and 24 hours of treatment with CP724714 compared to control (0 hours). There is a decrease of GREM1 expression at 4 hours treatment like that seen in B, this was not significant ($p > 0.05$)

6.3.2 Knockdown of HER2 resulted in reduced GREM1 expression

Two lentiviral short hairpin (SH) constructs were utilised for HER2 knockdown, SH5 and SH12, of which the SH5 construct showed greater efficacy on PCR and qPCR (Figure 6.2 A, B and C). This utilised the same methodology as the GREM1 lentiviral vector knockdown model, lentiviral particles are produced which carry DNA encoding an interference RNA sequence (the short hairpin RNA) that targets HER2 transcription and translation. From the below PCR and qPCR data this was more successful at knockdown of HER2 than the GREM1 constructs SH1 and SH2 were at reducing GREM1 expression. This may be due to improvement in methodology learning curve, or that the short hairpin sequence targeting HER2 is more efficient than the sequence targeting GREM1 in the SH1 and 2 constructs.

Interestingly when HER2 mRNA expression was reduced by knockdown, GREM1 mRNA expression was also reduced (Figure 6.2 B and D). This was evident mostly on qPCR (Figure 6.2 D, $p < 0.01$) and was further confirmed with whole cell lysate western blot of HER2 and Gremlin1 protein in scramble control cells, and the SH5 HER2 knockdown cells (Figure 6.2 E and F).

This finding supports the data from using the HER2 small molecule inhibitor CP724714(Figure 6.1), that there appears to be a regulatory connection between HER2 and GREM1 expression. The data cannot indicate if this is a direct or indirect regulatory relationship.

Figure 6-2 Effect of HER2 knockdown on GREM1

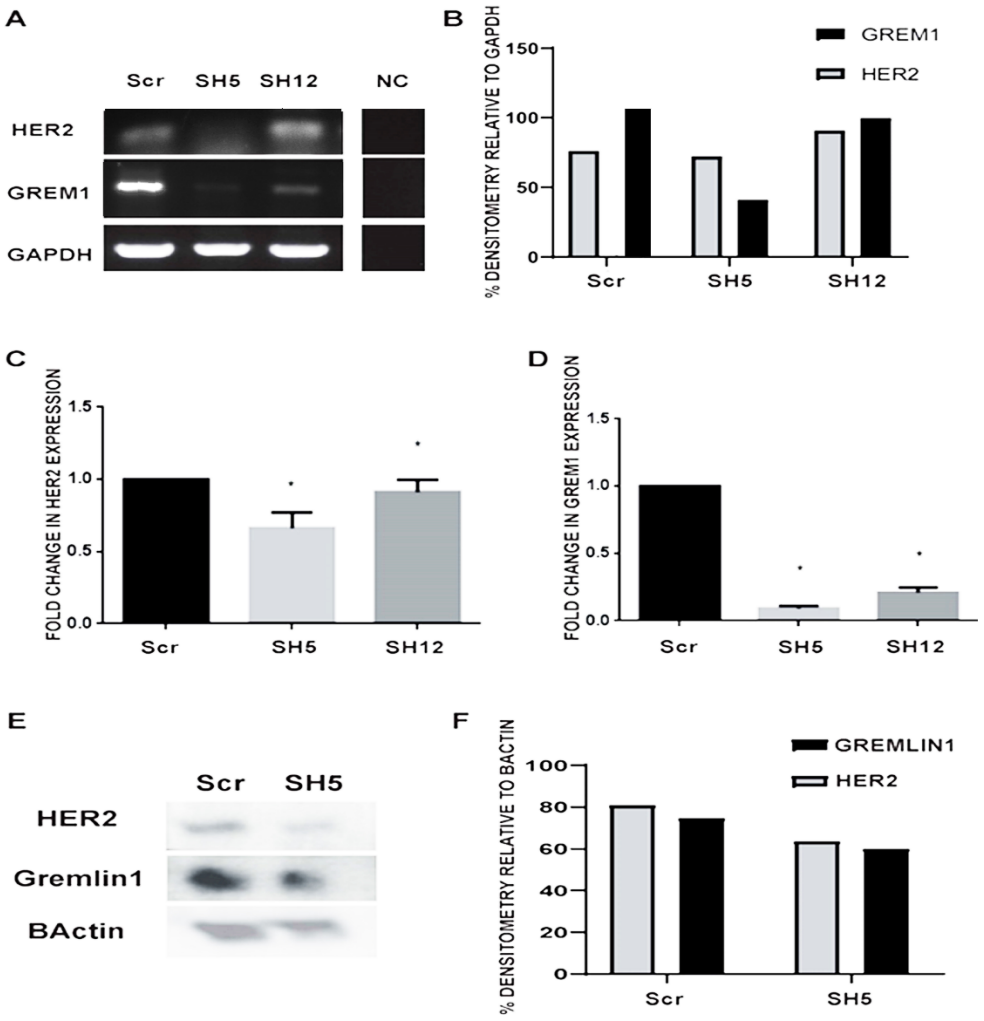

A) PCR at 35 cycles of GREM1 and HER2 expression when BT474 cells undergo HER2 knockdown with short hairpin (SH) lentivirus. Two lentiviral constructs are shown, SH5 and SH12, of which SH5 is the more successful knockdown compared to a scramble(nonsense) control vector (Scr). NC = Negative Control (sterile water)

B) Densitometry of the PCR from A using image J analysis of the PCR gel, by comparing the intensity of the GREM1 and HER2 PCR bands as a percentage relative to the intensity of the GAPDH band in each sample. This shows The SH5 lentiviral knockdown is most successful, and GREM1 expression decreased as HER2 expression reduced.

C) qPCR of fold change expression in HER2 with SH5 and SH12 HER2 knockdown compared to Scr control ($p < 0.01$, triplicate experimental repeat with mean + SEM (error bar)). HER2 expression reduced most with the SH5 knockdown.

D) qPCR showing fold change expression of GREM1 in SH5 and SH12 HER2 knockdown compared to Scr control ($p < 0.01$, triplicate experimental repeat with mean + SEM (error bar)). When HER2 knockdown occurs, GREM1 expression also reduced

E) Western blot of BT474 cells with HER2 knockdown, showing protein expression of HER2, Gremlin1 reduced in HER2 knockdown cells. The control is βActin.

F) Densitometry of E using ImageJ software semi quantified Gremlin1 and HER2 band intensity on the western blot relative to the intensity of the βActin bands. At the protein level Gremlin1 and HER2 appear reduced in SH5 HER2 knockdown compared to control (Scr)

6.3.3 HER2 inhibition abrogates the effects of GREM1 overexpression on cellular function

BT474^{PEF} and BT474^{GREM1} cells underwent growth assay over 5 days, with or without the addition of HER2 inhibitor CP724714 (Figure 6.3A). BT474^{GREM1} clearly had the greatest growth compared to BT474^{PEF}, although this levelled off by Day 5, in keeping with the findings of the previous chapter regarding GREM1 overexpression causing increased growth. When CP724714 was added to BT474^{PEF} there was significantly increased growth compared to BT474^{PEF} in normal medium (Figure 6.3 B, $P < 0.0001$ at day 3, 4 and 5), although growth was still less than BT474^{GREM1}(Figure 6.3 A).

The addition of CP724714 to BT474^{GREM1} conversely, significantly decreased growth (Figure 6.3 C, $P < 0.0001$ at day 2, 3 and 4) compared to BT474^{GREM1} in normal medium. The addition of HER2 inhibition reduced growth in GREM1 overexpression back to equivalence with the control cell line.

Migration was also seen to be increased in GREM1 overexpression in the previous chapter. With the addition of CP724714, although the changes were not significant, migration did appear to be reduced in the GREM1 overexpressing cells. BT474^{PEF} had an average of 109% migration through a transwell membrane when controlled for growth, with BT474^{GREM1} displaying 122% migration, which was reduced to 112% with the addition of CP724714(Figure 6.3 D).

In support of the 2D growth assays, similar results were seen with spheroid growth assay (Figure 6.4 A), with BT474^{GREM1} displaying the most prolific growth compared to BT474^{PEF}. Unlike the 2D growth assay, in the spheroid assay the addition of CP724714 did not seem to affect BT474^{PEF} growth (Figure 6.4 B). However, once again, the addition of HER2 inhibition to BT474^{GREM1} cells was shown to reduce growth significantly (Figure 6.4 C, $P < 0.0001$ at day 4, 6 and 8, photographic representation Figure 6.4 D). It appears that the cellular effects of increased GREM1 expression in HER2+ breast cancer cells are abrogated by HER2 inhibition.

The final experiments in this chapter examine which intracellular signalling mechanisms may be at play in Gremlin1's influence on HER2+ breast cancers.

Figure 6-3 Effect of HER2 inhibitor on 2D growth and migration in GREM1 overexpressing BT474 HER2+ cells

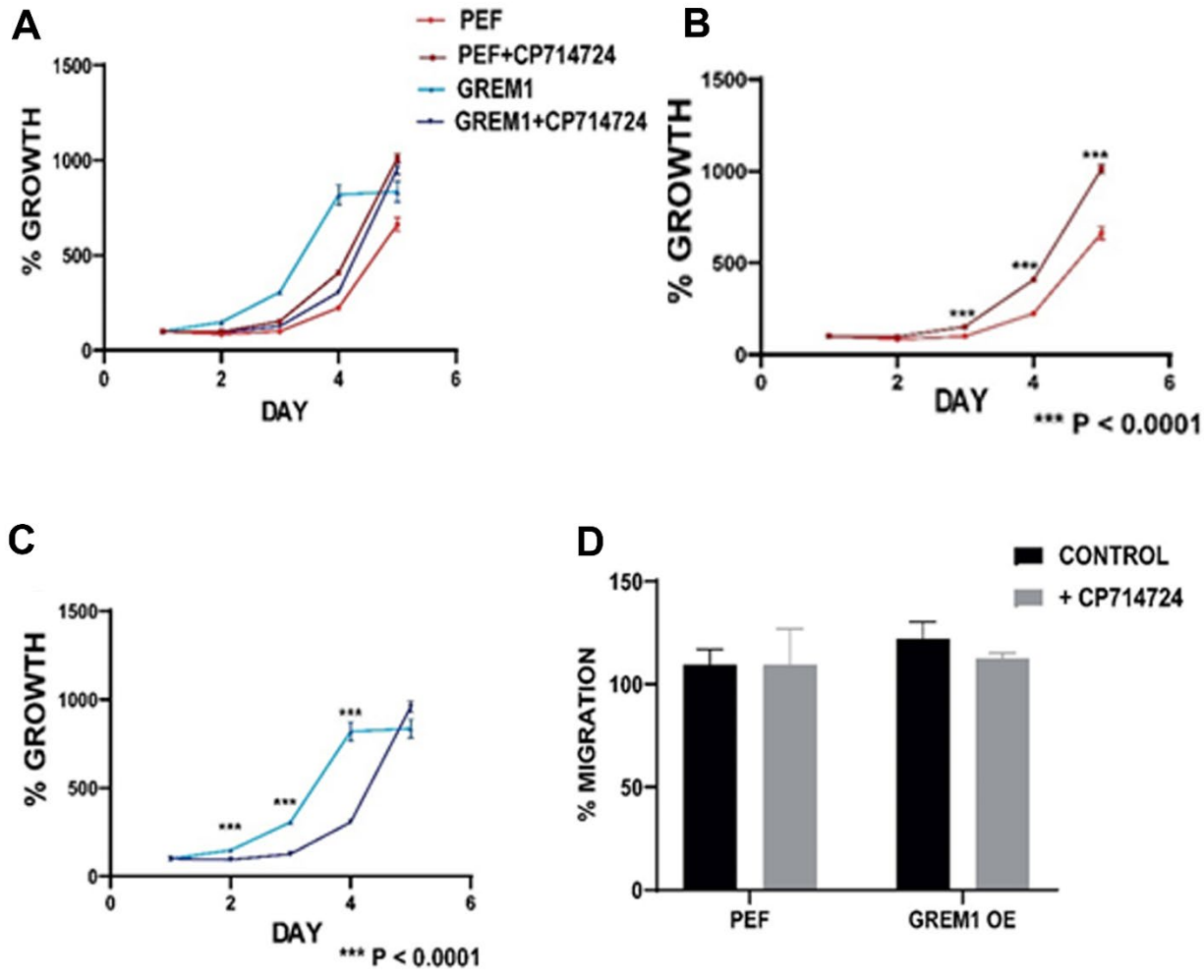

A) Growth assay of BT474^{PEF} and BT474^{GREM1} when treated with vehicle (normal media), or HER2 inhibitor CP724714. As in previous growth assays, cells are fixed and stained with crystal violet at day 1, day 3 and day 5 and the stain intensity measured. Results are then displayed as a percentage growth compared to day 1. The light red line is BT474^{PEF}, dark red line is BT474^{PEF} with addition of HER2 inhibitor CP724714, light blue line is BT474^{GREM1}, and dark blue line is BT474^{GREM1} with HER2 inhibitor CP724714 added. In each growth curve each data point is the mean of 3 experimental repeats +/- Standard Error of Mean (SEM)

B) In more detail of the graph in A, looking just at effect of HER2 inhibitor on control cells only.BT474^{PEF} showed significantly increased growth when CP724714 was added compared to control vehicle media, at day 3, 4 and 5. ($P < 0.0001$ Mann Whitney test)

C) In more detail of the graph in A looking only at GREM1 overexpressing cells with and without HER2 inhibitor.BT474^{GREM1} showed significantly decreased growth when CP724714 was added compared to control vehicle media, at day 2, 3 and 4. ($P < 0.0001$ Mann Whitney test)

D) Migration of BT474^{PEF} and BT474^{GREM1} through a porous membrane over 72 hours with either control media vehicle(black), or with addition of CP724714(grey). The average of 3 experimental repeats is shown (mean +/-SEM). There was no significant difference between BT474^{PEF} and BT474^{GREM1} with the addition of CP724714 ($p>0.05$)

Figure 6-4 Effect of HER2 inhibitor on 3D Spheroid growth of GREM1 overexpressing BT474 HER2+ cells

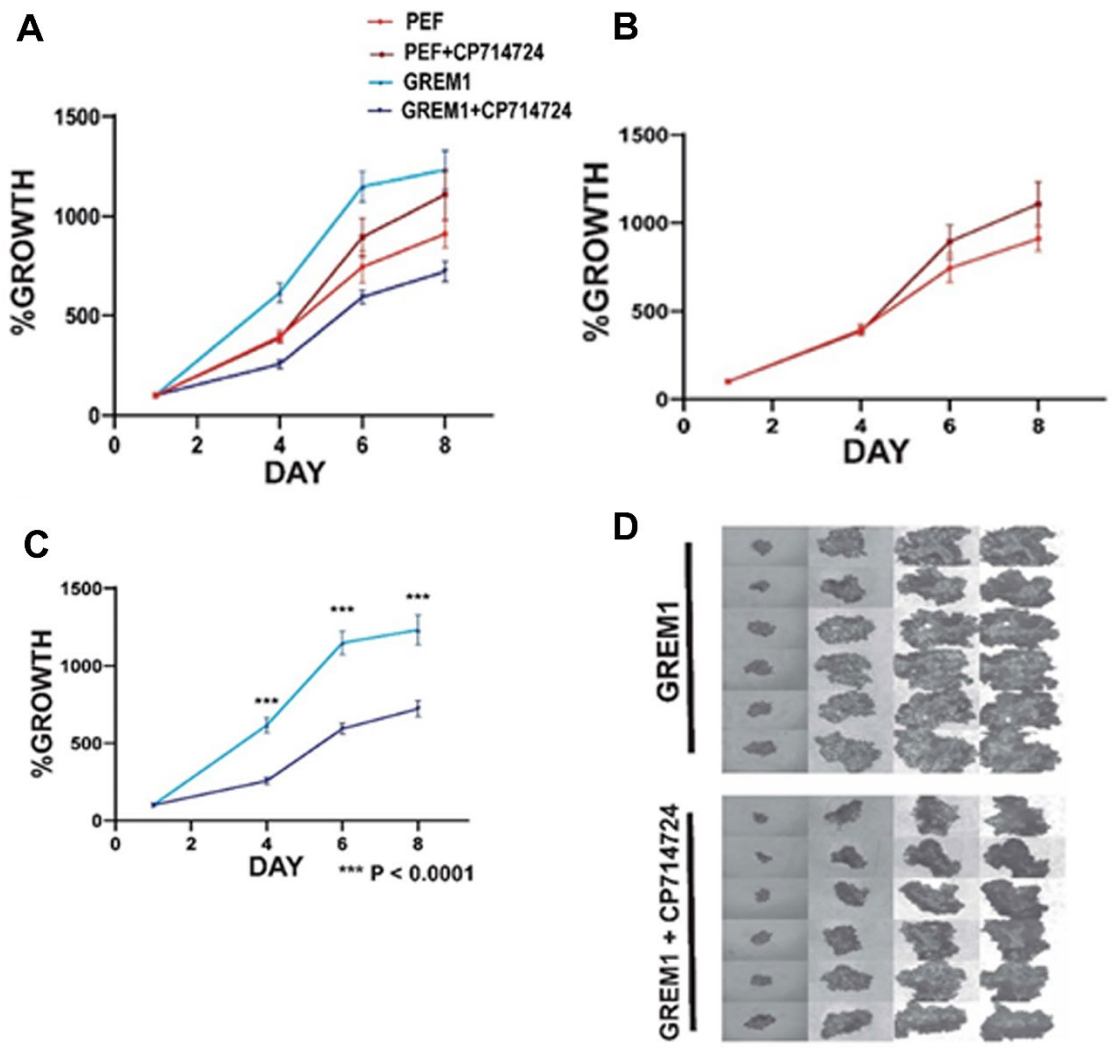

A) For 3D growth assay BT474^{PEF} and BT474^{GREM1}cells were grown in non-adherent u bottomed wells to create spheroids that then had the addition of HER2 inhibitor CP724714 or control vehicle media over 8 days, with Image J software used to quantify growth and this is displayed as a percentage growth compared to day 1. The light red line is BT474^{PEF,} dark red line is BT474^{PEF} with addition of HER2 inhibitor CP724714, light blue line is BT474^{GREM1,} and dark blue line is BT474^{GREM1} with HER2 inhibitor CP724714 added. In each growth curve each data point is the mean of 3 experimental repeats +/- Standard Error of Mean (SEM)

B) In looking more closely at the graph in A, there was no significant difference in 3D spheroid growth BT474^{PEF} when treated with vehicle (normal media), or HER2 inhibitor CP724714 ($p>0.05$).

C) When taking just BT474^{GREM1} spheroid growth from A, growth of GREM1 overexpressing BT474 cells is significantly inhibited with the addition of HER2 inhibitor CP724714 compared to control vehicle media at days 4, 6 and 8 ($p<0.0001$)

D) Microscopy photography (x10 magnification) of A, with BT474^{GREM1} spheroid growth on days 1, 4, 6 and 8(Upper group), and when CP724714 is added (Lower group). Growth is visibly reduced with the addition of CP724714.

6.3.4 Gremlin1 activates the AKT signalling pathway in HER2+ BT474 cells

BMPs are known to activate both canonical signalling via the smad1/5/8 pathway, and non-canonical signalling via MAPK pathways. To determine if Gremlin1 could exert its effects via BMP signalling pathways, or independent of them, I intended to treat BT474 cells with either recombinant BMP alone, recombinant Gremlin1 alone, and recombinant BMP followed by Gremlin1, examining phosphorylation of both the Smad1/5/8 and MAPK pathways. This required initial time trials to determine the optimal treatment time in which to capture phosphorylation of these pathways. When BT474 cells were treated for different times with 40ng/ml of BMP-4, maximal pSmad1/5/8 signal was seen at 1 hour (Figure 6.5 A). Interestingly, as one might expect from a negative regulatory feedback loop, the treatment with BMP-4 also increased Gremlin1 levels. There was also an increase in non-canonical signalling with pERK activity between 15 minutes and 2 hours, and a peak of pAKT at 1 hour, although the Western blot band was faint for AKT.

Having determined 1 hour treatment would adequately capture activity in these signalling pathways, the BT474 cells were then treated with recombinant Gremlin1, BMP-4 or both, with normal medium as control vehicle, and sodium orthovanadate as a positive control (Figure 6.5 B and relative densitometry represented in C). The pSmad1/5/8 unusually appeared at the same level when treated with BMP-4, and slightly increased when treated with Gremlin1. Gremlin1 did not abrogate pSmad1/5/8 when cells were treated with BMP-4. There appeared to be no effect of BMP-4 or Gremlin1 treatment on pERK, although, the positive control band was very strong, the 'noise' from which may have made more subtle changes in pERK difficult to detect. What was apparent was the strong pAKT signal when cells were treated with Gremlin1 alone. This did not occur when treated with BMP-4 alone, but only in the presence of Gremlin1.

This effect was seen in 2 of the three independent experimental repeats.

Interestingly in BT474^{GREM1} cells, PI3KCA was upregulated compared to control (Figure 6.5 D, P = 0.03). PI3KCA is a vital part of the PI3K/AKT/mTOR pathway that encodes the p110α catalytic subunit of the PI3K enzymes, resulting in cell proliferation and resistance to apoptosis *in vitro*. Gremlin1 may well exert its effects on tumour growth independent of BMP signalling, with direct action on the AKT pathway.

Figure 6-5 Gremlin1 effect on BMP and MAPK signalling pathways

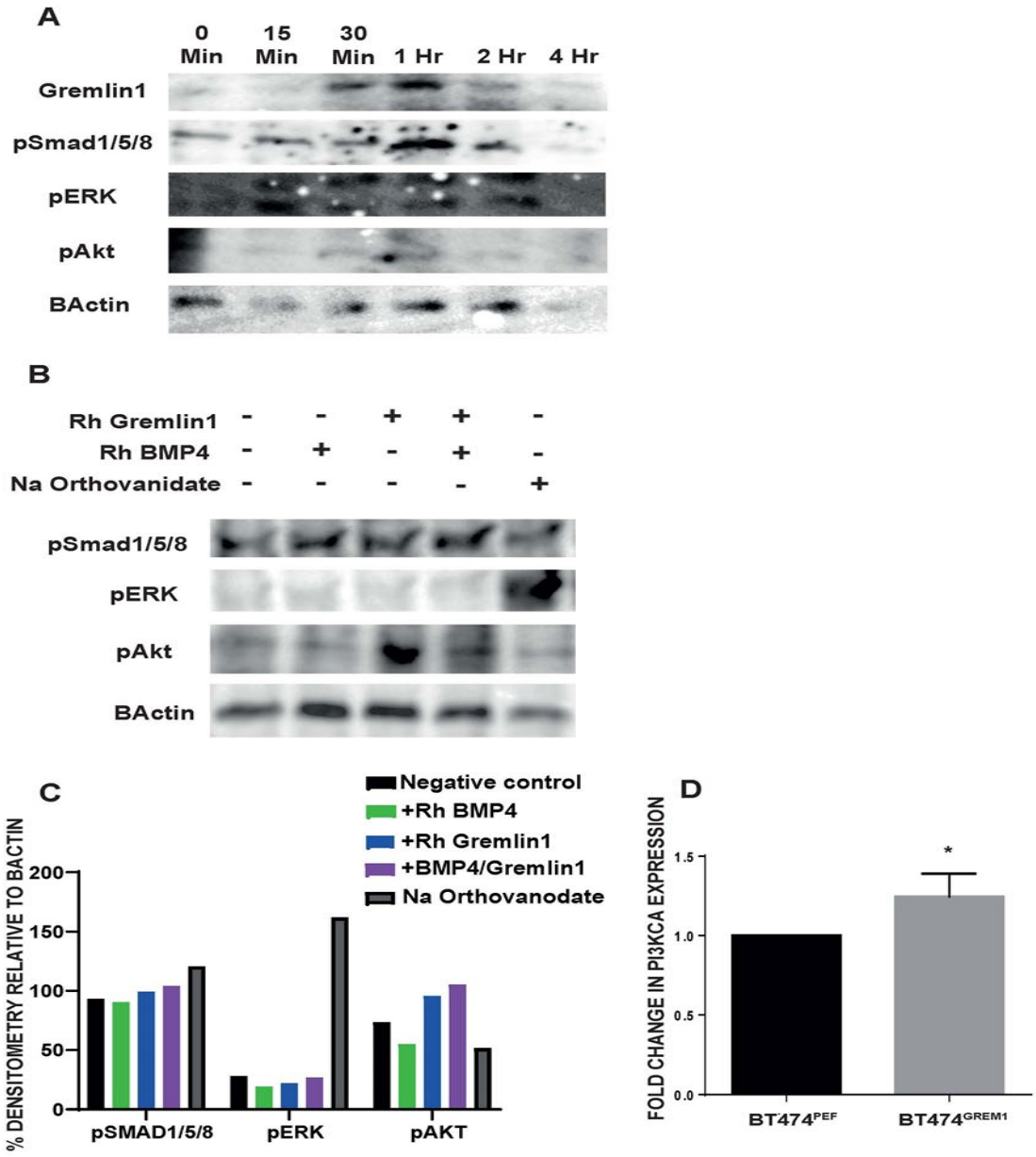

A) Western blot of BT474 cells treated with media only (0) or 40ng/ml BMP4 for 15 minutes, 30 minutes, 1 hour, 2 hours or 4 hours as a time trial. Whole cell lysate protein was then probed for Gremlin1, pSmad1/5/8, pERK, pAKT and housekeeping protein control βActin to see when the signalling pathways are activated. Peak activity was seen around 1 hour of treatment. Single representative image from same experimental repeat

B) Western blot of BT474 cells treated for 1 hour with normal media, 40ng/ml BMP4, 500ng/ml Gremlin1, BMP-4 then Gremlin1, or Sodium Orthovanadate (positive control causes phosphorylation). Whole cell lysate protein was then probed for pSmad1/5/8, pERK, pAKT and housekeeping protein control βActin. Neither BMP-4, nor Gremlin1 appear to affect Smad1/5/8 activity, but Gremlin1 appears to activate AKT independent of BMP-4. Single representative image from same experimental repeat

C) Densitometry of B using ImageJ software to semi quantify band intensity on the western blot relative to the intensity of the βActin bands, which corrects for loading volume differences. Gremlin1 appears to activate the AKT pathway, whilst BMP-4 does not.

D) qPCR of PI3KCA expression in BT474^{PEF} and BT474^{GREM1}, with significant increase in expression in GREM1 overexpression compared to control (* p = 0.03, mean of three repeats+/-SEM (error bars)). PI3KCA is an important part of the AKT pathway, and its overexpression in BT474^{GREM1} cells supports a link to the findings in B and C.

6.4 Discussion

In this chapter we have seen that there is a reciprocal interaction between HER2 and Gremlin1. In previous chapters, clinical cohort data had demonstrated the positive correlation between GREM1 and HER2, and the impact on poor clinical outcomes. When GREM1 was overexpressed, HER2 expression increased. Here we see that when HER2 is inhibited or knocked down, GREM1 expression decreases. This implies a regulatory feedback relationship in HER2+ breast cancer cells, which has not been previously identified. A more detailed analysis of regulatory control would be planned, with the use of GREM1 and HER2 gene reporter assays.

Interestingly, when examining the effect of HER2 inhibitor on cellular growth and migration in $BT474^{PEF}$ or $BT474^{GREM1}$ cells, the inhibition of HER2 in GREM1 overexpressing cells seemed to reduce cellular growth and migration back to the baseline rate of the control cell population. This adds weight to the established correlation between GREM1 and HER2, that HER2 inhibition or knockdown also results in reduction of GREM1 expression, and thus would inhibit the cellular effects of high GREM1 expression. The next question of interest is whether high GREM1 expression in HER2+ breast cancers would impact the sensitivity or resistance to treatment with HER2 blockade agents such as Trastuzumab and Pertuzumab. This data might suggest that the effects of high GREM1 expression are sensitive to HER2 blockade. Indeed, in the 3D spheroid growth assay, treatment with CP724714 reduced the growth rate the most in $BT4747^{GREM1}$. CP724714 however, did not result in a total reduction in growth, or increased apoptosis, $BT474^{GREM1}$ cells continued to grow, just at a slower rate. It may be, that had the experiments been run for a longer timeframe, sensitivity or resistance may have become more apparent and any expression changes in GREM1 with developing resistance could then be examined. There is also the matter of mechanisms of action.

CP724714 is a specific small molecule inhibitor of HER2, selectively inhibiting HER2 kinase phosphorylation, it does not have the same mechanisms of action as Trastuzumab or Pertuzumab, which are monoclonal antibodies. Trastuzumab targets the HER2 ectodomain promoting endocytosis and degradation, reducing receptor dimerisation and downstream MAPK and PI3K/AKT/mTOR signalling. When bound to HER2 at the cell surface, it also encourages innate immune system responses resulting in cancer cell death. Pertuzumab binds domain II of

HER2 blocking dimerisation with the other receptors required for HER2 signalling, particularly HER3 (Vernieri et al. 2019).The heterodimer of HER2-HER3 is strongly linked to PI3K/AKT/mTOR signalling pathway thought to be particularly relevant to HER2+ breast cancers (Nami et al. 2018; Vernieri et al. 2019).

Despite the success of these agents for HER2+ breast cancer patients, those that develop resistance have very poor outcomes. Many mechanisms of resistance have been described, such as alteration in HER2 expression or HER2 extracellular structure, shift to dimerising with alternative receptors such as EGFR, cross talk with ER signalling, activation of CyclinD1- CDK 4/6 axis, loss of p21 and activating mutations of PI3K catalytic subunit α (PI3KCA) (Nami et al. 2018; Vernieri et al. 2019). HER2 can also translate to the nucleus and effect direct gene expression effects via interaction with Signal Transducer and Activator of Transcription 3 (STAT3), which may be another mechanism of resistance to cell surface directed treatments (Aghazadeh and Yazdanparast 2017; Wang et al. 2018; Redmond et al. 2019).

There is very little published data on how Gremlin1 mediates its effects in cancer. It was first identified as a BMP antagonist (see Chapter 1) and although Gremlin1 has been shown to antagonise pSmad 1/5/8 BMP signalling in MDA MB 231 cells, resulting in increased invasiveness (Ren et al. 2019), it inhibits the effects of BMP-4 on MMP-9 mediated by Smad1/5/8 signalling in fibrosarcoma HT1080 cells (Laulan and St-Pierre 2015). Gremlin 1 also induces EMT in colorectal cancer cells by suppression of BMP signalling (Karagiannis et al. 2015). BMPs and their antagonists often have contradictory roles in cancer (Zabkiewicz et al. 2017) and interaction of Gremlin1 with cancer cells is unaffected by treatment with BMPs (Kim et al. 2012). Thus, other studies have focused on novel and BMP independent mechanisms of action. In angiogenesis and endothelial cells, Gremlin1 induces activation of focal adhesion kinase (FAK), ERK, NFκB and VEGFR2 (Stabile et al. 2007; Mitola et al. 2010; Grillo et al. 2016) . Sung et al, demonstrating GREM1 knockdown in MDA MB 453 cells, suppressed TGFβ induced migration, and Gremlin1 treatment induced markers of EMT, through ERK activation (Sung et al. 2020a). The same group found treatment of MDA MB 231 cells with Gremlin1 resulted in activation of STAT3 and subsequent increase in MMP13 expression, independent of BMP and EGFR signalling (Sung et al. 2020b). Interestingly, in another study from this group, treatment of SKBR3 cells with Gremlin1 resulted in activation of EGFR, resulting in downstream

phosphorylation of ERK and AKT, which was attenuated by an EGFR tyrosine kinase inhibitor (Park et al. 2020).

The results presented demonstrate Gremlin1 treatment of BT474 cells appears to induce AKT activation, independent of pSmad1/5/8, and overexpression of GREM1 upregulated PI3KCA, which is the catalytic subunit of PI3K. Hyperactivation of the PI3K/AKT pathway occurs in breast cancer on amplification of HER2 (Carmona et al. 2016), with overactivation of PI3K/AKT present in bone metastatic breast cancer cells and HER2+ tumours with metastasis to the bone (Kim et al. 2006; Hinz and Jücker 2021). Activated AKT impacts on several cell functions such as metabolism, proliferation, and cell survival. It promotes proliferation by inhibiting glycogen synthase kinase 3(GSK3), abating its inhibitory effect on CyclinD1, which promotes cell cycle. AKT also inactivates cell cycle checkpoint proteins p21 and p27 (Carmona et al. 2016; Martorana et al. 2021). In earlier chapters, GREM1 overexpression in BT474 cells decreased the expression of p21, although not to statistical significance (Chapter 5). In HER2+ cancers AKT activation also directly occurs on loss of PTEN, and this would be an interesting avenue to explore in GREM1 overexpressing or Gremlin1 treated cells, as to whether in addition to increased PI3KCA, PTEN is reduced and the subsequent impact of resistance to HER2 blockade. Aberrantly activated PI3KCA, or loss of PTEN, is important in HER2+ cancers, as this is thought to drive escape from upstream HER2 inhibition, through activation of PI3K/AKT/mTOR pathway, and clinical trials of AKT inhibitors as additional therapy in advanced and metastatic cancer are ongoing (Carmona et al. 2016; Martorana et al. 2021). Further studies are required to examine how Gremlin1 may act within the HER2/PI3K/AKT pathway and whether Gremlin1 provides a resistance mechanism to HER2 blockade in advanced and metastatic HER2+ breast cancers treated with Trastuzumab and Pertuzumab. Gremlin1 and its effect on HER2+ breast cancer metastasis, particularly to bone will be the subject of the subsequent chapter.

.

7 Effect of Gremlin1 on metastases of HER2+ Breast Cancers

7.1 Introduction

Osteolytic bone metastases are the most common metastatic lesions in breast cancer patients, and up to 70% of patients with metastatic disease will develop them (Pulido et al. 2017; Xiong et al. 2018). Bone metastatic breast cancer is considered incurable and has an associated increased risk of mortality. In addition, skeletal related events, such as fractures and spinal cord compression have significant morbidity and greatly add to disease burden (Brook et al. 2018; Parkes et al. 2018).

There is some evidence of propensity to metastatic site by breast cancer subtype. A recent article by Arciero et al examined around 85,000 cases of breast cancer from two national databases and concluded that those patients classified as ER+/HER2+ were more likely to have bone metastasis than ER-/HER2+patients(Arciero et al. 2019). This is in concordance with the findings of Xiao et al who also found that out of 295,000 cancers in the SEER (Surveillance, Epidemiology and End Results) database, ER+/HER2+ cancers had a higher incidence of bone metastasis at diagnosis compared to ER+/HER2- cancers. They also found that HER2+ cancers (whether ER+ or not) were significantly associated with a higher incidence of metastases to liver, brain, and lung(Xiao et al. 2018). Ignatov et al examined 12,000 patients with primary breast cancers which were non metastatic at diagnosis, and which were classified by biological criteria rather than clinical subtype. Patients with HER2+ and TNBC tumours had higher early recurrence and mortality, whereas Luminal A and B tumour patients had lower, but more long term, cancer recurrence risk. Both HER2 enriched and Luminal B (HER2+) tumours had similar metastatic patterns, with a higher rate of metastasis to bone and liver, although HER2 enriched subtype tumours had a higher propensity for brain metastasis than Luminal B (HER2+)(Ignatov et al. 2018).

As a regulator of the bone environment, bone morphogenetic protein (BMP) signalling is a natural area of interest with regards to skeletal metastases, with several studies identifying BMPs as promoting bone metastases in breast cancer (Alarmo et al. 2008; Katsuno et al. 2008; Ampuja et al. 2016). Our knowledge regarding the role of BMP antagonists such as Gremlin1 is much less well defined, although there is evidence that high levels of GREM1 are associated with metastasis of ER negative breast cancers (Neckmann et al. 2019), there is no published data on its role in other breast cancer subtypes, or the most common metastatic site, bone. The data presented thus far suggests that in clinical cohorts

high GREM1 in HER2+ breast cancers is associated with metastasis and poor distant metastasis free survival (Chapter 5) and that high GREM1 in HER2+ breast cancer cells lead to increased growth, migration and EMT, which is essential for metastasis. Gremlin1 activates the AKT pathway in HER2+ cells (Chapter 6), and AKT activity has been associated with bone metastasis in HER2+ tumours (Kim et al. 2006; Hinz and Jücker 2021). The first part of this chapter presents an *in vivo* model of GREM1 overexpression in HER2+ tumours, in terms of both primary tumour growth and metastasis. In Chapter 3, data suggested GREM1 expression was lower in primary tumours with metastasis to the bone, and in bone metastases themselves. The second part of this chapter will examine how HER2+ cells with high GREM1 expression behave in models of bone metastasis.

7.2 Methods

7.2.1 In Vivo primary tumour model

BT474^{PEF} and BT474^{GREM1} cells were prepared and counted on the day of injection, as described in Chapter 2.11,. There were 6 balb/c nude female mice in each group. At age 8 weeks, 2.5 x 10^6 cells (in 50:50 Matrigel: PBS) were injected into each 4th mammary fat pad, totalling 12 injection sites for each group. All mice were weighed and examined for tumour growth on a twice weekly basis for twelve weeks. At the end of the experiment mice were culled and the mammary fat pads excised and fixed. Tumour volume was calculated as follows –

Volume (mm^3) = (Length x Width x Width)/2

7.2.2 In Vivo metastatic model

BT474^{PEF} and BT474^{GREM1} cells were prepared and counted on the day of injection, as described in Chapter 2.11. There were initially 8 balb/c nude female mice in each group. In the BT474^{PEF} group, one mouse was terminated before experimentation due to a cystic growth, leaving 7 in this group that proceeded to experiment. At age 8 weeks, 150,000 cells in 150µl PBS were administered by intracardiac injection under inhaled anaesthesia. One mouse in the BT474^{GREM1} group had immediate periprocedural death, leaving 7 in this group for analysis. One further mouse in the BT474^{PEF} group required termination the day following injection, due to an apparent stroke, leaving 6 mice in this group for analysis.

Mice were weighed twice weekly and examined for signs of metastatic malignancy for 12 weeks. All then underwent PET CT under anaesthesia, having been starved for 12 hours, with tail vein injection of Fluorodeoxyglucose (18FDG) as contrast, to determine metastatic hotspots and direct subsequent autopsy dissection and tissue collection.

7.2.3 Bone Adhesion Model

Eight thousand Human Osteoblast hFob cells were seeded onto a 96 well plate the day before experiment. BT474^{PEF} and BT474^{GREM1} cells were stained with DiI (as per protocol in Chapter 2.9.2). Twenty thousand stained BT474^{PEF} or BT474^{GREM1} cells were seeded into each well of the hFob plates and incubated for two hours. Wells were then washed with PBS three times to remove non adherent cells. Confocal microscopy was then used to take three field images of each well with filter for DiI fluorescence. Cell counts were totalled for each well and averaged

over three wells, with three experimental repeats. Negative control was vehicle only with no cells onto the hFob plate and BT474^{PEF}/BT474^{GREM1} cells added into wells with no hFob cells.

7.2.4 Osteoblast co-culture and Bone Matrix Extract (BME) invasion and migration model

Forty thousand hFob cells were seeded onto a 24 well plate the day before transwell experiment. Thirty thousand BT474^{PEF} or BT474^{GREM1} were seeded into inserts in 200µl of Optimem medium, either lined with Matrigel (as per previous invasion assays) or without Matrigel (as per previous migration assays). In the bottom of each well were either the hFob cells in 600µl normal medium, 600µl of BME diluted to 100µg/ml in 10% FCS, or 600µl normal medium only. The control was also a 24 well plate with 30,000 BT474^{PEF} or BT474^{GREM1} cells in 600µl normal medium. The plates were then incubated at 37^{0}C for 3 days, with inserts and plates subsequently washed, fixed and stained with crystal violet. Migrated or invaded cells on the inserts were subsequently counted. Stained cells were then dissolved with 300 µl acetic acid (10% v/v) and plated into a 96 well plate for reading of absorbance at a wavelength of 540nm. Migration and invasion were calculated as compared to the control well with no insert, to account for baseline level of cell proliferation.

7.3 Results

7.3.1 BT474^{GREM1} grow larger volume tumours in vivo compared to BT474^{PEF}

Balb/c nude mice weight was similar in BT474^{PEF} and BT474^{GREM1} groups throughout the experiment (Figure 7.1 A). The BT474^{PEF} group were slightly heavier, but this only reached statistical significance on one measurement occasion. It can therefore be assumed that the two groups were comparable. The BT474^{PEF} group did not grow any macroscopic tumours within the mammary fat pads (Figure 7.1 B), whereas the BT474^{GREM1} group grew 4 tumours across the 12 injection sites (Figure 7.1 C), i.e., 33% of injections established tumour growth in the BT474^{GREM1} group compared to 0% of controls. The average tumour volume in the BT474^{GREM1} group was therefore higher than in the BT474^{PEF} group, significantly in the last 2 weeks of the experiment (Figure 7.1 D). As can be seen in graph 7.3D, there was an initial tumour nodule of cells and Matrigel that was established following injection, which then regressed so that there was no evident tumour. At around week 4 post injection, the first tumour nodules in the BT474^{GREM1} group started to appear and steadily increased in volume. There was no significant difference in initial nodule volume between the two groups (Figure 7.1 E). Therefore, the difference in subsequent tumour growth was not the product of differing injection volumes.

Figure 7-1 In vivo primary tumour model

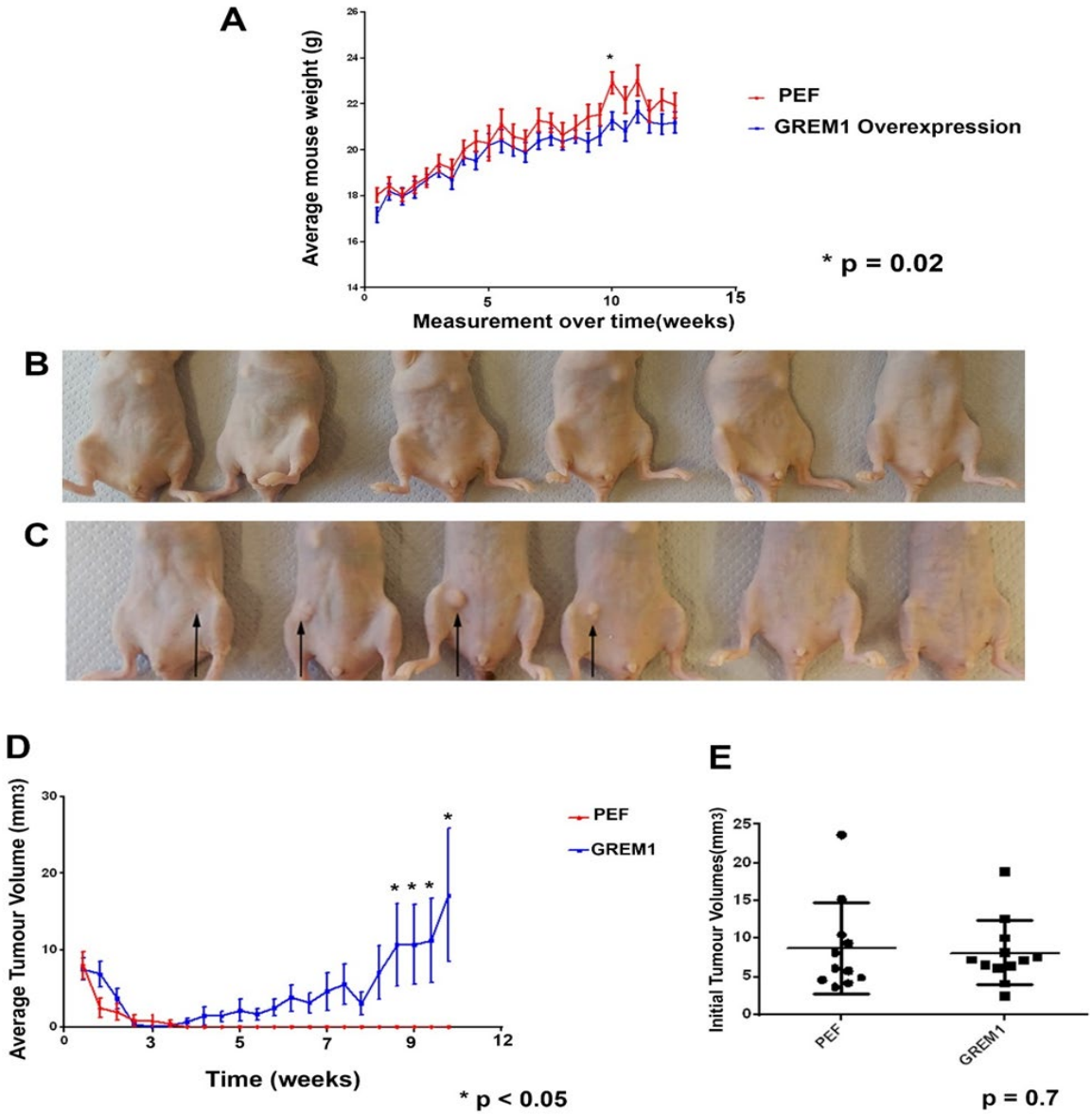

A) **Either BT474^{PEF} or BT474^{GREM1} cells were injected into abdominal mammary fat pads (MFP) of Balb/c nude mice. There were 6 mice in each group, with injection into both abdominal mammary pads on each mouse. Average weight measurements throughout the experiment were taken to ensure equivalence between the groups. The BT474^{PEF} group only had one statistically significant higher average weight on one measurement occasion in week 10, * p = 0.02. Otherwise, the groups were equivalent throughout. Graph plots mean weight over time +/- SEM (error bars)**

B) **Six control BT474^{PEF}mice at the end of the experimental period did not develop any clinically evident MFP tumours after the initial injection nodule regressed**

C) **Four of the six BT474^{GREM1} mice developed MFP tumours at a single injection site (black arrows), i.e., 4 out of 12 possible injection sites grew tumours.**

D) **Tumours were measured with callipers in width and length twice weekly. This was used to calculate tumour volume. The BT474^{GREM1} MFP tumours were significantly bigger than the control group tumours by week 9 after injection, p <0.05. Plot across time of mean tumour volume +/- SEM (error bars)**

E) **The initial volume of tumour nodule that formed after injection was equivalent between the two groups, p = 0.7, such that differences in tumour growth are not because of variable injection volumes. Graph plots individual values as circle or square, with mean +/- SEM**

7.3.2 *BT474^{GREM1} produce more metastases in vivo compared to BT474^{PEF}*

There were initially 8 mice injected intracardiac with BT474^{PEF}, and 8 mice injected with BT474^{GREM1}. In the control BT474^{PEF} group, 2 mice were culled from the group, one before the study due to a cystic malformation, and a second due to periprocedural complication. In the BT474^{GREM1} group one mouse was culled due to periprocedural complication. Thus, analysis proceeded on 6 control BT474^{PEF} and 7 BT474^{GREM1} injected mice (Figure.7.2 A and B). Although the control group trended towards a higher average weight, there was no significant statistical difference in average weight measurements overall, excepting one measurement occasion in week 4, whereby the control group weighed significantly more than the BT474^{GREM1} group (Figure 7.2 C, $p = 0.04$). There is therefore unlikely to be any significant difference in the condition of the two groups, particularly at the start of the intervention, that might Influence results.

18 FDG was injected into the tail vein of the mice (visible in Figure 7.2A and B in three mice), where it was taken up by high glucose metabolising cells, most commonly in mice in the brain, kidneys, heart and often the intestine. The 18 FDG was excreted via the renal tract and thus collected in the bladder. One mouse had an unsuccessful injection due to extravasation (Figure 7.2 B, Mouse 6), with no uptake visible in its heart, brain, kidney, or bladder. Rapidly metabolising cancer cells will also pick up the tracer and be identified as ‘hotspots’ (Figure 7.3). The PET CT images taken were analysed in coronal, sagittal, and axial planes to ensure hotspots were identified. In the control group, three of the six mice demonstrated hotspots, compared to six of the seven mice in the BT474^{GREM1} group (Table 7.1). The only mouse in the latter group that did not demonstrate hotspots was the single mouse where injection failed. The BT474^{GREM1} group also had nearly double the total number of hotspots compared to control (Table 7.1)

In both groups, the most common hotspots were seen in bone (Figure 7.3 A, C and Table 7.1), although this was seen more frequently in the BT474^{GREM1} group. The control group also saw hotspots in the liver, lung (Figure 7.3 D) and ovary (Figure 7.3 B). The BT474^{GREM1} group also had a lung hotspot, but in contrast to the control group, demonstrated more uptake in the adrenal region (Figure 7.3 E) and retroperitoneum, with the largest tumour at autopsy in the right adrenal region (Figure 7.3 F).

Figure 7-2 *In vivo* metastatic model

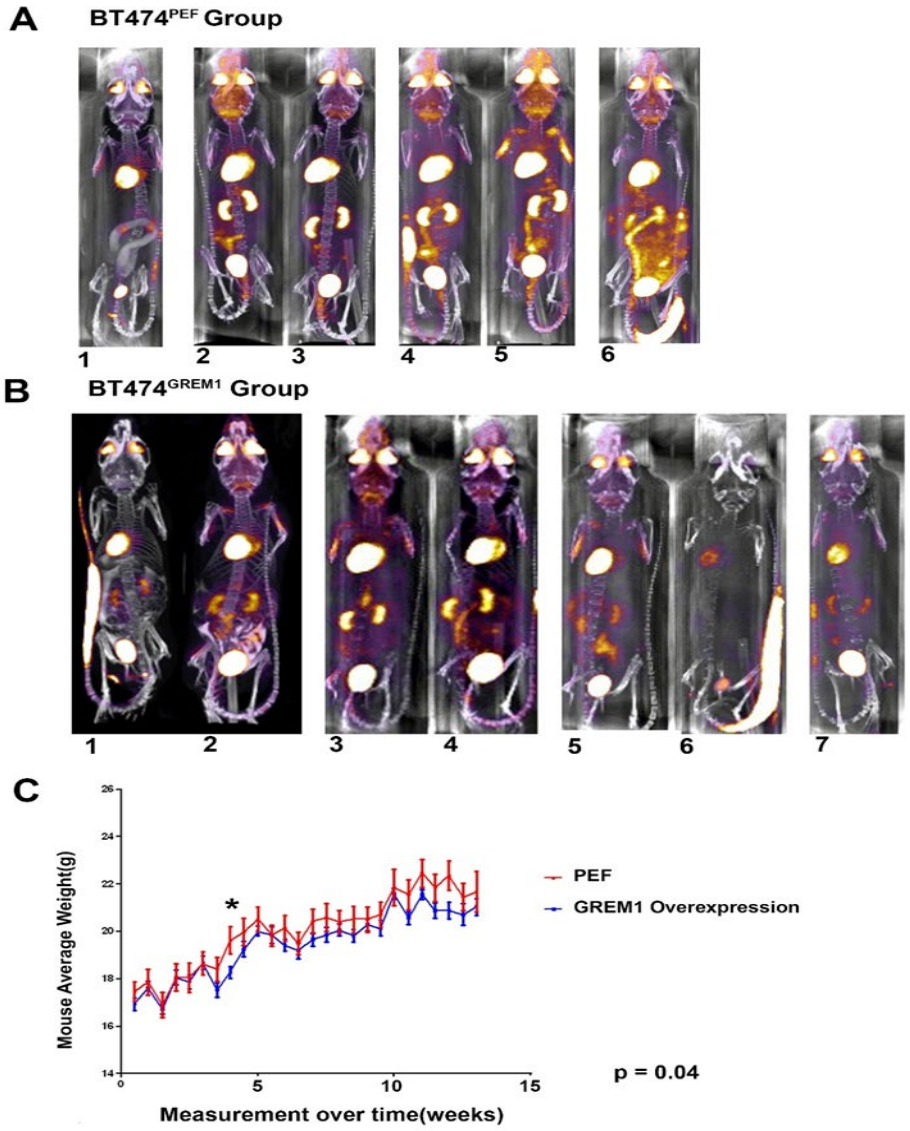

A) Balb/c nude mice underwent injection of BT474^{PEF} or BT474^{GREM1}cells into the heart to arterially seed metastatic deposits around the body. At 12 weeks after intracardiac injection positron emission tomography (PET) CT with a radioactive tracer(18FDG) injected into the tail vein was undertaken to pick up 'hotspots' of cancer metabolic activity. Figure A shows Group BT474^{PEF} PET CT background uptake view with expected intense radioactive tracer uptake in highly metabolic tissues of the eyes and heart and excretion signal in kidney and bladder. Mice 1, 5 and 6 demonstrated possible metastatic uptake hotspots on further imaging. Mouse 6 demonstrates radioactive tracer signal still at the injection site in the tail vein.

B) Group BT474^{GREM1} PET CT background uptake view with similar intense uptake as the BT474^{PEF} group (see A) in eyes, heart, kidney, and excretion signal in bladder. Mouse 6 shows poor injection, with the majority of 18FDG extravasated within the tail. This mouse did not have any subsequent hotspots, whereas the remaining 6 mice did.

C) Average mouse weight measurements throughout the experiment from the point of intracardiac injection over 12 weeks. The BT474^{PEF} group had statistically significant higher average weight on only one measurement in week 4, * p = 0.04. Overall, the groups were equivalent. Graph plots average weight +/- SEM

Figure 7-3 PET CT Hotspots images

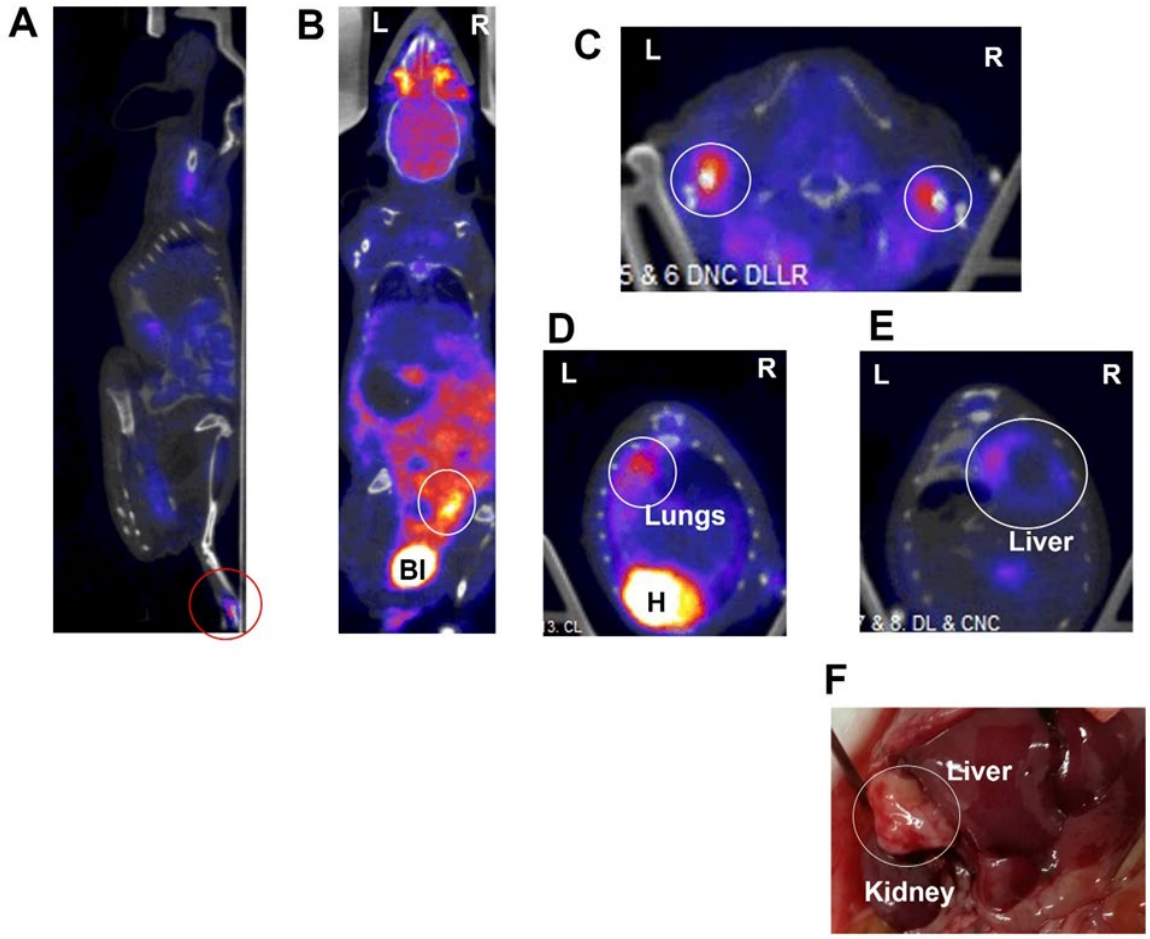

A) After injection of radioactive tracer 18FDG, which highlights metabolically active cancer 'hotspots' mice were scanned whilst lying on their front anaesthetised in a Nano PET CT scanner and tomographic sections were reviewed in both sagittal, coronal, and axial planes to identify hotspots, like the process of human PET CT scanning. Images were reviewed by me and Dr Paisey (expert in PET CT imaging) for agreement on high uptake hotspots. This picture is a Sagittal plane image of BT474^{GREM1} mouse 7, with uptake in the right foot (circled in red).

B) Coronal plane image of BT474^{PEF} mouse 6, with standard background uptake in brain (a high metabolism organ), intestine, and where tracer is excreted in the bladder (Bl). There is intense uptake in the region of the right ovary (circled white).

C) Axial plane image of prone BT474^{GREM1} mouse 5, with uptake hotspots in bilateral humerus (circled white) with the left more intense than the right. Humeral hotspots were seen in several mice.

D) Axial plane image of prone BT474^{PEF}mouse 6, with standard background uptake in the heart (H), and a hotspot at the posterior of the left lung (circled white)

E) Axial plane image of prone BT474^{GREM1} mouse 7 with hotspot on the right side, at the posterior edge of the liver in the region of the adrenal, with ring like enhancement (circled white)

F) The same mouse in E at autopsy showing a large mass in between kidney and liver (circled white), possibly an adrenal metastasis.

Table 7-1 PET CT identified hotspots

Site of hotspot	BT474^{PEF} (n=3 of 6 mice)	BT474 ^{GREM1} (n=6 of 7 mice)
Liver	2	0
Bone	4	11
Lung	1	1
Adrenal	0	3
Ovary	1	0
	8 TOTAL	15 TOTAL

7.3.3 Adhesion of BT474^{PEF} and BT474^{GREM1} in co-culture with hFob cells

GREM1 overexpressing BT474 cells, by average cell count, adhered significantly more after incubation with hFob cells compared to control BT474^{PEF} (Figure 7.4 A). Despite the same number of cells applied, and the short incubation time, to preclude higher cell numbers due to proliferation, DiI staining clearly showed higher density of BT474^{GREM1} than BT474^{PEF} at microscopy (Figure 7.4 C and B respectively). Neither were adherent when hFob cells were not plated (Figure 7.4 E).

Figure 7-4 Adhesion model BT474^{PEF} and BT4747^{GREM1} in co-culture with hFob cells

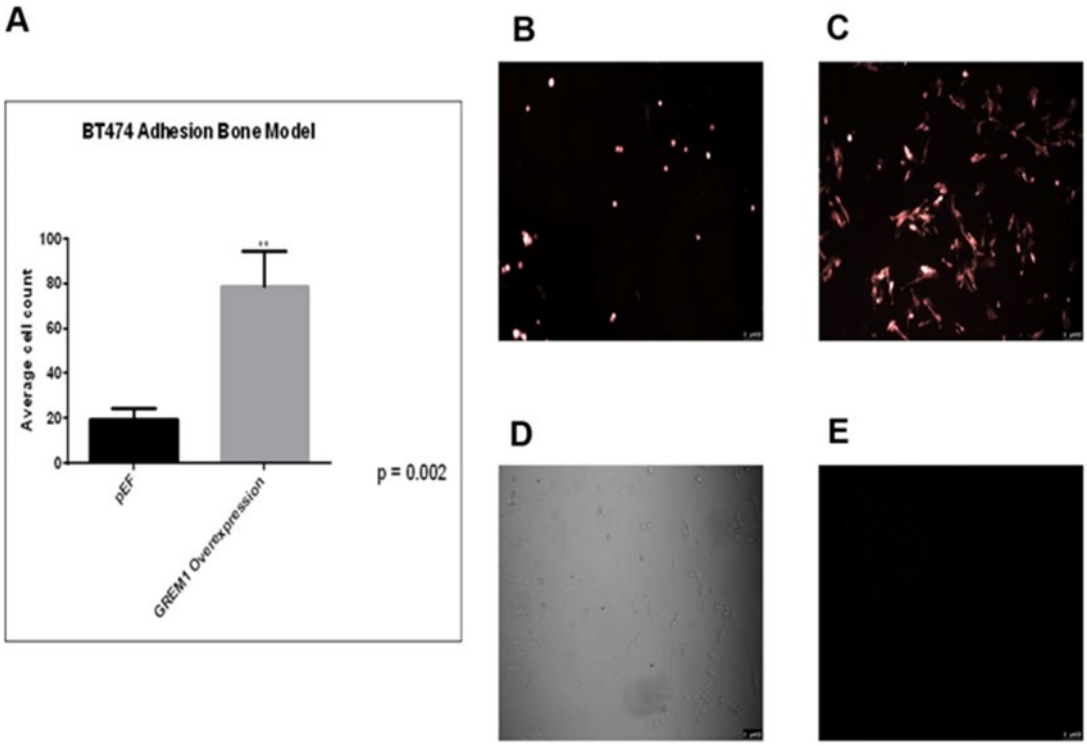

A) To determine if GREM1 overexpression resulted in a tendency to adhere in a bone environment BT474^{PEF} or BT474^{GREM1} cells that had been stained with a fluorescent dye (DiI) were co-cultured for 2 hours on a plate of human foetal osteoblast(hFob) cells. After 2 hours the plate was washed to remove any non-adherent cancer cells and fluorescence microscopy used to count the red/orange fluorescent cancer cells remaining adherent. The average count of adherent cells was significantly greater for BT474^{GREM1} cells compared to BT474^{PEF}, p = 0.002(Mann Whitney test, repeated in triplicate and displayed as mean count+/- standard error of the mean).

B) An example of adherent BT474^{PEF} stained with DiI, imaged with fluorescence microscopy at 549nm at x10 magnification. The red/orange fluorescent cancer cells can be seen sparsely across the plate.

C) An example of adherent BT474^{GREM1} stained with DiI, imaged with fluorescence microscopy at 549nm at x10 magnification. The red/orange fluorescent cancer cells are more numerous, indicating with GREM1 over expression, HER2+ BT474 cells will adhere more to osteoblast bone cells than control.

D) Standard microscopy of B, showing hFob cells are present on the plate, with the adherent BT474^{PEF} cells, such that there is no spurious staining of hFob cells. This shows only the BT474^{PEF} cells are responsible for the fluorescent signal.

E) Negative control plate, with no hFob cells, and DiI stained cancer cells applied for 2 hours, then imaged with fluorescence microscopy at 549nm to show no adherent DiI cells. This indicates the presence of the osteoblast cells is required for the BT474 cells to adhere within the 2-hour time frame.

7.3.4 Migration and invasion of BT474^{PEF} and BT4747^{GREM1} when in co-culture with hFob cells or BME

Based on cell count alone, the presence of osteoblasts and bone matrix extract (BME) significantly increased the migration of control BT474^{PEF} cells compared to normal medium (Figure 7.5 A). This significant increase was lost when analysing migration indirectly by crystal violet stain and absorbance (Figure 7.5 B).

For BT474^{GREM1} cells, concordant changes in migration were seen when assessed by either cell count or absorbance. The presence of osteoblasts increased migration, but interestingly BME significantly decreased migration of BT474^{GREM1} cells (Figure 7.5 A and B) compared to control normal medium.

The results for the invasion assays were more variable, and thus conclusions difficult to draw. From the cell count and absorbance readings, it appears that osteoblasts consistently and significantly increased invasion of BT474^{PEF} (Figure 7.5 C and D), but not BT474^{GREM1} cells. BME appeared to reduce the BT474^{PEF} invasion cell count, although this did not hold true on absorbance readings, whilst it did not statistically significantly alter invasion of BT474^{GREM1} cells (Figure 7.5 C and D).

Figure 7-5 BT474^{PEF} and BT474^{GREM1} migration and invasion in co-culture with hFob osteoblasts or BME

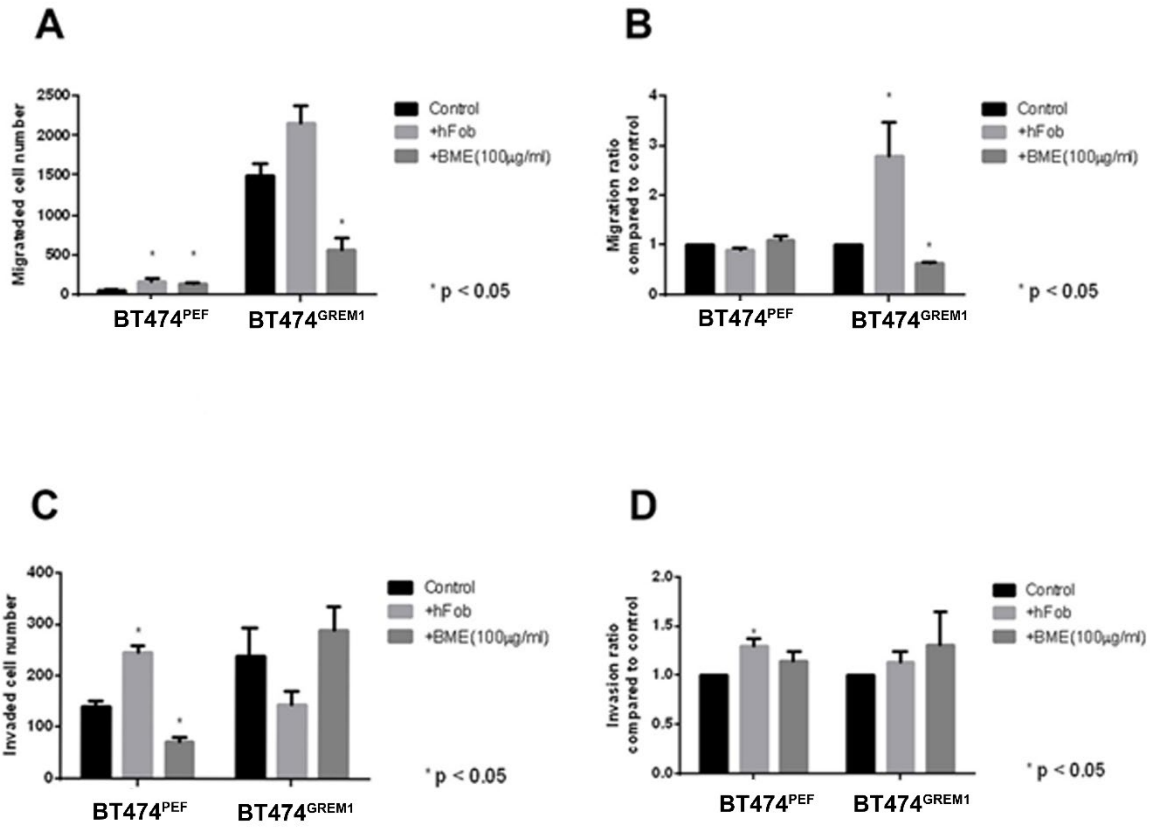

A) To demonstrate whether GREM1 overexpression contributes to migration of cells in a bone environment, 30,000 cancer cells (either BT474^{PEF} or BT474^{GREM1}) are seeded on one side of a porous membrane. On the other side of the membrane was either normal culture media, extracellular bone matrix extract (BME) or human foetal osteoblast(hFob)cells. Migration assay was run over 72 hours, with a control well for each experimental condition that had no membrane, to normalise for proliferation. Any cells that had migrated after 72 hours were fixed and counted. Both osteoblasts and BME appeared to encourage migration in BT474^{PEF}cells, and BME decreased migration whilst hFob cells increased migration in BT474^{GREM1} ($p<0.05$). Graph displayed as mean migrated cell count +/- standard error of the Mean (SEM).

B) After counting the migrated cells, the crystal violet stain was dissolved to provide absorbance readings of migrated cells in A, as a ratio compared to the absorbance of migration with normal media. This showed osteoblasts(hFob) increased migration of BT474^{GREM1,} but BME decreased migration($p<0.05$). Cytokines dynamically released by osteoblasts may be the reason that migration is promoted in GREM1 overexpressing cancer cells.

C) The experiment in A was repeated but with a Matrigel extracellular matrix coating to the porous membrane, such that invasion of BT474^{PEF} or BT474^{GREM1} was assessed over 72 hours in response to a bone environment stimulus versus normal media. Interestingly GREM1 overexpression had no different invasion in presence of BME or hFob cells compared to control, whereas BT474^{PEF}cells invasiveness increased in presence of hFob cells, and decreased with BME. Graph is mean invaded cell count+/-SEM

D) Subsequent staining and absorbance readings of invaded cells in C, as a ratio compared to the absorbance of invasion with normal media. Invasion did not change for GREM1 overexpressing cells in response to bone environment stimulus, but BT474^{PEF}became more invasive in the presence of hFob cells in comparison to normal culture media.

7.4 Discussion

In this small pilot mouse study, it was clear that GREM1 overexpression in BT474 cells resulted in a propensity to establish tumours in the mammary fat pad, compared to control BT474 cells, which did not establish any tumours. This difference was not due to any significant difference between the two groups in terms of the weight of the animals, nor the initial cell number or volume injected. The animals were housed in the same environments and fed the same diet. The difference between GREM1 overexpressing cells and controls is therefore quite clear, and this is in keeping with earlier experiments demonstrating GREM1 overexpression results in increased proliferation (see chapter 5).

The 4th mammary fat pads, for all mice in both groups, were extracted at autopsy and fixed for future examination, specifically haematoxylin and eosin (H&E) staining for tumour morphology, and immunohistochemistry for expression of GREM1 and HER2. The mammary lymph nodes were also harvested, in order to be examined in future for loco-regional metastases since, in other studies, 17% of mice developed axillary lymph node metastases with this cell line (Iorns et al. 2012). For these future tests, a control group tumour would have been of benefit, to compare the relative immunohistochemistry. It may be however that on H&E staining and sectioning, the mammary fat pads harbour some control cells in small tumours that could not be measured with callipers or seen macroscopically.

It is not a surprise that the control BT474 cells did not develop any primary tumours within the mammary fat pads. BT474 cells are not frequently used for *in vivo* models, as they are not as aggressive as other cell lines, such as the triple negative MDA MB 231 cells. Without exogenous high dose oestrogen administration, it can take well over two months for BT474 cells to even begin to produce tumours in the mammary fat pad, and they do not readily metastasise to other organs (Liang et al. 2010; Iorns et al. 2012).

On this basis therefore, other methods were utilised in the model of metastases with BT474 cells, to examine the homing of circulating cells to secondary organs. Intracardiac injection was chosen to allow wider dissemination of the tumour cells compared to tail vein injection, which results in higher propensity for lung deposits (Gómez-Cuadrado et al. 2017). As bone is the most common metastatic site for all breast cancers, intracardiac injection is also appropriate for modelling this, as it is

well established as a bone metastasis *in vivo* model (Kuchimaru et al. 2018). The method of intracardiac injection does however have disadvantages. It limits the number of cells that can be injected, as higher cell numbers can result in periprocedural complications such as embolism, with stroke, respiratory and cardiac arrest leading to death of the mouse, or severe impairment requiring termination. The limit to cell numbers means that metastases may not form very quickly if the cell line is not highly aggressive. However, if a more aggressive cell line is used, the metastases that form in the solid organs such as liver or brain, may result in the death of the animal before metastases to the bone can be detected (Kuchimaru et al. 2018).The BT474 cell line, being less aggressive in metastatic ability was, therefore, suitable from this perspective, with intracardiac injection deemed the most appropriate for reflecting clinical circulation of tumour cells and metastatic deposits.

In this metastasis model therefore, as expected, the most common hotspot on PET CT in both control and BT474^{GREM1} mice, was bone. BT474^{PEF} had fewer potential metastatic hotspots on PET CT overall, as only half of the mice in this group developed hotspots, and the target organs in the three mice included bone, liver, and lung. For the BT474^{GREM1} mice, nearly all had hotspots on PET CT, except the mouse with a failed injection, suggesting that GREM1 overexpression may result in a phenotype of Luminal B HER2+ cell that is better able to establish metastases once in circulation, and is more predisposed to the bone environment than control. Interestingly the next most common hot spot for BT474^{GREM1} compared to control was in the adrenal region, which resulted in the largest macroscopic tumour at autopsy. In humans, breast cancer metastases isolated to the adrenal are relatively uncommon and more often occur in conjunction with metastases to other organs (Bumpers et al. 1993; Barros et al. 2015). In a post-mortem series of metastatic breast cancer patients, 42% had adrenal gland metastases, with a predominance in patients with invasive lobular carcinoma. However, adrenal metastases are often clinically occult (Bumpers et al. 1993), and as such, rarely studied.

Further work is now required to examine the biological profiles of the hotspot tissue retrieved at autopsy, to confirm presence of metastasis and examine whether the phenotype of the cells was altered depending on metastatic niche.

Establishing breast cancer bone metastases requires circulating breast cancer cells to extravasate from the circulation, adhere, migrate, and invade, interacting

with the bone microenvironment, including the stromal cells of bone marrow and bone matrix. This interaction then allows tumour cells to survive, proliferate and in turn influence the activity of cells vital for bone turnover and homeostasis- osteoblasts and osteoclasts (Macedo et al. 2017; Brook et al. 2018).

Osteoblasts are required for normal bone deposition and produce bone matrix protein, Osteoblasts express cell surface receptor activator of nuclear factor κB (RANK) ligand (RANKL), and can also secrete a soluble form of RANKL, which binds RANK on osteoclast precursors, resulting in maturation to osteoclasts and bone resorption (Chen et al. 2018).

There are other factors shown to influence this homeostasis. BMPs, particularly BMP-2, are essential for osteoblast differentiation, as is Wnt signalling and parathyroid hormone (PTH). BMP signalling is essential for differentiation of mesenchymal stem cells (MSCs) into chondroblasts and osteoblasts, resulting in bone formation, but also induces osteoblasts to produce certain factors influential to osteoclast maturation and function (Zabkiewicz et al. 2017). PTH, oestrogen and other cytokines can regulate RANKL from osteoblasts, and thus have indirect influence on osteoclast differentiation and activity. Oestrogen favours osteoblast function, promoting bone formation and reducing osteoclast mediated resorption. OPG (osteoprotegerin) is also secreted by osteoblasts as a negative regulator of RANKL, blocking osteoclast activity (Allison et al. 2016; Brook et al. 2018). Transforming Growth Factor β (TGFβ), Insulin Growth Factor 1 (IGF-1), semaphorins, ephrins, and sphingosine-1-phosphate (S1P), are also involved in regulating osteoblast and osteoclast balance and function (Brook et al. 2018; Chen et al. 2018). Metastatic breast cancer cells are influenced by, and in turn influence and dysregulate these homeostatic mechanisms, leading to proliferation and survival of the cancer cells, along with osteoblastic, osteolytic, or mixed bone metastatic lesions.

A simple representation of the bone environment was created for these *in vitro* experiments, using either human osteoblasts (originally established from foetal limb tissue), or BME. BME contains proteins extracted from human femoral bones and thus provides a molecular environment for cancer cells when used in functional tests in keeping with the bone extracellular matrix. It is a mixture of collagens, fibronectin, and proteoglycans, produced by osteoblasts, which forms bone when mineralised. This matrix interacts with osteoblasts and osteoclasts to regulate bone homeostasis (Lin et al. 2020).

The *in vitro* work suggests that BT474^{GREM1} are more adherent than control cells in the presence of osteoblasts, reflecting the possibility that the bone environment favours establishment of breast cancer cells with higher levels of GREM1 expression. Co-culture with osteoblasts also increased cellular migration for both BT474^{GREM1} and BT474^{PEF} compared to culture media (control) alone, but this effect was greater in BT474^{GREM1} than BT474^{PEF} when normalised to control. Interestingly when examining invasion in co-culture with osteoblasts, the BT474^{PEF} cells were more invasive, but BT474^{GREM1} were not. This differential effect again was seen with co-culture using BME, which significantly reduced migration of GREM1 overexpressing cells, but appeared to have either no effect or increased the migration of low GREM1 expressing BT474^{PEF} cells. The effects of BME were then reversed for invasion of cells, with the low GREM1 expressing BT474^{PEF} cells seeing no change or reduced invasiveness, and the BT474^{GREM1} cells increased in invasiveness, albeit not significantly.

This reflects the complex dynamic between metastasising cells and the bone microenvironment, whereby the delicate balance of autocrine and paracrine cell signalling can determine whether tumour cells can survive and establish a tumour colony. High Gremlin1 expression in tumour cells may favour the initial steps in establishing metastasis in bone, but not necessarily in survival or progression within the niche, wherein lower Gremlin1 may be more beneficial. This may reflect the findings from clinical cohorts in Chapter 3, whereby fine needle aspirates of breast cancer metastases showed lower GREM1 expression in liver and bone, with low primary tumour GREM1 expression associated with bone metastases. Although, these were not HER2+ patients, so for future experiments a cohort of HER2+ patient matched primary tumour and bone metastasis tissue, as well as IHC from this *in vivo* study would help to examine this relationship. Further studies are required to establish the key mechanisms and signalling pathways, such as utilising conditioned media from BT4747^{GREM1} or recombinant Gremlin1, to examine effects on osteoblast and osteoclast activity, and to identify whether Gremlin1 has a canonical BMP mediated role, or whether, as shown in Chapter 6, the effect is BMP independent.

BMP signalling and BMP antagonists like Gremlin1 have been implicated in breast cancer bone metastasis. For example, high BMP-7 has been associated both with inhibiting and promoting breast cancer bone metastasis (Buijs et al. 2007; Alarmo et al. 2008; Sakai et al. 2012). BMP-9 suppresses the growth of tumour cells in

bone via down regulation of connective tissue growth factor (CTGF) (Wang et al. 2011; Ren et al. 2014b). High expression levels of the BMP antagonist Noggin are associated with bone metastases, in both cell line/murine models and clinical samples of breast cancer bone metastases (Tarragona et al. 2012), and can induce differentiation of osteoclasts *in vitro* (Mock et al. 2015). Meanwhile, there is very little evidence regarding Gremlin1 itself within the bone metastatic niche. It has been shown that Gremlin1 inhibits mesenchymal stem cell (MSC) differentiation to osteogenic cells like osteoblasts, via inhibition of the action of BMP-2, which usually promotes osteoblast differentiation and function (Hu et al. 2017). In this context, Gremlin1 is part of a regulatory feedback loop, as BMP-2, whilst promoting osteoblast differentiation, also induces osteoblast GREM1 expression (Pereira et al. 2000).

VEGF signalling is also important in bone homeostasis and breast cancer metastasis, and as Gremlin1 binds VEGFR2 it is possible there may be a role for Gremlin1 in this context. Osteoclast precursors and mature osteoclasts express VEGFR1 and VEGFR2, and these receptors and VEGF are seen at high expression in breast cancer bone metastases (Aldridge et al. 2005a,b). Finally, Gremlin1 results in activation of AKT, which is known to have a significant role in osteoclast differentiation. Increased PI3K/AKT activity has been found in HER2+ breast cancers with bone metastases and is increased in breast cancer cells colonising bone marrow (Hinz and Jücker 2021).

Dysregulation of this balance in BMP, VEGF and PI3K/AKT signalling by aberrant Gremlin1 could then result in alteration to both osteoblast and osteoclast function, promoting initial establishment of breast cancer bone metastasis.

8 General Conclusions

Breast cancer is a significant public health burden as the most common cancer worldwide, and the most common cause of cancer death in women, with a steadily rising incidence(Huang et al. 2021).

Significant progress over the last 50 years in diagnosis and treatment has resulted in a 97.9% 5-year survival for patients presenting with stage 1 disease (Table 1.1). However, for those presenting with metastatic disease this drops to 26.2%. Breast cancer metastasis is the source of greatest challenge for patients and healthcare systems, resulting in significant disease burden, loss of quality of life, and death. It is estimated the cases of metastatic breast cancer in the USA will have increased by 54.8%, and the costs by 140% by 2030 (Gogate et al. 2021).

Improving our ability to select patients at particular risk of metastatic disease, and to determine markers of benefit from certain treatments will reduce this burden, particularly for countries where resources are limited.

The most common metastatic site in breast cancer is to the bone, present in 70% of patients with metastases. Bone morphogenetic proteins are cytokines involved in the formation of bone, and a multiplicity of other effects controlling important steps in both tissue homeostasis and cancer, such as stem cell maintenance and regulation of cellular growth, differentiation and apoptosis (Zabkiewicz et al. 2017).

This study aimed to examine the role of Gremlin1 in breast cancer disease progression, as a novel area of breast cancer biology that may serve as a prognostic or therapeutic marker.

8.1 The role of Gremlin1 in Breast Cancer is subtype dependent

BMP signalling has been implicated in breast cancer with contradictory results (Alarmo and Kallioniemi 2010), as there are many different BMPs and regulatory mechanisms of BMP signalling, such as antagonists like Gremlin1, all with the potential to regulate cellular functions in different ways. There is also the question of signalling crosstalk, with BMP signalling having reciprocal relationships with both ER and MAPK pathways (Brazil et al. 2015; Chi et al. 2019). This will be variously relevant in different subtypes of breast cancer and may explain why, when looking at breast cancers, contradictory results appear.

As Gremlin1 is an antagonist of BMP activity it was important to examine not only the expression of GREM1 in breast cancer, but its BMP ligands. GREM1 appears to have increased expression in both breast cancer epithelial cells and stromal

cells, with most data suggesting increased GREM1 correlating with progression of disease and metastasis. Although there was variability in these findings, with our own tissue cohort implying lower GREM1 in advanced disease, this can be accounted for by variability of methodology and smaller numbers in our cohort. Gremlin1's preferred ligands however, had more variable expression findings, with BMP-2 and -4 being both raised and decreased in breast carcinoma compared to normal breast in different cohorts. Neckmann et al (Neckmann et al. 2019) published data after commencement of this work, examining expression of GREM1 and its preferred BMP ligands -2, -4 and -7, using a different public dataset, and similarly found that GREM1 expression was increased in breast cancer with poor clinical outcomes. They also found no correlation between high expression levels of BMP-2, -4 and -7 and prognosis, with co-expression of BMP and GREM1 not affecting the value of GREM1 as an indicator of poor prognosis.

The implication from these findings is that GREM1 impacts the prognosis and progression of breast cancer, independent of the expression of its BMP ligands.

Initial *in vitro* studies of the effect of Gremlin1 on cellular function implied loss of Gremlin1 had a significant impact on MDA MB 231 cells, increasing invasion and growth, in contradiction to subsequently published work correlating GREM1 knockdown with decreased proliferation and migration, and overexpression with increased invasiveness and metastasis in TNBC cell lines (Neckmann et al. 2019; Sung et al. 2020b).

Interestingly GREM1 knockdown in ER+ MCF7 cells did not have a significant impact on cellular function, but overexpression reduced growth and invasion *in vitro.* These variations in findings could be methodological, but the influence of each cell line having differences in signalling crosstalk pathways cannot be discounted. When examining GREM1 expression in the different clinical and molecular subtypes of breast cancer it became apparent that there were correlations of GREM1 expression with receptor status and molecular subtype, with high GREM1 particularly correlating with ER- and HER2+ tumours, at both the RNA and protein levels. This was particularly striking in HER2+ tumours, whereby high GREM1 expression significantly reduced distant metastasis free survival, and was a novel area not previously explored.

8.2 Elevated Gremlin1 in HER2+ Breast Cancer promotes EMT, metastasis, and poor clinical outcomes

This work demonstrates GREM1 overexpression clearly increases HER2+ cellular growth both *in vitro* and *in vivo*. Expression of cell cycle markers were also altered, with most effect seen in reduction of p21, but not to statistical significance, and this would be an area that could be explored further with flow cytometry.

In vitro migration also increased with GREM1 overexpression, in conjunction with reduced expression of E-Cadherin and increased expression of Slug and Snail, all of which imply Gremlin1 promotes EMT in HER2+ breast cancers, which is the initial step in the metastatic process. Although these *in vitro* tests did not demonstrate increased invasiveness, Park et al recently undertook GREM1 overexpression in SKBR3 cells, which are also a HER2+ cell line, and their findings confirmed an increased cellular viability and invasion with GREM1 overexpression (Park et al. 2020).

This increased propensity towards EMT also correlates with the findings that, in clinical cohorts of HER2+ patients, high GREM1 expression denotes increased likelihood of metastases and survival outcomes are significantly worse. The *in vivo* results also support this finding, with higher rates of metastases in BT4747^{GREM1} cells compared to control, particularly to the bone, which was supported by the increased adhesion of BT474^{GREM1}in co-culture with osteoblasts. Further work is required to confirm these findings of the *in vivo* model with IHC, which was unfortunately disrupted by laboratory closures during the COVID 19 pandemic.

Gremlin1 could therefore be proposed as a prognostic indicator of metastasis and poor outcome in HER2+ breast cancer patients.

8.3 Proposed relevant mechanisms

This work identifies that, as well as clinical implications, Gremlin1 has a significant reciprocal relationship with HER2, as GREM1 overexpression increased HER2 expression, and HER2 inhibition or knockdown decreased GREM1 expression, abrogating the effect of GREM1 overexpression on growth.

These effects may be direct or indirect. For example, HER2 is known to translocate to the nucleus and associate with STAT3 (Redmond et al. 2019), directly affecting gene transcription, making it possible that GREM1 could be directly regulated by HER2. GREM1 is also a downstream target of both BMP and

TGFβ signalling (Graham et al. 2014; Yin et al. 2017), and HER2 has a co-operative signalling relationship with these pathways. For example, HER2 and TGFβ signalling co-operate in inducing cell motility and invasion of MCF10A cells, with Trastuzumab blocking the promigratory effect of TGFβ on HER2 overexpressing cells. In reciprocal fashion, TGFβ can induce enhanced HER2/PI3K association and signalling, which can then render cells less sensitive to Trastuzumab (Wang 2011). It is possible that HER2 indirectly regulates GREM1 via co-operative signalling with TGFβ.

The finding that RhGremlin1 treatment activates AKT signalling independently of BMP signalling in HER2+ cells is interesting, considering PI3K/AKT/mTOR signalling is the predominant intracellular activity on HER2-HER3 dimerisation, that results in cellular proliferation and decreased apoptosis (Zuo et al. 2017). This would fit with the increased proliferation and growth *in vitro* and *in vivo* for $BT474^{GREM1}$ cells. Overexpression of GREM1 also upregulated PI3KCA, the catalytic subunit of PI3K.Gremlin1 may therefore serve to enhance the actions of HER2 in a co-operative manner, or as a positive feedback mechanism, by interacting with HER2 itself, or as an intermediary. There is evidence that Gremlin1 binds to the cancer cell surface independent of BMPs, and independent of its other known binding partner VEGFR2 (Kim et al. 2012). Recently, it has been suggested in SKBR3 cells that Gremlin1 interacts with EGFR(HER1), resulting in activation of downstream ERK and AKT signalling, which was abrogated by an EGFR tyrosine kinase inhibitor (Park et al. 2020).

GREM1 overexpressing cells had their increased proliferation abrogated by HER2 tyrosine kinase inhibition, but this does not reflect whether GREM1 overexpression denotes resistance or sensitivity to Trastuzumab or Pertuzumab treatment, as these agents work in a different manner and not directly on HER2 kinase inhibition unlike CP724714. Further experiments should be run, utilising Trastuzumab and/or Pertuzumab, to identify whether GREM1 overexpression denotes resistance to treatment in HER2+ breast cancers. However, it could be postulated that the enhanced PI3K/AKT activity induced by Gremlin1 could provide an ’escape route’ of resistance to HER2 monoclonal antibody blockade, as HER2+ breast cancer cells, with constitutionally active PI3K/AKT/mTOR pathway or upregulating mutations in PI3KCA, have shown resistance to treatment (Carmona et al. 2016). If this proved true, GREM1 could be a valuable marker of resistance to treatment,

and an indication for dual therapy with inhibitors that target the PI3K/AKT/mTOR pathway.

8.4 Future Works

As a novel area of breast cancer cell biology this work has raised several areas of enquiry for future study:

- A cohort of HER2+ patients with pre and post treatment tumour tissue samples, with matched tissue samples from any metastases, particularly bone metastases, would add further robustness to the clinical association of HER2 and Gremlin1 and demonstrate changes in Gremlin1 with HER2 blockade.
- As part of future studies on the increased proliferation and growth of GREM1 overexpressing HER2+ breast cancer cells, it would be intended that cell cycle flow cytometry studies of cell phase be undertaken, and Western blotting or immunostaining of nuclear and cytoplasmic cell cycle proteins, particularly p21, to better characterise the cell cycle effects
- To further explore how GREM1 may be regulated in HER2+ breast cancers a GREM1 promoter luciferase reporter system was purchased. This would be utilised in future work to determine if co-operative HER2/TGFβ signalling regulates GREM1 expression in HER2+ breast cancer cells, and if inhibition of certain intracellular pathways such as HER2, AKT and TGFβ influences GREM1 regulation independent of BMP signalling.
- Repeating the GREM1 overexpression cellular growth and migration assays with an AKT inhibitor, would provide further confirmation that Gremlin1 mediates its proliferative action in HER2+ cells via this pathway.
- Co-localisation studies to determine if Gremlin1 co-localises with HER2 at the cell membrane, or intracellularly as a potential method of Gremlin1/HER2 regulatory control.
- Completion of IHC work from the *in vivo* pilot study and development of further experiments for HER2+ GREM1 overexpressing cells in the bone environment, such as osteoblast and osteoclast function assays and 3D bone scaffold models.
- *In vitro* and *in vivo* models of whether GREM1 overexpression in HER2+ tumours denote resistance or sensitivity to Trastuzumab/Pertuzumab treatment and examining the mechanisms therein.

9 APPENDIX

9.1 APPENDIX I

9.1.1 ELISA Standard Curve

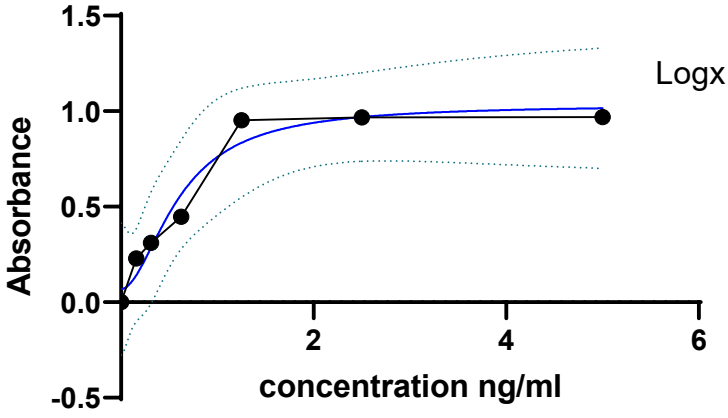

Logx = y - 0.6775/0.2547

9.2 APPENDIX II

9.2.1 GEO database set GDS3324 comparing GREM1 expression in stromal and epithelial cells

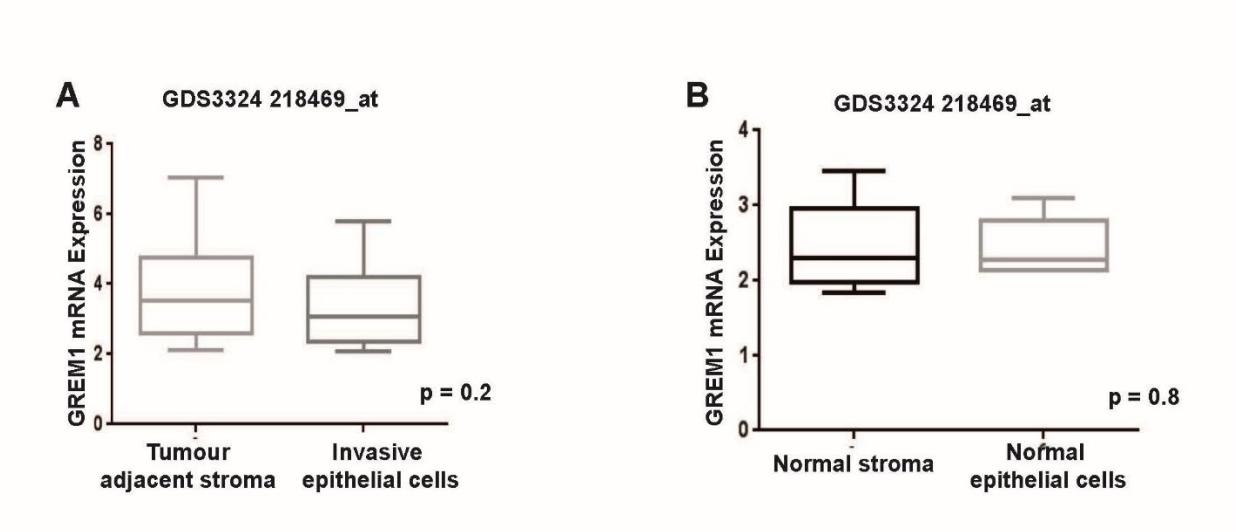

A) GREM1 expression value in LCM cells from tumour adjacent stroma and tumour epithelial cells is not significantly different, p = 0.2

B) LCM of cells from normal stroma and normal epithelium also show no difference in GREM1 values, p = 0.8

9.2.2 Breast Tumour Clinical Cohort

Table 9-1 Breast Tumour Clinical Cohort

	Patient Number	Mean Gremlin1 transcripts	SEM	P value
		(Copies/50ngRNA +/- SE mean)		
Breast Carcinoma	82	118184	42394	P = 0.19
Normal mammary tissue	24	56493	20950	
Histological type				
Ductal	59	91530	38431	
Lobular	11	64187	61105	P = 0.082
Histological grade				
Grade 1	12	263178	172452	
Grade 2	31	60502	31852	P = 0.27
Grade 3	5	2795	1645	P = 0.16
TNM staging				
TNM1	2	650	350	
TNM2	25	35382	15626	P = 0.036
TNM3	5	2795	1645	P = 0.27
TNM4	4	652696	631500	P = 0.38
Lymph node involvement				
Lymph node (-)	40	143981	58091	
Lymph node (+)	38	35977	17975	P = 0.082
Nottingham Prognostic Index (NPI)				
NPI1 (<3.4)	40	143981	58091	
NPI2 (3.4-5.4)	26	41870	25825	P = 0.11
NPI3 (>5.4)	12	23210	11640	P = 0.048
Clinical outcome				
Disease free	60	146209	56574	
Metastasis	4	39768	23024	P = 0.087
Local recurrence	4	7482	3461	P = 0.017
Died of breast cancer	10	5118	3175	P = 0.016
Poor prognosis	18	13343	6001	P = 0.023
Bone metastasis	7	18834	13159	P = 0.032

9.2.3 Clinical cohort GSE20685 GREM1 primary tumour expression by patient stage

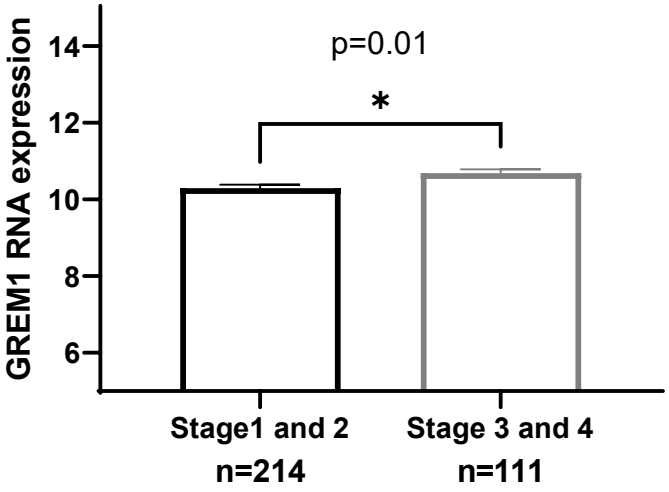

Due to low number of patients with stage 4 disease(n=8), those with stage 3 and 4 disease were grouped together for analysis, as were those with stage 1 and 2 disease, and the two compared with a Mann Whitney test. Those with stage 3 and 4 disease had higher GREM1 expression in primary tumours than those with stage 1 and 2 disease(p=0.01)

9.3 APPENDIX III

The first western blots undertaken for this thesis involved a panel of 9 breast cancer cell lines (Figure 4.2), whereby cells were grown to 80% confluency, washed with PBS, and lysed to extract the intracellular protein. The concentration of the protein was measured and the same amount of protein for each cell line loaded onto a gel for SDS PAGE electrophoresis and separation by protein size. The separated protein on the gel is then transferred onto a membrane and antibodies against the protein of interest applied. A secondary antibody that produces a fluorescent signal is also applied and finally a chemical added to produce the fluorescence and pictures taken. This method of western blot is specifically described in the methods section (Chapter 2, Section 2.4). The trouble shooting required to optimise western blotting involved the following stepwise approach as initial blots showed bands for the control housekeeping, but no bands for Gremlin1 at all on several repeats of the same initial method:

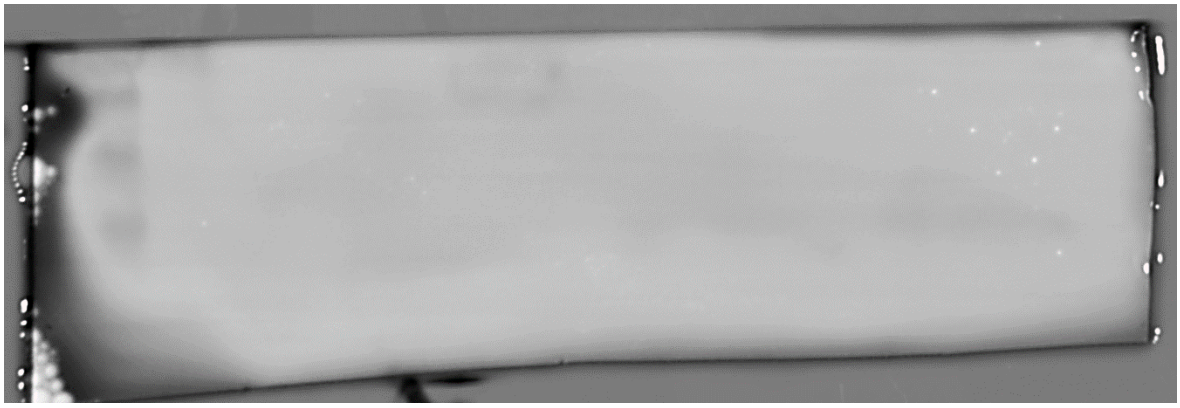

This could have been due to a long list of reasons as there are multiple points in western blotting that could go wrong. The fact that the protein ladder is visible (left hand side) meant that the transfer of protein from the gel to the membrane had been successful, and the fluorescent chemicals to produce a signal had worked.

Below is a further example of where the protein marker ladder was present, but no other protein bands and there were white patches, which shows where there might have been air bubbles and poor contact when undertaking western blot transfer.

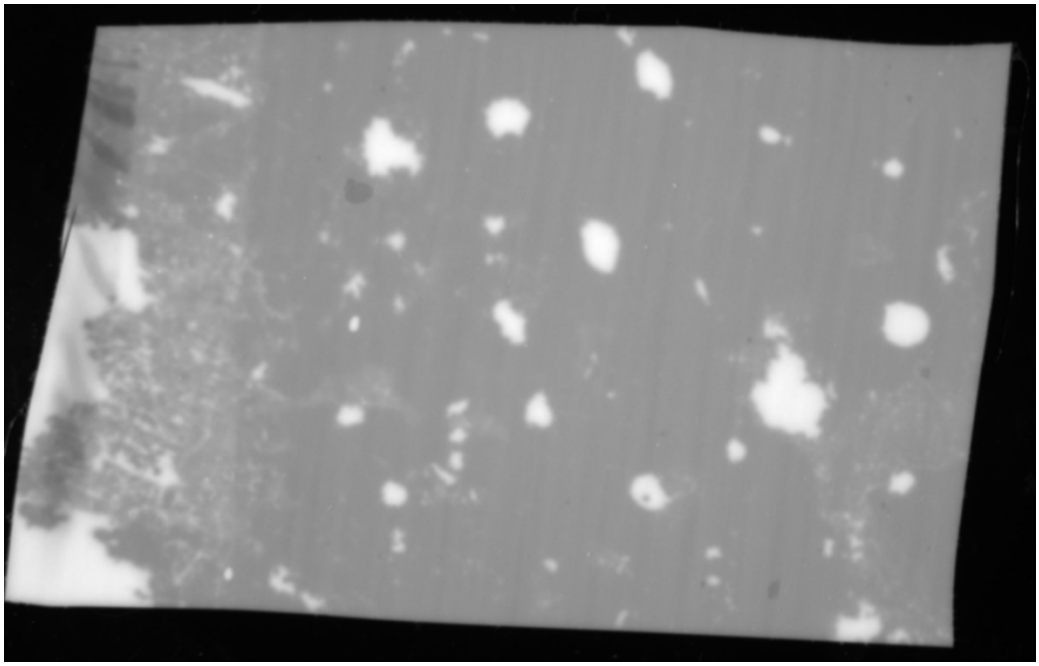

There are a multitude of reasons for not seeing protein bands on a western blot. That there was housekeeping control bands meant there was protein in the samples, but perhaps Gremlin1 was at such low levels that it was undetectable, although the recommended control cell line for Gremlin1, the lung cancer cell line A549 also did not show a band. Other possibilities included either the Gremlin1 antibody had not worked, blocking had not worked (leaving too much nonspecific antibody binding) the protein could have run off the gel if left for too long, or the gel% was incorrect. All reagents for making and running gels and blots were also shared within the lab and made in house, which meant there was also a possibility of incorrectly made buffers and variation on each time running a western blot.

My initial step therefore was to re make all the buffers and reagents for making and running the gels and transfers, and to keep my stock separately. I had initially been running the proteins on an 10% gel, but as Gremlin1 is a smaller protein at 21kDa, I began running Gremlin1 on a 15% gel for better separation and resolution, and the larger βActin housekeeping control protein at 42kDa on an 8% gel.

This produced the same result with no bands, so I then increased the Gremlin1 primary antibody concentration from the manufacturer's recommended 1:250, to 1:500.

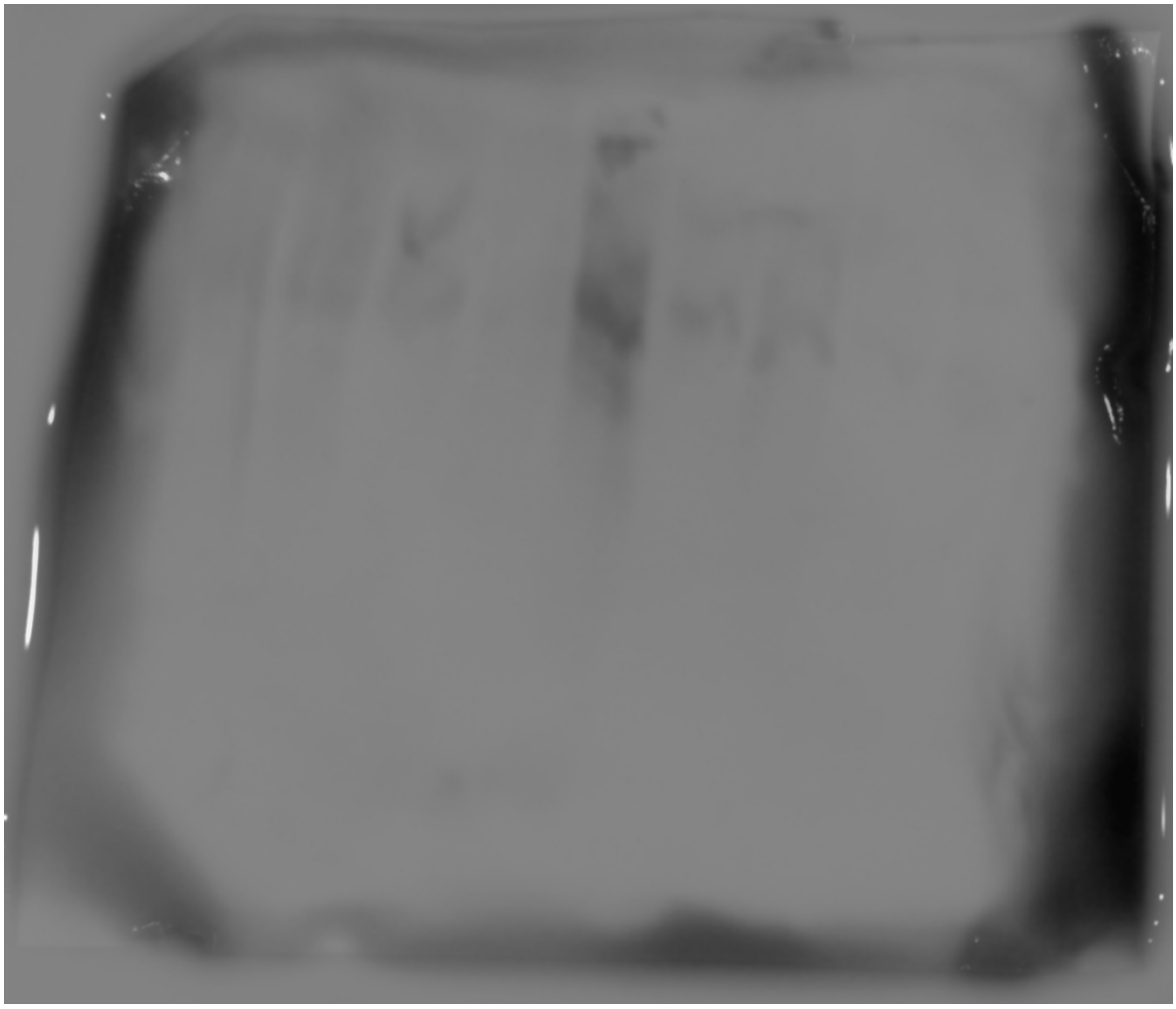

I had achieved Gremlin1 bands, but they were not straight, were very faint, and had smearing in the lanes. Again, there are multiple reasons for this.

The smearing of the bands can be due to nonspecific antibody binding/blocking solution issues, protein overloading or a problem when lysing or denaturing the protein samples. I began with the simpler step of adjusting the blocking solutions, increasing the milk solution from initial blocking of 5% to 10%, and applying the primary antibody with 5% up from 2.5%.

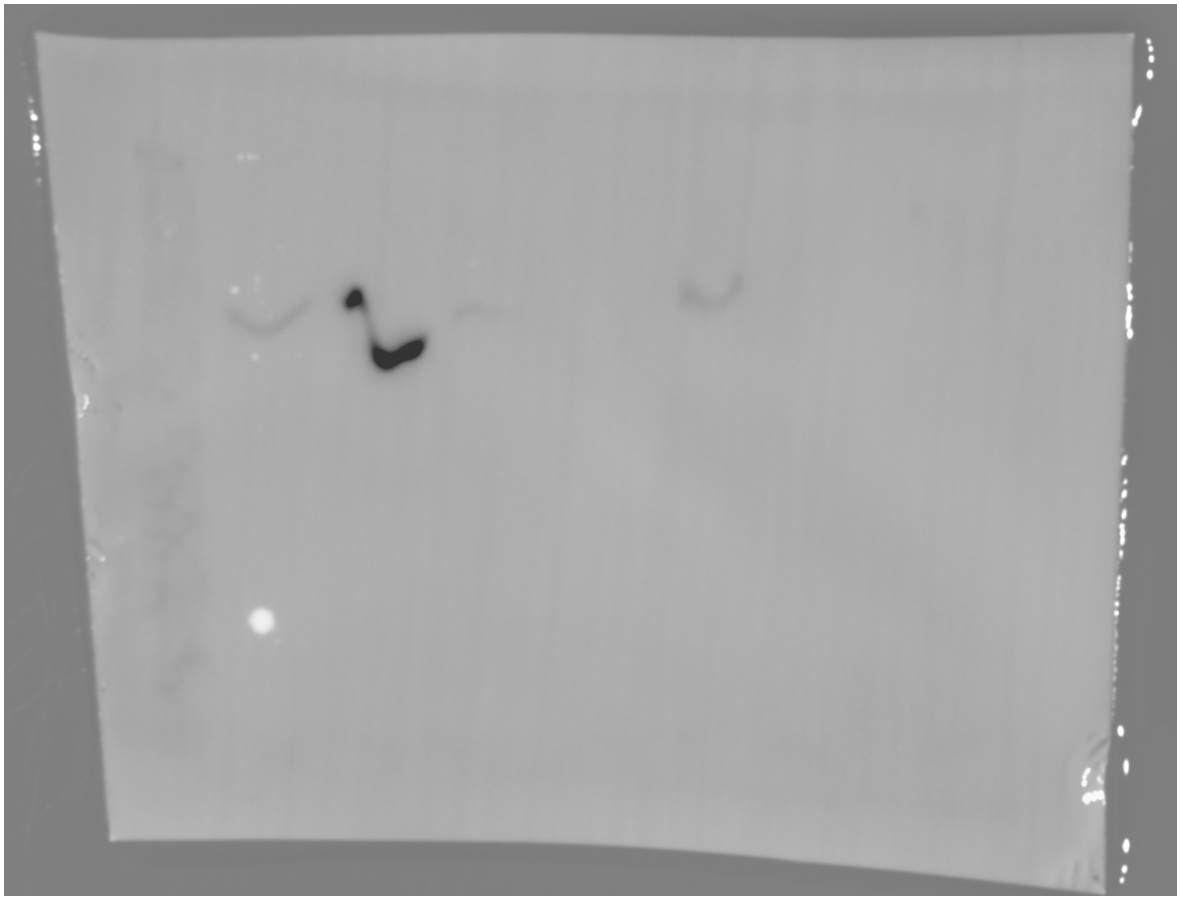

My bands were much cleaner, but still ‘wobbly’, and very faint in some of the cell lines. The ‘wobbly’ lines are often from either the gel preparation not setting uniformly, or the gel being run on too high a voltage. I remade and reran these gels several times, taking care to mix the gel reagents fully, I tried setting the gel on ice so that it didn’t set too quickly, and reduced the running voltage from 130 to 120V, with bands still coming out wobbly. The acrylamide and TEMED for making the gels were not made in house but purchased commercially. New bottles were opened to ensure reagents were fresh, with the same results. I then remade new Ammonium Persulfate (APS) for the gels and this, along with the lower running voltage improved the straightness of the bands. Although improved, I was still not getting much signal. I liaised with a colleague in a different laboratory to see if running the protein samples on commercially bought gels and reagents, with a more sensitive fluorescent chemical for visualisation would help.

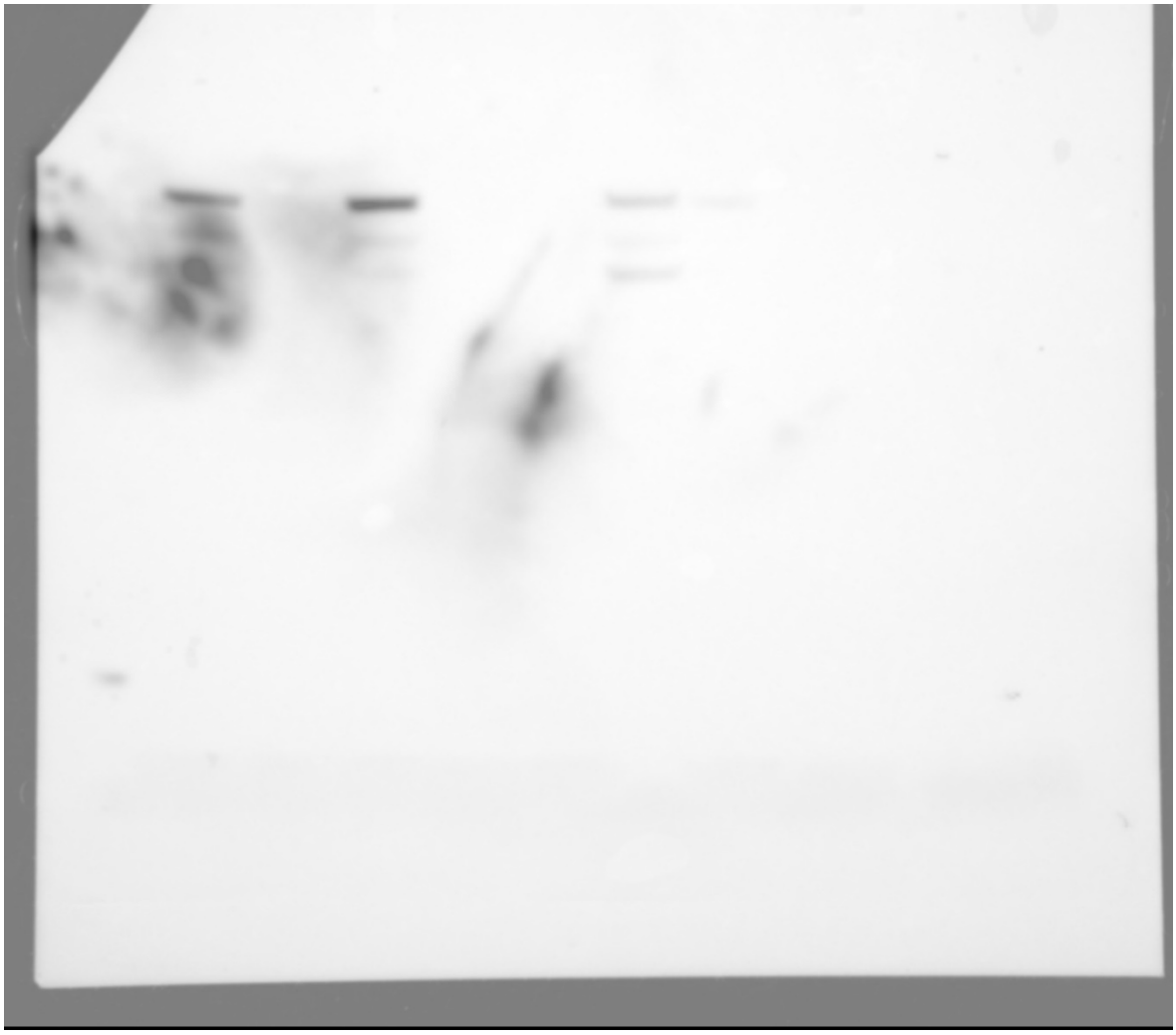

This gave crisp straight bands (although there are some spots, most likely from gel or membrane handling), and although the commercially bought reagents and gels weren't available to me for the duration of my project, a large proportion of my troubleshooting was to do with gels and reagents, and optimisation would have been more efficient were these available to me. I did however obtain and utilise the more sensitive fluorescent chemical for visualisation (EZ ECL). It was also apparent that there was not much Gremlin1 protein in my samples. I therefore re cultured all 9 cell lines, and re did protein extraction and denaturing, with the resulting images in the results section of the thesis.

This trouble shooting process had taken 5 months, and I could no longer expend further time optimising, or undertaking immunoprecipitation to concentrate the protein samples further, for a part of the work that was relatively small in terms of the aims of the thesis. Further optimisation might have been re-visited during the writing up period, as my western blotting technique was far improved by this point, but this was not possible due to lab closures during the COVID-19 pandemic.

9.3.1 ELISA results in concentration ng/ml

Cell Line	Average Absorbance	Average sample concentration result (ng/ml)	% Increase or decrease
MCF7^{Scr}	0.248123	0.1891667	
MCF7^{SH2}	0.232829	0.176336	- 6.782706933
MDA MB 231^{Scr}	0.238539	0.181127	
MDA MB 231^{SH2}	0.208658	0.1560585	- 13.84026567
BT474PEF	0.200117	0.1488936	
BT474 ^{GREM1}	0.238428	0.1810334	+ 21.58581713

In the following 3D spheroid graphs the raw data of pixel area on Image J software is charted, uncontrolled for variation in seeding of the spheroids, so that the variation in spheroid starting points of growth and invasion can be seen. In calculating statistical significance, this is done with day 1 variation accounted for.

9.3.2 3D Spheroid growth and invasion charts MDA MB 231^{SH2}

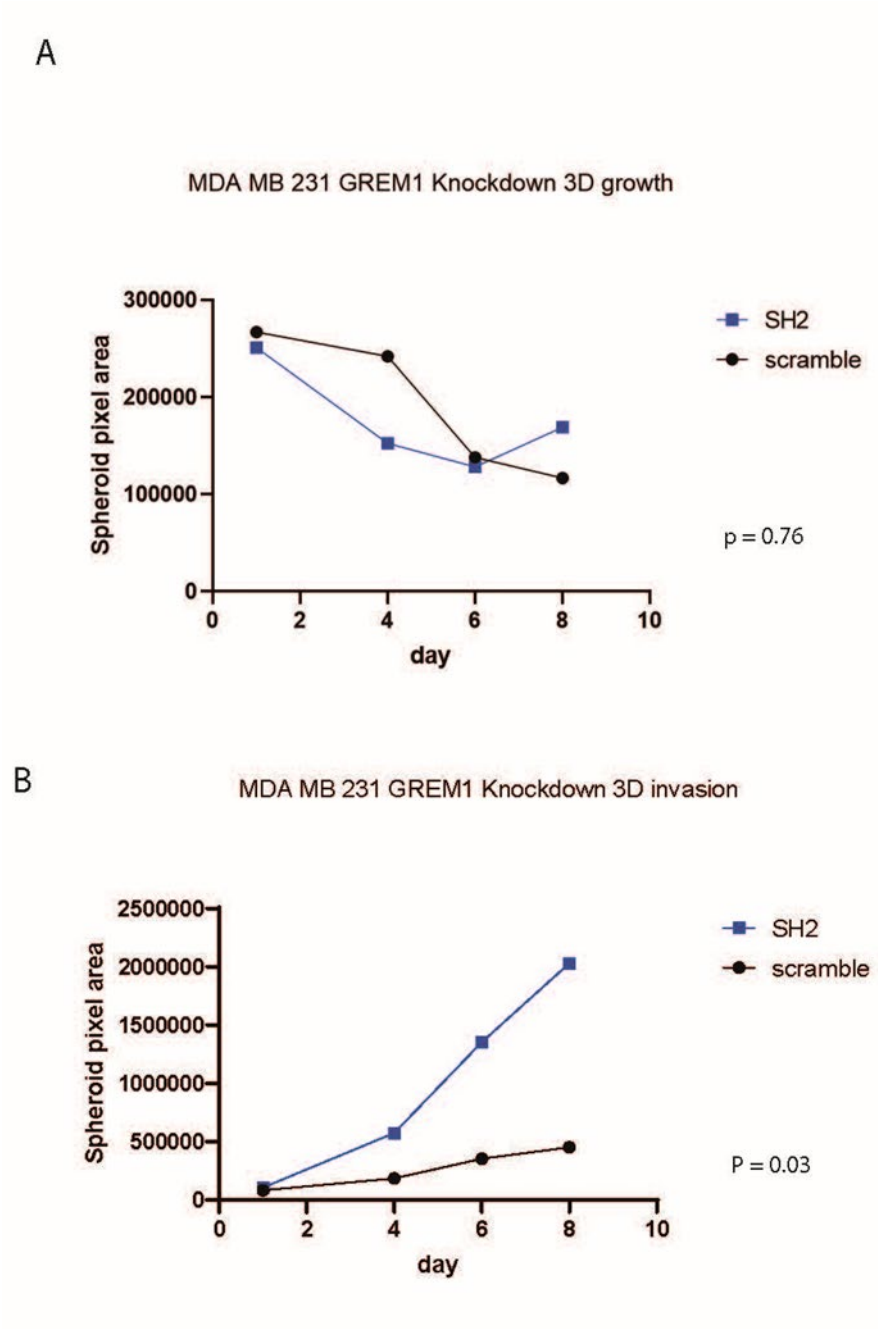

A) 3D spheroid growth by area of spheroid measured in Image J software. Spheroids have been seeded of equivalent size, but growth in both MDA MB 231^{Scr} and MDA MB 231^{SH2} decreases in a similar manner over time.

B) 3D spheroid invasion by area of spheroid measured in Image J software. Spheroids have been seeded with equivalent size and MDA MB 231^{SH2} shows significantly increased invasion compared to control, p = 0.03

9.3.3 3D Spheroid growth and invasion charts MCF7^{SH2}

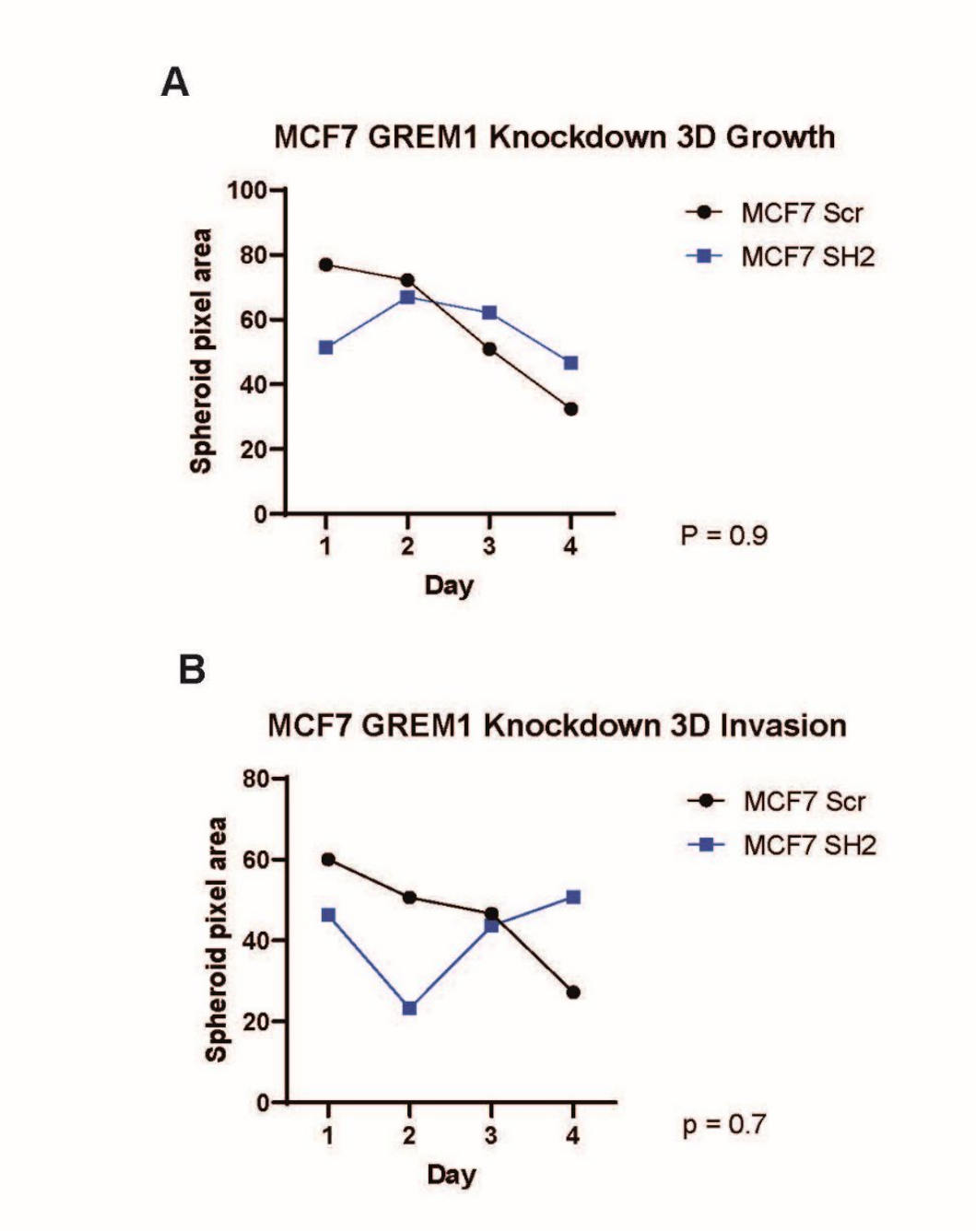

A) 3D spheroid growth by area of spheroid measured in Image J software. Spheroids have been seeded of different size, and growth in both MCF7^{Scr} and MCF7^{SH2} decreases over time, although MCF7^{SH2} does initially grow.

B) 3D spheroid invasion by area of spheroid measured in Image J software. As with A) spheroids are not seeded with equivalent size. MCF7^{SH2} initially decreases but then invasion area increases over time, whereas the control cells decrease in size over time.

9.3.4 3D Spheroid growth and invasion charts MDA MB 231^{GREM1}

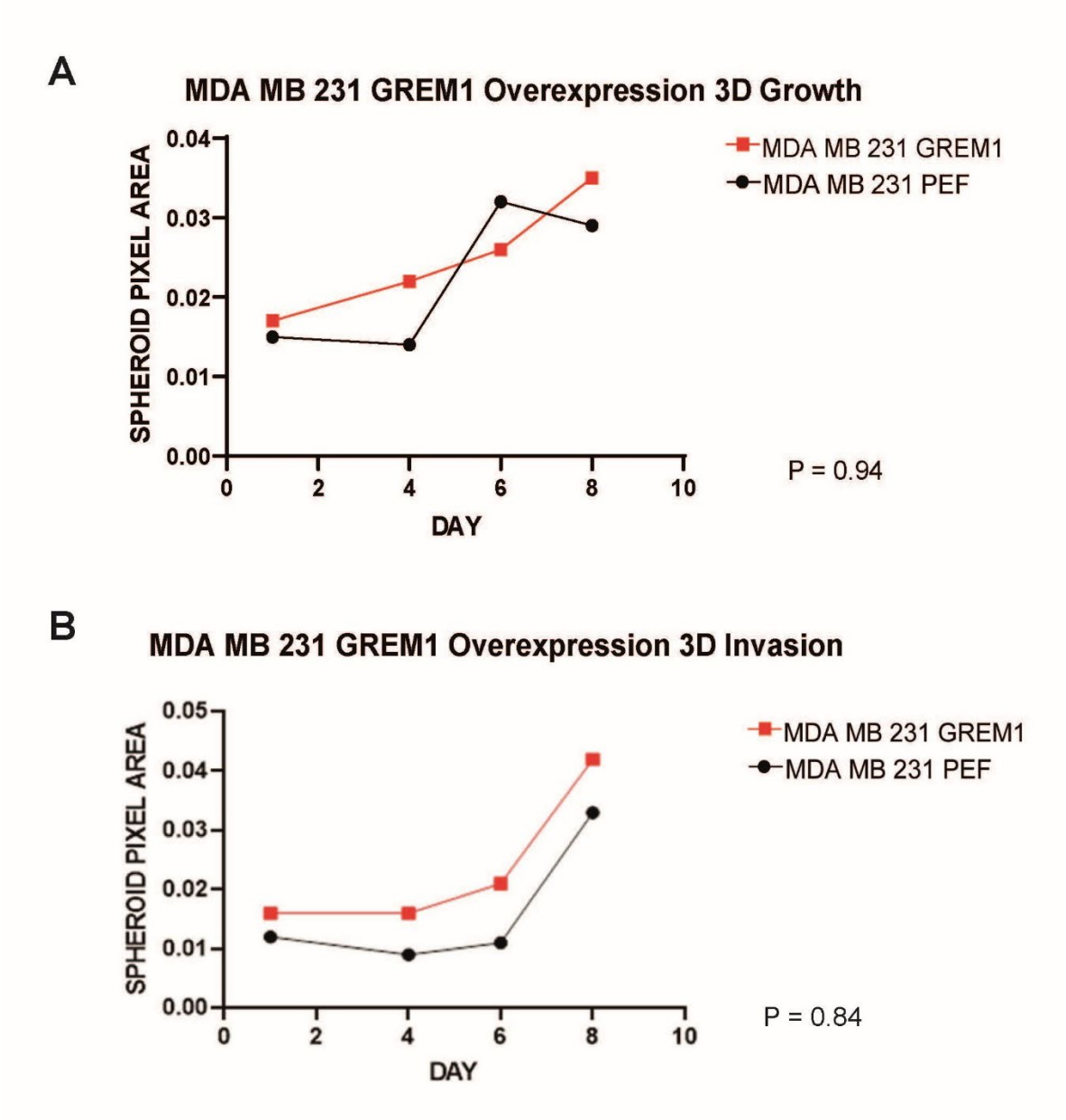

A) 3D spheroid growth by area of spheroid measured in Image J software. Spheroids have been seeded of similar size, and growth in both MDA MB 231^{PEF} and MDA MB 231^{GREM1} increases over time, with no significant difference, p = 0.94

B) 3D spheroid invasion by area of spheroid measured in Image J software. Spheroids are not seeded with equivalent size. both MDA MB 231^{PEF} and MDA MB 231^{GREM1} increases over time

9.3.5 3D Spheroid growth and invasion charts MCF7^{GREM1}

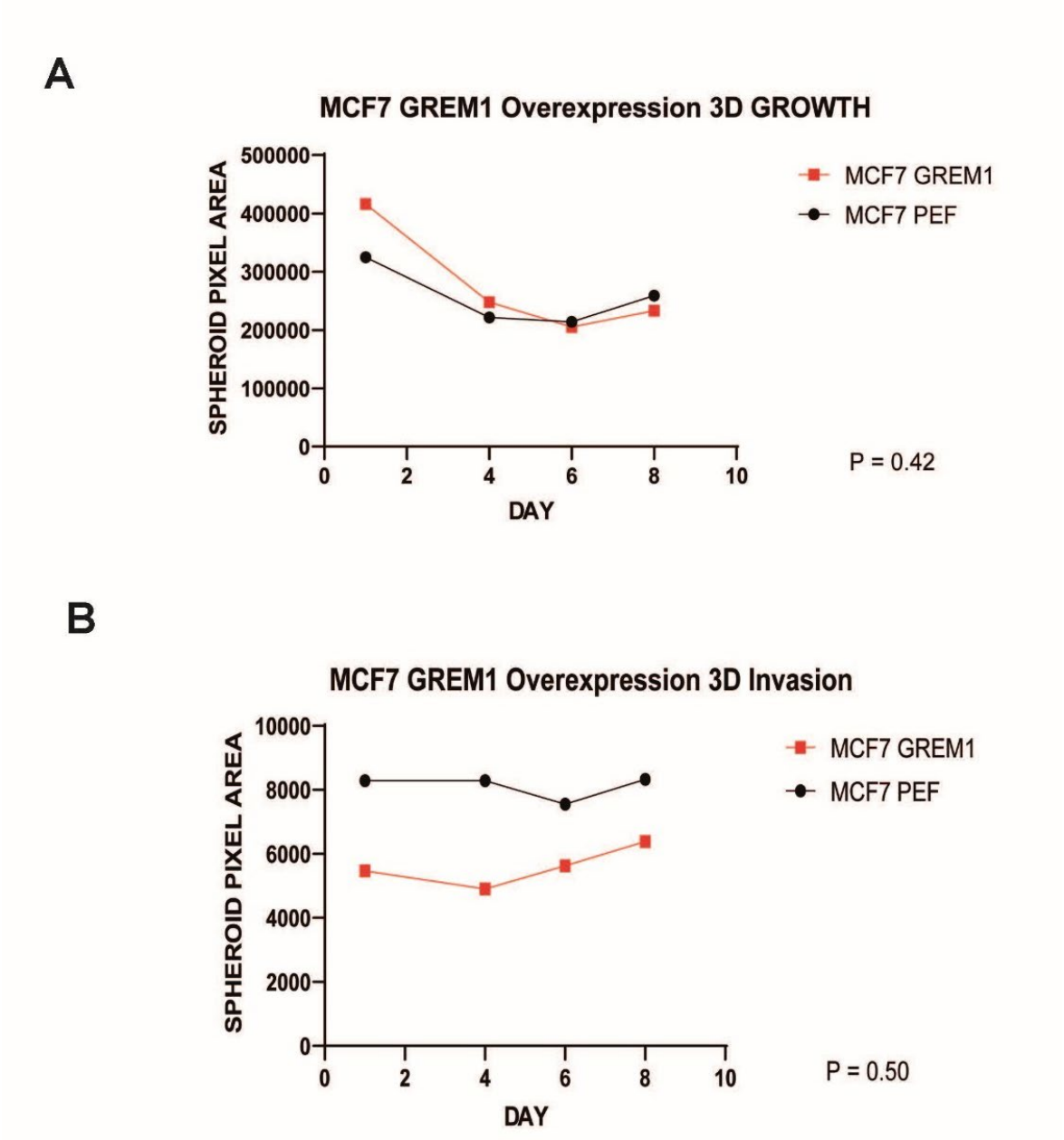

A) 3D spheroid growth by area of spheroid measured in Image J software. Spheroids have been seeded at different size, but growth in both MCF7^{PEF} and MCF7^{GREM1} decrease over time, with no significant difference, p = 0.94

B) 3D spheroid invasion by area of spheroid measured in Image J software. Spheroids were seeded at very different size, which could impact on results. Both MCF7^{PEF} and Mcf7^{GREM1} have the same invasion profile, which is flat, demonstrating very little invasion in either cell line.

9.3.6 EMT marker expression changes in Recombinant Gremlin1 treated MCF7 cells

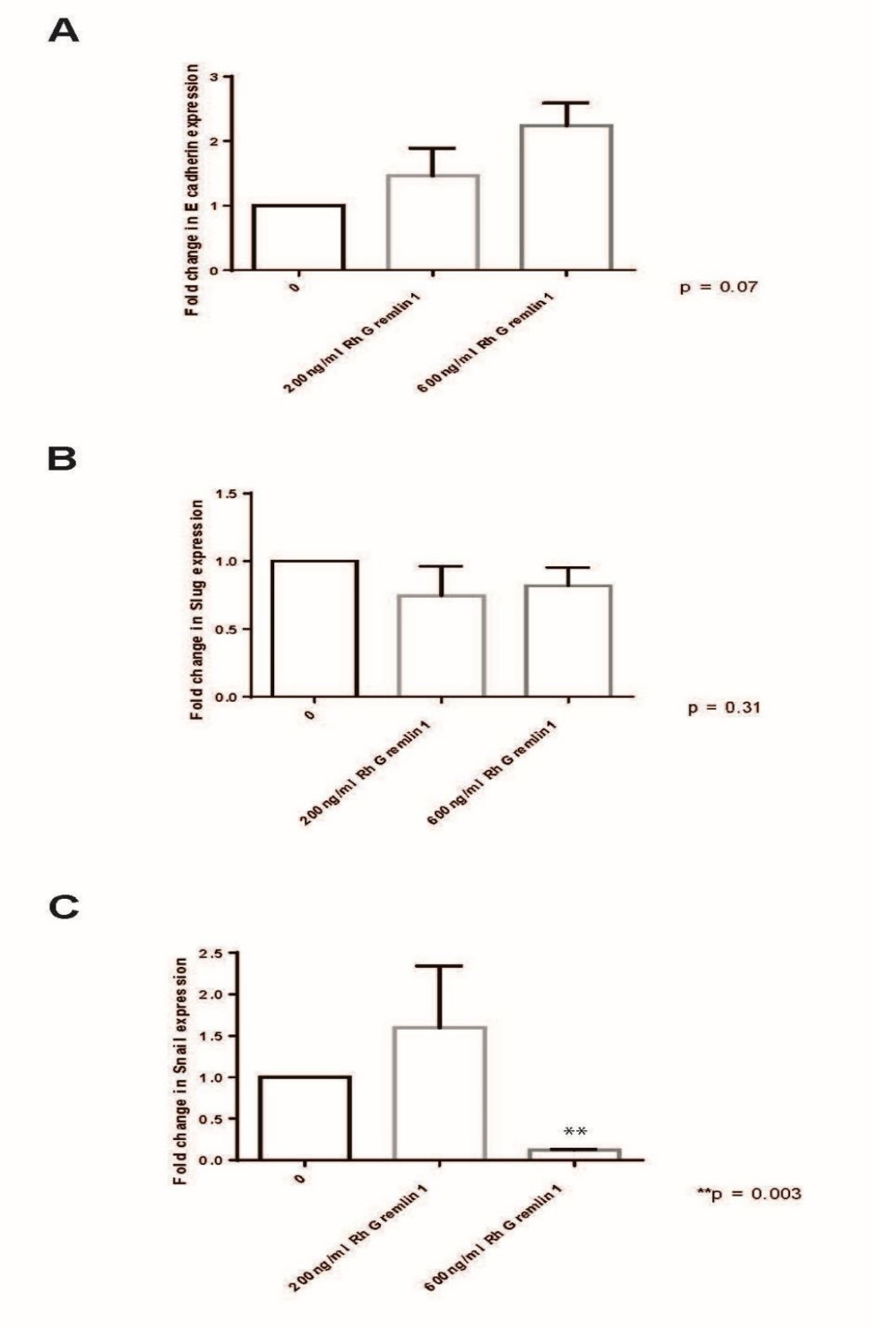

A) E- Cadherin expression on qPCR increases with RhGremlin1 treatment at low (200ng/ml) and high (600ng/ml) doses, but does not reach statistical significance, p = 0.07

B) Slug expression decreases on RhGremlin1 treatment, but not to statistical significance, p = 0.31

C) Snail expression increases on low concentration RhGremlin1 treatment, but then significantly decreases at high concentration, p = 0.003

9.4 APPENDIX IV

9.4.1 BT474 GREM1 Overexpression MTT assay

There was significant increase in MTT assay in BT474^{GREM1} cells compared to control, implying increased cell viability and proliferation (p = 0.002).

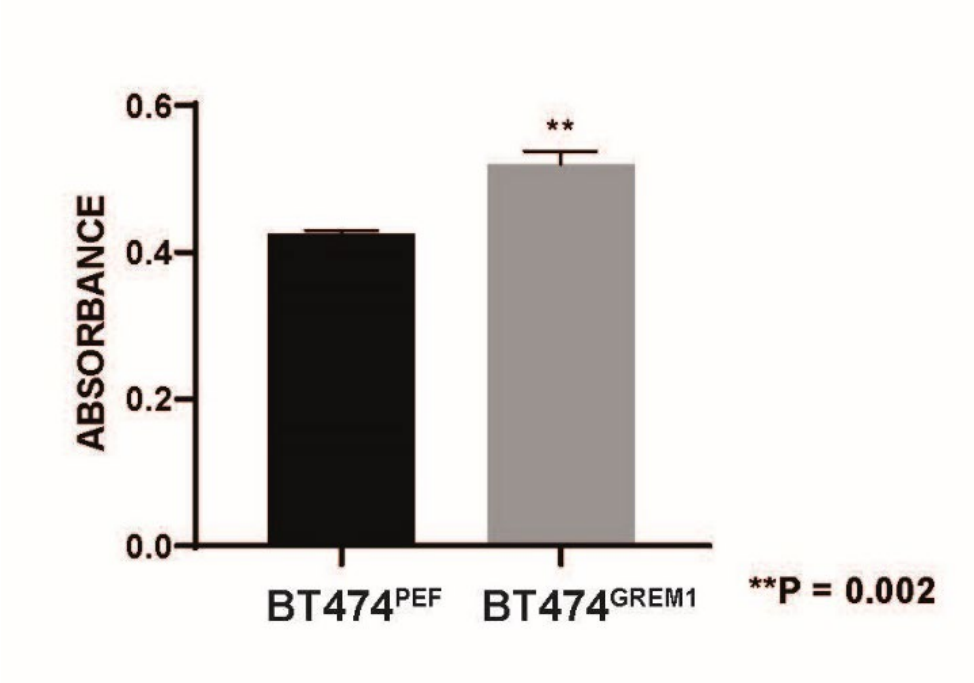

9.4.2 BT474 GREM1 overexpression spheroid invasion assay.

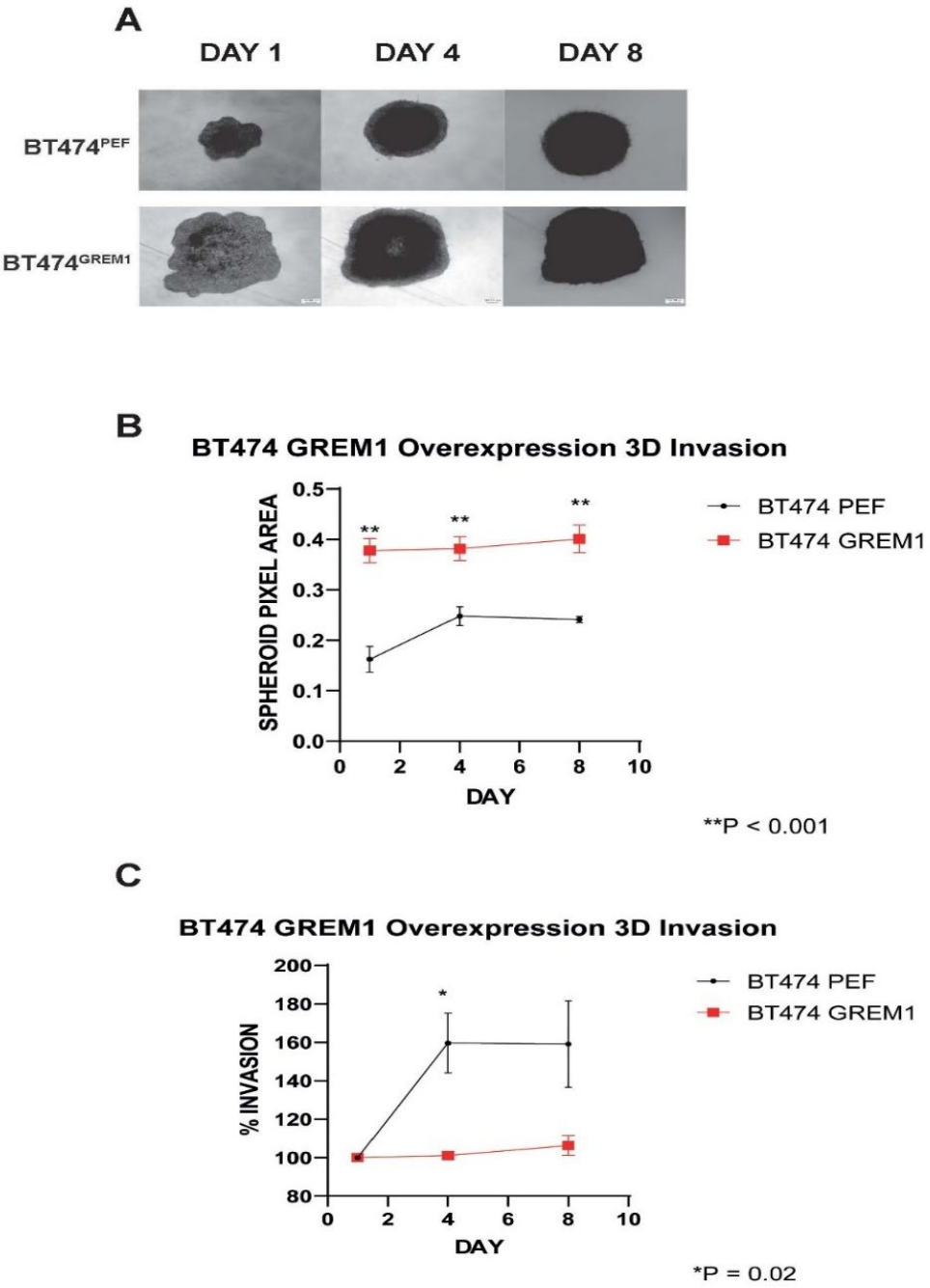

A) BT474^{GREM1} and BT474^{PEF} invasion assay representative microscopy photographs at x10 magnification

B) Graphic representation of spheroid area determined by Image J software. BT474^{GREM1} were seeded as significantly larger spheroids, and as such demonstrated significantly larger spheroids throughout, p < 0.001

C) When the difference in initial spheroid seeding was accounted for as percentage invasion compared to day 1, BT4747^{GREM1} spheroids demonstrated lower rates of invasion compared to BT4747^{PEF} which was significant on day 4, p = 0.02

9.4.3 Western Blot of EMT markers in BT474^{GREM1}

Western blot from whole cell lysate protein in BT474 cells with GREM1 overexpression for markers of EMT. Gremlin1, HER2, ID1 and Snail were all increased protein expression

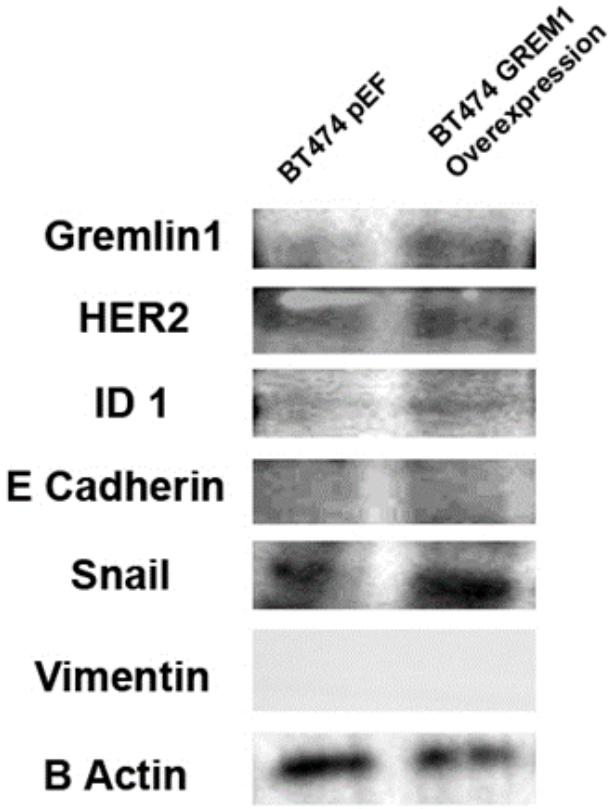

9.5 APPENDIX V

Home Office

No. I503919EB

ANIMALS (SCIENTIFIC PROCEDURES) ACT 1986

PERSONAL LICENCE

to

carry out regulated procedures on living animals.

In pursuance of the powers vested in him by the above Act, the Secretary of State hereby licenses

Miss Catherine Zabkiewicz
Cardiff University
c/o The Biological Standards Officer Cardiff University College of Biomedical & Life Sciences College House King George V Drive East Heath Park CF14 4EP

to apply regulated procedures of the category or categories specified below to animals of the species or groups specified below at places specified in authorised project licences subject to the restrictions and provisions contained in the Act, and subject also to the limitations and conditions contained in this licence and to such other conditions as the Secretary of State may from time to time prescribe:

Description of animal(s)

- Mice

Categories of regulated procedure:

A. Minor/minimally invasive procedures not requiring sedation, analgesia or general anaesthesia
B. Minor/minimally invasive procedures involving sedation, analgesia or brief general anaesthesia. Plus surgical procedures conducted under brief non-recovery general anaesthesia

This licence shall be in force until revoked by the Secretary of State and shall be periodically reviewed by him.

10 References

Abbas, T. and Dutta, A. 2009. p21 in cancer: intricate networks and multiple activities. *Nat Rev Cancer* 9(6), pp. 400-414. doi: 10.1038/nrc2657

Abukhdeir, A. M. and Park, B. H. 2008. P21 and p27: roles in carcinogenesis and drug resistance. *Expert reviews in molecular medicine* 10, p. e19. doi: 10.1017/S1462399408000744

Adamczyk, A. et al. 2017. Proteins Involved in HER2 Signalling Pathway, Their Relations and Influence on Metastasis-Free Survival in HER2-Positive Breast Cancer Patients Treated with Trastuzumab in Adjuvant Setting. *J Cancer* 8(1), pp. 131-139. doi: 10.7150/jca.16239

Aghazadeh, S. and Yazdanparast, R. 2017. Activation of STAT3/HIF-1α/Hes-1 axis promotes trastuzumab resistance in HER2-overexpressing breast cancer cells via down-regulation of PTEN. *Biochim Biophys Acta Gen Subj* 1861(8), pp. 1970-1980. doi: 10.1016/j.bbagen.2017.05.009

Al-Bader, M., Ford, C., Al-Ayadhy, B. and Francis, I. 2011. Analysis of estrogen receptor isoforms and variants in breast cancer cell lines. *Exp Ther Med* 2(3), pp. 537-544. doi: 10.3892/etm.2011.226

Al-Bari, A. A. and Al Mamun, A. 2020. Current advances in regulation of bone homeostasis. *FASEB Bioadv* 2(11), pp. 668-679. doi: 10.1096/fba.2020-00058

Alao, J. P. 2007. The regulation of cyclin D1 degradation: roles in cancer development and the potential for therapeutic invention. *Molecular cancer* 6, p. 24. doi: 10.1186/1476-4598-6-24

Alarmo, E. L. and Kallioniemi, A. 2010. Bone morphogenetic proteins in breast cancer: dual role in tumourigenesis? *Endocr Relat Cancer* 17(2), pp. R123-139. doi: 10.1677/ERC-09-0273

Alarmo, E. L., Korhonen, T., Kuukasjärvi, T., Huhtala, H., Holli, K. and Kallioniemi, A. 2008. Bone morphogenetic protein 7 expression associates with bone metastasis in breast carcinomas. *Ann Oncol* 19(2), pp. 308-314. doi: 10.1093/annonc/mdm453

Alarmo, E. L., Kuukasjärvi, T., Karhu, R. and Kallioniemi, A. 2007. A comprehensive expression survey of bone morphogenetic proteins in breast cancer highlights the importance of BMP4 and BMP7. *Breast Cancer Res Treat* 103(2), pp. 239-246. doi: 10.1007/s10549-006-9362-1

Alarmo, E. L., Rauta, J., Kauraniemi, P., Karhu, R., Kuukasjärvi, T. and Kallioniemi, A. 2006. Bone morphogenetic protein 7 is widely overexpressed in primary breast cancer. *Genes Chromosomes Cancer* 45(4), pp. 411-419. doi: 10.1002/gcc.20307

Alberts, B. 2008. *Molecular biology of the cell : Extended version*. 5th ed. New York: Garland Science.

Alborzinia, H. et al. 2013. Quantitative kinetics analysis of BMP2 uptake into cells and its modulation by BMP antagonists. *J Cell Sci* 126(Pt 1), pp. 117-127. doi: 10.1242/jcs.109777

Aldridge, S. E., Lennard, T. W., Williams, J. R. and Birch, M. A. 2005a. Vascular endothelial growth factor acts as an osteolytic factor in breast cancer metastases to bone. *Br J Cancer* 92(8), pp. 1531-1537. doi: 10.1038/sj.bjc.6602417

Aldridge, S. E., Lennard, T. W., Williams, J. R. and Birch, M. A. 2005b. Vascular endothelial growth factor receptors in osteoclast differentiation and function. *Biochem Biophys Res Commun* 335(3), pp. 793-798. doi: 10.1016/j.bbrc.2005.07.145

Alkarain, A., Jordan, R. and Slingerland, J. 2004. p27 deregulation in breast cancer: prognostic significance and implications for therapy. *J Mammary Gland Biol Neoplasia* 9(1), pp. 67-80. doi: 10.1023/B:JOMG.0000023589.00994.5e

Alkushi, A. 2009. Validation of tissue microarray biomarker expression of breast carcinomas in Saudi women. *Hematology/oncology and stem cell therapy* 2(3), pp. 394-398.

Allison, S. E. et al. 2016. Activation of the pro-migratory bone morphogenetic protein receptor 1B gene in human MDA-MB-468 triple-negative breast cancer cells that over-express CYP2J2. *Int J Biochem Cell Biol* 80, pp. 173-178. doi: 10.1016/j.biocel.2016.10.004

Alluri, P. and Newman, L. A. 2014. Basal-like and triple-negative breast cancers: searching for positives among many negatives. *Surg Oncol Clin N Am* 23(3), pp. 567-577. doi: 10.1016/j.soc.2014.03.003

Ampuja, M., Alarmo, E. L., Owens, P., Havunen, R., Gorska, A. E., Moses, H. L. and Kallioniemi, A. 2016. The impact of bone morphogenetic protein 4 (BMP4) on breast cancer metastasis in a mouse xenograft model. *Cancer Lett* 375(2), pp. 238-244. doi: 10.1016/j.canlet.2016.03.008

Arciero, C. A., Guo, Y., Jiang, R., Behera, M., O'Regan, R., Peng, L. and Li, X. 2019. ER+/HER2+ breast cancer has different metastatic patterns and better

survival than ER-/HER2+ breast cancer. *Clin Breast Cancer*, doi: 10.1016/j.clbc.2019.02.001

Augeri, D. J., Langenfeld, E., Castle, M., Gilleran, J. A. and Langenfeld, J. 2016. Inhibition of BMP and of TGFβ receptors downregulates expression of XIAP and TAK1 leading to lung cancer cell death. *Mol Cancer* 15, p. 27. doi: 10.1186/s12943-016-0511-9

Baird, R. 2017. *A Pre operative window study of Letrozole plus PR agonist(Megestrol Acetate) versus Letrozole alone in post menopausal patients with ER positive breast cancer(PIONEER)*. Available at: www.clinicaltrials.gov [Accessed: May].

Baltimore, D. 1970. RNA-dependent DNA polymerase in virions of RNA tumour viruses. *Nature* 226(5252), pp. 1209-1211. doi: 10.1038/2261209a0

Barrett-Lee, P. J. et al. 2009. Expert opinion on the use of anthracyclines in patients with advanced breast cancer at cardiac risk. *Ann Oncol* 20(5), pp. 816-827. doi: 10.1093/annonc/mdn728

Barros, N. A., Ferreira, A., Rocha, M. J. and Castro, L. 2015. Unusual breast cancer metastasis. *BMJ Case Rep* 2015, doi: 10.1136/bcr-2014-209125

Baselga, J. and Swain, S. M. 2010. CLEOPATRA: a phase III evaluation of pertuzumab and trastuzumab for HER2-positive metastatic breast cancer. *Clin Breast Cancer* 10(6), pp. 489-491. doi: 10.3816/CBC.2010.n.065

Bastien, R. R. et al. 2012. PAM50 breast cancer subtyping by RT-qPCR and concordance with standard clinical molecular markers. *BMC Med Genomics* 5, p. 44. doi: 10.1186/1755-8794-5-44

Bertucci, F., Finetti, P. and Birnbaum, D. 2012. Basal breast cancer: a complex and deadly molecular subtype. *Curr Mol Med* 12(1), pp. 96-110. doi: 10.2174/156652412798376134

Bialkowska, K., Komorowski, P., Bryszewska, M. and Milowska, K. 2020. Spheroids as a Type of Three-Dimensional Cell Cultures-Examples of Methods of Preparation and the Most Important Application. *Int J Mol Sci* 21(17), doi: 10.3390/ijms21176225

Bobinac, D., Marić, I., Zoricić, S., Spanjol, J., Dordević, G., Mustać, E. and Fuckar, Z. 2005. Expression of bone morphogenetic proteins in human metastatic prostate and breast cancer. *Croat Med J* 46(3), pp. 389-396.

Boers, W., Aarrass, S., Linthorst, C., Pinzani, M., Elferink, R. O. and Bosma, P. 2006. Transcriptional profiling reveals novel markers of liver fibrogenesis: gremlin and insulin-like growth factor-binding proteins. *J Biol Chem* 281(24), pp. 16289-16295. doi: 10.1074/jbc.M600711200

Bragdon, B., Moseychuk, O., Saldanha, S., King, D., Julian, J. and Nohe, A. 2011. Bone morphogenetic proteins: a critical review. *Cell Signal* 23(4), pp. 609-620. doi: 10.1016/j.cellsig.2010.10.003

Bray, F., Ferlay, J., Soerjomataram, I., Siegel, R. L., Torre, L. A. and Jemal, A. 2018. Global cancer statistics 2018: GLOBOCAN estimates of incidence and mortality worldwide for 36 cancers in 185 countries. *CA Cancer J Clin* 68(6), pp. 394-424. doi: 10.3322/caac.21492

Brazil, D. P., Church, R. H., Surae, S., Godson, C. and Martin, F. 2015. BMP signalling: agony and antagony in the family. *Trends Cell Biol* 25(5), pp. 249-264. doi: 10.1016/j.tcb.2014.12.004

Brook, N., Brook, E., Dharmarajan, A., Dass, C. R. and Chan, A. 2018. Breast cancer bone metastases: pathogenesis and therapeutic targets. *Int J Biochem Cell Biol* 96, pp. 63-78. doi: 10.1016/j.biocel.2018.01.003

Buijs, J. T. et al. 2007. Bone morphogenetic protein 7 in the development and treatment of bone metastases from breast cancer. *Cancer Res* 67(18), pp. 8742-8751. doi: 10.1158/0008-5472.CAN-06-2490

Buijs, J. T. et al. 2012. The BMP2/7 heterodimer inhibits the human breast cancer stem cell subpopulation and bone metastases formation. *Oncogene* 31(17), pp. 2164-2174. doi: 10.1038/onc.2011.400

Bumpers, H. L., Hassett, J. M., Penetrante, R. B., Hoover, E. L. and Holyoke, E. D. 1993. Endocrine organ metastases in subjects with lobular carcinoma of the breast. *Arch Surg* 128(12), pp. 1344-1347. doi: 10.1001/archsurg.1993.01420240052009

Burguin, A., Furrer, D., Ouellette, G., Jacob, S., Diorio, C. and Durocher, F. 2020. Trastuzumab effects depend on HER2 phosphorylation in HER2-negative breast cancer cell lines. *PLoS One* 15(6), p. e0234991. doi: 10.1371/journal.pone.0234991

Bussard, K. M., Mutkus, L., Stumpf, K., Gomez-Manzano, C. and Marini, F. C. 2016. Tumor-associated stromal cells as key contributors to the tumor

microenvironment. *Breast cancer research : BCR* 18(1), p. 84. doi: 10.1186/s13058-016-0740-2

Cahill, E. et al. 2012. Gremlin plays a key role in the pathogenesis of pulmonary hypertension. *Circulation* 125(7), pp. 920-930. doi: 10.1161/CIRCULATIONAHA.111.038125

Calpe, S. et al. 2015. Effective Inhibition of Bone Morphogenetic Protein Function by Highly Specific Llama-Derived Antibodies. *Mol Cancer Ther* 14(11), pp. 2527-2540. doi: 10.1158/1535-7163.MCT-14-0956

Camp, R. L., Charette, L. A. and Rimm, D. L. 2000. Validation of tissue microarray technology in breast carcinoma. *Laboratory investigation; a journal of technical methods and pathology* 80(12), pp. 1943-1949.

Canalis, E., Parker, K. and Zanotti, S. 2012. Gremlin1 is required for skeletal development and postnatal skeletal homeostasis. *J Cell Physiol* 227(1), pp. 269-277. doi: 10.1002/jcp.22730

Cancer, I. A. f. R. o. 2012. *Breast Cancer Factsheet*. Available at: https://gco.iarc.fr [Accessed: 29/12/2019].

Cao, Y. et al. 2014. BMP4 inhibits breast cancer metastasis by blocking myeloid-derived suppressor cell activity. *Cancer Res* 74(18), pp. 5091-5102. doi: 10.1158/0008-5472.CAN-13-3171

Capulli, M., Paone, R. and Rucci, N. 2014. Osteoblast and osteocyte: games without frontiers. *Arch Biochem Biophys* 561, pp. 3-12. doi: 10.1016/j.abb.2014.05.003

Cardoso, F. et al. 2019. Early breast cancer: ESMO Clinical Practice Guidelines for diagnosis, treatment and follow-up. *Ann Oncol*, doi: 10.1093/annonc/mdz189

Carey, L. A. et al. 2006. Race, breast cancer subtypes, and survival in the Carolina Breast Cancer Study. *JAMA* 295(21), pp. 2492-2502. doi: 10.1001/jama.295.21.2492

Carmona, F. J., Montemurro, F., Kannan, S., Rossi, V., Verma, C., Baselga, J. and Scaltriti, M. 2016. AKT signaling in ERBB2-amplified breast cancer. *Pharmacol Ther* 158, pp. 63-70. doi: 10.1016/j.pharmthera.2015.11.013

Carreira, A. C., Lojudice, F. H., Halcsik, E., Navarro, R. D., Sogayar, M. C. and Granjeiro, J. M. 2014. Bone morphogenetic proteins: facts, challenges, and future perspectives. *J Dent Res* 93(4), pp. 335-345. doi: 10.1177/0022034513518561

Carroll, J. S. 2016. Mechanisms of oestrogen receptor (ER) gene regulation in breast cancer. *Eur J Endocrinol* 175(1), pp. R41-49. doi: 10.1530/EJE-16-0124

Carroll, J. S., Hickey, T. E., Tarulli, G. A., Williams, M. and Tilley, W. D. 2017. Deciphering the divergent roles of progestogens in breast cancer. *Nat Rev Cancer* 17(1), pp. 54-64. doi: 10.1038/nrc.2016.116

Casey, T. et al. 2009. Molecular signatures suggest a major role for stromal cells in development of invasive breast cancer. *Breast cancer research and treatment* 114(1), pp. 47-62. doi: 10.1007/s10549-008-9982-8

Chandler, C., Liu, T., Buckanovich, R. and Coffman, L. G. 2019. The double edge sword of fibrosis in cancer. *Transl Res* 209, pp. 55-67. doi: 10.1016/j.trsl.2019.02.006

Cheang, M. C. et al. 2009. Ki67 index, HER2 status, and prognosis of patients with luminal B breast cancer. *J Natl Cancer Inst* 101(10), pp. 736-750. doi: 10.1093/jnci/djp082

Cheang, M. C. et al. 2015. Defining breast cancer intrinsic subtypes by quantitative receptor expression. *Oncologist* 20(5), pp. 474-482. doi: 10.1634/theoncologist.2014-0372

Chen, B., Athanasiou, M., Gu, Q. and Blair, D. G. 2002. Drm/Gremlin transcriptionally activates p21(Cip1) via a novel mechanism and inhibits neoplastic transformation. *Biochem Biophys Res Commun* 295(5), pp. 1135-1141. doi: 10.1016/s0006-291x(02)00828-8

Chen, M. H. et al. 2013. Expression of gremlin 1 correlates with increased angiogenesis and progression-free survival in patients with pancreatic neuroendocrine tumors. *J Gastroenterol* 48(1), pp. 101-108. doi: 10.1007/s00535-012-0614-z

Chen, Q. et al. 2017. An Experimental Analysis of the Molecular Effects of Trastuzumab (Herceptin) and Fulvestrant (Falsodex), as Single Agents or in Combination, on Human HR+/HER2+ Breast Cancer Cell Lines and Mouse Tumor Xenografts. *PLoS One* 12(1), p. e0168960. doi: 10.1371/journal.pone.0168960

Chen, X., Wang, Z., Duan, N., Zhu, G., Schwarz, E. M. and Xie, C. 2018. Osteoblast-osteoclast interactions. *Connect Tissue Res* 59(2), pp. 99-107. doi: 10.1080/03008207.2017.1290085

Chen, Z., Fang, Z. and Ma, J. 2021. Regulatory mechanisms and clinical significance of vimentin in breast cancer. *Biomed Pharmacother* 133, p. 111068. doi: 10.1016/j.biopha.2020.111068

Chi, L. H., Burrows, A. D. and Anderson, R. L. 2019. Bone morphogenetic protein signaling in breast cancer progression. *Growth Factors* 37(1-2), pp. 12-28. doi: 10.1080/08977194.2019.1626378

Chiarle, R., Pagano, M. and Inghirami, G. 2001. The cyclin dependent kinase inhibitor p27 and its prognostic role in breast cancer. *Breast Cancer Res* 3(2), pp. 91-94.

Chiodelli, P., Mitola, S., Ravelli, C., Oreste, P., Rusnati, M. and Presta, M. 2011. Heparan sulfate proteoglycans mediate the angiogenic activity of the vascular endothelial growth factor receptor-2 agonist gremlin. *Arterioscler Thromb Vasc Biol* 31(12), pp. e116-127. doi: 10.1161/ATVBAHA.111.235184

Chung, J. Y. et al. 2021. TGF-beta Signaling: From Tissue Fibrosis to Tumor Microenvironment. *Int J Mol Sci* 22(14), doi: 10.3390/ijms22147575

Church, R. H. et al. 2017. Gremlin1 plays a key role in kidney development and renal fibrosis. *Am J Physiol Renal Physiol* 312(6), pp. F1141-F1157. doi: 10.1152/ajprenal.00344.2016

Church, R. H. et al. 2015. Gremlin1 preferentially binds to bone morphogenetic protein-2 (BMP-2) and BMP-4 over BMP-7. *Biochem J* 466(1), pp. 55-68. doi: 10.1042/BJ20140771

Ciatto, S., Bonardi, R., Zappa, M. and Giorgi, D. 1997. Risk of breast cancer subsequent to histological or clinical diagnosis of fibroadenoma--retrospective longitudinal study of 3938 cases. *Ann Oncol* 8(3), pp. 297-300. doi: 10.1023/a:1008263522021

Ciuclan, L. et al. 2013. Treatment with anti-gremlin 1 antibody ameliorates chronic hypoxia/SU5416-induced pulmonary arterial hypertension in mice. *Am J Pathol* 183(5), pp. 1461-1473. doi: 10.1016/j.ajpath.2013.07.017

Clement, J. H., Sänger, J. and Höffken, K. 1999. Expression of bone morphogenetic protein 6 in normal mammary tissue and breast cancer cell lines and its regulation by epidermal growth factor. *Int J Cancer* 80(2), pp. 250-256.

Coleman, R. et al. 2020. Adjuvant denosumab in early breast cancer (D-CARE): an international, multicentre, randomised, controlled, phase 3 trial. *Lancet Oncol* 21(1), pp. 60-72. doi: 10.1016/S1470-2045(19)30687-4

Cominetti, M. R., Altei, W. F. and Selistre-de-Araujo, H. S. 2019. Metastasis inhibition in breast cancer by targeting cancer cell extravasation. *Breast Cancer (Dove Med Press)* 11, pp. 165-178. doi: 10.2147/BCTT.S166725

Costello, C. M., Cahill, E., Martin, F., Gaine, S. and McLoughlin, P. 2010. Role of gremlin in the lung: development and disease. *Am J Respir Cell Mol Biol* 42(5), pp. 517-523. doi: 10.1165/rcmb.2009-0101TR

Costello, C. M. et al. 2008. Lung-selective gene responses to alveolar hypoxia: potential role for the bone morphogenetic antagonist gremlin in pulmonary hypertension. *Am J Physiol Lung Cell Mol Physiol* 295(2), pp. L272-284. doi: 10.1152/ajplung.00358.2007

CRUK. 2021. *Twenty most common cancers*. Available at: www.cancerresearchuk.org/health-professional/cancer-statistics/incidence [Accessed: 23/08/2021].

Dai, X., Cheng, H., Bai, Z. and Li, J. 2017. Breast Cancer Cell Line Classification and Its Relevance with Breast Tumor Subtyping. *J Cancer* 8(16), pp. 3131-3141. doi: 10.7150/jca.18457

Dai, X., Li, T., Bai, Z., Yang, Y., Liu, X., Zhan, J. and Shi, B. 2015. Breast cancer intrinsic subtype classification, clinical use and future trends. *Am J Cancer Res* 5(10), pp. 2929-2943.

Davies, S. and Jiang, W. G. 2010. ALCAM, activated leukocyte cell adhesion molecule, influences the aggressive nature of breast cancer cells, a potential connection to bone metastasis. *Anticancer Res* 30(4), pp. 1163-1168.

Davies, S. R., Watkins, G., Douglas-Jones, A., Mansel, R. E. and Jiang, W. G. 2008. Bone morphogenetic proteins 1 to 7 in human breast cancer, expression pattern and clinical/prognostic relevance. *J Exp Ther Oncol* 7(4), pp. 327-338.

Davis, H. et al. 2015. Aberrant epithelial GREM1 expression initiates colonic tumorigenesis from cells outside the stem cell niche. *Nat Med* 21(1), pp. 62-70. doi: 10.1038/nm.3750

Davis, H., Raja, E., Miyazono, K., Tsubakihara, Y. and Moustakas, A. 2016. Mechanisms of action of bone morphogenetic proteins in cancer. *Cytokine Growth Factor Rev* 27, pp. 81-92. doi: 10.1016/j.cytogfr.2015.11.009

Dituri, F., Cossu, C., Mancarella, S. and Giannelli, G. 2019. The Interactivity between TGFβ and BMP Signaling in Organogenesis, Fibrosis, and Cancer. *Cells* 8(10), doi: 10.3390/cells8101130

Droguett, A. et al. 2014. Tubular overexpression of gremlin induces renal damage susceptibility in mice. *PLoS One* 9(7), p. e101879. doi: 10.1371/journal.pone.0101879

Droguett, A. et al. 2019. Gremlin, A Potential Urinary Biomarker of Anca-Associated Crescentic Glomerulonephritis. *Sci Rep* 9(1), p. 6867. doi: 10.1038/s41598-019-43358-5

Duffy, M. J., Harbeck, N., Nap, M., Molina, R., Nicolini, A., Senkus, E. and Cardoso, F. 2017. Clinical use of biomarkers in breast cancer: Updated guidelines from the European Group on Tumor Markers (EGTM). *Eur J Cancer* 75, pp. 284-298. doi: 10.1016/j.ejca.2017.01.017

Dutton, L. R., O' Neill, C. L., Medina, R. J. and Brazil, D. P. 2019. No evidence of Gremlin1-mediated activation of VEGFR2 signalling in endothelial cells. *J Biol Chem*, doi: 10.1074/jbc.AC119.010148

Dyrstad, S. W., Yan, Y., Fowler, A. M. and Colditz, G. A. 2015. Breast cancer risk associated with benign breast disease: systematic review and meta-analysis. *Breast Cancer Res Treat* 149(3), pp. 569-575. doi: 10.1007/s10549-014-3254-6

Eroles, P., Bosch, A., Pérez-Fidalgo, J. A. and Lluch, A. 2012. Molecular biology in breast cancer: intrinsic subtypes and signaling pathways. *Cancer Treat Rev* 38(6), pp. 698-707. doi: 10.1016/j.ctrv.2011.11.005

Evans, M. K. and Longo, D. L. 2014. PALB2 mutations and breast-cancer risk. *N Engl J Med* 371(6), pp. 566-568. doi: 10.1056/NEJMe1405784

Farkas, L., Farkas, D., Gauldie, J., Warburton, D., Shi, W. and Kolb, M. 2011. Transient overexpression of Gremlin results in epithelial activation and reversible fibrosis in rat lungs. *Am J Respir Cell Mol Biol* 44(6), pp. 870-878. doi: 10.1165/rcmb.2010-0070OC

Ferlay, J. et al. 2019. Estimating the global cancer incidence and mortality in 2018: GLOBOCAN sources and methods. *Int J Cancer* 144(8), pp. 1941-1953. doi: 10.1002/ijc.31937

Ferzoco, R. M. and Ruddy, K. J. 2016. The Epidemiology of Male Breast Cancer. *Curr Oncol Rep* 18(1), p. 1. doi: 10.1007/s11912-015-0487-4

Finn, R. S., Aleshin, A. and Slamon, D. J. 2016. Targeting the cyclin-dependent kinases (CDK) 4/6 in estrogen receptor-positive breast cancers. *Breast cancer research : BCR* 18(1), p. 17. doi: 10.1186/s13058-015-0661-5

Fong, Y. C. et al. 2008. BMP-2 increases migration of human chondrosarcoma cells via PI3K/Akt pathway. *J Cell Physiol* 217(3), pp. 846-855. doi: 10.1002/jcp.21568

Ford, C. H., Al-Bader, M., Al-Ayadhi, B. and Francis, I. 2011. Reassessment of estrogen receptor expression in human breast cancer cell lines. *Anticancer Res* 31(2), pp. 521-527.

Fouad, Y. A. and Aanei, C. 2017. Revisiting the hallmarks of cancer. *Am J Cancer Res* 7(5), pp. 1016-1036.

Frey, P., Devisme, A., Schrempp, M., Andrieux, G., Boerries, M. and Hecht, A. 2020. Canonical BMP Signaling Executes Epithelial-Mesenchymal Transition Downstream of SNAIL1. *Cancers (Basel)* 12(4), doi: 10.3390/cancers12041019

Galamb, O. et al. 2008. Diagnostic mRNA expression patterns of inflamed, benign, and malignant colorectal biopsy specimen and their correlation with peripheral blood results. *Cancer Epidemiol Biomarkers Prev* 17(10), pp. 2835-2845. doi: 10.1158/1055-9965.EPI-08-0231

Gao, H. et al. 2012. The BMP inhibitor Coco reactivates breast cancer cells at lung metastatic sites. *Cell* 150(4), pp. 764-779. doi: 10.1016/j.cell.2012.06.035

Garibyan, L. and Avashia, N. 2013. Polymerase chain reaction. *J Invest Dermatol* 133(3), pp. 1-4. doi: 10.1038/jid.2013.1

Gazzerro, E., Pereira, R. C., Jorgetti, V., Olson, S., Economides, A. N. and Canalis, E. 2005. Skeletal overexpression of gremlin impairs bone formation and causes osteopenia. *Endocrinology* 146(2), pp. 655-665. doi: 10.1210/en.2004-0766

Gazzerro, E., Smerdel-Ramoya, A., Zanotti, S., Stadmeyer, L., Durant, D., Economides, A. N. and Canalis, E. 2007. Conditional deletion of gremlin causes a transient increase in bone formation and bone mass. *J Biol Chem* 282(43), pp. 31549-31557. doi: 10.1074/jbc.M701317200

Ghosh-Choudhury, N., Ghosh-Choudhury, G., Celeste, A., Ghosh, P. M., Moyer, M., Abboud, S. L. and Kreisberg, J. 2000a. Bone morphogenetic protein-2 induces cyclin kinase inhibitor p21 and hypophosphorylation of retinoblastoma protein in

estradiol-treated MCF-7 human breast cancer cells. *Biochim Biophys Acta* 1497(2), pp. 186-196.

Ghosh-Choudhury, N., Woodruff, K., Qi, W., Celeste, A., Abboud, S. L. and Ghosh Choudhury, G. 2000b. Bone morphogenetic protein-2 blocks MDA MB 231 human breast cancer cell proliferation by inhibiting cyclin-dependent kinase-mediated retinoblastoma protein phosphorylation. *Biochem Biophys Res Commun* 272(3), pp. 705-711. doi: 10.1006/bbrc.2000.2844

Ghosh Choudhury, G., Jin, D. C., Kim YSs, Celeste, A., Ghosh-Choudhury, N. and Abboud, H. E. 1999. Bone morphogenetic protein-2 inhibits MAPK-dependent Elk-1 transactivation and DNA synthesis induced by EGF in mesangial cells. *Biochem Biophys Res Commun* 258(2), pp. 490-496. doi: 10.1006/bbrc.1999.0599

Gogate, A., Wheeler, S. B., Reeder-Hayes, K. E., Ekwueme, D. U., Fairley, T. L., Drier, S. and Trogdon, J. G. 2021. Projecting the Prevalence and Costs of Metastatic Breast Cancer From 2015 through 2030. *JNCI Cancer Spectr* 5(4), p. pkab063. doi: 10.1093/jncics/pkab063

Goldvaser, H. et al. 2017. The association between smoking and breast cancer characteristics and outcome. *BMC Cancer* 17(1), p. 624. doi: 10.1186/s12885-017-3611-z

Gomez-Cuadrado, L., Tracey, N., Ma, R., Qian, B. and Brunton, V. G. 2017. Mouse models of metastasis: progress and prospects. *Dis Model Mech* 10(9), pp. 1061-1074. doi: 10.1242/dmm.030403

Gómez-Cuadrado, L., Tracey, N., Ma, R., Qian, B. and Brunton, V. G. 2017. Mouse models of metastasis: progress and prospects. *Dis Model Mech* 10(9), pp. 1061-1074. doi: 10.1242/dmm.030403

Goodwin, P. J. and Stambolic, V. 2015. Impact of the obesity epidemic on cancer. *Annu Rev Med* 66, pp. 281-296. doi: 10.1146/annurev-med-051613-012328

Graham, J. R., Williams, C. M. and Yang, Z. 2014. MicroRNA-27b targets gremlin 1 to modulate fibrotic responses in pulmonary cells. *J Cell Biochem* 115(9), pp. 1539-1548. doi: 10.1002/jcb.24809

Grillo, E. et al. 2016. Monomeric gremlin is a novel vascular endothelial growth factor receptor-2 antagonist. *Oncotarget* 7(23), pp. 35353-35368. doi: 10.18632/oncotarget.9286

Guan, Y., Cheng, W., Zou, C., Wang, T. and Cao, Z. 2017a. Gremlin1 promotes carcinogenesis of glioma in vitro. *Clin Exp Pharmacol Physiol* 44(2), pp. 244-256. doi: 10.1111/1440-1681.12697

Guan, Y., Cheng, W., Zou, C., Wang, T. and Cao, Z. 2017b. Gremlin1 promotes carcinogenesis of glioma in vitro. *Clinical and experimental pharmacology & physiology* 44(2), pp. 244-256. doi: 10.1111/1440-1681.12697

Guimei, M., Baddour, N., Elkaffash, D., Abdou, L. and Taher, Y. 2012. Gremlin in the pathogenesis of hepatocellular carcinoma complicating chronic hepatitis C: an immunohistochemical and PCR study of human liver biopsies. *BMC Res Notes* 5, p. 390. doi: 10.1186/1756-0500-5-390

Guo, D., Huang, J. and Gong, J. 2012. Bone morphogenetic protein 4 (BMP4) is required for migration and invasion of breast cancer. *Mol Cell Biochem* 363(1-2), pp. 179-190. doi: 10.1007/s11010-011-1170-1

Guo, X. and Wang, X. F. 2009. Signaling cross-talk between TGF-beta/BMP and other pathways. *Cell Res* 19(1), pp. 71-88. doi: 10.1038/cr.2008.302

Haagenson, K. K. and Wu, G. S. 2010. The role of MAP kinases and MAP kinase phosphatase-1 in resistance to breast cancer treatment. *Cancer Metastasis Rev* 29(1), pp. 143-149. doi: 10.1007/s10555-010-9208-5

Hamajima, N. et al. 2002. Alcohol, tobacco and breast cancer--collaborative reanalysis of individual data from 53 epidemiological studies, including 58,515 women with breast cancer and 95,067 women without the disease. *Br J Cancer* 87(11), pp. 1234-1245. doi: 10.1038/sj.bjc.6600596

Hanahan, D. and Weinberg, R. A. 2000. The hallmarks of cancer. *Cell* 100(1), pp. 57-70. doi: 10.1016/s0092-8674(00)81683-9

Hanahan, D. and Weinberg, R. A. 2011. Hallmarks of cancer: the next generation. *Cell* 144(5), pp. 646-674. doi: 10.1016/j.cell.2011.02.013

Harris, L. N. et al. 2016. Use of Biomarkers to Guide Decisions on Adjuvant Systemic Therapy for Women With Early-Stage Invasive Breast Cancer: American Society of Clinical Oncology Clinical Practice Guideline. *J Clin Oncol* 34(10), pp. 1134-1150. doi: 10.1200/JCO.2015.65.2289

Hartmann, L. C. et al. 2005. Benign breast disease and the risk of breast cancer. *N Engl J Med* 353(3), pp. 229-237. doi: 10.1056/NEJMoa044383

Hatschek, T. et al. 2012. Individually tailored treatment with epirubicin and paclitaxel with or without capecitabine as first-line chemotherapy in metastatic

breast cancer: a randomized multicenter trial. *Breast cancer research and treatment* 131(3), pp. 939-947. doi: 10.1007/s10549-011-1880-9

Hefti, M. M., Hu, R., Knoblauch, N. W., Collins, L. C., Haibe-Kains, B., Tamimi, R. M. and Beck, A. H. 2013. Estrogen receptor negative/progesterone receptor positive breast cancer is not a reproducible subtype. *Breast Cancer Res* 15(4), p. R68. doi: 10.1186/bcr3462

Helms, M. W., Packeisen, J., August, C., Schittek, B., Boecker, W., Brandt, B. H. and Buerger, H. 2005. First evidence supporting a potential role for the BMP/SMAD pathway in the progression of oestrogen receptor-positive breast cancer. *J Pathol* 206(3), pp. 366-376. doi: 10.1002/path.1785

Hinz, M., Krappmann, D., Eichten, A., Heder, A., Scheidereit, C. and Strauss, M. 1999. NF-kappaB function in growth control: regulation of cyclin D1 expression and G0/G1-to-S-phase transition. *Mol Cell Biol* 19(4), pp. 2690-2698. doi: 10.1128/mcb.19.4.2690

Hinz, N. and Jücker, M. 2021. AKT in Bone Metastasis of Solid Tumors: A Comprehensive Review. *Cancers (Basel)* 13(10), doi: 10.3390/cancers13102287

Holliday, D. L. and Speirs, V. 2011a. Choosing the right cell line for breast cancer research. *Breast Cancer Res* 13(4), p. 215. doi: 10.1186/bcr2889

Holliday, D. L. and Speirs, V. 2011b. Choosing the right cell line for breast cancer research. *Breast cancer research : BCR* 13(4), p. 215. doi: 10.1186/bcr2889

Hong, D. et al. 2018. Gremlin1 Delivered by Mesenchymal Stromal Cells Promoted Epithelial-Mesenchymal Transition in Human Esophageal Squamous

Cell Carcinoma. *Cell Physiol Biochem* 47(5), pp. 1785-1799. doi: 10.1159/000491060

Honma, R. et al. 2018. Clinicopathological and Prognostic Significance of Epithelial Gremlin1 Expression in Gastric Cancer. *Anticancer research* 38(3), pp. 1419-1425. doi: 10.21873/anticanres.12366

Hu, K., Sun, H., Gui, B. and Sui, C. 2017. Gremlin-1 suppression increases BMP-2-induced osteogenesis of human mesenchymal stem cells. *Mol Med Rep* 15(4), pp. 2186-2194. doi: 10.3892/mmr.2017.6253

Huang, J. et al. 2021. Global incidence and mortality of breast cancer: a trend analysis. *Aging (Albany NY)* 13(4), pp. 5748-5803. doi: 10.18632/aging.202502

Hugh, J. et al. 2009. Breast cancer subtypes and response to docetaxel in node-positive breast cancer: use of an immunohistochemical definition in the BCIRG 001 trial. *J Clin Oncol* 27(8), pp. 1168-1176. doi: 10.1200/JCO.2008.18.1024

Huntley, R., Jensen, E., Gopalakrishnan, R. and Mansky, K. C. 2019. Bone morphogenetic proteins: Their role in regulating osteoclast differentiation. *Bone Rep* 10, p. 100207. doi: 10.1016/j.bonr.2019.100207

Ibrahim, T. et al. 2000. Expression of bone sialoprotein and osteopontin in breast cancer bone metastases. *Clin Exp Metastasis* 18(3), pp. 253-260. doi: 10.1023/a:1006754605901

Ignatov, A., Eggemann, H., Burger, E. and Ignatov, T. 2018. Patterns of breast cancer relapse in accordance to biological subtype. *J Cancer Res Clin Oncol* 144(7), pp. 1347-1355. doi: 10.1007/s00432-018-2644-2

Ingthorsson, S., Andersen, K., Hilmarsdottir, B., Maelandsmo, G. M., Magnusson, M. K. and Gudjonsson, T. 2016. HER2 induced EMT and tumorigenicity in breast epithelial progenitor cells is inhibited by coexpression of EGFR. *Oncogene* 35(32), pp. 4244-4255. doi: 10.1038/onc.2015.489

Iorns, E. et al. 2012. A new mouse model for the study of human breast cancer metastasis. *PLoS One* 7(10), p. e47995. doi: 10.1371/journal.pone.0047995

Jaeger, E. et al. 2012. Hereditary mixed polyposis syndrome is caused by a 40-kb upstream duplication that leads to increased and ectopic expression of the BMP antagonist GREM1. *Nat Genet* 44(6), pp. 699-703. doi: 10.1038/ng.2263

Jang, B. G. et al. 2017. Prognostic significance of stromal GREM1 expression in colorectal cancer. *Hum Pathol* 62, pp. 56-65. doi: 10.1016/j.humpath.2016.12.018

Jani, J. P. et al. 2007. Discovery and pharmacologic characterization of CP-724,714, a selective ErbB2 tyrosine kinase inhibitor. *Cancer Res* 67(20), pp. 9887-9893. doi: 10.1158/0008-5472.CAN-06-3559

Jezequel, P., Frenel, J. S., Campion, L., Guerin-Charbonnel, C., Gouraud, W., Ricolleau, G. and Campone, M. 2013. bc-GenExMiner 3.0: new mining module computes breast cancer gene expression correlation analyses. *Database (Oxford)* 2013, p. bas060. doi: 10.1093/database/bas060

Jezequel, P., Gouraud, W., Ben Azzouz, F., Guerin-Charbonnel, C., Juin, P. P., Lasla, H. and Campone, M. 2021. bc-GenExMiner 4.5: new mining module computes breast cancer differential gene expression analyses. *Database (Oxford)* 2021, doi: 10.1093/database/baab007

Jiralerspong, S. and Goodwin, P. J. 2016. Obesity and Breast Cancer Prognosis: Evidence, Challenges, and Opportunities. *J Clin Oncol* 34(35), pp. 4203-4216. doi: 10.1200/JCO.2016.68.4480

Jones, M. E., Schoemaker, M. J., Wright, L. B., Ashworth, A. and Swerdlow, A. J. 2017. Smoking and risk of breast cancer in the Generations Study cohort. *Breast Cancer Res* 19(1), p. 118. doi: 10.1186/s13058-017-0908-4

Kamath, S. D., Kircher, S. M. and Benson, A. B. 2019. Comparison of Cancer Burden and Nonprofit Organization Funding Reveals Disparities in Funding Across Cancer Types. *J Natl Compr Canc Netw* 17(7), pp. 849-854. doi: 10.6004/jnccn.2018.7280

Kao, K. J., Chang, K. M., Hsu, H. C. and Huang, A. T. 2011. Correlation of microarray-based breast cancer molecular subtypes and clinical outcomes: implications for treatment optimization. *BMC cancer* 11, p. 143. doi: 10.1186/1471-2407-11-143

Kapalczynska, M. et al. 2018. 2D and 3D cell cultures - a comparison of different types of cancer cell cultures. *Arch Med Sci* 14(4), pp. 910-919. doi: 10.5114/aoms.2016.63743

Kapoor, P., Suva, L. J., Welch, D. R. and Donahue, H. J. 2008. Osteoprotegrin and the bone homing and colonization potential of breast cancer cells. *J Cell Biochem* 103(1), pp. 30-41. doi: 10.1002/jcb.21382

Karagiannis, G. S., Afaloniati, H., Karamanavi, E., Poutahidis, T. and Angelopoulou, K. 2016. BMP pathway suppression is an early event in

inflammation-driven colon neoplasmatogenesis of uPA-deficient mice. *Tumour Biol* 37(2), pp. 2243-2255. doi: 10.1007/s13277-015-3988-8

Karagiannis, G. S. et al. 2015. Bone morphogenetic protein antagonist gremlin-1 regulates colon cancer progression. *Biol Chem* 396(2), pp. 163-183. doi: 10.1515/hsz-2014-0221

Katsuno, Y. et al. 2008. Bone morphogenetic protein signaling enhances invasion and bone metastasis of breast cancer cells through Smad pathway. *Oncogene* 27(49), pp. 6322-6333. doi: 10.1038/onc.2008.232

Khalili, P., Arakelian, A., Chen, G., Singh, G. and Rabbani, S. A. 2005. Effect of Herceptin on the development and progression of skeletal metastases in a xenograft model of human breast cancer. *Oncogene* 24(44), pp. 6657-6666. doi: 10.1038/sj.onc.1208790

Khojasteh Poor, F. et al. 2021. Mini review: The FDA-approved prescription drugs that target the MAPK signaling pathway in women with breast cancer. *Breast Dis*, doi: 10.3233/BD-201063

Khokha, M. K., Hsu, D., Brunet, L. J., Dionne, M. S. and Harland, R. M. 2003. Gremlin is the BMP antagonist required for maintenance of Shh and Fgf signals during limb patterning. *Nat Genet* 34(3), pp. 303-307. doi: 10.1038/ng1178

Kim, H. S. et al. 2017. GREM1 is expressed in the cancer-associated myofibroblasts of basal cell carcinomas. *PLoS One* 12(3), p. e0174565. doi: 10.1371/journal.pone.0174565

Kim, M., Yoon, S., Lee, S., Ha, S. A., Kim, H. K., Kim, J. W. and Chung, J. 2012. Gremlin-1 induces BMP-independent tumor cell proliferation, migration, and invasion. *PLoS One* 7(4), p. e35100. doi: 10.1371/journal.pone.0035100

Kim, M. O. et al. 2011. Embryonic stem-cell-preconditioned microenvironment induces loss of cancer cell properties in human melanoma cells. *Pigment Cell Melanoma Res* 24(5), pp. 922-931. doi: 10.1111/j.1755-148X.2011.00891.x

Kim, R., Arihiro, K., Emi, M., Tanabe, K. and Osaki, A. 2006. Potential role of HER-2; in primary breast tumor with bone metastasis. *Oncol Rep* 15(6), pp. 1477-1484.

Kimbung, S., Kovacs, A., Bendahl, P. O., Malmstrom, P., Ferno, M., Hatschek, T. and Hedenfalk, I. 2014. Claudin-2 is an independent negative prognostic factor in breast cancer and specifically predicts early liver recurrences. *Molecular oncology* 8(1), pp. 119-128. doi: 10.1016/j.molonc.2013.10.002

Kimura, F. et al. 2017. Hereditary breast cancer associated with Cowden syndrome-related PTEN mutation with Lhermitte-Duclos disease. *Surg Case Rep* 3(1), p. 83. doi: 10.1186/s40792-017-0355-6

Kisonaite, M., Wang, X. and Hyvonen, M. 2016. Structure of Gremlin-1 and analysis of its interaction with BMP-2. *The Biochemical journal* 473(11), pp. 1593-1604. doi: 10.1042/BCJ20160254

Kišonaitė, M., Wang, X. and Hyvönen, M. 2016. Structure of Gremlin-1 and analysis of its interaction with BMP-2. *Biochem J* 473(11), pp. 1593-1604. doi: 10.1042/BCJ20160254

Koba, W., Jelicks, L. A. and Fine, E. J. 2013. MicroPET/SPECT/CT imaging of small animal models of disease. *Am J Pathol* 182(2), pp. 319-324. doi: 10.1016/j.ajpath.2012.09.025

Kodach, L. L. et al. 2008a. The bone morphogenetic protein pathway is active in human colon adenomas and inactivated in colorectal cancer. *Cancer* 112(2), pp. 300-306. doi: 10.1002/cncr.23160

Kodach, L. L. et al. 2008b. The bone morphogenetic protein pathway is inactivated in the majority of sporadic colorectal cancers. *Gastroenterology* 134(5), pp. 1332-1341. doi: 10.1053/j.gastro.2008.02.059

Koh, J. and Kim, M. J. 2019. Introduction of a New Staging System of Breast Cancer for Radiologists: An Emphasis on the Prognostic Stage. *Korean J Radiol* 20(1), pp. 69-82. doi: 10.3348/kjr.2018.0231

Koketsu, K., Yoshida, D., Kim, K., Ishii, Y., Tahara, S., Teramoto, A. and Morita, A. 2015. Gremlin, a bone morphogenetic protein antagonist, is a crucial angiogenic factor in pituitary adenoma. *Int J Endocrinol* 2015, p. 834137. doi: 10.1155/2015/834137

Koli, K., Myllärniemi, M., Vuorinen, K., Salmenkivi, K., Ryynänen, M. J., Kinnula, V. L. and Keski-Oja, J. 2006. Bone morphogenetic protein-4 inhibitor gremlin is overexpressed in idiopathic pulmonary fibrosis. *Am J Pathol* 169(1), pp. 61-71. doi: 10.2353/ajpath.2006.051263

Kretschmer, C., Sterner-Kock, A., Siedentopf, F., Schoenegg, W., Schlag, P. M. and Kemmner, W. 2011. Identification of early molecular markers for breast cancer. *Molecular cancer* 10(1), p. 15. doi: 10.1186/1476-4598-10-15

Kuchimaru, T. et al. 2018. A reliable murine model of bone metastasis by injecting cancer cells through caudal arteries. *Nat Commun* 9(1), p. 2981. doi: 10.1038/s41467-018-05366-3

Lademann, F., Hofbauer, L. C. and Rauner, M. 2020. The Bone Morphogenetic Protein Pathway: The Osteoclastic Perspective. *Front Cell Dev Biol* 8, p. 586031. doi: 10.3389/fcell.2020.586031

Langley, R. R. and Fidler, I. J. 2011. The seed and soil hypothesis revisited--the role of tumor-stroma interactions in metastasis to different organs. *Int J Cancer* 128(11), pp. 2527-2535. doi: 10.1002/ijc.26031

Larrea, M. D., Wander, S. A. and Slingerland, J. M. 2009. p27 as Jekyll and Hyde: regulation of cell cycle and cell motility. *Cell Cycle* 8(21), pp. 3455-3461. doi: 10.4161/cc.8.21.9789

Laulan, N. B. and St-Pierre, Y. 2015. Bone morphogenetic protein 4 (BMP-4) and epidermal growth factor (EGF) inhibit metalloproteinase-9 (MMP-9) expression in cancer cells. *Oncoscience* 2(3), pp. 309-316. doi: 10.18632/oncoscience.144

Laurila, R., Parkkila, S., Isola, J., Kallioniemi, A. and Alarmo, E. L. 2013. The expression patterns of gremlin 1 and noggin in normal adult and tumor tissues. *International journal of clinical and experimental pathology* 6(7), pp. 1400-1408.

Lavoz, C. et al. 2015. Gremlin regulates renal inflammation via the vascular endothelial growth factor receptor 2 pathway. *J Pathol* 236(4), pp. 407-420. doi: 10.1002/path.4537

Lavoz, C. et al. 2018. Gremlin activates the Notch pathway linked to renal inflammation. *Clin Sci (Lond)* 132(11), pp. 1097-1115. doi: 10.1042/CS20171553

Lee, A., Moon, B. I. and Kim, T. H. 2020. /. *Ann Lab Med* 40(2), pp. 114-121. doi: 10.3343/alm.2020.40.2.114

Lee, Y. C. et al. 2011. BMP4 promotes prostate tumor growth in bone through osteogenesis. *Cancer Res* 71(15), pp. 5194-5203. doi: 10.1158/0008-5472.CAN-10-4374

Li, B. T., Wong, M. H. and Pavlakis, N. 2014. Treatment and Prevention of Bone Metastases from Breast Cancer: A Comprehensive Review of Evidence for Clinical Practice. *J Clin Med* 3(1), pp. 1-24. doi: 10.3390/jcm3010001

Li, J. P. and Kusche-Gullberg, M. 2016. Heparan Sulfate: Biosynthesis, Structure, and Function. *Int Rev Cell Mol Biol* 325, pp. 215-273. doi: 10.1016/bs.ircmb.2016.02.009

Li, Q., Birkbak, N. J., Gyorffy, B., Szallasi, Z. and Eklund, A. C. 2011. Jetset: selecting the optimal microarray probe set to represent a gene. *BMC Bioinformatics* 12, p. 474. doi: 10.1186/1471-2105-12-474

Li, Z. et al. 2015. Methylation profiling of 48 candidate genes in tumor and matched normal tissues from breast cancer patients. *Breast Cancer Res Treat* 149(3), pp. 767-779. doi: 10.1007/s10549-015-3276-8

Lian, W. J., Liu, G., Liu, Y. J., Zhao, Z. W., Yi, T. and Zhou, H. Y. 2013. Downregulation of BMP6 enhances cell proliferation and chemoresistance via

activation of the ERK signaling pathway in breast cancer. *Oncol Rep* 30(1), pp. 193-200. doi: 10.3892/or.2013.2462

Liang, Y., Benakanakere, I., Besch-Williford, C., Hyder, R. S., Ellersieck, M. R. and Hyder, S. M. 2010. Synthetic progestins induce growth and metastasis of BT-474 human breast cancer xenografts in nude mice. *Menopause* 17(5), pp. 1040-1047. doi: 10.1097/gme.0b013e3181d3dd0c

Liao, S., Li, J., Wei, W., Wang, L., Zhang, Y., Wang, C. and Sun, S. 2011. Association between diabetes mellitus and breast cancer risk: a meta-analysis of the literature. *Asian Pac J Cancer Prev* 12(4), pp. 1061-1065.

Lim, K. J., Brandt, W. D., Heth, J. A., Muraszko, K. M., Fan, X., Bar, E. E. and Eberhart, C. G. 2015. Lateral inhibition of Notch signaling in neoplastic cells. *Oncotarget* 6(3), pp. 1666-1677. doi: 10.18632/oncotarget.2762

Lin, X., Patil, S., Gao, Y. G. and Qian, A. 2020. The Bone Extracellular Matrix in Bone Formation and Regeneration. *Front Pharmacol* 11, p. 757. doi: 10.3389/fphar.2020.00757

Liu, L. L., Zhao, H., Ma, T. F., Ge, F., Chen, C. S. and Zhang, Y. P. 2015. Identification of valid reference genes for the normalization of RT-qPCR expression studies in human breast cancer cell lines treated with and without transient transfection. *PLoS One* 10(1), p. e0117058. doi: 10.1371/journal.pone.0117058

Liu, M. C. et al. 2016. PAM50 gene signatures and breast cancer prognosis with adjuvant anthracycline- and taxane-based chemotherapy: correlative analysis of C9741 (Alliance). *NPJ Breast Cancer* 2, doi: 10.1038/npjbcancer.2015.23

Liu, Y., Li, Y., Hou, R. and Shu, Z. 2019. Knockdown GREM1 suppresses cell growth, angiogenesis, and epithelial-mesenchymal transition in colon cancer. *J Cell Biochem* 120(4), pp. 5583-5596. doi: 10.1002/jcb.27842

Liu, Y. et al. 2018. Knockdown of Bone Morphogenetic Proteins Type 1a Receptor (BMPR1a) in Breast Cancer Cells Protects Bone from Breast Cancer-Induced Osteolysis by Suppressing RANKL Expression. *Cell Physiol Biochem* 45(5), pp. 1759-1771. doi: 10.1159/000487784

Lokuhetty, D., White, V., Watanabe, R. and Cree, I. 2019. *WHO Classification of Tumours: Breast Tumours*. 5th ed.

Ma, X. J., Dahiya, S., Richardson, E., Erlander, M. and Sgroi, D. C. 2009. Gene expression profiling of the tumor microenvironment during breast cancer progression. *Breast cancer research : BCR* 11(1), p. R7. doi: 10.1186/bcr2222

Ma, X. J. et al. 2003. Gene expression profiles of human breast cancer progression. *Proceedings of the National Academy of Sciences of the United States of America* 100(10), pp. 5974-5979. doi: 10.1073/pnas.0931261100

Macedo, F., Ladeira, K., Pinho, F., Saraiva, N., Bonito, N., Pinto, L. and Goncalves, F. 2017. Bone Metastases: An Overview. *Oncol Rev* 11(1), p. 321. doi: 10.4081/oncol.2017.321

Magnoni, F., Accardo, G., Rossi, E., Veronesi, P. and Corso, G. 2019. Anatomy is not enough: the crucial role of biology and genetics in AJCC eighth edition of the TNM classification for breast cancer. *Ann Transl Med* 7(Suppl 1), p. S34. doi: 10.21037/atm.2019.02.12

Martinez-Morilla, S. et al. 2020. Quantitative assessment of PD-L1 as an analyte in immunohistochemistry diagnostic assays using a standardized cell line tissue microarray. *Lab Invest* 100(1), pp. 4-15. doi: 10.1038/s41374-019-0295-9

Martorana, F. et al. 2021. AKT Inhibitors: New Weapons in the Fight Against Breast Cancer? *Front Pharmacol* 12, p. 662232. doi: 10.3389/fphar.2021.662232

Masciari, S. et al. 2012. Breast cancer phenotype in women with TP53 germline mutations: a Li-Fraumeni syndrome consortium effort. *Breast Cancer Res Treat* 133(3), pp. 1125-1130. doi: 10.1007/s10549-012-1993-9

McPherson, K., Steel, C. M. and Dixon, J. M. 2000. ABC of breast diseases. Breast cancer-epidemiology, risk factors, and genetics. *BMJ* 321(7261), pp. 624-628. doi: 10.1136/bmj.321.7261.624

Meftahi, G. H., Bahari, Z., Zarei Mahmoudabadi, A., Iman, M. and Jangravi, Z. 2021. Applications of western blot technique: From bench to bedside. *Biochem Mol Biol Educ* 49(4), pp. 509-517. doi: 10.1002/bmb.21516

Meiers, P., Cil, T., Guller, U. and Zuber, M. 2013. Sentinel lymph node biopsy in early-stage breast cancer patients: improved survival through better staging? *Langenbecks Arch Surg* 398(5), pp. 687-690. doi: 10.1007/s00423-012-1037-2

Mezzano, S., Droguett, A., Lavoz, C., Krall, P., Egido, J. and Ruiz-Ortega, M. 2018. Gremlin and renal diseases: ready to jump the fence to clinical utility? *Nephrol Dial Transplant* 33(5), pp. 735-741. doi: 10.1093/ndt/gfx194

Michos, O. et al. 2007. Reduction of BMP4 activity by gremlin 1 enables ureteric bud outgrowth and GDNF/WNT11 feedback signalling during kidney branching morphogenesis. *Development* 134(13), pp. 2397-2405. doi: 10.1242/dev.02861

Michos, O., Panman, L., Vintersten, K., Beier, K., Zeller, R. and Zuniga, A. 2004. Gremlin-mediated BMP antagonism induces the epithelial-mesenchymal feedback signaling controlling metanephric kidney and limb organogenesis. *Development* 131(14), pp. 3401-3410. doi: 10.1242/dev.01251

Milanes-Yearsley, M. et al. 2002. Tissue micro-array: a cost and time-effective method for correlative studies by regional and national cancer study groups. *Mod Pathol* 15(12), pp. 1366-1373. doi: 10.1097/01.MP.0000036345.18944.22

Mitola, S. et al. 2010. Gremlin is a novel agonist of the major proangiogenic receptor VEGFR2. *Blood* 116(18), pp. 3677-3680. doi: 10.1182/blood-2010-06-291930

Mitri, Z., Constantine, T. and O'Regan, R. 2012. The HER2 Receptor in Breast Cancer: Pathophysiology, Clinical Use, and New Advances in Therapy. *Chemother Res Pract* 2012, p. 743193. doi: 10.1155/2012/743193

Mittal, V. 2018. Epithelial Mesenchymal Transition in Tumor Metastasis. *Annu Rev Pathol* 13, pp. 395-412. doi: 10.1146/annurev-pathol-020117-043854

Miyazono, K., Kamiya, Y. and Morikawa, M. 2010. Bone morphogenetic protein receptors and signal transduction. *J Biochem* 147(1), pp. 35-51. doi: 10.1093/jb/mvp148

Mock, K., Preca, B. T., Brummer, T., Brabletz, S., Stemmler, M. P. and Brabletz, T. 2015. The EMT-activator ZEB1 induces bone metastasis associated genes including BMP-inhibitors. *Oncotarget* 6(16), pp. 14399-14412. doi: 10.18632/oncotarget.3882

Mohammadizadeh, F., Hani, M., Ranaee, M. and Bagheri, M. 2013. Role of cyclin D1 in breast carcinoma. *Journal of research in medical sciences : the official journal of Isfahan University of Medical Sciences* 18(12), pp. 1021-1025.

Mulvihill, M. S. et al. 2012. Gremlin is overexpressed in lung adenocarcinoma and increases cell growth and proliferation in normal lung cells. *PLoS One* 7(8), p. e42264. doi: 10.1371/journal.pone.0042264

Murphy, N. et al. 2016. Altered Expression of Bone Morphogenetic Protein Accessory Proteins in Murine and Human Pulmonary Fibrosis. *Am J Pathol* 186(3), pp. 600-615. doi: 10.1016/j.ajpath.2015.10.032

Myllärniemi, M. et al. 2008. Gremlin-mediated decrease in bone morphogenetic protein signaling promotes pulmonary fibrosis. *Am J Respir Crit Care Med* 177(3), pp. 321-329. doi: 10.1164/rccm.200706-945OC

Nam, S. et al. 2020. Introduction to digital pathology and computer-aided pathology. *J Pathol Transl Med* 54(2), pp. 125-134. doi: 10.4132/jptm.2019.12.31

Nami, B., Maadi, H. and Wang, Z. 2018. Mechanisms Underlying the Action and Synergism of Trastuzumab and Pertuzumab in Targeting HER2-Positive Breast Cancer. *Cancers (Basel)* 10(10), doi: 10.3390/cancers10100342

Namkoong, H. et al. 2006. The bone morphogenetic protein antagonist gremlin 1 is overexpressed in human cancers and interacts with YWHAH protein. *BMC Cancer* 6, p. 74. doi: 10.1186/1471-2407-6-74

Nassar, A. et al. 2015. Complex fibroadenoma and breast cancer risk: a Mayo Clinic Benign Breast Disease Cohort Study. *Breast Cancer Res Treat* 153(2), pp. 397-405. doi: 10.1007/s10549-015-3535-8

NCBI. *Primer BLAST*. National Center for Biotechnology Information. Available at: www.ncbi.nlm.nih.gov/tools/primer-blast/primertool [Accessed: 01/03/2022].

Neckmann, U. et al. 2019. GREM1 is associated with metastasis and predicts poor prognosis in ER-negative breast cancer patients. *Cell Commun Signal* 17(1), p. 140. doi: 10.1186/s12964-019-0467-7

NICE. 2011. *Gene expression profiling and expanding IHC tests to guide selection of chemotherapy regimes in breast cancer management*. Available at: www.nice.org.uk/guidance/dg10 [Accessed.

NICE. 2017. *Early breast cancer (preventing recurrence and improving survival): adjuvant bisphosphonates*

Evidence summary [ES15]. Available at: https://www.nice.org.uk/advice/es15/chapter/Key-points [Accessed: 10/02/2022].

NICE. 2018. Early and locally advanced breast cancer : Diagnosis and management Guideline NG101. National Institute for Health and Care Excellence.

Nicolini, A., Ferrari, P. and Duffy, M. J. 2018. Prognostic and predictive biomarkers in breast cancer: Past, present and future. *Semin Cancer Biol* 52(Pt 1), pp. 56-73. doi: 10.1016/j.semcancer.2017.08.010

Nissim, S., Hasso, S. M., Fallon, J. F. and Tabin, C. J. 2006. Regulation of Gremlin expression in the posterior limb bud. *Dev Biol* 299(1), pp. 12-21. doi: 10.1016/j.ydbio.2006.05.026

Nohe, A., Keating, E., Knaus, P. and Petersen, N. O. 2004. Signal transduction of bone morphogenetic protein receptors. *Cell Signal* 16(3), pp. 291-299. doi: 10.1016/j.cellsig.2003.08.011

O'Brien, K. M. et al. 2010. Intrinsic breast tumor subtypes, race, and long-term survival in the Carolina Breast Cancer Study. *Clin Cancer Res* 16(24), pp. 6100-6110. doi: 10.1158/1078-0432.CCR-10-1533

Ong, D. B., Colley, S. M., Norman, M. R., Kitazawa, S. and Tobias, J. H. 2004. Transcriptional regulation of a BMP-6 promoter by estrogen receptor alpha. *J Bone Miner Res* 19(3), pp. 447-454. doi: 10.1359/JBMR.0301249

Ouahoud, S., Hardwick, J. C. H. and Hawinkels, L. J. A. C. 2020. Extracellular BMP Antagonists, Multifaceted Orchestrators in the Tumor and Its Microenvironment. *Int J Mol Sci* 21(11), doi: 10.3390/ijms21113888

Ouyang, W., Ma, Q., Li, J., Zhang, D., Liu, Z. G., Rustgi, A. K. and Huang, C. 2005. Cyclin D1 induction through IkappaB kinase beta/nuclear factor-kappaB pathway is responsible for arsenite-induced increased cell cycle G1-S phase transition in human keratinocytes. *Cancer Res* 65(20), pp. 9287-9293. doi: 10.1158/0008-5472.CAN-05-0469

Owens, P. et al. 2012. Disruption of bone morphogenetic protein receptor 2 (BMPR2) in mammary tumors promotes metastases through cell autonomous and paracrine mediators. *Proc Natl Acad Sci U S A* 109(8), pp. 2814-2819. doi: 10.1073/pnas.1101139108

Owens, P. et al. 2015. Inhibition of BMP signaling suppresses metastasis in mammary cancer. *Oncogene* 34(19), pp. 2437-2449. doi: 10.1038/onc.2014.189

Owens, P. et al. 2013. Bone Morphogenetic Proteins stimulate mammary fibroblasts to promote mammary carcinoma cell invasion. *PLoS One* 8(6), p. e67533. doi: 10.1371/journal.pone.0067533

Park, S. A., Sung, N. J., Choi, B. J., Kim, W., Kim, S. H. and Surh, Y. J. 2020. Gremlin-1 augments the oestrogen-related receptor α signalling through EGFR activation: implications for the progression of breast cancer. *Br J Cancer* 123(6), pp. 988-999. doi: 10.1038/s41416-020-0945-0

Parkes, A., Clifton, K., Al-Awadhi, A., Oke, O., Warneke, C. L., Litton, J. K. and Hortobagyi, G. N. 2018. Characterization of bone only metastasis patients with respect to tumor subtypes. *NPJ Breast Cancer* 4, p. 2. doi: 10.1038/s41523-018-0054-x

Pawlak, J. B. and Blobe, G. C. 2021. TGF-β superfamily co-receptors in cancer. *Dev Dyn*, doi: 10.1002/dvdy.338

Pelli, A., Väyrynen, J. P., Klintrup, K., Mäkelä, J., Mäkinen, M. J., Tuomisto, A. and Karttunen, T. J. 2016. Gremlin1 expression associates with serrated pathway and favourable prognosis in colorectal cancer. *Histopathology* 69(5), pp. 831-838. doi: 10.1111/his.13006

Pereira, R. C., Economides, A. N. and Canalis, E. 2000. Bone morphogenetic proteins induce gremlin, a protein that limits their activity in osteoblasts. *Endocrinology* 141(12), pp. 4558-4563. doi: 10.1210/endo.141.12.7851

Perou, C. M. et al. 2000. Molecular portraits of human breast tumours. *Nature* 406(6797), pp. 747-752. doi: 10.1038/35021093

Peshkin, B. N., Alabek, M. L. and Isaacs, C. 2010. BRCA1/2 mutations and triple negative breast cancers. *Breast Dis* 32(1-2), pp. 25-33. doi: 10.3233/BD-2010-0306

Peshkin, B. N., DeMarco, T. A. and Schwartz, M. D. 2002. Oophorectomy in carriers of BRCA mutations. *N Engl J Med* 347(13), pp. 1037-1040; author reply 1037-1040.

Pickup, M. W. et al. 2015. BMPR2 loss in fibroblasts promotes mammary carcinoma metastasis via increased inflammation. *Molecular oncology* 9(1), pp. 179-191. doi: 10.1016/j.molonc.2014.08.004

Picon-Ruiz, M., Morata-Tarifa, C., Valle-Goffin, J. J., Friedman, E. R. and Slingerland, J. M. 2017. Obesity and adverse breast cancer risk and outcome: Mechanistic insights and strategies for intervention. *CA: a cancer journal for clinicians* 67(5), pp. 378-397. doi: 10.3322/caac.21405

Pilarski, R. 2009. Cowden syndrome: a critical review of the clinical literature. *J Genet Couns* 18(1), pp. 13-27. doi: 10.1007/s10897-008-9187-7

Prat, A. and Perou, C. M. 2011. Deconstructing the molecular portraits of breast cancer. *Mol Oncol* 5(1), pp. 5-23. doi: 10.1016/j.molonc.2010.11.003

Pulido, C., Vendrell, I., Ferreira, A. R., Casimiro, S., Mansinho, A., Alho, I. and Costa, L. 2017. Bone metastasis risk factors in breast cancer. *Ecancermedicalscience* 11, p. 715. doi: 10.3332/ecancer.2017.715

Qu, Y. et al. 2015. Evaluation of MCF10A as a Reliable Model for Normal Human Mammary Epithelial Cells. *PLoS One* 10(7), p. e0131285. doi: 10.1371/journal.pone.0131285

Quigley, D. A. et al. 2017. Age, estrogen, and immune response in breast adenocarcinoma and adjacent normal tissue. *Oncoimmunology* 6(11), p. e1356142. doi: 10.1080/2162402X.2017.1356142

Rahman, M. S., Akhtar, N., Jamil, H. M., Banik, R. S. and Asaduzzaman, S. M. 2015. TGF-β/BMP signaling and other molecular events: regulation of osteoblastogenesis and bone formation. *Bone Res* 3, p. 15005. doi: 10.1038/boneres.2015.5

Rahman, N. et al. 2007. PALB2, which encodes a BRCA2-interacting protein, is a breast cancer susceptibility gene. *Nat Genet* 39(2), pp. 165-167. doi: 10.1038/ng1959

Raida, M., Clement, J. H., Leek, R. D., Ameri, K., Bicknell, R., Niederwieser, D. and Harris, A. L. 2005. Bone morphogenetic protein 2 (BMP-2) and induction of tumor angiogenesis. *J Cancer Res Clin Oncol* 131(11), pp. 741-750. doi: 10.1007/s00432-005-0024-1

Rakha, E. A. et al. 2010. Breast cancer prognostic classification in the molecular era: the role of histological grade. *Breast Cancer Res* 12(4), p. 207. doi: 10.1186/bcr2607

Redmond, A. M., Omarjee, S., Chernukhin, I., Le Romancer, M. and Carroll, J. S. 2019. Analysis of HER2 genomic binding in breast cancer cells identifies a global role in direct gene regulation. *PLoS One* 14(11), p. e0225180. doi: 10.1371/journal.pone.0225180

Reinholz, M. M., Iturria, S. J., Ingle, J. N. and Roche, P. C. 2002. Differential gene expression of TGF-beta family members and osteopontin in breast tumor tissue: analysis by real-time quantitative PCR. *Breast cancer research and treatment* 74(3), pp. 255-269.

Ren, J. et al. 2019. Cancer-associated fibroblast-derived Gremlin 1 promotes breast cancer progression. *Breast Cancer Res* 21(1), p. 109. doi: 10.1186/s13058-019-1194-0

Ren, W. et al. 2014a. BMP9 inhibits proliferation and metastasis of HER2-positive SK-BR-3 breast cancer cells through ERK1/2 and PI3K/AKT pathways. *PLoS One* 9(5), p. e96816. doi: 10.1371/journal.pone.0096816

Ren, W. et al. 2014b. BMP9 inhibits the bone metastasis of breast cancer cells by downregulating CCN2 (connective tissue growth factor, CTGF) expression. *Mol Biol Rep* 41(3), pp. 1373-1383. doi: 10.1007/s11033-013-2982-8

Ribatti, D., Tamma, R. and Annese, T. 2020. Epithelial-Mesenchymal Transition in Cancer: A Historical Overview. *Transl Oncol* 13(6), p. 100773. doi: 10.1016/j.tranon.2020.100773

Rizzardi, A. E. et al. 2012. Quantitative comparison of immunohistochemical staining measured by digital image analysis versus pathologist visual scoring. *Diagn Pathol* 7, p. 42. doi: 10.1186/1746-1596-7-42

Rodrigues-Diez, R. et al. 2012. Gremlin is a downstream profibrotic mediator of transforming growth factor-beta in cultured renal cells. *Nephron Exp Nephrol* 122(1-2), pp. 62-74. doi: 10.1159/000346575

Rojas, K. and Stuckey, A. 2016. Breast Cancer Epidemiology and Risk Factors. *Clin Obstet Gynecol* 59(4), pp. 651-672. doi: 10.1097/GRF.0000000000000239

Rousset-Jablonski, C. and Gompel, A. 2017. Screening for familial cancer risk: Focus on breast cancer. *Maturitas* 105, pp. 69-77. doi: 10.1016/j.maturitas.2017.08.004

Saadatmand, S., Bretveld, R., Siesling, S. and Tilanus-Linthorst, M. M. 2015. Influence of tumour stage at breast cancer detection on survival in modern times: population based study in 173,797 patients. *BMJ* 351, p. h4901. doi: 10.1136/bmj.h4901

Sakai, H. et al. 2012. Augmented autocrine bone morphogenic protein (BMP) 7 signaling increases the metastatic potential of mouse breast cancer cells. *Clin Exp Metastasis* 29(4), pp. 327-338. doi: 10.1007/s10585-012-9453-9

Sanchez-Duffhues, G., Hiepen, C., Knaus, P. and Ten Dijke, P. 2015. Bone morphogenetic protein signaling in bone homeostasis. *Bone* 80, pp. 43-59. doi: 10.1016/j.bone.2015.05.025

Sanchez-Duffhues, G., Williams, E., Goumans, M. J., Heldin, C. H. and Ten Dijke, P. 2020. Bone morphogenetic protein receptors: Structure, function and targeting by selective small molecule kinase inhibitors. *Bone* 138, p. 115472. doi: 10.1016/j.bone.2020.115472

Sapkota, G., Alarcón, C., Spagnoli, F. M., Brivanlou, A. H. and Massagué, J. 2007. Balancing BMP signaling through integrated inputs into the Smad1 linker. *Mol Cell* 25(3), pp. 441-454. doi: 10.1016/j.molcel.2007.01.006

Sarker, D. et al. 2022. A multi-modular phase I/II study of UCB6114, a first-in-class, fully human IgG4P anti-Gremlin-1 monoclonal antibody, as monotherapy and in combination with mFOLFOX6 or trifluridine/tipiracil, for patients with advanced gastrointestinal (GI) tumors. *Journal of Clinical Oncology* 40(4_suppl), pp. TPS221-TPS221. doi: 10.1200/JCO.2022.40.4_suppl.TPS221

Scherberich, A., Tucker, R. P., Degen, M., Brown-Luedi, M., Andres, A. C. and Chiquet-Ehrismann, R. 2005. Tenascin-W is found in malignant mammary tumors, promotes alpha8 integrin-dependent motility and requires p38MAPK activity for BMP-2 and TNF-alpha induced expression in vitro. *Oncogene* 24(9), pp. 1525-1532. doi: 10.1038/sj.onc.1208342

Schnitt, S. J. 2010. Classification and prognosis of invasive breast cancer: from morphology to molecular taxonomy. *Mod Pathol* 23 Suppl 2, pp. S60-64. doi: 10.1038/modpathol.2010.33

Schuetz, C. S. et al. 2006. Progression-specific genes identified by expression profiling of matched ductal carcinomas in situ and invasive breast tumors, combining laser capture microdissection and oligonucleotide microarray analysis. *Cancer research* 66(10), pp. 5278-5286. doi: 10.1158/0008-5472.CAN-05-4610

Schwalbe, M., Sänger, J., Eggers, R., Naumann, A., Schmidt, A., Höffken, K. and Clement, J. H. 2003. Differential expression and regulation of bone morphogenetic protein 7 in breast cancer. *Int J Oncol* 23(1), pp. 89-95.

Schwaninger, R. et al. 2007. Lack of noggin expression by cancer cells is a determinant of the osteoblast response in bone metastases. *Am J Pathol* 170(1), pp. 160-175. doi: 10.2353/ajpath.2007.051276

Scimeca, M. et al. 2018. Breast Osteoblast-like Cells: A Reliable Early Marker for Bone Metastases From Breast Cancer. *Clin Breast Cancer* 18(4), pp. e659-e669. doi: 10.1016/j.clbc.2017.11.020

Sejben, A., Nyári, T., Zombori, T. and Cserni, G. 2020. Comparison of Nottingham Prognostic Index, PREDICT and PrognosTILs in Triple Negative Breast Cancer -a Retrospective Cohort Study. *Pathol Oncol Res* 26(4), pp. 2443-2450. doi: 10.1007/s12253-020-00846-8

Senkus, E., Kyriakides, S., Penault-Llorca, F., Poortmans, P., Thompson, A., Zackrisson, S. and Cardoso, F. 2013. Primary breast cancer: ESMO Clinical Practice Guidelines for diagnosis, treatment and follow-up. *Annals of oncology : official journal of the European Society for Medical Oncology* 24 Suppl 6, pp. vi7-23. doi: 10.1093/annonc/mdt284

Shao, H. and Varamini, P. 2022. Breast Cancer Bone Metastasis: A Narrative Review of Emerging Targeted Drug Delivery Systems. *Cells* 11(3), doi: 10.3390/cells11030388

Siersbæk, R., Kumar, S. and Carroll, J. S. 2018. Signaling pathways and steroid receptors modulating estrogen receptor α function in breast cancer. *Genes Dev* 32(17-18), pp. 1141-1154. doi: 10.1101/gad.316646.118

Smittenaar, C. R., Petersen, K. A., Stewart, K. and Moitt, N. 2016. Cancer incidence and mortality projections in the UK until 2035. *Br J Cancer* 115(9), pp. 1147-1155. doi: 10.1038/bjc.2016.304

Sneddon, J. B. et al. 2006. Bone morphogenetic protein antagonist gremlin 1 is widely expressed by cancer-associated stromal cells and can promote tumor cell proliferation. *Proc Natl Acad Sci U S A* 103(40), pp. 14842-14847. doi: 10.1073/pnas.0606857103

Soguel, L., Durocher, F., Tchernof, A. and Diorio, C. 2017. Adiposity, breast density, and breast cancer risk: epidemiological and biological considerations. *Eur J Cancer Prev* 26(6), pp. 511-520. doi: 10.1097/CEJ.0000000000000310

Sørlie, T. et al. 2001. Gene expression patterns of breast carcinomas distinguish tumor subclasses with clinical implications. *Proc Natl Acad Sci U S A* 98(19), pp. 10869-10874. doi: 10.1073/pnas.191367098

Sosa, J. M., Huber, D. E., Welk, B. and Fraser, H. L. 2014. Development and application of MIPAR™: a novel software package for two- and three-dimensional microstructural characterization. *Integrating Materials and Manufacturing Innovation* 3(1), pp. 123-140. doi: 10.1186/2193-9772-3-10

Sotiriou, C. et al. 2003. Breast cancer classification and prognosis based on gene expression profiles from a population-based study. *Proc Natl Acad Sci U S A* 100(18), pp. 10393-10398. doi: 10.1073/pnas.1732912100

Stabile, H. et al. 2007. Bone morphogenic protein antagonist Drm/gremlin is a novel proangiogenic factor. *Blood* 109(5), pp. 1834-1840. doi: 10.1182/blood-2006-06-032276

Strouhalova, K., Přechová, M., Gandalovičová, A., Brábek, J., Gregor, M. and Rosel, D. 2020. Vimentin Intermediate Filaments as Potential Target for Cancer Treatment. *Cancers (Basel)* 12(1), doi: 10.3390/cancers12010184

Sun, J. et al. 2006. BMP4 activation and secretion are negatively regulated by an intracellular gremlin-BMP4 interaction. *J Biol Chem* 281(39), pp. 29349-29356. doi: 10.1074/jbc.M603833200

Sun, Z., Cai, S., Liu, C., Cui, Y., Ji, J., Jiang, W. G. and Ye, L. 2020. Increased Expression of Gremlin1 Promotes Proliferation and Epithelial Mesenchymal Transition in Gastric Cancer Cells and Correlates With Poor Prognosis of Patients With Gastric Cancer. *Cancer Genomics Proteomics* 17(1), pp. 49-60. doi: 10.21873/cgp.20167

Sung, N. J., Kim, N. H., Bae, N. Y., Jo, H. S. and Park, S. A. 2020a. DHA inhibits Gremlin-1-induced epithelial-to-mesenchymal transition via ERK suppression in human breast cancer cells. *Biosci Rep* 40(3), doi: 10.1042/BSR20200164

Sung, N. J., Kim, N. H., Surh, Y. J. and Park, S. A. 2020b. Gremlin-1 Promotes Metastasis of Breast Cancer Cells by Activating STAT3-MMP13 Signaling Pathway. *Int J Mol Sci* 21(23), doi: 10.3390/ijms21239227

Suvannasankha, A. and Chirgwin, J. M. 2014. Role of bone-anabolic agents in the treatment of breast cancer bone metastases. *Breast Cancer Res* 16(6), p. 484. doi: 10.1186/s13058-014-0484-9

Takahashi, M. et al. 2008. Bone morphogenetic protein 6 (BMP6) and BMP7 inhibit estrogen-induced proliferation of breast cancer cells by suppressing p38 mitogen-activated protein kinase activation. *J Endocrinol* 199(3), pp. 445-455. doi: 10.1677/JOE-08-0226

Tan, C. C. et al. 2016. Breast cancer cells obtain an osteomimetic feature via epithelial-mesenchymal transition that have undergone BMP2/RUNX2 signaling pathway induction. *Oncotarget* 7(48), pp. 79688-79705. doi: 10.18632/oncotarget.12939

Tarragona, M. et al. 2012. Identification of NOG as a specific breast cancer bone metastasis-supporting gene. *J Biol Chem* 287(25), pp. 21346-21355. doi: 10.1074/jbc.M112.355834

Todd, G. M., Gao, Z., Hyvönen, M., Brazil, D. P. and Ten Dijke, P. 2020. Secreted BMP antagonists and their role in cancer and bone metastases. *Bone* 137, p. 115455. doi: 10.1016/j.bone.2020.115455

Todd, J. H. et al. 1987. Confirmation of a prognostic index in primary breast cancer. *Br J Cancer* 56(4), pp. 489-492. doi: 10.1038/bjc.1987.230

Topol, L. Z. et al. 2000. Biosynthesis, post-translation modification, and functional characterization of Drm/Gremlin. *J Biol Chem* 275(12), pp. 8785-8793. doi: 10.1074/jbc.275.12.8785

UK, C. R. 2021. *Twenty most common cancers*. Available at: www.cancerresearchuk.org/health-professional/cancer-statistics/incidence [Accessed: 23/08/2021].

UK, P. H. E. N. C. I. N. a. C. R. 2014. *Cancer by deprivation in England: Incidence, 1996-2010, Mortality, 1997-2011*.

Urist, M. R. and Strates, B. S. 1971. Bone morphogenetic protein. *J Dent Res* 50(6), pp. 1392-1406. doi: 10.1177/00220345710500060601

Valabrega, G., Montemurro, F. and Aglietta, M. 2007. Trastuzumab: mechanism of action, resistance and future perspectives in HER2-overexpressing breast cancer. *Ann Oncol* 18(6), pp. 977-984. doi: 10.1093/annonc/mdl475

Vanderveen, K. A., Schneider, P. D., Khatri, V. P., Goodnight, J. E. and Bold, R. J. 2006. Upstaging and improved survival of early breast cancer patients after implementation of sentinel node biopsy for axillary staging. *Ann Surg Oncol* 13(11), pp. 1450-1456. doi: 10.1245/s10434-006-9109-6

Verheyden, J. M. and Sun, X. 2008. An Fgf/Gremlin inhibitory feedback loop triggers termination of limb bud outgrowth. *Nature* 454(7204), pp. 638-641. doi: 10.1038/nature07085

Vernieri, C. et al. 2019. Resistance mechanisms to anti-HER2 therapies in HER2-positive breast cancer: Current knowledge, new research directions and therapeutic perspectives. *Crit Rev Oncol Hematol* 139, pp. 53-66. doi: 10.1016/j.critrevonc.2019.05.001

Vollaire, J. et al. 2019. The Bone Morphogenetic Protein Signaling Inhibitor LDN-193189 Enhances Metastasis Development in Mice. *Front Pharmacol* 10, p. 667. doi: 10.3389/fphar.2019.00667

Wallden, B. et al. 2015. Development and verification of the PAM50-based Prosigna breast cancer gene signature assay. *BMC Med Genomics* 8, p. 54. doi: 10.1186/s12920-015-0129-6

Walsh, D. W., Godson, C., Brazil, D. P. and Martin, F. 2010. Extracellular BMP-antagonist regulation in development and disease: tied up in knots. *Trends Cell Biol* 20(5), pp. 244-256. doi: 10.1016/j.tcb.2010.01.008

Walsh, D. W. et al. 2008. Co-regulation of Gremlin and Notch signalling in diabetic nephropathy. *Biochim Biophys Acta* 1782(1), pp. 10-21. doi: 10.1016/j.bbadis.2007.09.005

Wang, C. X., Koay, D. C., Edwards, A., Lu, Z., Mor, G., Ocal, I. T. and Digiovanna, M. P. 2005. In vitro and in vivo effects of combination of Trastuzumab (Herceptin) and Tamoxifen in breast cancer. *Breast Cancer Res Treat* 92(3), pp. 251-263. doi: 10.1007/s10549-005-3375-z

Wang, D. J. et al. 2012. The bone morphogenetic protein antagonist Gremlin is overexpressed in human malignant mesothelioma. *Oncol Rep* 27(1), pp. 58-64. doi: 10.3892/or.2011.1463

Wang, H. and Cui, Z. 2015. The Distribution and Expression of BAMBI in Breast Cancer Cell Lines. *Open Access Library Journal* 2(11), pp. 1-7. doi: 10.4236/oalib.1102147

Wang, K. et al. 2011. BMP9 inhibits the proliferation and invasiveness of breast cancer cells MDA-MB-231. *J Cancer Res Clin Oncol* 137(11), pp. 1687-1696. doi: 10.1007/s00432-011-1047-4

Wang, L., Wang, Q., Gao, M., Fu, L., Li, Y., Quan, H. and Lou, L. 2018. STAT3 activation confers trastuzumab-emtansine (T-DM1) resistance in HER2-positive breast cancer. *Cancer Sci* 109(10), pp. 3305-3315. doi: 10.1111/cas.13761

Wang, R., Zhu, Y., Liu, X., Liao, X., He, J. and Niu, L. 2019. The Clinicopathological features and survival outcomes of patients with different metastatic sites in stage IV breast cancer. *BMC Cancer* 19(1), p. 1091. doi: 10.1186/s12885-019-6311-z

Wang, S. E. 2011. The Functional Crosstalk between HER2 Tyrosine Kinase and TGF-β Signaling in Breast Cancer Malignancy. *J Signal Transduct* 2011, p. 804236. doi: 10.1155/2011/804236

Wellbrock, J. et al. 2015. Intrinsic BMP Antagonist Gremlin-1 as a Novel Circulating Marker in Pulmonary Arterial Hypertension. *Lung* 193(4), pp. 567-570. doi: 10.1007/s00408-015-9735-5

Wesolowski, R. and Ramaswamy, B. 2011. Gene expression profiling: changing face of breast cancer classification and management. *Gene Expr* 15(3), pp. 105-115.

Williams, C. and Lin, C. Y. 2013. Oestrogen receptors in breast cancer: basic mechanisms and clinical implications. *Ecancermedicalscience* 7, p. 370. doi: 10.3332/ecancer.2013.370

Wishart, G. C. et al. 2010. PREDICT: a new UK prognostic model that predicts survival following surgery for invasive breast cancer. *Breast Cancer Res* 12(1), p. R1. doi: 10.1186/bcr2464

Wordinger, R. J., Zode, G. and Clark, A. F. 2008. Focus on molecules: gremlin. *Exp Eye Res* 87(2), pp. 78-79. doi: 10.1016/j.exer.2007.11.016

Wu, Q. et al. 2017. Breast cancer subtypes predict the preferential site of distant metastases: a SEER based study. *Oncotarget* 8(17), pp. 27990-27996. doi: 10.18632/oncotarget.15856

Xiao, W., Zheng, S., Yang, A., Zhang, X., Zou, Y., Tang, H. and Xie, X. 2018. Breast cancer subtypes and the risk of distant metastasis at initial diagnosis: a population-based study. *Cancer Manag Res* 10, pp. 5329-5338. doi: 10.2147/CMAR.S176763

Xiong, Z. et al. 2018. Bone metastasis pattern in initial metastatic breast cancer: a population-based study. *Cancer Manag Res* 10, pp. 287-295. doi: 10.2147/CMAR.S155524

Yamamoto, T., Saatcioglu, F. and Matsuda, T. 2002. Cross-talk between bone morphogenic proteins and estrogen receptor signaling. *Endocrinology* 143(7), pp. 2635-2642. doi: 10.1210/endo.143.7.8877

Yamasaki, Y. et al. 2018. Expression of gremlin1 in gastric cancer and its clinical significance. *Med Oncol* 35(3), p. 30. doi: 10.1007/s12032-017-1073-4

Yang, K., Hitomi, M. and Stacey, D. W. 2006. Variations in cyclin D1 levels through the cell cycle determine the proliferative fate of a cell. *Cell Div* 1, p. 32. doi: 10.1186/1747-1028-1-32

Yang, T., Chen, S. L., Lu, X. J., Shen, C. Y., Liu, Y. and Chen, Y. P. 2012. Bone morphogenetic protein 7 suppresses the progression of hepatic fibrosis

and regulates the expression of gremlin and transforming growth factor β1. *Mol Med Rep* 6(1), pp. 246-252. doi: 10.3892/mmr.2012.892

Yang, X. R. et al. 2007. Hormonal markers in breast cancer: coexpression, relationship with pathologic characteristics, and risk factor associations in a population-based study. *Cancer Res* 67(21), pp. 10608-10617. doi: 10.1158/0008-5472.CAN-07-2142

Yardley, D. A. 2016. Pharmacologic management of bone-related complications and bone metastases in postmenopausal women with hormone receptor-positive breast cancer. *Breast Cancer (Dove Med Press)* 8, pp. 73-82. doi: 10.2147/BCTT.S97963

Ye, J., Coulouris, G., Zaretskaya, I., Cutcutache, I., Rozen, S. and Madden, T. L. 2012. Primer-BLAST: a tool to design target-specific primers for polymerase chain reaction. *BMC Bioinformatics* 13, p. 134. doi: 10.1186/1471-2105-13-134

Ye, L., Bokobza, S. M. and Jiang, W. G. 2009. Bone morphogenetic proteins in development and progression of breast cancer and therapeutic potential (review). *Int J Mol Med* 24(5), pp. 591-597. doi: 10.3892/ijmm_00000269

Ye, L., Lewis-Russell, J. M., Davies, G., Sanders, A. J., Kynaston, H. and Jiang, W. G. 2007. Hepatocyte growth factor up-regulates the expression of the bone morphogenetic protein (BMP) receptors, BMPR-IB and BMPR-II, in human prostate cancer cells. *Int J Oncol* 30(2), pp. 521-529.

Ye, L., Lewis-Russell, J. M., Sanders, A. J., Kynaston, H. and Jiang, W. G. 2008. HGF/SF up-regulates the expression of bone morphogenetic protein 7 in prostate cancer cells. *Urol Oncol* 26(2), pp. 190-197. doi: 10.1016/j.urolonc.2007.03.027

Ye , L., Mansel , R. and Jiang, W. 2009. Noggin, impact on in vitro cell growth, expression pattern and the prognostic value in breast cancer. *Cancer Research* 69(2), doi: 10.1158/0008-5472.SABCS-2084

Yersal, O. and Barutca, S. 2014. Biological subtypes of breast cancer: Prognostic and therapeutic implications. *World J Clin Oncol* 5(3), pp. 412-424. doi: 10.5306/wjco.v5.i3.412

Yin, M. et al. 2017. Gremlin-1 is a key regulator of the invasive cell phenotype in mesothelioma. *Oncotarget* 8(58), pp. 98280-98297. doi: 10.18632/oncotarget.21550

Yin, Y., Yang, Y., Yang, L., Li, C., Liu, X. and Qu, Y. 2016. Overexpression of Gremlin promotes non-small cell lung cancer progression. *Tumour Biol* 37(2), pp. 2597-2602. doi: 10.1007/s13277-015-4093-8

Zabkiewicz, C., Resaul, J., Hargest, R., Jiang, W. and Ye, L. 2017. Bone morphogenetic proteins, breast cancer, and bone metastases: striking the right balance. *Endocr Relat Cancer*, doi: 10.1530/ERC-17-0139

Zhang, H. et al. 2018. Incidence, risk factors and prognostic characteristics of bone metastases and skeletal-related events (SREs) in breast cancer patients: A systematic review of the real world data. *J Bone Oncol* 11, pp. 38-50. doi: 10.1016/j.jbo.2018.01.004

Zhang, M., Yan, J. D., Zhang, L., Wang, Q., Lü, S. J., Zhang, J. and Zhu, T. H. 2005. Activation of bone morphogenetic protein-6 gene transcription in MCF-7 cells by estrogen. *Chin Med J (Engl)* 118(19), pp. 1629-1636.

Zhang, Q. et al. 2010. In vivo delivery of Gremlin siRNA plasmid reveals therapeutic potential against diabetic nephropathy by recovering bone morphogenetic protein-7. *PLoS One* 5(7), p. e11709. doi: 10.1371/journal.pone.0011709

Zhao, X. K. et al. 2014. Effect of Danshao Huaxian capsule on Gremlin and bone morphogenetic protein-7 expression in hepatic fibrosis in rats. *World J Gastroenterol* 20(40), pp. 14875-14883. doi: 10.3748/wjg.v20.i40.14875

Zhao, Z., Bo, Z., Gong, W. and Guo, Y. 2020. Inhibitor of Differentiation 1 (Id1) in Cancer and Cancer Therapy. *Int J Med Sci* 17(8), pp. 995-1005. doi: 10.7150/ijms.42805

Ziadeh, C., Ziogas, A. and Anton-Culver, H. 2017. Cancer risk in different generations of Middle Eastern immigrants to California, 1988-2013. *Int J Cancer* 141(11), pp. 2260-2269. doi: 10.1002/ijc.30928

Ziegler, R. G. et al. 1993. Migration patterns and breast cancer risk in Asian-American women. *J Natl Cancer Inst* 85(22), pp. 1819-1827. doi: 10.1093/jnci/85.22.1819

Zuo, T. et al. 2017. The influence of stage at diagnosis and molecular subtype on breast cancer patient survival: a hospital-based multi-center study. *Chin J Cancer* 36(1), p. 84. doi: 10.1186/s40880-017-0250-3